ELECTROCHEMICALLY SYNTHESISED POLYANILINE FOR THE GAS AND AQUEOUS DETECTION OF AMMONIA

Anja Korent

Doctoral Dissertation
Jožef Stefan International Postgraduate School
Ljubljana, Slovenia

Supervisor: Prof. Dr. Kristina Žužek, Jožef Stefan Institute and Jožef Stefan International Postgraduate School, Jamova cesta 39, SI-1000, Ljubljana, Slovenia

Evaluation Board:
Prof. Dr. Uroš Cvelbar, Chair, Jožef Stefan Institute and Jožef Stefan International Postgraduate School, Jamova cesta 39, SI-1000, Ljubljana, Slovenia
Asst. Prof. Gregor Marolt, Member, University of Ljubljana, Faculty of Chemistry and Chemical Technology, Večna pot 113, SI-1000, Ljubljana, Slovenia
Prof. Dr. Cristian Fabrega Gallego, Member, University of Barcelona, Faculty of Physics, Department of Electronics and Biomedical Engineering, Martí Franquès 1, 08028 Barcelona, Spain

MEDNARODNA PODIPLOMSKA ŠOLA JOŽEFA STEFANA
JOŽEF STEFAN INTERNATIONAL POSTGRADUATE SCHOOL

Anja Korent

ELECTROCHEMICALLY SYNTHESISED POLYANILINE FOR GAS AND AQUEOUS DETECTION OF AMMONIA

Doctoral Dissertation

ELEKTROKEMIJSKO SINTETIZIRAN POLIANILIN ZA PLINSKO IN TEKOČINSKO ZAZNAVANJE AMONIJAKA

Doktorska disertacija

Supervisor: Prof. Dr. Kristina Žužek

Ljubljana, Slovenia, November 2022

Acknowledgements

The PhD process was a long, ups-and-downs road, and I had many people by my side, guiding and encouraging me to reach the finishing line. I would like to express my gratitude to each of them for being there where I needed them to be.

Starting from my first days at the Jožef Stefan Institute and the Department for Nanostructured Materials (K7). I was just a bachelor's student with the idea of working afternoons in a chemical laboratory to gain work experience and earn a little extra. 😊 Prof. Saša Novak and Dr. Aljaž Iveković saw the potential in me and gave me the opportunity to work. I would not be here if Saša did not pay attention to my interests and guided me towards them. She introduced me to Dr. Martina Lorenzetti and gave me the opportunity to be a part of the ISO-Food project with my bachelor thesis. Prof. Saša Novak, you believed in me from the start and opened the doors to the scientific world for me. You were there for my bachelor's thesis, encouraged me to enrol for a master's thesis at Jožef Stefan Postgraduate School and left me to spread my wings when I decided on a PhD position. Saša and Martina, you were my beginning on this crazy scientific road, and I am grateful that you were there. Thank you!

When I started to think about a PhD position, I was indecisive. My supervisor Prof. Kristina Žužek offered me a topic that immediately attracted me at the time. She introduced me to the world of electrochemistry, taught me how to think and behave like a scientist and gave me the opportunity to be a part of her group. It was not always easy to follow her instructions and expectations, but a PhD is not meant to be easy if you want to learn something new. She forced me to do quality work, of which I could be proud. I was not always easy to work, but she found a way to communicate with me and guide me through the process. Tina, thank you for taking your time and being there. Your office was always open. Thank you, especially for allowing me to go for the Erasmus+ traineeship in France. This was the highlight of my PhD years.

At the beginning of my third year of PhD studies, I was given the opportunity to go as an Erasmus+ student on a traineeship. Prof. Jean-Luc Wojkiewicz from the Institut Mines Télécom Lille Douai, France, Department of Atmospheric Science and Environment Engineering accepted me with open arms. Working under his and Dr. Caroline Duc's supervision gave me a whole new perspective on polyaniline, a material I was struggling with at the time. Thank you and to the other members of the department, Dr. Nathalie Redon, Thomas Fagniez for accepting me and letting me work in your department and, most importantly, to learn from you.

Even though I previously worked at the K7 department as a student, being a PhD student brought a lot of new things. I was lucky enough to share an office with Dr. Špela Trafela for most of my PhD studies. At the time, she was a student too, and she was the one I looked up to. She showed me everything she knew, helped me with my topic, gave me constructive critique when I needed it, and most importantly, she became my friend, with whom I could talk and discuss numerous topics. Thank you.

There are many people who helped me during my PhD and without them, my days at the K7 would not be the same:

- "Electrochemical and sensor group". Thank you for all discussions, helpful comments and encouragement. Special thanks go to Dr. Kristina Žagar Soderžnik for helping me with the topic and articles;

- Our “young group”: Špela Trafela, Luka Kelhar, Matic Korent, Matej Kocen, Bojan Ambrožič, Luka Suhadolnik, Hermina Hudelja, Aleksander Učakar, Živa Marinko and Monika Kušter, gave me a lot of joyful memories, unforgettable team buildings, lunches and one o’clock coffee breaks;
- Room E51 (Luka, Matic, Živa, and Monika) for accepting me in the office. I appreciate our discussions and attempts to maintain a calm and peaceful environment. Thanks for your support, help and conversations;
- Thanks to all members of the department for their help, friendly discussions and laughs.

Finally, I would like to thank my family and friends for always being there, not giving up on me and encouraging me till the end. My mother, Suzana, father, Janko and sister Saša. It was not always easy to listen to and understand me, but you did it at every step of the way. My husband, Matic. We started this PhD road together, and now, a year after you, I finally reached the end. I cannot express my gratitude for everything you did for me during the “PhD” years.

This thesis was funded by several projects:

- The ARRS young-researcher project, grant number PR-08337;
- the ARRS project High performance nanostructured acrylamide sensors, grant number J2-1739;
- The ARRS project Development of high performance sensors for the detection of persistent and mobile chemicals in the environment (sense PMC), grant number J2-3051;
- the Erasmus+ program of the European Union, Jožef Stefan International Postgraduate School project, grant number 2019-1-SI01-KA103-060202;
- The ARRS project Catalytically-assisted high efficiency and low-cost nanostructured sensors based on modified screen-printed electrodes for analytical chemistry, grant number J2-8182;
- The ARRS project From the synthesis of metal oxides to the humidity and oxygen prototype nanosensors, grant number Z2-6757;
- Program Nanostructured Materials, grant number P2-0084.

Abstract

An everyday awareness of the presence of harmful chemicals around us has led to the development of a way to report overexposure through the reactions of these compounds with specifically prepared materials - sensory elements. In this doctoral dissertation we focused on the electrochemical synthesis (electropolymerization) of conductive polymer polyaniline (PANI) and on its ability to detect ammonia (NH_3). The main objectives included the electrochemical synthesis of PANI, the study of its electronic and electrochemical properties and its use for detecting NH_3. The latter was detected in the gaseous and aqueous states, which divided this work into three chapters presented in scientific articles.

NH_3 is a well-known compound, indispensable in industry, part of the natural nitrogen cycle and a common decomposition product of nitrogen compounds. Due to its extremely irritating and harmful effects when exposed to excessive concentrations and its presence in exhaled air as a consequence of organ failure, the detection of NH_3 gas is of great scientific interest. PANI, the most commonly studied and widely used conductive polymer, is known for its specific interaction with NH_3, which is why it is also a commonly used material for constructing NH_3 sensors.

In our study, PANI was prepared electrochemically from 0.1M aniline (ANI) in 1.0 M HCl solution by cyclic voltammetry (CV) from −0.3 to 1.0 V vs Ag reference electrode at 50 mV s^{-1}. The resulting polymer was directly deposited on a working electrode of commercial screen-printed electrodes (SPEs). Since PANI's electrochemical, optical and electronic properties are interconnected, their correlation during the PANI formation was observed with the spectro-electrochemical technique. The experiment was performed *in-situ* in the specifically designed electrochemical cell for SPEs with space for the optical probe. The CV result shows the ANI oxidation at a high positive potential (0.9 V vs Ag), the successful deposition of PANI during each cycle, observed in a current increase, and characteristic electrochemical transformations of already-deposited PANI (from leucoemeraldine, emeraldine, to pernigraniline). While the spectroscopic results showed characteristic absorbance peaks such as for the formation of dimers, the formation of charge carriers during the PANI polymerization, and the structural changes in PANI (i.e., quinoid ring formation). The PANI electropolymerization process carried out by CV under certain conditions produces a compact deposition of PANI directly on the SPE in a conductive protonated emeraldine form suitable for further use in sensorics.

Such an electrochemically synthesized PANI layer, compactly attached to the SPE (PANI-Au-SPE), was the starting material for producing NH_3 gas-sensor platforms. The PANI-deposit was characterized with scanning electron microscopy (SEM), profilometry, and Fourier-transformation infrared spectroscopy (FTIR) to determine the morphology, surface roughness and to confirm the form of emeraldine salt. The electrochemical preparation requires using a three-electrode system, while for subsequent sensor measurements, only two electrodes connected via the PANI were needed. The SPE was converted into a system suitable for electrical measurements by creating a new contact with Au sputtering, connecting the PANI to the counter and reference electrodes. The electrodes prepared in this way were exposed to the humidity and NH_3 in the gas chamber, and the material's response was monitored by observing changes in the PANIs' resistance. The simultaneous use of a commercial NH_3 analyser confirms the immediate response and possibility for realistic measurements. Considering the system's simplicity from the point of view of preparation and the PANI itself (simple acid dopant, without the addition of nanomaterials), detections of low NH_3 concentrations (detection limit 23 ppb) were achieved, giving the developed system an applied value.

As a highly water-soluble gas, NH_3 is also present in water sources and biological fluids in the body, where it can indicate diseases and organ failure. The last part of the thesis focuses on the

electrochemical detection of liquid NH_3 in a neutral medium. In the previous study, electrochemically prepared PANI ($PANI_{el}$) in the form of emeraldine salt demonstrated an excellent affinity for NH_3 gas. Therefore, the same material was also tested against aqueous NH_3. Due to the aim of the biomedical application, the phosphate buffered saline (PBS, pH = 7) was used as a working electrolyte. Awareness of PANI's electronic behaviour was important, as its conductivity depends on the electrochemical conditions and environmental pH. The $PANI_{el}$ electrochemical behaviour was therefore observed in acidic (0.1 M H_2SO_4) and neutral (PBS) media to determine the most appropriate conditions for further use in sensorics. NH_3 detection was performed using chronoamperometry (CA) at a constant applied potential of 0.2 V vs Ag by injecting a 1µL sample aliquot into a 50 µL drop of PBS, placed directly on the SPE. The current response is explained by the mechanism involving $PANI_{el}$ deprotonation, $PANI_{el}$ re-oxidation due to the previous reduction caused by NH_4^+ oxidation. To improve the $PANI_{el}$ responses, Au NPs of different sizes were added, where 20-nm Au NPs ($PANI_{el}$-Au20) showed the highest contribution to the $PANI_{el}$'s electronic properties. Thus, the detection limit was lowered from 24.64 µM NH_3 to 1.44 µM, i.e., 17 times, and the quantification limit form 51 µM NH_3 to 2.55 µM, i.e., 20 times lower. The capability for real-sample measurement was studied by observing the $PANI_{el}$-Au20 response to NH_3 in artificial saliva of different pH values, where it exhibits a recovery rate of 90–99.5 %. Thus, the $PANI_{el}$-Au20 demonstrated suitability for measuring more complex samples containing a variety of ions and consequently proved the high affinity of PANI for NH_3.

Overall, the PANI prepared by electropolymerization on SPE demonstrated the applicability for NH_3 gas and aqueous sensing, demonstrating the versatility of the studied material.

Povzetek

Zavedanje o vsesplošni prisotnosti škodljivih kemikalij okoli nas, je privedlo do razvoja načina zaznavanja naše prekomerne izpostavljenosti. Slednje se vrši preko reakcij teh spojin s specifično pripravljenimi materiali – senzornimi elementi. V doktorskem delu smo se osredotočili na elektrokemijsko sintezo (elektropolimerizacijo) prevodnega polimera polianilina (PANI) za namen zaznavanja amonijaka (NH_3). Glavni cilji so zajemali elektrokemijsko sintezo PANI-ja preučevanje njegovih elektronskih in elektrokemijskih lastnosti ter njegovo uporabo za zaznavanje NH_3. Slednjega smo zaznavali tako v plinskem kot v tekočinskem stanju. Glede na cilje, je omenjeno delo razdeljeno na tri poglavja, predstavljena s tremi izvirnimi znanstvenimi članki.

Amonijak je splošno znana spojina, nepogrešljiva v industriji in je del naravnega dušikovega cikla in pogost produkt pri razkroju dušikovih spojin. Zaradi izredno dražilnega in škodljivega učinka ob izpostavitvi previsokim koncentracijam ter njegovi prisotnosti v izdihanem zraku kot posledici odpovedovanja določenih organov, ima zaznavanje plinskega NH_3 velik znanstveni in uporabni pomen.

PANI, kot eden izmed najbolj preučevanih in uporabljenih prevodnih polimerov, je znan po svoji specifični interakciji z NH_3, zaradi česar je pogosto uporabljen material za izdelavo senzorjev amonijaka. V tej raziskavi smo PANI pripravili elektrokemijsko z uporabo ciklične voltametrije (CV) v prisotnosti 1 M HCl raztopine z vsebnostjo 0.1 M monomera anilina (ANI). CV smo izvedli v potencialnem območju od −0.3 do 1 V glede na referenčno elektrodo na osnovi Ag s hitrostjo preleta 50 mV s^{-1}. Tako pripravljen polimer je bil direktno nanešen na delovno elektrodo komercialno dostopne sitotiskane elektrode (“screen printed electrodes-SPE”).

Ker so elektrokemijske, optične in elektronske lastnosti PANI-ja med seboj povezane, smo njihovo odvisnost in povezavo tekom elektrokemijske priprave PANI-ja, preučili z uporabo spektroelektrokemijske tehnike. *In-situ* poskus spektroelektrokemije smo izvedli v posebni elektrokemijski celici za SPE, ki je vsebovala prostor za vstavitev optične sonde. Rezultati, pridobljeni s CV-jem so pokazali oksidacijo ANI-ja pri visokih pozitivnih potencialih (0.9 V proti Ag), ter uspešen nanos PANI-ja z vsakim izvedenim ciklom, kar je bilo razvidno iz porasta toka. Prav tako smo opazil značilne elektrokemijske prehode med različnimi oblikami nanesenega PANI-ja in sicer iz leukoemeraldina v emeraldin ter v pernigranilin. Spektroskopski rezultati so pokazali absorpcijske vrhove, ki so značilni za nastanek dimerov in nosilcev nabojev ter strukturne spremembe v PANI-ju (na primer nastanek kinoidnega obroča). Ugotovili smo, da izvedba elektropolimerizacije pod danimi pogoji zagotovi neposreden kompakten nanos PANI-ja na zlato elektrodo, ki je del SPE. Nanešen PANI je v prevodni protonirani obliki (emeraldin soli), ki je primerna za nadaljnjo uporabo v senzoriki.

Tako pripravljen sloj PANI-ja, kompaktno nanešen na zlato elektrodo na tiskanem elektrodnem sistemu SPE, smo uporabili kot začetni material za izdelavo plinskega senzorja za NH_3. Z uporabo vrstičnega elektronskega mikroskopa (SEM), profilometra in infrardeče spektroskopije s Fourierjevo transformacijo (FTIR), smo preučiti morfologijo in hrapavost površine nanešenega sloja, ter potrdili najbolj prevodno obliko PANI-ja, t.j. emeraldin sol. Za elektrokemijsko pripravo PANI-ja smo potrebovali posebno prirejen tri-elektrodni sistem, kjer smo PANI nanašali na zlato elektrodo na SPE, medtem ko sta bili za nadaljnje senzorne meritve potrebni le dve elektrodi povezani s PANI-jem. S pomočjo naprševanja Au, smo PANI povezali s proti in referenčno elektrodo ter tako pretvorili komercialen SPE, v sistem primeren za izvedbo električnih meritev upornosti. Tako pripravljene elektrode smo v plinski komori izpostavili vlagi in NH_3 ter spremljali odziv PANI-ja – oz. njegove spremembe v upornosti. Sočasna uporaba komercialnega detektorja za NH_3 je omogočila potrditev takojšnjega odziva in sposobnost realnih meritev. PANI, pripravljen z uporabo preprostega kislinskega dopanta in brez dodatkov

nanomaterialov, je uspešno zaznaval nizke koncentracije NH_3 in dosegel mejo zaznavanja 23 ppb, kar mu daje potencial za nadaljnjo uporabo.

Nadalje, NH_3 je izredno dobro topen plin, zaradi česar je prisoten tudi v vodnem okolju in bioloških raztopinah v človeškem telesu. Njegova prisotnost v telesu lahko nakazuje na bolezni in okvare organov. Na podlagi tega smo se v zadnjem delu doktorskega dela osredotočili na elektrokemijsko zaznavanje NH_3 v tekočem stanju pri nevtralnem pH-ju. Na podlagi prejšnje raziskave, kjer smo dokazali odlično interakcijo med elektrokemijsko pripravljenim PANI-jem ($PANI_{el}$) v obliki emeraldin soli in NH_3 v plinskem stanju, smo enak material nato preizkusili tudi za zaznavanje amonijaka v tekočinah. S ciljem potencialne uporabe senzornega sistema v biomedicinske namene smo za delovni elektrolit izbrali fiziološko raztopino ("phosphate-buffered saline" – PBS) s pH = 7. Zavedali smo se, da so elektronske lastnosti PANI-ja in posledično njegova prevodnost odvisne od elektrokemijskih pogojev in pH okolja, zato smo najprej preučili njegovo elektrokemijsko obnašanje tako v kislem (0,1 M H_2SO_4) kot nevtralnem elektrolitu (PBS) ter tako določili optimalne pogoje za nadaljnjo uporabo. NH_3 smo zaznali z uporabo kronoamperometrije, pri konstantnem potencialu 0,2 V proti Ag elektrodi, ob injiciranju 1 µL vzorca v 50 µL kapljico PBS, ki je bila predhodno nanešena neposredno na SPE. Tokovni odziv, s katerim smo opisali zaznavanje amonijaka, smo razložili s pomočjo mehanizma, ki je sestavljen iz reakcij deprotonacije $PANI_{el}$ in njegove ponovne oksidacije, zaradi predhodne redukcije, ki jo povzroči oksidacija NH_4^+. Odzive $PANI_{el}$ smo izboljšali z dodatkom zlatih nanodelcev (Au NPs) različnih velikosti, med katerimi je dodatek 20 nm velikih zlatih nanodelcev (Au20 NPs) pokazal največji prispevek k elektronskim lastnostim $PANI_{el}$-ja. Tako smo mejo zaznavanja znižali za 17-krat, s 24,64 µM NH_3 na 1,44 µM, in mejo količinske določitve kar za 20-krat, z 51 µM NH_3 na 2,55 µM. Sposobnost merjenja in zaznavanja NH_3 v realnih vzorcih smo dokazali z merjenjem odziva $PANI_{el}$-Au20 na NH_3 v umetni slini z 90–99,5 % odzivom napram meritvam v čistem elektrolitu. S tem smo dokazali sposobnost merjenja amonijaka v bolj kompleksnih vzorcih z matrico različnih ionov in dokazali visoko interakcijo $PANI_{el}$ z NH_3.

Če povzamemo, PANI, ki smo ga pripravili z elektropolimerizacijo pod določenimi pogoji ($PANI_{el}$ na SPE), s katerimi smo namensko vplivali na njegove elektronske lastnosti, se je izkazal kot izjemno učinkovit material pri zaznavanju NH_3 tako v plinskem kot v tekočem stanju.

Contents

List of Figures

List of Tables

Abbreviations

HA	. . .	Acid electrolyte
NH_3	. . .	Ammonia
NH_4^+	. . .	Ammonium ion
$(NH_4)_2S_2O_8$	. . .	Ammonium persulfate
ANI	. . .	Aniline
ATR	. . .	Attenuated total reflection
BIA	. . .	Batch injection analysis
CA	. . .	Chronoamperometry
CPs	. . .	Conducting polymers
CE	. . .	Counter electrode
CV	. . .	Cyclic voltammetry
$PANI_{el}$	. . .	Electrochemically synthesized polyaniline
E_g	. . .	Energy band gap
$FeCl_3$	. . .	Ferric chloride
FEG-SEM	. . .	Field-emission-gun scanning electron microscopy
FTIR	. . .	Fourier-transformation infrared spectroscopy
HOMO	. . .	Highest occupied molecular orbital
HCl	. . .	Hydrochloric acid
H_2O_2	. . .	Hydrogen peroxide
ITO	. . .	Indium-tin-oxide glass
IHP	. . .	Inner Helmholtz plane
$FeCl_3$	. . .	Iron (III) chloride
LOD	. . .	Limit of detection
LSV	. . .	Linear sweep voltammetry
LUMO	. . .	Lowest unoccupied molecular orbital
NPs	. . .	Nanoparticles
NIR	. . .	Near-infrared region
NHE	. . .	Normal hydrogen electrode
iR	. . .	Ohmic drop
OHP	. . .	Outer Helmholtz plane
I_p^{ox}	. . .	Oxidation peak current
E_p^{ox}	. . .	Oxidation peak potential
E_0	. . .	Oxidation potential
PBS	. . .	Phosphate buffered saline
POC	. . .	Point-of-care
PA	. . .	Polyacetylene
PANI	. . .	Polyaniline
PPy	. . .	Polypyrrole
I_p^{red}	. . .	Reduction peak current
E_p^{red}	. . .	Reduction peak potential
RE	. . .	Reference electrode
SCE	. . .	Saturated calomel electrode
SPE	. . .	Screen-printed electrode
Ag/AgCl	. . .	Silver/silver chloride
Rs	. . .	Solution resistance
SHE	. . .	Standard hydrogen electrode
H_2SO_4	. . .	Sulfuric acid

TEM	. . .	Transmission electron microscopy
UV-Vis	. . .	Ultraviolet-visible spectroscopy
WE	. . .	Working electrode
XPS	. . .	X-ray photoelectron spectroscopy

Symbols

a . . . Activity
E . . . Actual/equilibrium potential
I_a . . . Anodic (oxidation) current
I_C . . . Capacitive current
I_c . . . Cathodic (reduction) current
q . . . Charge
k_a . . . Charge-transfer-rate constant for oxidation at electrode
k_c . . . Charge-transfer-rate constant for reduction at electrode
c . . . Concentration
I . . . Current
j . . . Current density
D . . . Diffusion coefficient
A^- . . . Doping anion
y . . . Doping degree
$\boldsymbol{E}$ . . . Electric field strength
E_{cell} . . . Electrochemical cell potential
ϕ . . . Electrostatic potential
E_g . . . Energy band gap
E_{eq} . . . Equilibrium potential
I_0 . . . Exchange current
I_F . . Faradaic current
F . . . Faraday constant
E_F . . . Fermi energy level
J . . . Flux
R . . . Gas constant
E_i . . . Initial potential
R_0 . . . Initial resistance
z . . . Ion charge
L . . . Length
k_d . . . Mass-transfer coefficient
M . . . Monomer
n . . . Number of reacting electrons
m . . . Number of reacting protons
η . . . Overpotential
Ox . . . Oxidised species
I_p . . . Peak current
ΔE_p . . . Peak-to-peak separation
E . . . Potential
E_{anode} . . . Potential at anode
$E_{cathode}$ . . . Potential at cathode
Red . . . Reduced species
R_r . . . Resistance
R_{max} . . . Resistance upon exposure to analyte
ρ . . . Resistivity
υ . . . Scan rate
m_{slope} . . . Slope of calibration curve
Rs . . . Solution resistance

σ . . Standard deviation of blank
E^0 . . . Standard potential
k_0 . . . Standard rate constant
E_f . . . Stopping potential
A . . . Surface area
Γ . . . Surface coverage
t . . . Time
α . . . Transfer coefficient

Chapter 1

Introduction

The research work presented in this thesis was published in three scientific papers. The focus of the PhD was to study electrochemically synthesized polyaniline and its subsequent application in ammonia sensing. The following introduction is an overall state-of-the-art review based on electrochemistry and the conductive polymer polyaniline (PANI), which is suitable for NH_3 sensing in gas and aqueous media. The introduction is followed by the aims and hypothesis section, where we describe the mechanisms and the methodology for constructing the NH_3 sensors based on PANI.

The chapters presenting the research work are presented as three first-author papers. Each one has a focused and detailed literature review of the problem and the aim of the research. Together they form a story of the electrochemical study of polyaniline and its versatile application in the electrical sensing of ammonia gas and the electrochemical sensing of aqueous ammonia.

1.1 The Basic Concepts of Electrochemistry

Electrochemistry is a branch of chemistry and physics that studies chemical reactions combined with the electric-charge (electron) transfer, current, and potential. Chemical phenomena associated with charge transfer can occur homogeneously in a solution (one phase) or heterogeneously on the surface of an electrode (between two different phases). Each electrochemical reaction represents a half-reaction. To ensure electroneutrality, two opposite half-reactions need to take place simultaneously. In the case of heterogeneous reactions, the two half-reactions occur separately, usually at different electrodes immersed in the solution in a cell. Charge transfer between electrodes can occur if the electrodes are connected externally (via electric wires) and in solution (electrolyte). The sum of the overall energy from both electrodes can be negative, in which case spontaneous electrode reactions occur (energy can be stored, e.g., batteries), or positive, used to force the electrode reaction and convert the chemical species (electrolysis) [1].

The electrode reaction is the heterogeneous chemical process of adding or removing an electron, i.e., charge transfer, to or from the electrode surface. The electrode reaction can be an anodic or a cathodic process. In the case of an anodic process, the species are oxidised, which is a reaction of donating electrons, i.e., oxidation (Eq. (1.1) to the left). Thus, the species lose electrons to the electrode. The opposite reaction is a cathodic process, where the species are reduced. Reduction means receiving electrons (Eq. (1.1) to the right). In this case, chemical species gain electrons from the electrode. The species that cause oxidation to occur are oxidants or oxidising agents, and the species which cause reduction to occur are reductants or reducing agents. An oxidant is always reduced (Ox – oxidised species, which tends to gain electrons), and a reductant is always oxidised (Red – reduced species, which tends to donate electrons) [1], [2].

$$\mathrm{Ox} + \mathrm{ne}^- \leftrightarrow \mathrm{Red} \tag{1.1}$$

$$I = \frac{\mathrm{d}q}{\mathrm{d}t} \tag{1.2}$$

$$j = \frac{\mathrm{d}I}{\mathrm{d}A} \tag{1.3}$$

The output of the charge transfer is an electric current, which is a measure of the rate of the electrochemical reaction and gives us the gradient of charge (q [C]) in a period of time (t [s]) (Eq. 1.2). The current density (j [A cm^{-2}] is the amount of current flowing through a defined surface area (A [cm^2]) (Eq. 1.3). In the case of the anodic process (oxidation), the current density is positive, and in the case of the cathodic process (reduction), the current density is negative [1], [2]. The electron-transfer reaction (reduction/oxidation), which is caused by the applied current and is proportional to the amount of electricity passed, is a Faradaic electrode process. The result of which is the Faradaic current (i_F [A]). The current that is not a result of electron transfer is non-Faradaic, i.e., capacitive current (i_C [A]), resulting from the double-layer charging (explained later). The total current is (Eq. 1.4) [1]:

$$I = I_F + I_C \tag{1.4}$$

The involved species (donor and acceptor) must have coherence between the energies of the electron orbitals, where the electron transfer takes place. In a metal electrode, this level is the highest filled orbital, i.e., the Fermi energy level (E_F), which is the electrochemical potential of the electrons in the electrode. In soluble species, the outer shell with valence electrons is the one that gives or receives electrons. Figure 1.1 presents the energy levels of a metal electrode and electrolyte for unsuccessful and successful reduction (Figure 1.1a) as well as successful oxidation (Figure 1.1b). For reduction to occur, there is a minimum energy that must be provided for electron transfer from the electrode (E_F of electrode > the lowest unoccupied molecular orbital (LUMO) of soluble species, Figure 1.1a), which corresponds to a sufficiently high, negative potential (in volts). On the other hand, for oxidation, there is a maximum energy that the LUMO of the electrode can have and still receives the electrons from the species in solution, corresponding to a sufficiently high, positive potential (in volts, Figure 1.1b) [1].

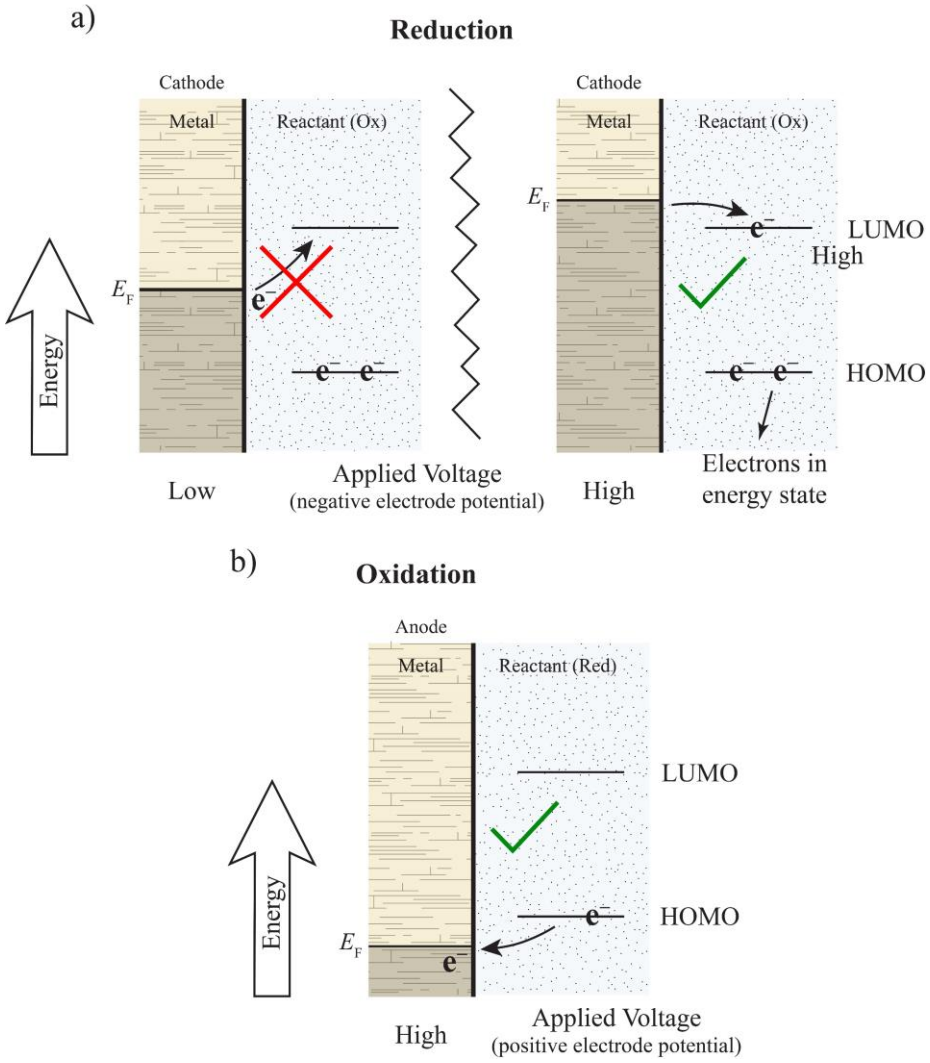

Figure 1.1: Schematic of a) unsuccessful and successful reactant reduction reaction; and b) successful reactant oxidation reaction (Adapted from [1]).

The electroactive species involved in electrochemical reactions can be organic or inorganic, neutral or charged, dissolved in solution, the solvent itself, a film on the electrode surface or the electrode material itself. Figure 1.2 illustrates a few types of electrode reduction (Figure 1.2a, b, f) and oxidation (Figure 1.2c, d, e) reactions [2].

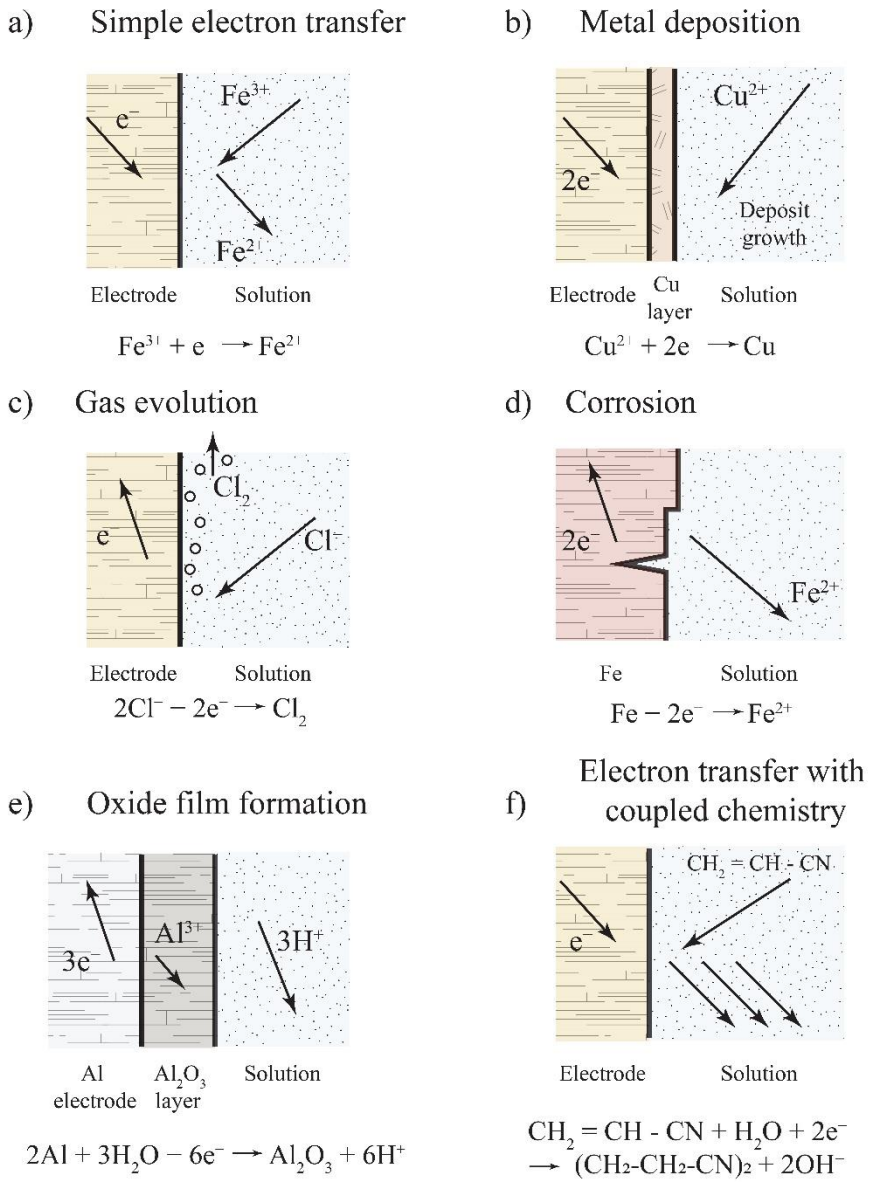

Figure 1.2: Schematic of various types of fundamental electrochemical reactions (Adapted from [2]).

1.1.1 Electrolysis

Electrolysis is a process where the output energy is used to drive the electrode reaction and convert chemical species, i.e., causing a chemical change. It takes place in an electrochemical cell made up of a cathode, an anode and an electrolyte. Electrode reactions (oxidation or reduction) are half-reactions. The extent of the reduction reaction at the cathode must be equal to that of the oxidation reaction at the anode. Conventionally, both half-reactions are expressed as reductions and are associated with a standard electrode potential (E^0 [V]), which is measured relative to the normal hydrogen electrode (NHE) [1], [2].

The electrical energy that comes from transforming a spontaneous chemical reaction into an electron movement is studied in a type of electrochemical cell called a galvanic cell. In the case of electrolysis, the energy needs to be supplied for the reaction to occur, i.e., the conversion of electrical energy into chemical energy. This happens in an electrolytic cell. The main difference between these two cells is the charge of the electrodes (Table 1.1).

Table 1.1: Difference between electrochemical cells [1].

Electrochemical cell	Anode	Cathode
Galvanic cell	-	+
Electrolytic cell	+	-

As the focus of this thesis is on electrolysis, the electrochemical cell will subsequently be referred to as the electrolytic cell. Electrochemical experiments are performed in two- or three-electrode systems immersed in an electrolyte (Figure 1.3). A two-electrode system is composed of a working electrode (WE) and a reference electrode (RE). The potential at the WE is monitored relative to the RE. Therefore, the potential of the RE must maintain a constant value. Due to the possibility of a current passing through the RE and causing a variation of its potential, the three-electrode system was developed. In the three-electrode system, a counter/auxiliary electrode (CE) is added. Figure 1.3a presents the cross-section of a three-electrode system with the potential profile of a solution between the WE and the CE. The WE potential is still monitored relative to the potential of the RE, but the current now passes through the WE and the CE. Therefore, only a negligible current passes through RE, causing almost no polarizability and thus it is a reliable electrode for potential control. The position of the RE should be as close as possible to the WE in order to minimise the solution's resistance. At the same time, the RE should not interfere with the mass transfer of the electrolyte species [1], [3]. The process of interest is happening on the surface of the WE. The CE is used to complete the electrical circuit. When one half-reaction (e.g., reduction) takes place on the WE, the opposite half-reaction (e.g., oxidation) takes place on the CE, as shown with the potential profile in Figure 1.3a. The CE should have a much larger area than the WE to ensure that the half-reaction at the CE is sufficiently fast, so it does not limit the process at the WE, and to minimize the polarization of the CE [1]. Figure 1.3b presents an electrochemical cell where a platinum mesh is used as the CE to ensure a larger surface area compared to the flat WE. The measured potential between the WE and the RE is smaller than the equilibrium potential (E_{eq} [V]) due to the product of the current i passing through the cell and the solution resistance (Rs), called the ohmic drop (iR). If the iR is smaller than 2 mV, a two-electrode system can be used. In the case of iR > 2 mV, the introduction of a CE and, therefore, a three-electrode system, is needed. The introduction of the CE decreases the amount of current passing between the WE and the RE, thus causing a lower iR. The iR can be additionally reduced by positioning the RE as close as possible to the WE [1], [4].

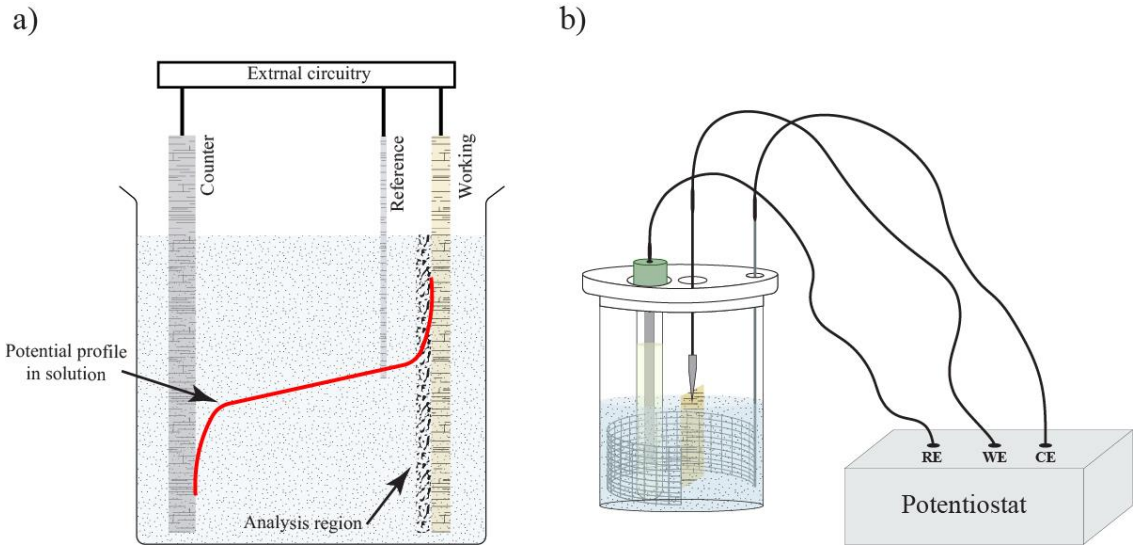

Figure 1.3: Schematic of: a) a three-electrode system with the potential profile and b) a three-electrode electrochemical cell connected to the power supply – potentiostat (RE: reference electrode, WE: working electrode, CE: counter electrode).

Electrode reactions occur at the interface between the bulk electrode and the solution called the electrolyte double-layer region. In the interfacial region, the value of the electrostatic potential (the potential caused by the charged species, ϕ) differs from that in the bulk solution. An electrical double layer is described by a model that refers to the molecules' interactions at the electrode surface. The most accurate model is a combination of several models developed over time. The Helmholtz model explains the double layer as a compact layer of oppositely charged ions to the electrode surface charge due to the applied potential. Later, the Gouy-Chapman model examined the influence of the applied potential and the electrolyte concentration on the double-layer capacity. The double-layer was presented not as a compact layer of ions next to the electrode, but as a diffuse layer where the ions are free to move. The Stern model combines both models and describes the electric double layer as a compact layer of ions next to the electrode surface followed by a diffuse layer extending into the bulk solution. Considering the specific adsorption (Grahame model), the electric double layer is divided into three parts. The inner Helmholtz plane (IHP) is the border that passes through the centre of the specifically adsorbed ions that lost their solvation. The next border is the outer Helmholtz plane (OHP) that passes through the centre of the solvated ions, non-specifically adsorbed ions. All the ions that pass the OHP are located in the diffuse layer. Figure 1.4 presents the distribution of ions and solvent molecules, forming an electric double layer according to the Gouy-Chapmn-Stern model [1].

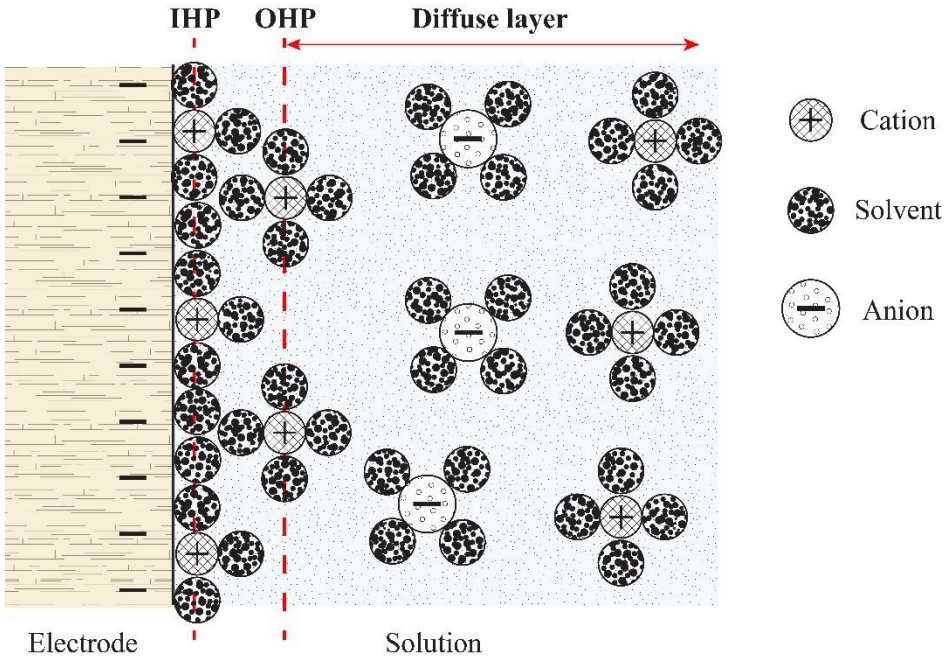

Figure 1.4: Schematic of Gouy-Chapman-Stern model for electric double layer, where IHP stands for the Inner Helmholtz plane and OHP for the Outer Helmholtz plane (Adapted from [1], [5]).

1.1.1.1 Transports in electrolysis

For a successful electrolysis, the electron transfer must occur at the electrode surface, and the ions must pass through the electrolyte in which the electrodes are immersed. The solvated ions move either by a diffusion or migration process, depending on the ion size and charge. Diffusion is the process of movement due to the concentration gradient, and migration is the movement due to the electric field effect (potential gradient). Diffusion is described by Fick's two laws. The first law (Eq. (1.5)) describes the flux of the species i (J_i [mol m^2 s^{-1}] of concentration c_i [mol L^{-1}] in direction x. The diffusion coefficient (D_i [m^2 s^{-1}]) is the proportionality factor between the flux and the concentration gradient ($\partial c_i/\partial x$) [1].

$$J_{\mathrm{i}} = -D_{\mathrm{i}} \frac{\partial c_i}{\partial x} \tag{1.5}$$

Fick's second law (Eq. (1.6)) describes the relationship between the flux of the species and the concentration of the substance as a function of time (t [s]) and position x [m] [1].

$$J_{\mathrm{i}} = -D_{\mathrm{i}} \frac{\partial c_{\mathrm{i}}(x,t)}{\partial x} \; ; \; \frac{\partial c_{\mathrm{i}}}{\partial t} = \mathrm{D}_{\mathrm{i}} \frac{\partial^2 c_{\mathrm{i}}}{\partial x^2} \tag{1.6}$$

In the presence of an electric field of strength $\boldsymbol{E}$ (electric field gradient = $\partial\phi/\partial x$ [V m^{-1}]), the flux of the species is given by Eq. (1.7):

$$J_{\mathrm{i}} = -D_{\mathrm{i}} \frac{\partial c_{\mathrm{i}}}{\partial x} - z_{\mathrm{i}} c_{\mathrm{i}} \frac{F}{RT} \boldsymbol{E} \tag{1.7}$$

where z is the ion charge. The second contribution to the flux is the migration and importance of the ion charge of the species. The movement of ions in a solution under the influence of an electric field results in the conductivity of the solution. For a high-intensity electric field, the conductivity increases with the field strength [1].

1.1.1.2 The mechanism of electron transfer at the electrode

When examining the electron transfer, we will consider the electrochemical reaction without a chemical transformation, an example being Eq. (1.8):

$$\mathrm{Fe}^{3+}\,(\mathrm{aq}) + \mathrm{e}^{-}\,(\mathrm{electrode}) \leftrightarrow \mathrm{Fe}^{2+}\,(\mathrm{aq}) \tag{1.8}$$

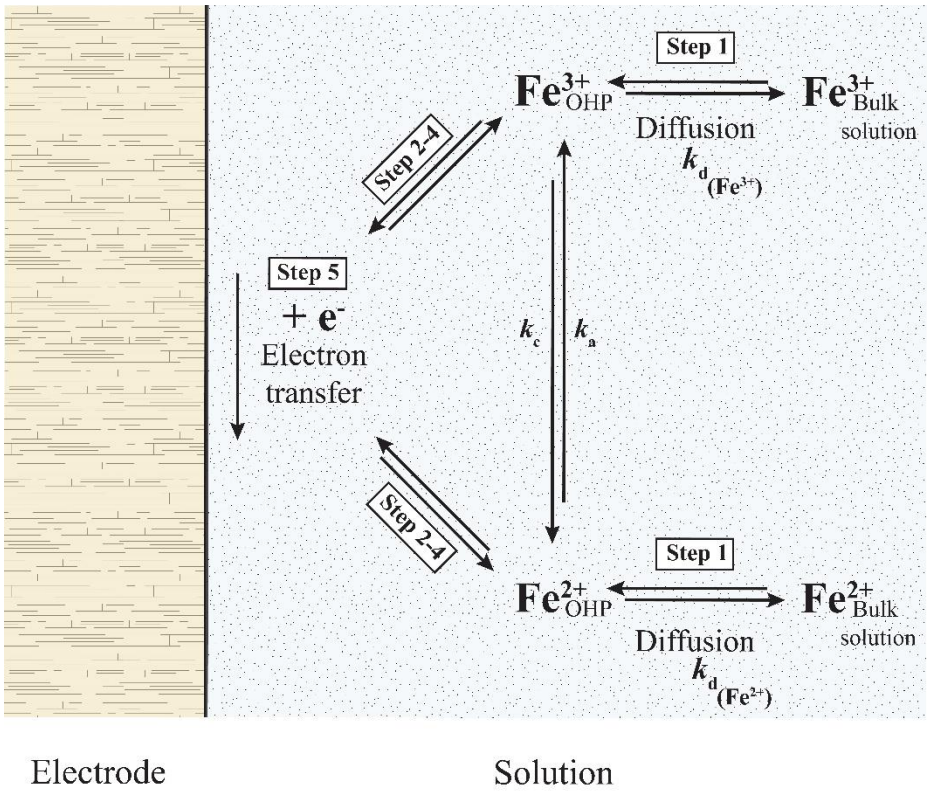

Figure 1.5: Scheme of electron transfer at an electrode (Adapted from [1], [3]).

The process of a simple electrochemical reaction involves several steps (Figure 1.5) [1]:

- Mass transport of reactant ions between diffuse layer and OHP near the electrode surface where the reaction occurs (Figure 1.5, Step 1);
- Rearrangement of Fe^{3+} ions (Figure 1.5, Step 2-4);
- Reorientation of the solvent dipoles at the OHP for specific adsorption at the electrode surface (Figure 1.5, Step 2-4);

- Changes in the distance between the centre of the Fe^{3+} ions and ligands from the surrounding (Figure 1.5, Step 2-4);
- Heterogeneous electron transfer between the conductive electrode and Fe^{3+} ions (Figure 1.5, Step 5).

During steps 2–4, the Fe^{3+} ions reach a pre-equilibrium state before the electron transfer. Meanwhile, during the electron transfer, the positions of the ions are frozen [1].

The electrochemical reaction rate (i.e., the speed at which an electrochemical reaction takes place; equations presented in the subchapter 1.1.1.4) is dependent on many factors (Figure 1.5): the mass transfer of the reactant towards the electrode surface described by the mass-transfer coefficient (k_d [cm s^{-1}]), the kinetics of electron transfer at the electrode, described by the charge transfer constant (k_a and k_c), preceding and ensuing reactions (e.g., migration of the products away from the electrode surface), and surface adsorption reactions. k_d describes the rate of diffusion within the diffusion layer, and k_a and k_c the charge-transfer rate constants for the oxidation and reduction processes, respectively. The slowest process determines the reaction rate. The first step is the mass transfer, which can be described by Fick's law of diffusion Eq. (1.5). Reactions at the electrode surface are limited by the transport of species from the bulk solution to the electrode. If all the species that reach the electrode surface are oxidised or reduced, the current will not increase further. In the case of there being no effects from migration, the current is limited to the diffusion process. The maximum current is thus called the diffusion-limited current. When species are transported via migration, the resulting current can be mass-transfer limited. The mass-transfer-limited current is correlated with the number of reacting electrons, the Faraday constant, the surface area, the mass-transfer coefficient, and the concentration of electrochemically active species converted at the electrode. In the ideal case, the concentration of reacted analyte is equal to the initial bulk concentration of the analyte. When all the processes correlated with the transport of reactive species are fast, the limiting factor becomes the electron transfer. Preceding the electron transfer, electroactive species can undergo a chemical reaction, influencing the reaction rate. When the electron transfer at the electrode occurs before reaching the chemical equilibrium, the slowest chemical reaction is the rate-determining step and has the most significant influence on the Faradaic current. Reactions such as adsorption, desorption, and crystallisation can change the electrode surface and, therefore, affect the electron-transfer kinetics of the electrode [1], [3].

1.1.1.3 Fundamental electrochemical equations

Knowledge of the fundamental laws (laws of thermodynamics, Fick's laws etc.) is essential for a description of the processes in electrochemistry and enables a derivation of the basic electrochemical equations. These are the Nernst, Cottrell, Randles-Ševčík, Butler-Volmer, and Tafel equations. Their use makes it possible to predict the potentials, electrode kinetics, electroactive species behaviour, changes on the electrode surface, etc. Thus, experiments and system behaviour can be predicted in advance. Used with the experimental data, fundamental equations help us to understand the system and to provide a theoretical explanation.

- Nernst equation
  When the electrode is placed in solution, it develops a surface charge. Under equilibrium conditions, the potential difference between the electrode and the solution is correlated with the electrode material and the concentration of the analyte in a solution. The Nernst equation gives the correlation between the equilibrium potential of a half-reaction to the standard electrode potential relative to the normal hydrogen electrode (Eq. (1.9)):

$$E = E^0 + \frac{RT}{nF} \ln \frac{[\mathrm{Ox}]}{[\mathrm{Red}]} \tag{1.9}$$

  where E and E^0 are the actual/equilibrium and standard potentials [V], R is the gas constant [8.314 J mol K^{-1}], T is the temperature [K], n is the number of reacting electrons, F is the Faraday constant at room temperature [96,485 C mol^{-1}], [Ox] and [Red] are concentrations of the oxidised and reduced species [$mol\ L^{-1}$]. This form of the equation is valid only for dilute solutions. In relatively concentrated solutions there are interionic interactions that do not occur in very dilute solutions because of the large interionic

distances. These interactions have influence on velocity of ion migration and consequently on ionic activity. The relation between activity and concentration is activity coefficient ($a = \gamma_c \cdot c$), which vary with concentration. Thus, in the case of concentrated solutions, the concentrations are replaced by their chemical activities (a_{Ox}/a_{Red}). The Nernst equation can be used to calculate the electrochemical cell potential (E_{cell} [V]), which is calculated from the electrode potential of both half-reactions ($E_{cell} = E_{cathode} - E_{anode}$). E_{cell} presents the maximum work/energy that the cell can supply [1], [5].

- Cottrell equation
The Cottrell equation describes the current changes in time and is valid for diffusion-controlled processes. Suppose we apply a potential step at time zero (t = 0 s) to an electrode in a solution containing electroactive species. In that case, the system moves from the non-reaction state to where all the electroactive species that reach the electrode react. The resulting diffusion current, therefore, varies with time. For a planar electrode, the current for the oxidation/reduction can be expressed using (Eq. (1.10)) [1], [3]:

$$I_{\mathrm{ox}} = nFAD\left(\frac{\partial c}{\partial x}\right)_0 \; ; \; I_{\mathrm{red}} = -nFAD\left(\frac{\partial c}{\partial x}\right)_0 \tag{1.10}$$

The solution of differential equation, combining Eq. (1.10) and Fick's second law (Eq. (1.6)), considering the boundary conditions: 1) t = 0; c_0 (at the electrode) = c_∞ (in bulk solution); 2) $t \geq 0$; lim(x → ∞) $c = c_\infty$; and 3) $t > 0$ and x = 0; c_0 = 0, gives the Cottrell equation (Eq. (1.11)) [1], [3]:

$$I(t) = I_{\mathrm{d}}(t) = \frac{nFAD^{1/2}c_\infty}{(\pi t)^{1/2}} \tag{1.11}$$

where π ("pi") is a mathematical constant approximately equal to 3.14159.

- Randles-Ševčík equation
Let us consider a simple electron-transfer reaction Eq. (1.8). The resulting Faradaic current depends on the electroactive species' kinetics and diffusion towards the electrode. As mentioned above, Fick's second law (Eq. (1.3)) needs to be solved to observe the concentration-time dependence in the diffusion-controlled process. As it represents a partial differential equation, the boundary conditions must be selected. The first three boundary conditions describe the behaviour of the species' concentrations at certain positions and time. The fourth one explains the change in the applied potential at a certain time by considering the scan rate. The last boundary condition expresses the kinetic regime of the electrode reaction, which Randles and Ševčík described first. The Randles-Ševčík equation (Eq. (1.12)) describes the dependence of the peak current (I_p [A], the maximum value of current) on the electrode properties (surface area, electron-transfer reaction, concentration of electroactive species), and experimental conditions (υ - scan rate [mV s^{-1}]) [1].

$$I_{\mathrm{p}} = 2.69 \cdot 10^5 n^{3/2} A D^{1/2} c \upsilon^{1/2} \tag{1.12}$$

The Randles-Ševčík equation can be used to study reaction mechanism, to determine either diffusion or absorption-controlled process. In the case of diffusion-controlled process, the experimental results will give linear relationship between I_p and $\upsilon^{1/2}$ which is one of the conditions for a reversible reaction. From the slope of a linear relationship between I_p and $\upsilon^{1/2}$, by knowing the number of electrons involved in a reaction and the diffusion coefficient of reacted species, the surface area involved in the electrochemical reaction can be determined [1].

- Butler-Volmer equation

The Butler-Volmer equation is a fundamental electrochemical equation for studying the electrode kinetics in a well-stirred cell. It is used to predict the currents resulting from the overpotential when there are no mass-transfer limitations (i.e., currents are not diffusion-controlled). Eq. (1.8) will be taken as an example of a simple electron-transfer reaction, where k_a stands for a charge-transfer-rate constant for oxidation at the electrode and k_c a charge-transfer-rate constant for reduction at the electrode (Figure 1.5). The resulting overall current of the reaction (I [A] = $I_c - I_a$) is the difference between the cathodic (reduction) current (I_c [A]) and the anodic (oxidation) current (I_a [A]). Each current can be separately described as a value proportional to their corresponding rate constant (Eq. (1.13)) [3]:

$$I_c = FAk_c[Fe^{3+}](0,t)\ ;\ I_a = FAk_a[Fe^{2+}](0,t) \tag{1.13}$$

where $[Fe^{3+}]$ and $[Fe^{2+}]$ are the concentrations of oxidised and reduced species [mol cm^{-3}] at a distance x [cm] from the electrode at time t [s]. In this case, the reaction at the electrode surface is considered, and therefore x = 0. Both rate constants can be expressed as a function of the standard heterogeneous rate constant k_0 [cm s^{-1}] and the applied potential (Eq. (1.14)) [3]:

$$k_c = k_0 e^{\frac{-\alpha F\eta}{RT}}\ ;\ k_a = k_0 e^{\frac{(1-\alpha)F\eta}{RT}} \tag{1.14}$$

where α is the transfer coefficient (dimensionless parameter with a value between 0 and 1), and η is the overpotential [V]. k_0 is a measure of the kinetic facility of a redox system. The larger the k_0 value, the shorter is the time scale needed for the system to reach equilibrium. By dividing the equations for rate constants by each other (Eq. (1.14)), the resulting equation (Eq. (1.15)) expresses the electrode kinetics not only in equilibrium cases, but in all cases [3].

$$\frac{k_a}{k_c} = e^{\frac{F\eta}{RT}} \tag{1.15}$$

Combining all the equations expressing the overall current and rate constants (Eq. (1.13 – 1.15)) gives the complete current-potential characteristic and represents the basis for the Butler-Volmer equation. In the equilibrium state, when the applied potential is the same as the equilibrium potential (η = 0), the overall current, i.e., the exchange current (i_0 [A]) is zero, as the cathodic current is balanced by equal and opposite anodic currents ($i_c = -i_a$). In this case, the exchange current can be written as (Eq. (1.16)) [3]:

$$I_0 = FAk_0[Fe^{3+}]^{*(1-\alpha)}[Fe^{2+}]^{*(\alpha)} \tag{1.16}$$

where $[Fe^{3+}]^*$ and $[Fe^{2+}]^*$ stand for the bulk concentration. By considering that the concentration of the bulk solution and the concentration at the electrode surface are equal (no mass-transfer limitations), the final Butler-Volmer equation (Eq. (1.17)) provides a correlation between the current and the difference between the rate of the reduction and oxidation reactions [3].

$$I = I_0\left[e^{-\alpha\frac{F\eta}{RT}} - e^{(1-\alpha)\frac{F\eta}{RT}}\right] \tag{1.17}$$

- Tafel equation

The exchange current (I_0) and transfer coefficient (α) used in the Butler-Volmer equation (Eq. (1.17)) can be calculated from the slopes and the intercept at the equilibrium potential (E_{qe}) in the Tafel plots (Figure 1.6). A Tafel plot is a graph presenting the relationship between $\log|I|$ and η. The plot has an anodic branch for positive overpotentials (oxidation) and a cathodic branch for negative overpotentials (reduction). If the overpotentials are small (η < 50 mV), the slope increases due to the larger contribution of the backward reaction and changing the relative concentration at

the electrode surface. In this case, the current flows in both directions (positive and negative) and the system is reversible. If the overpotentials are very large (η > few hundred mV), the mass-transfer limitations influence the deviation of the line from the prediction of the Tafel equation. Such a system is irreversible. The Tafel equation (Eq. (1.18)) describes the correlation between the overpotential and the current [3].

$$\eta = \frac{RT}{\alpha F}\ln(I_0) - \frac{RT}{\alpha F}\log(I) \tag{1.18}$$

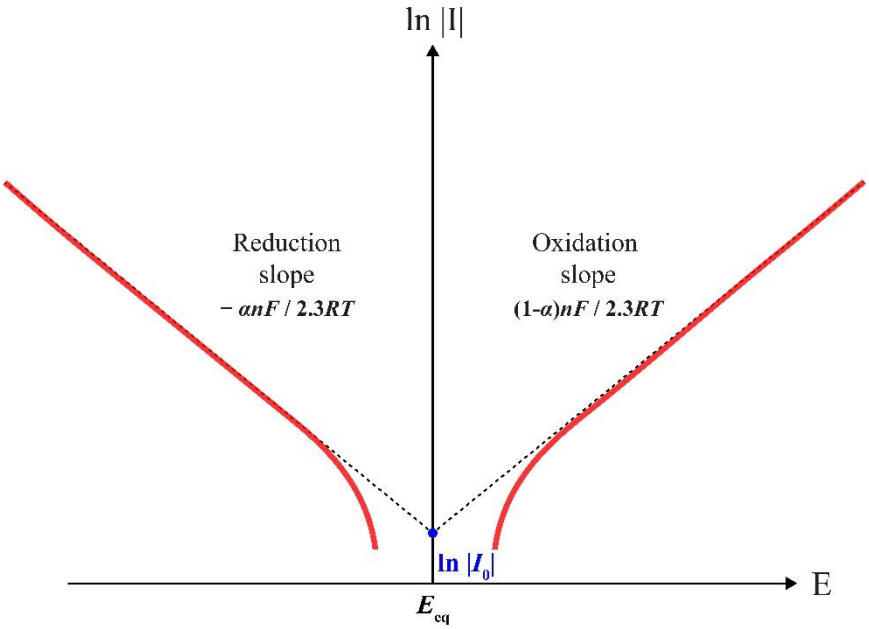

Figure 1.6: Tafel plot (Adapted from [1]).

1.1.1.4 Reversibility of electrochemical system

The electrode reaction is reversible if it follows the conditions of thermodynamic reversibility. The reversibility of an electrode reaction is correlated with the mass transport of species from the bulk solution and the kinetics of the electrode reaction. The mass transport is expressed by the mass-transfer coefficient k_d and the electrode reaction kinetics by a standard rate constant k_0. The electrochemical reaction is reversible if the kinetics of the electrode reaction is faster than the kinetics of mass transport ($k_0 >> k_d$). In the case of the opposite conditions ($k_0 << k_d$), the reaction cannot be reversible, i.e., it is irreversible due to the too high kinetic barrier to be overcome by the addition of extra potential, called the overpotential (η [V]). The overpotential ($\eta = E - E_{eq}$) is the potential difference that needs to be added to the equilibrium potential (E_{eq} [V]) for the reaction to occur. If the overpotential is relatively small so that its addition can reverse the reaction, the reaction is quasi-reversible [1], [3].

1.1.2 Studying electrode reactions

Electrochemical reactions are experimentally studied via electrochemical techniques. They make it possible to monitor the current as a function of potential (controlled/constant potential, i.e., potentiostatic mode) or the potential as a function of the current (controlled/constant current, i.e., galvanostatic mode) (Figure 1.7) to obtain information about the nature of a reaction, its course and kinetics. The classical methods are divided into the potential sweep methods, the pulse techniques, the impedance methods, and the static methods. Linear sweep voltammetry (LSV) and cyclic voltammetry (CV) are the most common methods for studying electrode processes. They enable a rapid identification of redox potentials that are specific to the electro-active species under investigation and give information about the thermodynamics of the redox process, the kinetics of heterogeneous electron-transfer reactions and the analysis of coupled electrochemical reactions [1], [3].

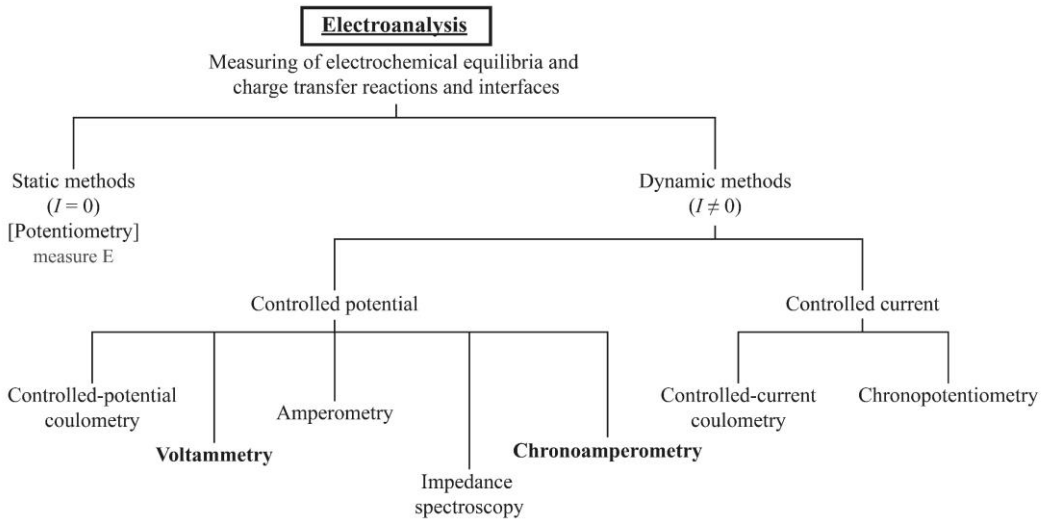

Figure 1.7: Family tree of electrochemical techniques.

1.1.2.1 Linear sweep and cyclic voltammetry

LSV and CV are voltammetric methods that apply a continuously linearly time-varying potential to the WE. The resulting current reveals the oxidation or reduction reactions of the electroactive species in solution (Faradaic current), the adsorption of species according to the potential, and double-layer charging (capacitive current). The sweep rate of the potential, i.e., the scan rate (υ [mV s^{-1}]) is defined as $|dE/dt|$ (slope of curve $E(t)$, Figure 1.8). In LSV, the potential scan starts at the initial potential (E_i [V]) and ends at the stopping potential (E_f [V]) (Figure 1.8, red line). The scan direction can be positive (observing an oxidation reaction) or negative (observing a reduction reaction). In CV, the scan starts at E_i and proceeds towards $E_{max,}$ and after reaching it, the potential direction is inverted until E_{min}. After completing the cycle, the experiment stops at E_f (Figure 1.8, blue line). This presents one cycle of the cyclic voltammogram. In the case of studying film formation, multiple cycles can be recorded. The initial step before performing voltammetry is choosing the waveform parameter (E_i, E_{max}, E_{min}, E_f), since they determine the sweep direction [1], [3].

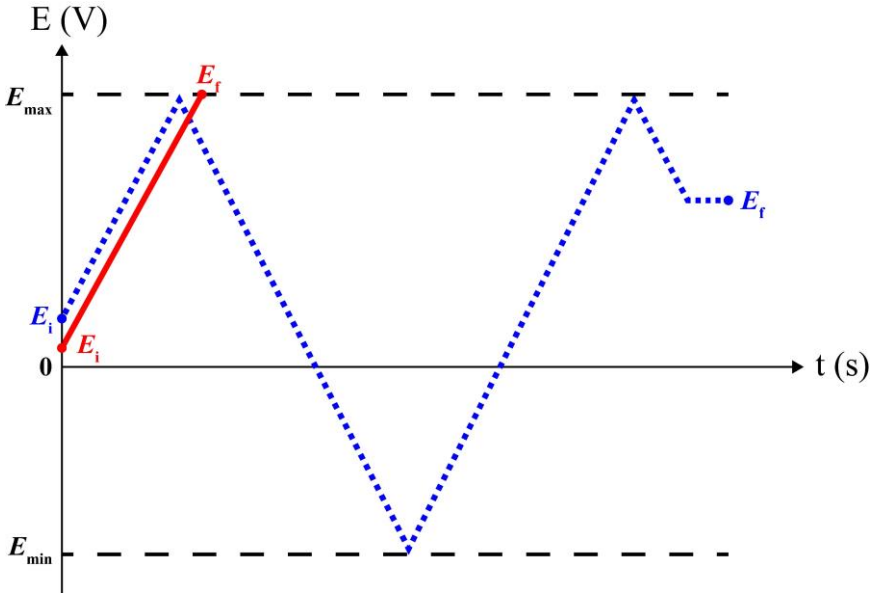

Figure 1.8: Variation of applied potential with time in linear sweep voltammetry (red) and cyclic voltammetry (dotted blue) (Adapted from [1]).

The output of voltammetric methods are current-voltage (*I* vs *E*) curves that reveal the reaction mechanism's characteristics and kinetic conditions. The LSV presents the potential scan in one direction (positive or negative), while the CV potential scan goes in both directions. Graphically, the cyclic voltammogram (Figure 1.9a) combines positive (A-C) and negative (C-E) scans of LSV. Considering a simple electrochemical reaction Eq. (1.1), a peak in the current-voltage curve represents an equilibrium between Red and Ox, and is described by the Nernst equation (Eq. (1.9)). The Nernst equation predicts the system's behaviour due to the concentration or potential change [1], [6]. In a diffusion-limited system (no stirring) containing Red, the oxidation is performed by scanning towards positive potentials (A-C). The oxidation of R results in an oxidation-current rise (positive current) and achieves the maximum value of the current, the oxidation peak current (I_p^{ox}, B) at the oxidation peak potential (E_p^{ox}). Later, the current decreases due to the lack of reactant Red supply just before the peak current. When the switching potential (C) is reached, the scan direction is reversed to a negative direction (C-E). While the concentration of Red at the electrode was consumed, the Ox concentration increased according to the Nernst equation. Applying a negative potential causes a reduction of Ox, resulting in an increase in the reduction currents (negative currents). The current rises until reaching the maximum value, the reduction peak current (I_p^{red}, D) at the reduction peak potential (E_p^{red}). Due to the consumption of Red, the oxidation current decreases until all Red was reacted [1], [6].

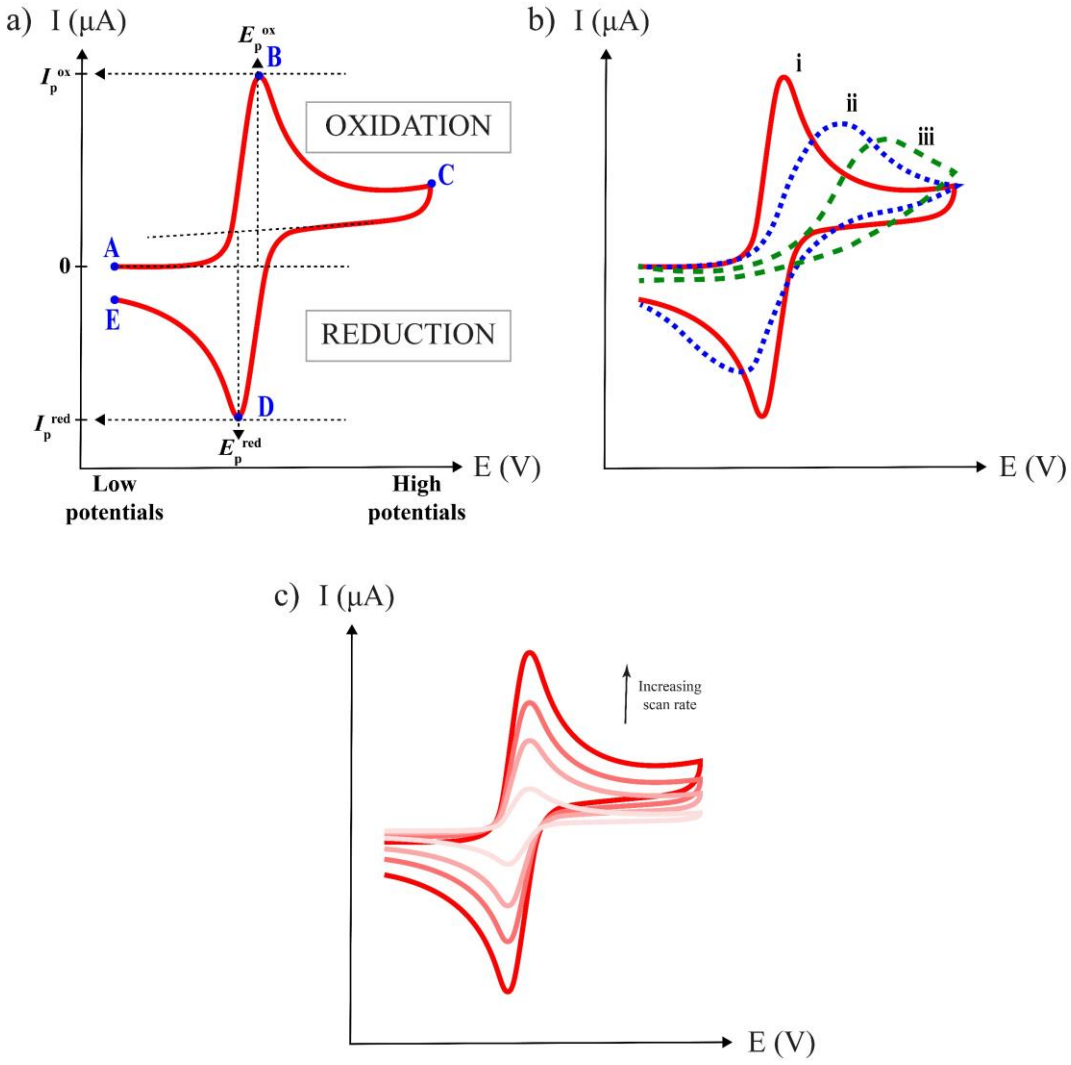

Figure 1.9: a) Cycling voltammograms (IUPAC Convention): a) presenting the peak positions and pea height; b) for (i) reversible, (ii) quasi-reversible, and (iii) irreversible electron reactions; and c) the effect of scan rate on current (Adapted from [1], [6]).

The shape of the cyclic voltammogram reflects the kinetics of the electrochemical process under observation, defined by the electrode reaction rate and the mass transport. The reaction is chemically reversible if the analyte is stable upon reduction and can be subsequently re-oxidized. Electrochemical reversibility relates the electron-transfer kinetics to the height of the electron-transfer barrier. If the barrier is sufficiently low, the Nernst equilibrium is immediately established upon any applied potential change. An electrochemically reversible reaction has a comparable or higher rate constant of electron transfer than the mass transport. The difference between the oxidation and reduction peak potentials (i.e., peak-to-peak separation ΔE_p) of the reversible system is 57 mV at 25 °C ($2.22RT/F$, Figure 1.9b (i)). When the mass-transfer coefficient (k_d, defined in Chapter. 1.1.1.2) increases, the peaks broaden, and the peak separation increases due to the higher electron transfer barrier, i.e., a greater overpotential is needed for the same electron transfer (quasi-reversible system, Figure 1.9b (ii)). The faster the mass transport, the less pronounced the reverse peak until it disappears in the case of an irreversible system (Figure 1.9b (iii)) [4], [6].

The scan rate (ν, [mV s^{-1}]) defined as $|dE/dt|$ controls the potential scan speed and influences the shape of the current-voltage curves. The faster the scan rate, the higher the currents that are observed due to the decrease in the size of the diffusion layer (Figure 1.9c). If the scan rate is slow, the diffusion layer starts to grow much further from the electrode, resulting in a slower flux of the solution species towards the electrode surface. For a reversible diffusion-controlled reaction, the current changes linearly with the square root of the scan rate, described with the Randles-Ševčík equation (Eq. (1.12)) [1], [6].

1.1.2.2 Chronoamperometry

Chronoamperometry (CA) is an amperometric method for studying the variation in the current response with time (current-time behaviour) under an applied potential (i.e., potentiostatic control). CA is performed by applying a potential step to a WE exposed to an analyte solution (Figure 1.10a). Considering a solution containing only Ox at a concentration of c_0. At E_i no electrochemical reaction occurs at the WE. After applying a potential step to E_f, almost all of the Ox located at the electrode surface is reduced to Red according to the Eq. (1.1) and any additional Ox that diffused towards the electrode is immediately reacted, and thus the Ox concentration at the electrode surface is zero (Figure 1.10b). The changes in current (Figure 1.10c) appear due to the diffusion of Ox towards the electrode surface and changes in the diffuse layer. The CA experiments can be performed as a single potential step (only forward potential) or a double potential step. In the case of a double step, the returning potential is applied after a given period of time. The concentration gradient and diffusion are theoretically described with Fick's second law (Eq. (1.6)), which with the appropriate boundary conditions gives the Cottrell equation (Eq. (1.11)) and expresses the current obtained at each point in time [3], [5].

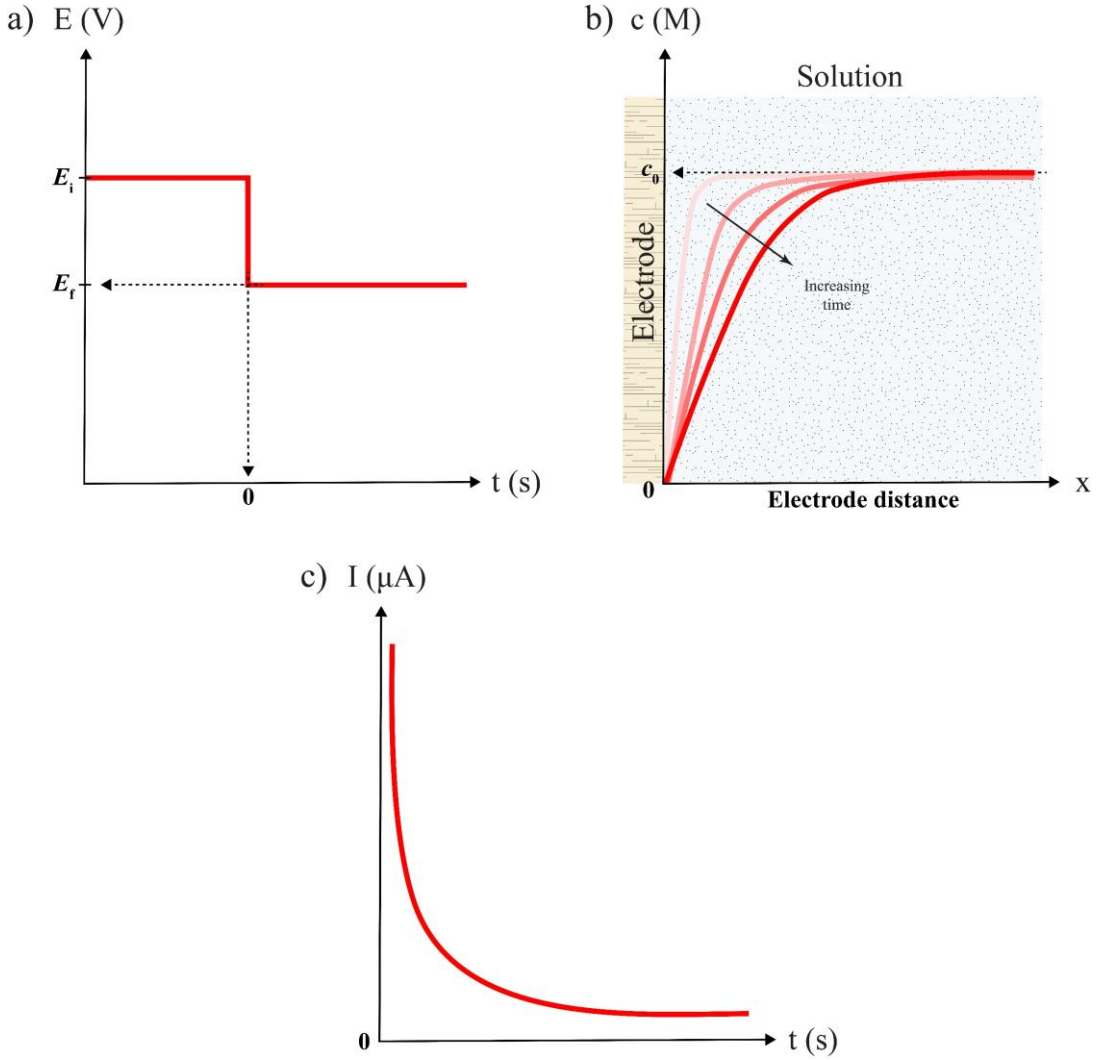

Figure 1.10: Chronoamperometry experiment to a planar electrode: a) potential-time waveform; b) change of concentration gradient; and c) current-time response (Adopted from [3], [5]).

1.2 Application of Electrochemistry

Understanding electrochemical reactions can help us to tailor electrode reactions (enhancing the desired or inhibiting the unwanted electrode reactions, cleaning electrodes, developing new electrode materials), study complex systems and measure the concentrations of electroactive species [1]. The voltammetric and amperometric methods are the most frequently used techniques within the field of electrochemistry. They are applied in industrial electrolysis, electroplating, batteries, fuel cells, electrochemical machining, and for sensing analytes we encounter in quality management, environmental control, forensics, biomedical and food applications etc. [1], [7].

1.2.1 Spectro-electrochemistry

Electrochemistry provides thermodynamic and kinetic information about the electron-transfer process. By itself, it is not sufficient for a clear identification of the electroactive species, as molecular identity is typically inferred from the measured physical properties of a known standard system. To identify the reaction intermediates, monitor the concentration profile of the reacting species, and study the surface properties, spectroscopic techniques (e.g., infrared spectroscopy, nuclear magnetic resonance, ultraviolet-visible spectroscopy – UV-Vis) are applied *in situ* in an electrochemical cell. Such a combination can provide spectroscopic molecular

information for species under potential/current control, such as vibration frequencies, molar absorptivities, luminescence intensities, and electronic and magnetic resonance frequencies. Conventional spectro-electrochemistry is a correlative study of the bulk electrolysis of an analyte in a small electrochemical cell combined *in situ* with a spectroscopic technique. It makes possible quantitative measurements that are useful for a structural characterization of the redox state of the intermediate. The technique itself is experimentally demanding, as the experimental cell must be designed according to the spectroscopic technique. At the same time, it must have appropriate geometrical arrangements to avoid basic electrochemical problems such as iR drop and low current densities. The most frequently used spectro-electrochemistry is the combination of electronic spectroscopy and electrochemistry (electronic spectro-electrochemistry). It has a straightforward usage and capability to obtain quantitative and qualitative information about the electrochemical process. Electrochemistry addresses the electron transfer of an electroactive analyte resulting in a change in electronic states. Such transitions occur in the ultra-violet or visible regions (UV-Vis, 190–700 nm) and sometimes also in the near-infrared region (NIR, 700–3000 nm). The redox processes are frequently investigated either with transmittance or reflectance spectroscopy. Transmittance spectroscopy is the most facile and straightforward for investigating solution-phase analytes using an optically transparent WE. Meanwhile, reflectance spectroscopy is used to study thin films, solid deposits, or self-assembled mono- and multilayers. Electronic spectroscopy is helpful when investigating the electronic changes caused by a redox process [2], [4].

1.2.2 Electrochemical sensors

Sensors are devices that translate physical, chemical, or biological information into a signal. They give qualitative and quantitative information regarding the existence of ions or molecules (analytes) with sensitivity and specificity on a molecular scale. In general, sensors operate following three basics steps [8], [9]. Figure 1.11 presents the operating steps for the example of an electrochemical sensor.

- Capture and recognition (Figure 1.11a): The most important step is to prepare effective receptor material suitable for the specific detection of a target analyte. The binding of molecules into the recognition element triggers the sensing effect, physical (e.g., absorbance, refractive index, conductivity, temperature or mass change), chemical (e.g., chemical reaction with the participation of the analyte) or biochemical (biochemical processes) changes. The material should allow a sensing effect with only the target analyte (selectivity), a high response towards a small number of target molecules (high sensitivity) and at the same time have the ability to detect a larger number of molecules without saturation (wide detection range);
- Transduction (Figure 1.11b): The changes in the material's physical or chemical properties are converted into a measured signal. According to the operating principle, chemical sensors may be classified as optical (converting light-based properties), electrochemical (converting the result of an electrochemical reaction between the analyte and the electrode), electrical (converting changes in physical parameters), mass-sensitive (converting a mass change at a specifically modified surface), magnetic (converting the changes in magnetic field magnitude and variations) or thermal sensors (converting the measuring temperature). The transducer’s characteristics should include high sensitivity, good resolution and a large dynamic range (the concentration range between the minimum concentration, of which the response can be distinguished from the noise, and maximum concentration before saturation);
- Measurement and analysis (Figure 1.11c): the signal from the transducer is measured, recorded and converted into information on the quantity of molecular activity.

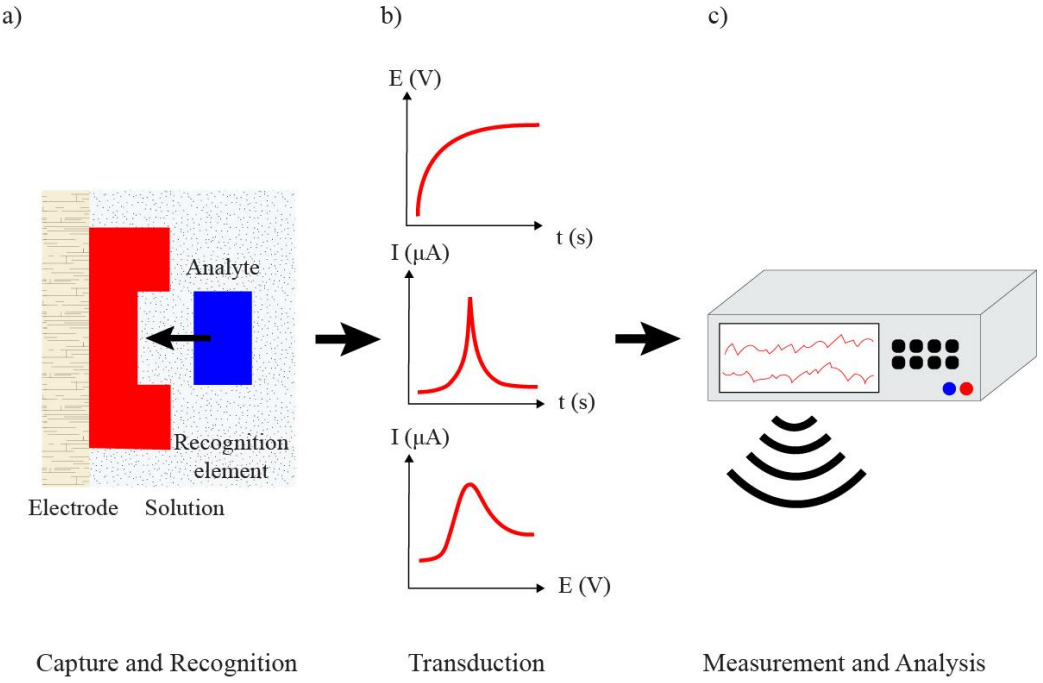

Figure 1.11: Basic steps for a sensor, presented on the example of an electrochemical sensor: a) capture and recognition; b) transduction and c) measurement and analysis (Adapted from [8]).

Electrochemical sensors (Figure 1.11) are devices that transform the effect of electrochemical events (electron-transfer reactions) into the electric signal of a voltage or current that can be directly connected to the analyte concentration. The electrochemical sensors can be divided in terms of working principle [1], [9]:

- Potentiometric: where the potential of the WE is measured against the RE. Measurements are carried out under equilibrium conditions where the sum of the partial anodic and cathodic currents resulting from electrochemical activities at the electrode is equal to zero. Ion-selective electrodes are the best example of a potentiometric sensor.
- Voltammetric or amperometric: where a current is measured as a function of an applied potential sweep or step. An amperometric sensor measures current at fixed potential (fixed-potential voltammetric sensor).
- Conductometric: where a change in conductivity during a reaction is measured
- Impedimetric: where an impedance or its components such as the resistance and capacitance of an electrode material are measured using an applied alternating voltage.

Electrochemical sensors represent an important area of modern analytical chemistry. Their major advantages are sensitivity and inherent selectivity using a simple fabrication process, high reproducibility, a linear profile of response vs concentration, low power requirement, and cost-effectiveness for routine analysis. They have great practical utility as on-site monitoring and point-of-care measurements [9], [10]. The opposite of an electrochemical sensor is an electrical sensor, where the output signal is an electrical property.

1.3 Screen-Printed Electrodes

Electrochemical techniques are more affordable than complex analytical laboratory techniques (e.g., ultraviolet-visible spectroscopy, x-ray spectroscopy, mass spectrometer, microscopic techniques, chromatographic methods, etc.). They can provide sensitive and complex results with less equipment in a shorter time. Thus, they have a great potential in applicable science. In the field of biomedical, pharmaceutical, industrial, and environmental analyses, *in-situ* and point-of-care (POC) measurements/testing are needed. The main equipment for electrochemical experiments is the power supply, a potentiostat/galvanostat, an

electrochemical cell composed of a minimum of two electrode, and a computer to analyse the data. For the transition of the laboratory into the field, battery-powered portable potentiostat/galvanostat with wireless connection to a smart device and screen-printed electrodes (SPEs) as an electrochemical sensing platform can be used for miniaturisation [7], [10].

The analytical performance of electrochemical experiments is fundamentally linked to the assembly of an electrochemical cell or electrochemical sensing platform, e.g., electrodes material and electrode positions. The SPEs are low-cost and straightforward design electrode platforms composed of conductive paste or ink deposited on various substrates. SPEs are manufactured using industrial printers to position ink on a substrate (Figure 1.12). Their production offers diversity in terms of electrode design (size and positions of electrodes) and the choice of material and enables mass production [7], [11]. SPEs consist of a chemically inert insulating substrate, which can be flexible (plastic-based material) or firm (ceramics, glass), on which two or more electrodes are printed. The basic electrodes are WE (wide range of inks), CE (the most used gold, platinum, carbon) and RE (Ag, Ag/AgCl). The most used inks for WE are carbon or modifications of carbon (e.g., graphene, graphite, carbon nanotubes, and fullerene), gold and platinum. SPEs can be produced with one WE or the whole array of WEs, which can be further modified with a variety of nanostructures or biological components (e.g., enzymes and antibodies) for enhancing the electrical response (i.e., sensitivity) and the detection of specific compounds (i.e., selectivity). In addition, SPEs can be produced on a transparent substrate with a thin enough layer of ink that transmits light, suitable for electro- and/or optical devices [10]–[13]. Therefore, SPE devices are in widespread use in analytical chemistry.

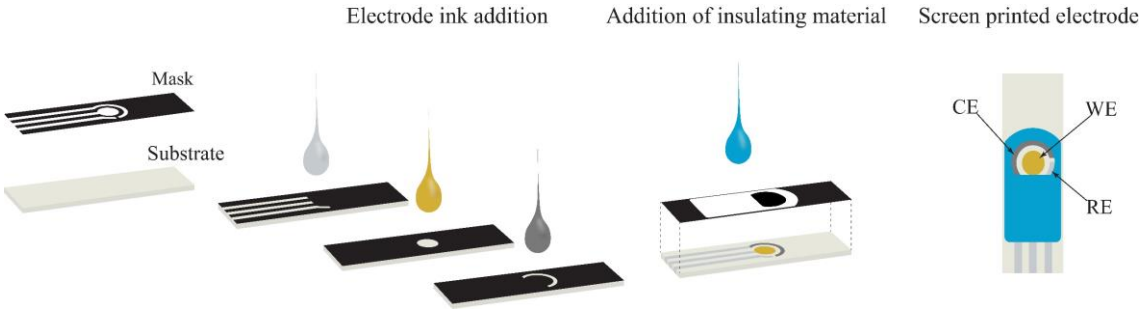

Figure 1.12: Schematic of the production of the screen-printed electrode (Adapted from [7]).

Electrochemical techniques in combination with SPEs are an efficient combination that can be used for constructing low-cost, robust, and fast-response sensing devices. Their use enables small sample volumes analysis, faster analysis times, *in-situ* analyses, automation procedures, and increased reliability and repeatability [7], [11]. SPEs can serve as reusable or single-use disposable devices, especially in the case of biosensing [13].

1.4 Conducting Polymers

Conducting polymers (CPs) were discovered in 1976 by studying the semiconducting properties of trans-polyacetylene (PA) [14], [15]. It was observed that exposing PA to halogen vapours caused the formation of charge-transfer complexes that increased the polymer conductivity at room temperature. Introducing so-called dopants caused metal-insulator transitions. The discovery and applicability of conductive polymers awarded A. J. Heeger [16], A. G. MacDiarmid [17], and H. Shirakawa with the Nobel Prize in Chemistry in 2000 [18] and triggered a great interest in studying CPs for a variety of applications.

CPs are conjugated polymers with one unpaired electron (the π-electron) per carbon atom. Carbon orbitals are in the sp^2p_z configuration with overlapping orbitals, leading to electron delocalisation. The π-electron transfer tends to delocalise the electronic wavefunctions, which is the main reason for charge mobility along the polymeric chain, and it is limited by disorder (tendency towards localised wavefunctions) and by Coulomb interaction (binding of moving electrons to a nearby repeat unit, leaving a positive charge, i.e., a hole) [16].

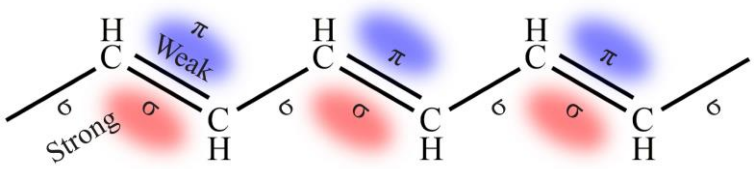

Figure 1.13: Chemical structure of PA. The backbone of conjugated double bonds (Adopted from [19]).

The electronic structure in CPs is determined by the chain symmetry, providing semiconducting or even metallic properties [16]. PA is the simplest member of CPs with a linear conjugated single-chain structure. Each carbon is σ bonded to a hydrogen atom and π bonded to a neighbouring carbon atom, having sp^2 hybridisation (Figure 1.13) [14], [16]. The conjugated π bonds allow the delocalisation of electrons into a band [14], [16], while σ bonds are responsible for holding the polymer together [20]. The PA structure is presented as a $(\text{-CH=CH})_n$ repeating unit and has a π-band divided into π- and π^*-bands, where the π-band is filled and the π^*-band is empty of electrons. The energy difference between π- (the highest occupied molecular orbital – HOMO level, i.e., the valance band in semiconductor terminology) and π^*-band (the lowest unoccupied molecular orbital – LUMO level, i.e., conduction band) is the π- π^* energy band gap, E_g. The bond-alternated structure of PA is characteristic of conjugated polymers. The members of the CP family are presented in Figure 1.14, all of them with conjugated double bonds in the form of an aromatic ring, with the exception of PA. The E_g of CPs depends on the molecular structure of the repeated units [16].

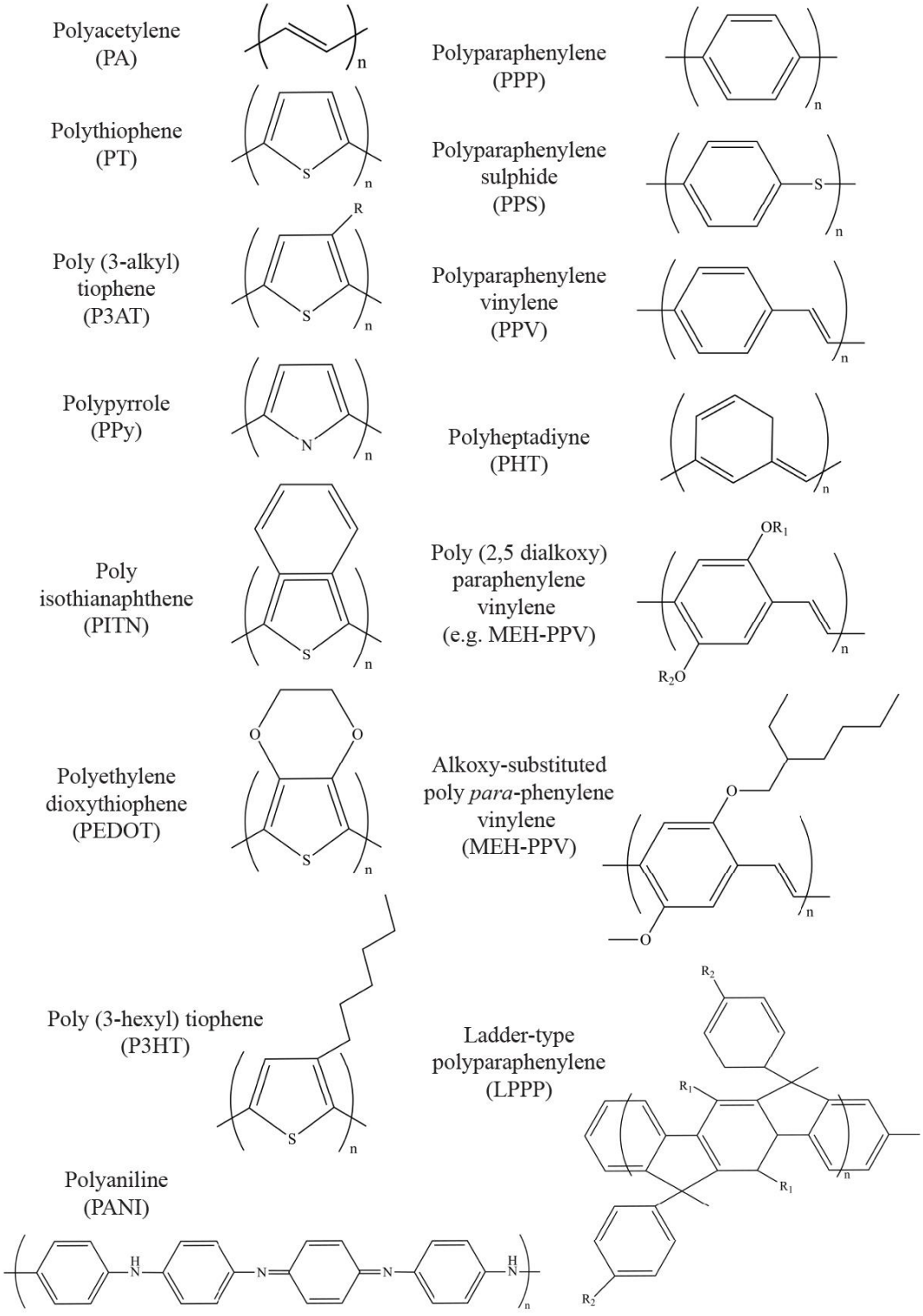

Figure 1.14: Molecular structure of a few CPs with characteristic bond-alternated structure (Adopted from [16]).

1.4.1 The conductivity of conducting polymers

CPs have an E_g larger than 1.5 eV, which categorises them as insulators. The electrical conductivity of CPs can be tailored from insulator to metal by reversible "doping", which causes the formation of unfilled electronic bands between the valance and conduction bands [16], [20]. "Doping" is a charge-injection process into conjugated, insulating/semiconducting

macromolecular chains. It can be performed chemically, electrochemically, photochemically, or by charge injection at the metal-polymer interface and causes the formation of charge carriers. The ability of charge carriers to move along a π-bonded structure results in electrical conductivity [16]. During the doping process, a neutral polymer is converted into an ionic complex of polymeric cation/anion and a counter-ion [20]. All the above-mentioned types of doping are redox doping (number of electrons change during the process), with the presence of counter dopant ion in the case of chemical and electrochemical doping, and its absence in the case of photo- and charge-injection doping [17].

Chemical and electrochemical "doping" are the most used type of doping and result in permanent electrical conductivity until the charge carriers are chemically compensated or removed by "undoping". An acid-based reaction and redox reaction cause the movement of the electrochemical potential (the Fermi level) into an energy region with a high density of electronic states. The neutrality of such a system is maintained by introducing counter-ions [16]. Counter-ions can bind to the polymer either by ionic interaction or ring-attachment to a polymer backbone. For example, Yue et al. [21] showed with an X-ray photoelectron spectroscopy (XPS) study that the ring-attachment of a $-SO_3^-$ counter ion to PANI backbone phenyl groups. Meanwhile, no covalent bond was found for the Cl^- counter-ion, meaning it is associated with PANI in ionic form (ionically bonded to positively charged nitrogen). Metallic polymers are categorised as salts [16].

Chemical doping is a straightforward procedure usually difficult to control. It can often result in inhomogeneous doping, which can be solved via electrochemical doping. In electrochemical doping, the electrode supplies the redox charge, and the electrolyte supplies the ion for neutrality. Electrochemical doping makes it possible to achieve doping at any level by controlling the voltage between the CP and the CE [16]. Doping involves the addition (reduction) or removal (oxidation) of electrons to or from the π-system [17]. Thus, CPs can be doped by n-type or p-type [16], [19]. p-Doping is the partial oxidation of the π-system by exposing the polymer to an oxidising agent (e.g., iodine) or immersing it in an electrolyte and connecting to a positive DC power source. Due to oxidation, electrons in the π-bond are removed from the valence band of the polymer to the dopant and create a hole in the polymer chain. Conversely, n-doping is a partial reduction of the polymer π-system by treating it with a reducing agent (e.g., sodium naphthalene, $C_{10}H_8Na$) or by performing cathodic reduction with an electrolyte and negative DC power source. Thus, electrons are transferred from the dopant to the conduction band of the polymer, resulting in an increased electron density. In all chemical and electrochemical p-/n-doping, counter-ions are introduced to the system to stabilise the charge on the polymer backbone. Generally, p-doping is more popular than n-doping due to the higher stability of the positively charged carriers [17], [19], [20].

CPs can also be doped by a non-redox type of doping, where the number of electrons associated with the polymer does not change during the process, yet the energy levels are rearranged. An example of non-redox doping is the protonation of polyaniline (PANI), where a stable polysemiquinone radical can be obtained by treating the emeraldine base with aqueous protonic acid to produce a protonated emeraldine salt [17]. All types of doping with advantages and disadvantages are summarised in Table 1.2.

Table 1.2: Different types of doping CPs (Taken from [19]).

Type of doping	Controlled variables	Advantages	Disadvantages
Chemical doping	• Vapour pressure • Exposure time	• Simple procedure (exposing to vapour or immersing into solution) • Low cost	• Slow procedure to avoid inhomogeneous doping • Unstable doping levels with respect to time • Electrical conductivity decay due to the structural distortion • Low reversibility

Electrochemical doping	Amount of current passed	• Easily controlled doping level • High reversibility • Various dopants • Low cost	Electrical conductivity decays due to the structural distortion
Photo doping	Radiation energy of light beam	• Charge carrier formed without chemical compound • No distortion of the material structure • No counter-ions	Loss in the electrical conductivity when irradiation is discontinued
Charge-injection doping	Potential applied to the polymer structure	• No counter-ions • Minimised distortion	Strong coulombic interactions between charge and dopant (change in the energetics)
Non-redox doping	Protonic acid strength	No change in the number of electrons	Low conductivities for some CPs

Doping causes the self-localisation of injected charges, associated with the formation of solitons, polarons, and bi-polarons (nonlinear excitations). Therefore, it leads to structural relaxation (distortion) and the formation of electronic states in the energy gap [16], [22]. The injected charge moves along the conjugated chains with interchain hopping, a necessary secondary and rate-determining step, to produce the conductivity [20], [22].

Organic polymers have usually different equilibrium geometries in the ionised state than in the ground state (e.g., a transformation from benzene to quinoid). To adopt the equilibrium geometry of the ionised state, these molecules were first distorted in the ground state, which leads to an upward shift of the valance band (π-band) and a downward shift of the conduction band (π*-band) for the same portion. In the presence of a charge in the polymeric chain, it is energetically favourable to localise it by distortion/relaxation of the lattice, which causes the formation of nonlinear excitations, e.g., polarons [20]. Removing a charge from the quinoid structure is more favourable than from an aromatic structure, i.e., a benzenoid, due to the lower ionisation potential and higher electron affinity [1], [19], [22].

Systems with different equilibrium geometries in the ionised state than in the ground state, i.e., two possible bond alternation patterns with different energies in the ground state (e.g., aromatic and quinoid-like geometric structures), are non-degenerated systems (e.g., polythiophene, Figure 1.15a). The injection of charge causes a stable nonlinear excitation and charge storage in the form of polarons and bi-polarons. Removal of the first electron from the polymer chain causes the formation of localised structural distortions in the form of polarons. A polaron (positively or negatively charged) is a radical cation/anion, a quasiparticle with a single occupation and is associated with a local geometrical relaxation of the bond lengths (lattice distortion) and the presence of localised electronic states in the gap (Figure 1.15b). Its formation retains a full valance band and an empty conduction band. The second electron can be removed from the polymeric chain, causing the formation of two polarons, or from a polaron causing the formation of a bi-polaron. A bi-polaron is a pair of like charges. A positive/negative bipolaron is a spinless dication/dianion with an enhanced geometrical relaxation of the bond lengths (Figure 1.15b, c). At high doping levels, the bipolaron states overlap, causing the formation of bipolaron bands. The origin of bipolaron states is from the valence and conduction edges, thus, the bandgap at high doping levels becomes wider (Figure 1.15b). Bipolaron formation causes a larger decrease in the ionisation energy than two polarons. Thus, it is thermodynamically more stable. Due to the stronger lattice relaxation around two charges than around one, the electronic states appearing in the gap for a bipolaron are further away from the band edges than for the polaron (e.g., the polaron binding energy for polypyrrole (PPy) is 0.12 eV, and for a bipolaron it is 0.45 eV) [16], [19], [20], [22].

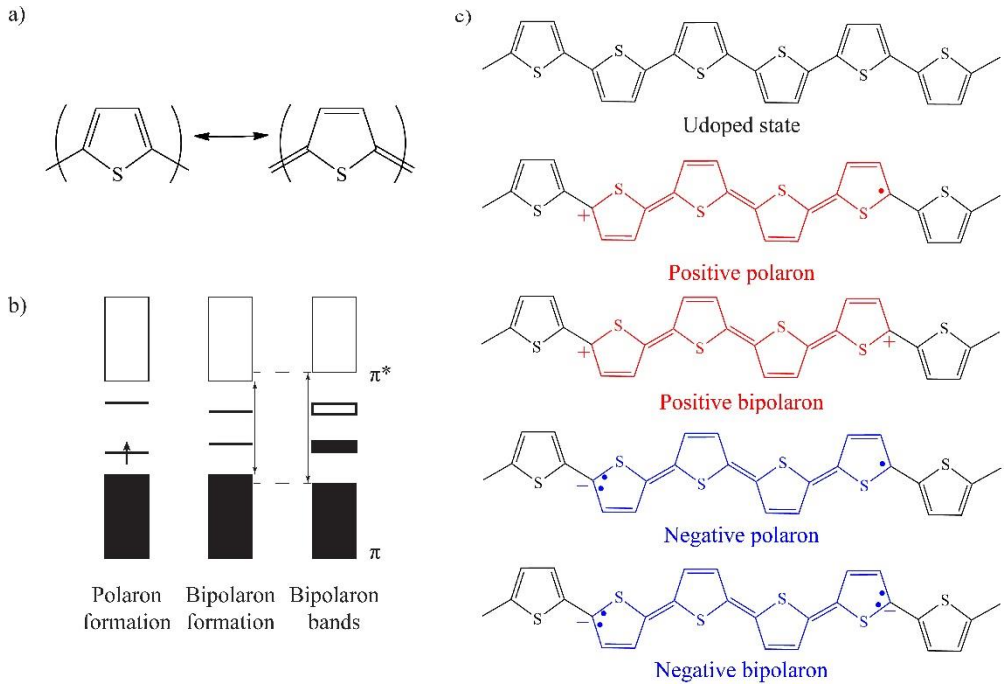

Figure 1.15: Polythiophene: a) aromatic (ground state) and quinoid-like geometric structure; b) electronic bands (low, moderate, and high doping level) and c) chemical structures illustrating undoped state, polarons and bipolarons (Adapted from [16], [19], [20]).

The degenerated systems have two identical geometric structures in the ground state, corresponding to the same total energy (e.g., *trans*-PA (Figure 1.16a, b). In the case of degenerated polymers, structural relaxation is associated with the formation of polarons, bipolarons, and solitons [16], [19], [20]. The removal of two electrons causes the formation of a bipolaron. The bipolarons' two charges can readily separate since there is no increase in the distortion energy due to there being the same energy of geometric structure between the two charges as on the other side of the charges. Isolated charges present a boundary between the two segments (Figure 1.16c). The charge associated with a boundary or domain wall is called a soliton because it possesses solitary wave properties [20]. A soliton causes a structural relaxation nearby the domain boundary extended over approximately seven carbon atoms (Figure 1.16d). The localised electronic state associated with the soliton is a non-bonding state with an energy between the π- and π^*-band (Figure 1.16e). If the state is unoccupied (doubly occupied), a soliton is positively (negatively) charged. In the case of a single occupation, the soliton state neutralises the electronic charge on the carbon nucleus. At a high doping level, individual charged solitons can overlap, forming a soliton band located in the middle of the valence and conduction bands [16], [19], [20].

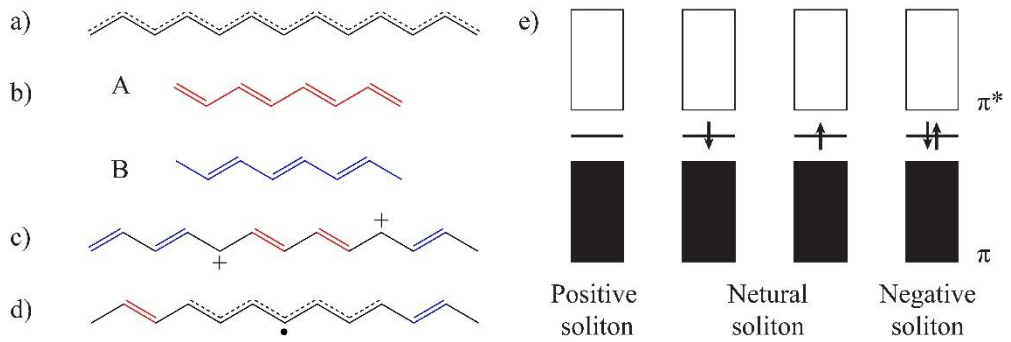

Figure 1.16: *trans*-PA geometric structures: a) undimerized structure; b) degenerated A and B phase; c) two charged solitons; d) neutral soliton; and e) the band structure of trans-PA (Adapted from [16], [19], [20]).

During the doping process, polymer as an insulator or semiconductor with a conductivity in the range 10^{-10} to 10^{-5} S cm^{-1}, is converted to a polymer with metallic conductivity (1-10^4 S cm^{-1}). Doping can therefore increase the conductivity of CPs by several orders of magnitude from the semiconductor regime. These polymers are generally referred to as "electronic polymers". Figure 1.17 illustrates the rise of *trans*-PA and polyaniline (PANI) conductivity by doping. The conductivity of the polymer can vary from a low- to a high-conducting polymer by controlling the doping level [17]. The conductivity increases rapidly at the beginning of the doping and stabilises with very little change at a certain point, even though the polymer has a higher degree of doping [23]. The maximum dopant concentrations are typically around several mole percent per repeat unit (e.g., up to 20 % for PA doped with iodine) [20].

In addition to the degree of doping, the conductivity strongly depends on the nature of the dopant (e.g., the conductivity of PPy can vary from 0.3 S cm^{-1} for HSO_4^- to 100 S cm^{-1} for BF_4^- dopant). They are categorised as small cations/anions (e.g., Na^+, Cl^-, and ClO_4^-) and a large polymeric species (e.g., polystyrene sulfonate and polyvinyl sulfonate). Small dopants can be readily inserted/de-inserted into/from the polymeric chain. Meanwhile, large dopants can change the polymer's density, and they are strongly bonded to the polymeric chain, thus preventing leaching. Reversible doping (charging/discharging) is an important feature of CPs for various applications. However, in the case of large, strongly bonded dopants, the de-doping process becomes difficult, since the doping/de-doping process is diffusion controlled [19].

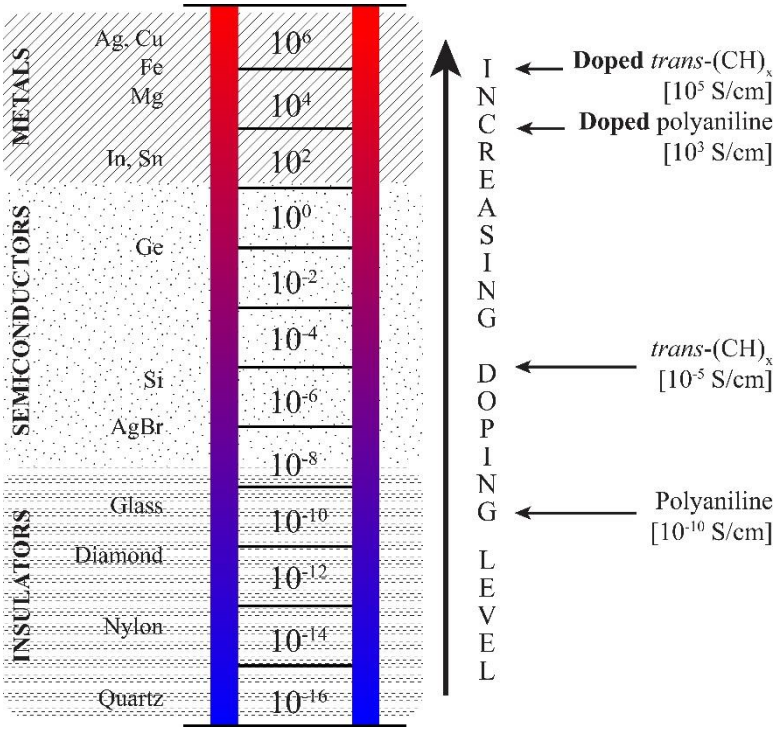

Figure 1.17: Conductivity of CPs (Adapted from [17]).

1.4.2 Properties and applications of conductive polymers

CPs have a unique intrinsic anisotropy in terms of electrical and optical properties, originating from the π-electron delocalisation along the polymer backbone [19], [22]. These physical properties are affected by the conjugation length, the degree of crystallinity, the degree of doping, and the intra-/inter-chain interactions, which can be improved via orientation and chain-alignment [17], [19], [22]. Each charged polymer has a characteristic spectroscopic signature given by the solitons, polarons and bipolarons [17]. For example, a bipolaron causes two possible optical transitions: from the valance band to a lower bipolaron level or an upper bipolaron level [20].

CPs show wide chemical diversity, low density, good flexibility, corrosion resistance, and an easily tuneable shape, morphology and conductivity. They enable solubility and processability

from common solvents and the fabrication of transparent electronics and semiconductors, in which the Fermi energy can be controlled and shifted over a wide range. This class of materials can reversibly store charge and energy and present a candidate for high-energy-density, high-power-density polymer battery electrodes. Additionally, due to their attractive electrochemical and electrochromic properties, they are used as a material in chemical sensors. Thus, CPs are very interesting due to their application in "plastic electronic" devices. To further improve the properties, various CPs-based composites and hybrids (introduction of nanomaterials, other polymers) are studied and produced [16], [19], [22].

1.4.2.1 Electrochemical properties of conductive polymers

CPs have attractive electrochemical properties mainly due to the reversible doping/de-doping process. The simplest way to understand and study them is by using CV. The polymer chain becomes positively charged during the positive, i.e., anodic scan (oxidation). While the negative, i.e., cathodic scan (reduction), results in a negatively charged polymer chain. The current peak for a reversible system caused by the doping/de-doping process can be calculated using Eq. (1.19) [19]:

$$I_p = n^2F^2A\Gamma\upsilon\left[\frac{\exp\theta}{RT\,(1+\exp\theta)}\right] \tag{1.19}$$

where $\vartheta = (nF/RT)(E\text{-}E°)$. According to the equation, the current peak is directly proportional to the surface coverage (Γ) and the potential scan rate. An increased scan rate does not change the current peak position, which only applies to thin CP films doped with ions that have a small diffusion coefficient, where the system is not diffusion-controlled. In this case, the cyclic voltammogram for the one-electron redox process shows completely symmetrical redox peaks (Figure 1.18a) and they do not change if the solutions are stirred. When a polymer is doped with larger ions, the reversibility of doping becomes diffusion-controlled. The result is an asymmetrical cyclic voltammogram, with the current proportional to $\upsilon^{1/2}$, and a shift in the current peak position with a scan-rate increases. In the case of the multi-electron redox process, the cyclic voltammogram shows several redox couple peaks (Figure 1.18b). The CV behaviour of CPs can also vary due to the type of acid electrolyte used, dopants and ions of different sizes. In the given potential range that is material specific, the redox behaviour of CPs is stable and reversible. However, scanning a CP electrode over 1 V vs Ag/AgCl can cause a rapid structural degradation and a loss of electro-activity. This oxidation is irreversible and is referred to as an over-oxidation process [19].

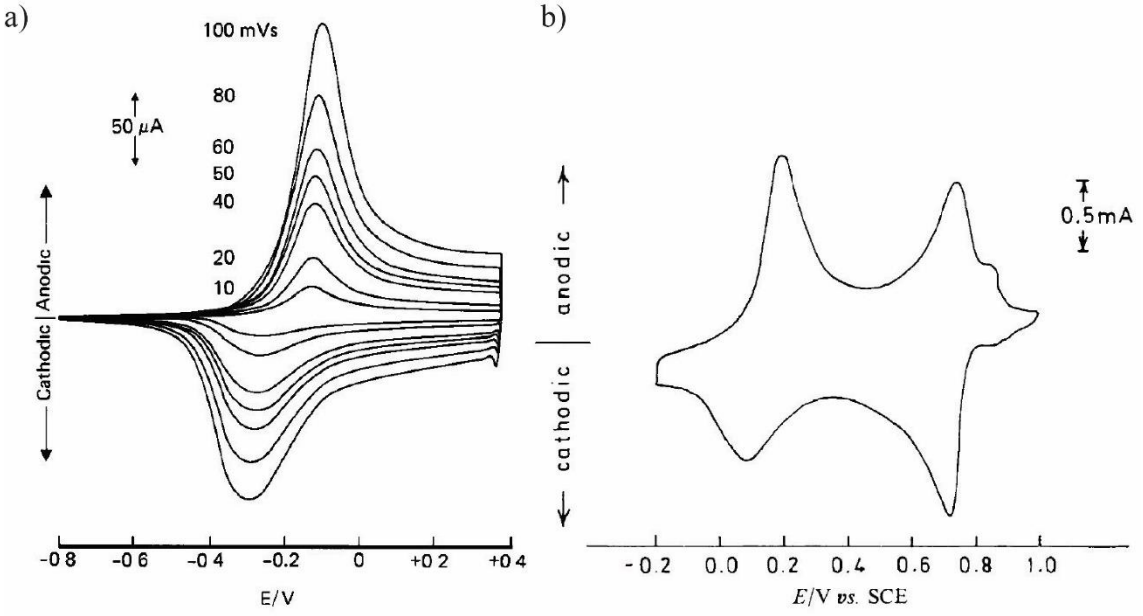

Figure 1.18: Cyclic voltamogram of a) PPy – one-electron redox process (Taken from [24]; "Used with permission of Royal Society of Chemistry (2022), License Number: 1272627-1); b) PANI – multi-electron redox process (Taken form [25]; Used with permission of Elsevier (2022), License Number: 5380740749407).

Properties that are also categorised as electrochemical due to the tight connection with the redox behaviour of CPs are the capability of charge storage, electrochromism, and swelling of the polymer, i.e., a change in volume. CPs can reversibly store charge due to the redox reactions, which makes them interesting for applications in electrochemical capacitors as a type of pseudo-capacitor. The redox reactions of CPs are tightly connected with the doping/de-doping of CPs. As already explained, doping introduces a reorganisation in the electronic structure of the polymer, resulting in the reduced E_g and new sub-bands due to the charge carriers acting as polarons and bipolarons. The visible colour change of CPs is related to the energy gap and electron transitions, so it is affected by reversible redox processes, i.e., electrochromism. Swelling/de-swelling is caused by a change in the redox state of CPs and can be result in changes to the bond lengths and the insertion/removal of solvent molecules into/from the polymer (i.e., osmotic expansion). It is a property of CPs that makes them suitable candidates for actuators, i.e., a material that converts an external stimulation into a mechanical response [19].

1.5 Polyaniline

PANI is a widely studied and the most industrially applicable CP due to being an inexpensive monomer, having a straightforward polymerisation reaction with a high yield, excellent environmental stability, and reversible redox and pH-switching properties [16], [26]–[28]. As polymers, PANIs can refer to derivations from a polymer with a general structure (Figure 1.19a) composed of repeated reduced (Figure 1.19a, red) and oxidised (Figure 1.19a, blue) units. The average oxidation state, (1-y) can vary from 0 (y = 1; completely reduced polymer), 0.5 (y = 0.5; half-oxidized polymer), to 1 (y = 0; completely oxidized polymer). Each oxidation state has its own term: 'leucoemeraldine', i.e., completely reduced PANI (Figure 1.19b), 'emeraldine', i.e., half-oxidised PANI (Figure 1.19c), and 'pernigraniline', i.e., completely oxidised PANI (Figure 1.19d) [17], [28]. According to the generalised formula of PANI (Figure 1.19a), this can exist in a continuum of oxidation states. MacDiarmid et al. [29] showed that in the range between y = 1 and y = 0.5, only two chromophores, i.e., part of the molecule responsible for colour, characteristic of a completely reduced and half-oxidised state exists. All the intermediate

oxidation states are at a molecular level composed of the mixtures of these chromophores. The same phenomenon is true for the range between y = 0.5 and y = 0, where all the intermediates are composed of a mixture of chromophores characteristic of half-oxidised and completely oxidised states. All the states can exist either in a base form, e.g., emeraldine base, or in a salt form, e.g., emeraldine salt. Half or completely protonated imine nitrogen atom gives the corresponding salt. The degree of protonation depends on the degree of the oxidation state and the pH of the aqueous acid [17].

The emeraldine base is the most useful and commonly synthesised state of PANI due to its good stability at room temperature and its classification as a semiconductor. Leucoemeraldine is known to be unstable, i.e., it can be easily oxidised, and is without an increase in the conductivity after protonation of the leucoemeraldine base (~10^{-10} S cm^{-1}). Pernigraniline is easily degraded due to the instability of the quinonediimine groups in the presence of nucleophiles (e.g., water) [23], [27], [30].

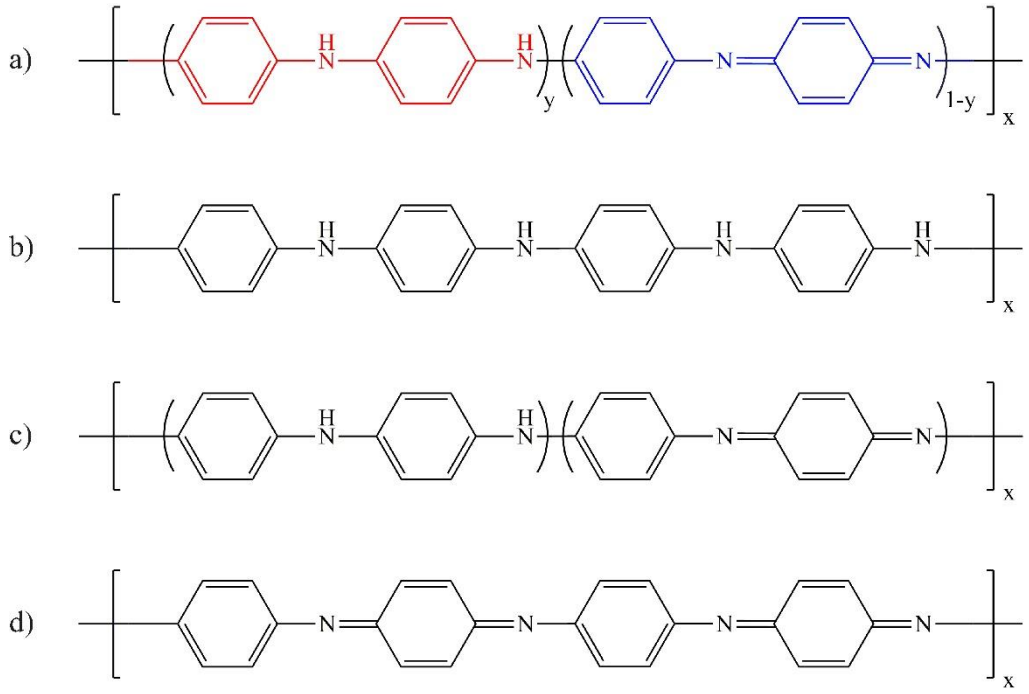

Figure 1.19: PANI base: a) general composition of PANI (red – reduced unit, blue – oxidised unit), b) completely reduced PANI, i.e., leucoemeraldine base, c) half-oxidised PANI, i.e., emeraldine base, and d) completely oxidised PANI, i.e., pernigraniline base (Adapted from [17], [28]).

1.5.1 Polyaniline synthesis

Generally, the most common preparation of CPs is via chemical or electrochemical synthesis involving the oxidation of a monomer. In the first step, monomers are oxidised at high potentials (0.9 V vs saturated calomel electrode (SCE) for aniline (ANI) [31]) into low-molecular-weight oligomers. The low-molecular-weight oligomers are oxidised at lower potentials than the oxidation of the monomer to form a polymer. In the case of chemical synthesis, monomers are oxidised by oxidants with high oxidation potentials (E_0, vs SHE), such as ferric chloride ($FeCl_3$, E_0 = 0.77 V) and ammonium persulfate ($(NH_4)_2S_2O_8$, E_0 = 1.94 V). The polymerisation is performed in acidic conditions (pH < 3) to minimise the formation of undesirable secondary products and enhance the head-to-tail coupling. The resulting polymer precipitates out of the chemical reaction solution in the form of powdery nanostructures. In electrochemical polymerisation, i.e., electropolymerisation, a monomer is oxidised by applying a positive potential or current (anodic oxidation process) and can be performed via one of three electrochemical techniques: potentiostatic (application of a constant voltage), galvanostatic (application of a constant current) or potentiodynamic (a variable current and voltage). It is performed using a three-electrode system: CE, RE, and WE. As the chemical polymerisation, electropolymerisation is also

performed in an acid electrolyte (HA) with pH < 2. Acidic conditions ensure the solubilization of monomers in water, the formation of short conjugation oligomers, an improvement of head-tail bonding, the formation of a doped emerald salt, and the prevention of undesirable by-products [27], [31]–[34]. The growth of a polymer due to the insertion of a dopant anion, i.e., a counter-ion, in electrochemical polymerisation, can be presented as a generalised stochiometric equation (Eq. (1.20)):

$$\mathrm{nM} + \mathrm{nyA}^{-} \xrightarrow{\text{oxidation}} \left[\mathrm{M}^{y+}(\mathrm{A}^{-})^{y-}\right]_{\mathrm{n}} + \mathrm{n}(2+\mathrm{y})\mathrm{e}^{-} \tag{1.20}$$

where M refers to the monomer, A is a dopant anion for the neutralisation of positive charge at the anode, and y is a doping degree defined as the ratio between the number of charges in the polymer and the number of monomer units (usually between 0.1 and 0.4) [35]. The resulting polymer deposited on the surface of the WE is a film, composed of different nanostructures, e.g., nanofibers, nanoparticles, nanoflowers, nanosheets, as presented on Figure 1.20 [32], [33], [36].

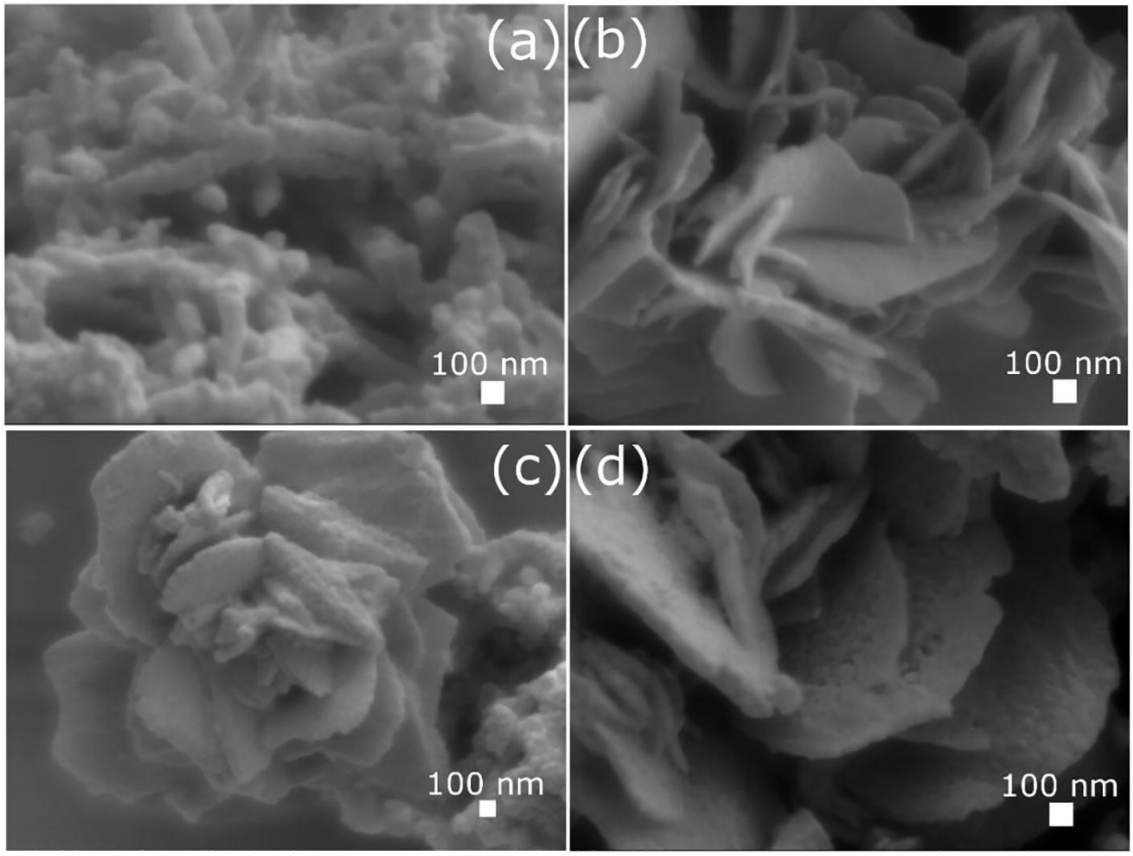

Figure 1.20: Scanning electron microscope images of different PANI morphologies: a) nanofibers; b) nanosheets; c) nanoflowers; and d) magnified nanoflower petal (Taken from [36]; Used with permission of Elsevier (2022), License Number: 5384130611972).

PANI can be synthesised via the chemical or electrochemical oxidation of ANI. Both syntheses proceed via a radical propagation mechanism in four steps. Figure 1.21 presents the PANIs' chemical and electrochemical synthesis with reactions, presented using molecular structures. The 1st and 2nd step, oxidation of the ANI and radical coupling and re-aromatization, respectively, are the same in both syntheses. The figure presents the difference in 3rd and 4th step, chain propagation and final formation of the polymer. The first step in the PANI polymerisation mechanism is the oxidation of the ANI monomer to a radical cation, which exists in a three-resonance structure. The most stable structure is the one with a radical on the para position of the benzene ring (Figure 1.21a). This is the slowest step in the polymerisation, and thus it is the

rate-determining step in the PANI synthesis. In the second step (Figure 1.21b), head-to-tail coupling of the *N*- and *para*- radical cation takes place. The resulting dimer further undergoes the re-aromatisation process and eliminates two protons, resulting in the *p*-aminodiphenylamine formation. In the case of electrochemical synthesis, the third step is the dimer oxidation on the surface of the electrode from the formation of dimer radical cation (Figure 1.21c_E). The chain propagation results from monomer radical cation and dimer radical cation coupling. The polymer is oxidised and doped in an acid solution to the final product PANI/HA in the last stage (Figure 1.21d_E). In the chemical synthesis, the initial product in the chain propagation step (Figure 1.21c_C) is a fully oxidised pernigraniline salt. The pernigraniline salt is reduced by unreacted aniline to the green emeraldine salt after running out of oxidant in the last step (Figure 1.21d_C) [28].

By changing the synthesis parameters, i.e., temperature, time, the type of oxidant, nature of doping anion, the electrode material, pH of electrolyte, scan rate and deposition time, PANI can possess a different structures, morphology, and redox state [30], [37]. In contrast to other CPs such as PPy, polythiophene, PANI has an intrinsic nature to grow 1-dimensionally, i.e., a nanofibrillar morphology [33], [38]. With electrochemical polymerisation, PANI nanofibers can be obtained directly without any additional usage of a template or surfactant. They can be formed simply by controlling the electrochemical polymerisation kinetics [33]. For example, by increasing the scan rate (from 10 to 50 mV s^{-1}) during potentiodynamic deposition, the fibres' average diameter and length decrease. While the fibres become very short and completely merged at a too-high scan rate (100 mV s^{-1})[37]. Other shapes (e.g., wires, rods, tubes, and ribbons) can be achieved by using various templates and surfactants [32], [33].

Electrochemical polymerisation has several advantages over chemical polymerisation. Due to there being no require for an oxidant agent, it can give the purest product, free of admixtures and does not need special procedures for the purification of PANI from the solvent, unreacted monomer, and initiator molecules. Additionally, electrochemical polymerisation enables a straightforward (one-step) deposition of a compact and integrated layer of polymer directly on to the conducting surface, ensuring good ohmic contact between the electrode and the polymer and easier control over the thickness and the uniformity of the deposit [30], [31], [38] On the other hand, chemical polymerisation has a higher yield, the product characterisation is not limited to surface-analysis techniques, and the prepared polymer can be applied to any substrate [30], [39].

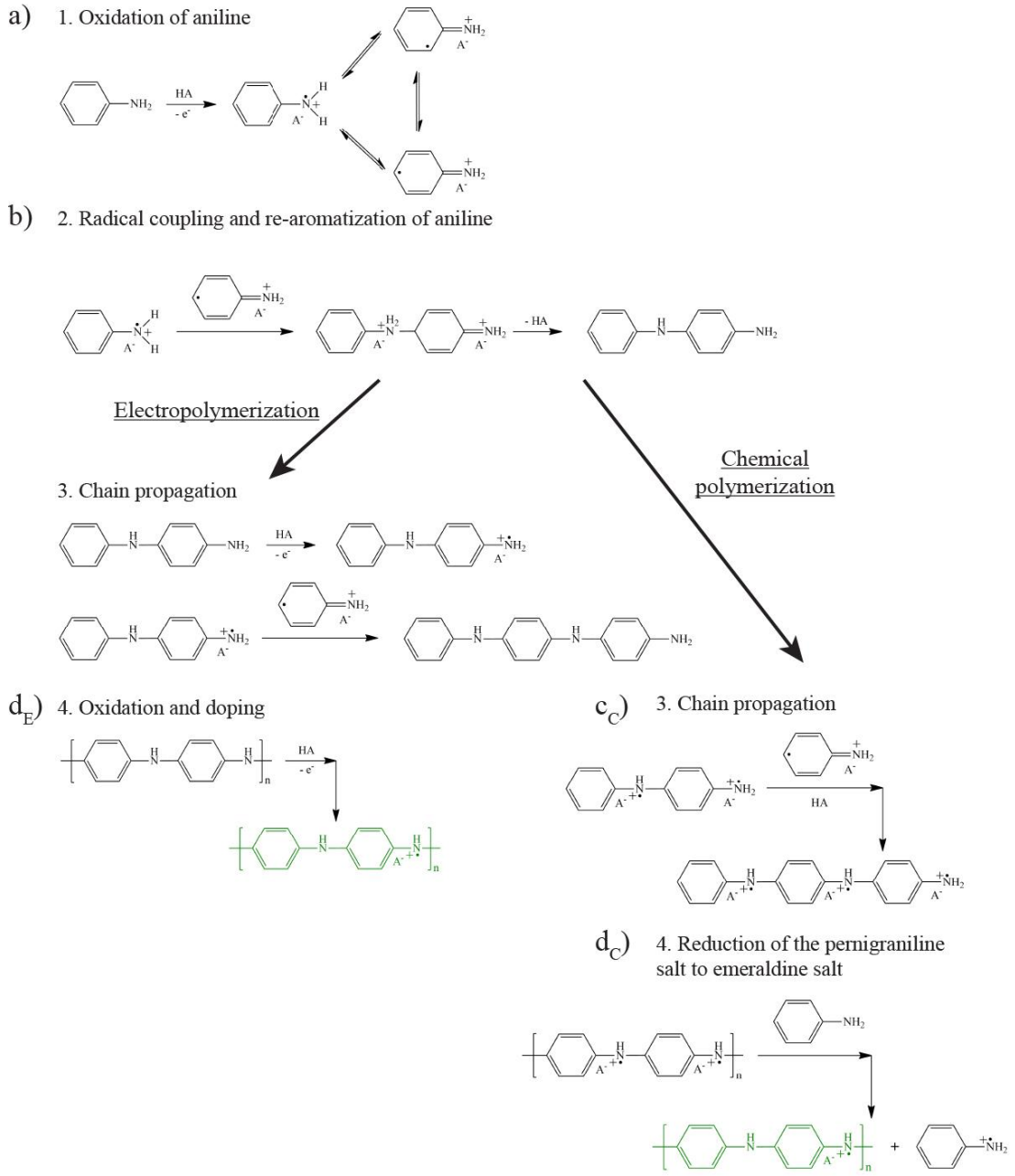

Figure 1.21: PANI polymerisation mechanism (Adapted from [28]).

1.5.1.1 Electrochemical polymerization

Electrochemical polymerisation is usually performed in a three-electrode electropolymerisation cell. This setup is composed of a WE (anode), a CE, (cathode) and a RE to ensure effective potential control and maximise the polymerisation process's reproducibility. The WE is the electrode on which the monomer is oxidised, and the resulting polymer is deposited. The role of the CE is to pass currents, opposite that the ones passing through WE, thus ensuring no current flow through the RE. Its position is critical to the determination of the generated electric field, which influences the quality of the deposited polymer. The RE has stable and well-known potential. It enables control over the potentials used in electrochemical experiments. A two-electrode system can also perform the polymerisation (without RE). However, special care and control over the potential needs to be taken to avoid over-oxidation [28].

In electrochemical polymerisation, a monomer is oxidised by applying a sufficiently positive potential [28]. ANI monomer oxidation is an irreversible reaction at 0.9 V vs SCE. In the electrochemical polymerization of the ANI, the chosen potential should be positive enough (0.9

V vs SCE) to ensure a sufficiently fast polymerization rate and at the same time must not be too positive (more than 1 V vs SCE) to avoid the process of excessive oxidation.

PANI is commonly prepared using the potentiodynamic method. Polymerisation by the potentiodynamic method involves the application of CV. In the case of PANI polymerisation, potentials are usually scanned from −0.2 V to 0.7–1.2 V vs. SCE [30]. During the polymerisation, the polymer is subjected to oxidation/reduction reactions, i.e., the insertion/removal of electrons and ions, which causes a change in the bond lengths and the polymer volume. Additional processes to the polymerisation mechanism add another dimension to electropolymer growth, and they need to be considered. For example, redox reactions of PPy during its polymerisation via CV results in a more ordered structure [28]. Figure 1.22 presents an example of PANI electropolymerization by CV on a Pt electrode from 0.2 M ANI in 0.6 M HCl solution and from 0 to 1 V vs Ag/AgCl at 48 mV s^{-1}. In the first cycle (marked as 1 in Figure 1.22), the oxidation current starts to rise after passing the potential 0.8 V vs Ag/AgCl, indicating the start of the ANI oxidation with a maximum current at ~0.9 V. After performing a few cycles (2 and 3 in Figure 1.22), characteristic peaks for the polymerization appear on the cyclic voltammogram. The first anodic current peak at ~0.2 V vs Ag/AgCl (Figure 1.22 peak A) refers to the oxidation of leucoemeraldine to the emeraldine form of PANI. The second small oxidation peak (Figure 1.22 peak B) refers to the formation and oxidation of intermediate products (p-benzoquinone). A further increase of the potential leads to the formation of fully-oxidized pernigraniline at ~0.7 V vs Ag/AgCl (Figure 1.22 peak C). The reduction peak corresponds to the opposite reactions: at 0.65 V vs Ag/AgCl pernigraniline reduces to emelardine (Figure 1.22 peak D); peak at ~0.45 V vs Ag/AgCl is the reduction of intermediate products (Figure 1.22 peak E); and ~0.1 V vs Ag/AgCl emeraldine is reduced to leucoemeraldine (Figure 1.22 peak F). Each performed cycle results in higher peak currents, indicating the successful formation and a thicker amount of deposited PANI [31], [40].

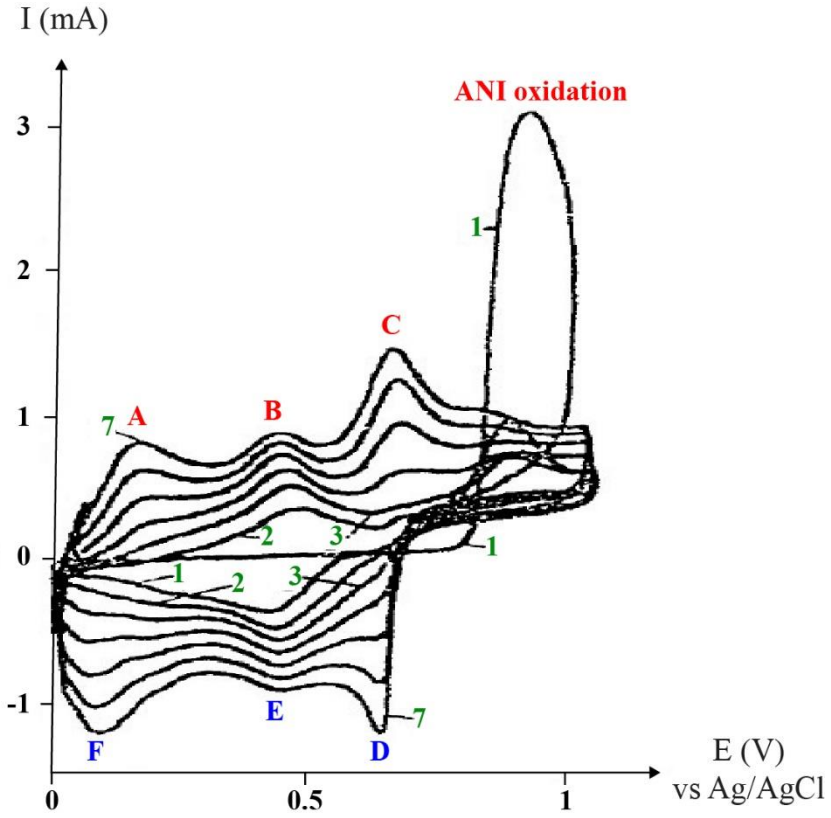

Figure 1.22: Electropolymerization of PANI by CV from 0.2 M ANI in 0.6 M HCl solution and from 0 to 1 V vs Ag/AgCl at 48 mV s^{-1} (WE: Pt) (Adapted from [40]).

Another way of electropolymerizing PANI is the potentiostatic and galvanostatic methods [27]. For the potentiostatic PANI polymerisation, the potential is set to a fixed value between 0.7 and 1.2 V vs. SCE [30]. For galvanostatic polymerization, the fixed value of the current density should not exceed 10 mA cm^{-2}. Since the rate of polymerisation is determined by the applied constant potential or the current density, care needs to be taken not to have too slow a rate, where no deposition occurs, or too high a rate, which would cause over-oxidation [28].

The application of potentiodynamic polymerisation results in the deposition of PANI with strong adhesion to the electrode surface. However, the resulting film is flexible and compact. Meanwhile, the use of galvanostatic polymerisation results in weaker adhesion and a powdery or flaky film. Potentiostatic polymerisation produces a polymer with the lowest adhesion. Potentiodynamic polymerisation results in a more uniformly deposited PANI film, in comparison to the other two methods. Due to the heterogeneity of electrode substrates, polymer growth caused by applying a constant potential does not result in an even coating being formed. Additionally, constant potential growth is more sensitive to iR drop, as the electrode resistance changes due to the deposited polymer of the surface of the electrode [28], [35], [38].

The electrochemical polymerisation of ANI is an autocatalytic process. As the oxidation of the ANI monomer is the rate-determining step in electropolymerization, the subsequent formation of the polymer on the already-formed/deposited polymer has a quicker polymerisation rate. In the CV polymerization of PANI, the anodic peak potential for the ANI oxidation shifts towards negative potentials by about 80 mV from the first to the second cycle (Figure 1.22), which confirms the autocatalytic behaviour [31], [40].

Electrochemical conditions for electropolymerisation process

The construction of an electrochemical cell setup for electropolymerisation has two major considerations, i.e., the iR drop and the hydrodynamics of the cell [28]. The iR drop contributes to the electrode potential, caused by the solution resistance between two electrodes during the electric current's flow through the cell. It is influenced by the rate of ion flow between the electrodes (the magnitude of current, electrolyte conductivity, and the distance between the two electrodes) [41]. As mentioned above, during the electropolymerisation, a polymer is deposited on the surface of the WE. Therefore, the resistance of the "new" electrode (i.e., the electrode with the deposited polymer layer) usually increases, causing changes in the rate of the ion flow between the electrodes. The hydrodynamics of the cell is responsible for the movements of the reactants (monomers, oligomers) and products (polymers). The changes to the polymerization rate and the mass transfer of reactants and products can influence the final polymer product. During the reduction process on WE, the CE is exposed to high positive potentials that can cause the oxidation of the ANI, resulting in the deposition of the PANI [1], which is unwanted and influences the electrochemical system. For this reason, it is important to either have a separate CE or place it downstream [28].

Working electrode

The choice of WE material is important due to its influence on the initial stage of polymerisation, i.e., the monomer oxidation rate, the degree of absorption of the monomer and other products, and the properties of the final polymer surface [42]. Due to the use of a high potential for the oxidation of monomers, it is difficult to apply to substrates that form a non-conductive metal oxide at these potentials (e.g., tantalum, aluminium, stainless steel). However, if the oxide formation rate is sufficiently slow and the polymer can be deposited before the metal oxide forms, a film of excellent quality can be obtained. In addition to the type of material, the size of the WE can also influence the polymerisation. In the case of larger WEs, the conductivity decrease during the polymerisation is minimised. On the other hand, smaller electrodes (< 20 µm diameter) enable electropolymerisation in low-conductive media. Electrodes can also be used as a template for the deposition of nanostructures. PANI can be deposited on various WEs, such as platinum, gold, glassy carbon, reticulated vitreous carbon and indium-tin-oxide glass (ITO) [28].

Electrolyte

The electrolyte is composed of solvent and counter ions. The solvent should be as pure as possible, capable of dissolving the monomer and the counter ion at appropriate concentrations and be stable at the potential of electropolymerisation. Aqueous solvents are preferred over

organic ones due to the cost, handling, safety, and wide range of counter-ion choices [28]. The prepared electrolytes should be oxygen-free, i.e., purged with inert gas, due to possible reaction of oxygen with radical intermediates and its reduction at the CE, which can cause the formation of a hydroxide. The latter can affect the quality of the formed PANI. The electrochemical polymerization of the PANI is usually performed in a strongly acidic aqueous medium, i.e., an acidic electrolyte (pH < 2) to avoid the formation of short conjugation oligomers and a smaller polydispersity [28], [31].

The concentration and type of counter ions influence the electrolyte's conductivity, the polymerisation rate, and the polymer's properties (e.g., polymer-solvent interactions, structure, morphology), e.g., the diameter of the produced PANI fibres and the polymerisation rate decrease with different anions: HSO_4^->NO_3^->Cl^->ClO_4^-. Thus, counter ions can have an important effect on the polymerisation process. As a solvent, counter ions should also be chemically and electrochemically stable. In the case of the electrolyte, when containing a surfactant, i.e., dodecyl sulphate, the surface properties of the electrode influence the surface properties of the final polymer. The substrate can influence the orientation of the surfactant counter ion within the polymer. For example, polymers deposited on the hydrophilic substrate have more hydrophobic properties and vice versa. Examples of good and effective counter ions are sulfonated aromatics, e.g., *para*-toluene sulfonate. They are known to improve the conductivity and mechanical properties, as they induce a degree of crystallinity, and they exhibit surfactant-like behaviour [28].

1.5.2 Polyaniline properties

Among CPs, PANI has the most interesting electrochemical, optical, and conductive properties. The electrochemical and optical properties are interconnected, as optical properties immediately change with the oxidation state of the PANI. PANI is a mixed-oxidation-state polymer with three characteristics states (leucoemeraldine, emeraldine, and pernigraniline) either in the form of a salt or a base. Figure 1.23 presents the chemical structures of all the PANI's characteristic states and the transformation reactions between them. Each of these states has its characteristic colour. The switching between the oxidation states is caused by a redox reaction (oxidation/reduction), while the salt and base forms depend on the pH due to the protonation of a nitrogen atom. All this redox and protonation switching is accompanied by a visible colour change. The optical absorbance can be directly connected to the electronic structure of the polymer. Thus, this information can be used to calculate the electronic band gap PANI states [27].

The changes in the oxidation level and pH of PANI cause the transfer of electronic and ionic charges (i.e., transformation between leucoemeraldine, emeraldine and pernigraniline) and protons (i.e., transformation between salt and base form; Figure 1.23). Leucoemeraldine has a pKa between 0 and 1. Thus, its protonation begins at approximately pH 2 and is completed at pH −1. The pKa of emeraldine is approximately 3 and for pernigraniline below 0. Their salt forms are electro-active in acids with a pH below 3–4. Above pH 4, the conductive emeraldine salt cannot be formed. The exact pH at which the polymer protonation/deprotonation occurs is dependent on the type of acid and the incorporated dopants. For example, in the case of polyelectrolyte dopants, the transition between conducting and non-conducting PANI can be shifted towards higher pH (comparison between Figure 1.24a and b) [28], [43].

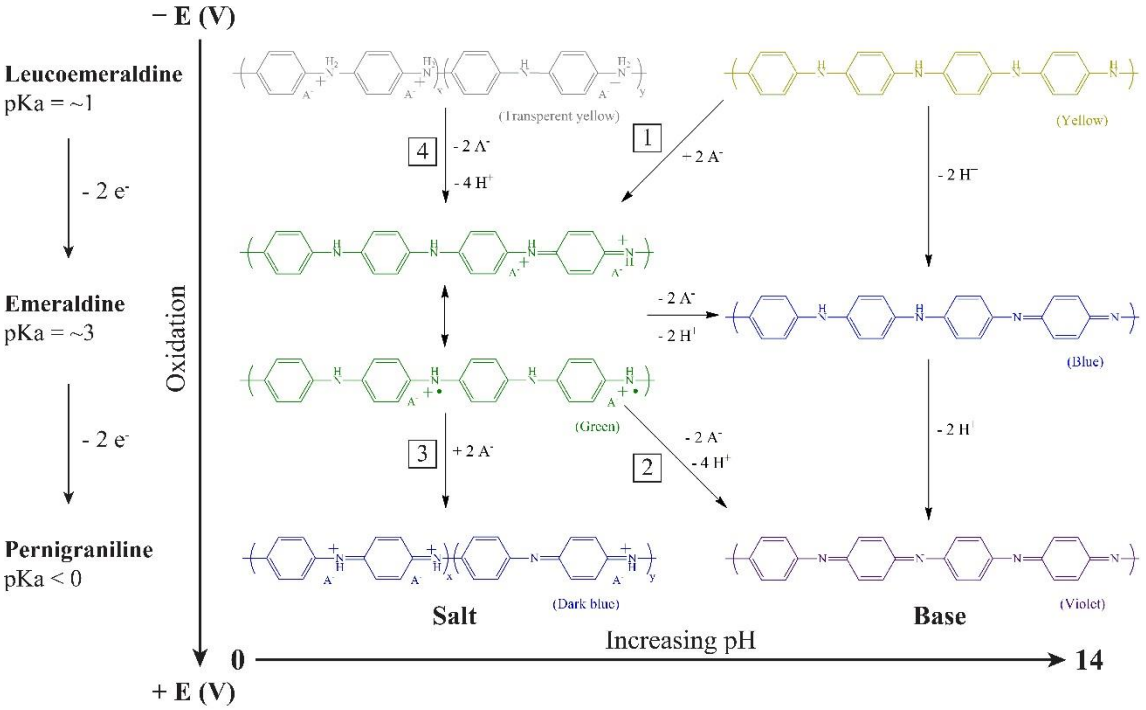

Figure 1.23: PANI switching: redox/protonation states and colours. Note that all the reactions are reversible (Adapted from [19], [43], [44]).

The electrochemical switching can be readily observed via a CV. Figure 1.24a is an example of a characteristic cyclic voltammogram of PANI in 1 M HCl electrolyte. In the protonated state, PANI undergoes two redox processes: transformation from leucoemeraldine to emeraldine and from emeraldine to pernigraniline. In the potential range between −0.2 and 0.9 V vs Ag/AgCl in HCl electrolyte (pH = 1) the first redox couple (leucoemeraldine/emeraldine; Figure 1.24a A/D) occurs between 0 and 0.25 V vs. Ag/AgCl, and the second one (emeraldine/pernigraniline; Figure 1.24a B/C) between 0.6 and 0.8 V vs. Ag/AgCl. The most conductive emeraldine salt occurs between 0.20 and 0.60 V vs Ag/AgCl. At lower potentials, PANI exists in the leucoemeraldine state and at higher in the pernigraniline state [28], [38].

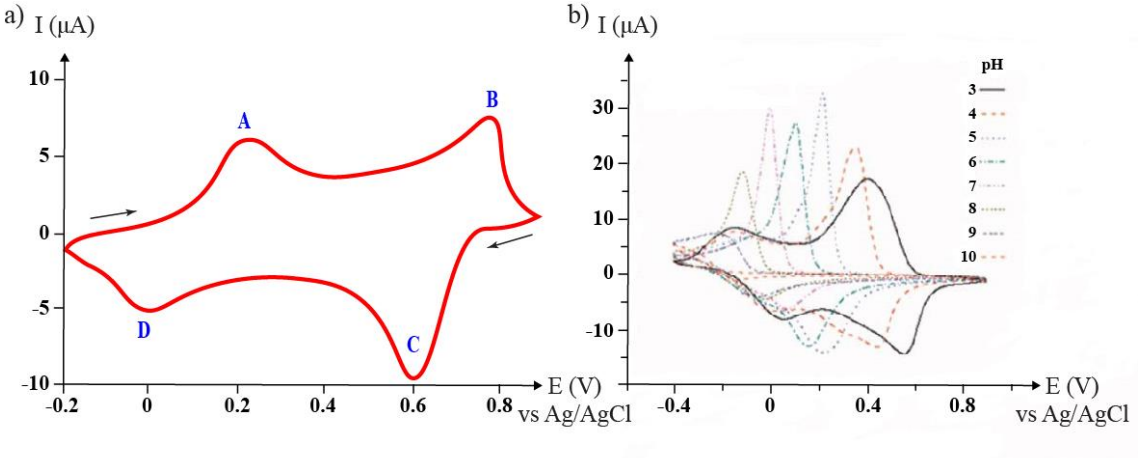

Figure 1.24: Cyclic voltammogram of PANI a) HCl-doped PANI in 1 M HCl showing the characteristics of two redox couples: A/D and B/C (Adapted from [38]); and b) polymer-acid-doped PANI in buffer solutions of varying pH (Adapted from [45]).

However, potentiometric methods alone cannot answer whether the emeraldine salt or base is formed. They can be distinguished by determining the pH dependence of the potentials of the redox couples. Figure 1.24b presents the cyclic voltammograms of PANI in a buffered electrolyte with different pH values. Increasing the pH from 3 to 7 causes shifts in the peak potentials of the second redox couple (B/C), while the first one (A/D) is largely pH independent. Above pH 7, the redox couples overlap into a single one. The pH dependence of the potentials of a simple redox reaction Eq. (1.21) can be described by the Nernst equation (Eq. (1.9)) by including the influence of the pH (Eq. (1.22)) [41], [44]:

$$\mathrm{Ox} + \mathrm{ne}^- + \mathrm{mH}^+ \leftrightarrow \mathrm{Red} \tag{1.21}$$

$$E = \left(E^0 + \frac{0.059}{n} \ln \frac{[\mathrm{Ox}]}{[\mathrm{Red}]}\right) - 0.059 \frac{m}{n} \mathrm{pH} \tag{1.22}$$

where 0.059 is the ratio between the gas constant and the Faraday constant at room temperature and *m* is the number of reacting protons. For example, the transition between pernigraniline base and emeraldine base (Figure 1.23) involves the exchange of 2 electrons (*n* = 2) and 2 protons (*m* = 2), meaning $E - E^0$ = −59 mV/decade of pH. Thus, in the case of the formation of the emeraldine base, the potential of the redox couple associated with this transition would shift by −59 mV/decade of pH. For the transition between the pernigraniline base and the emeraldine salt (Figure 1.23), two electrons (*n* = 2) and four protons (*m* = 4) are exchanged, giving a shift in potential of −118 mV/decade of pH. The transition between the leucoemeraldine base and the emeraldine salt (Figure 1.23) includes only the electron exchange (*n* = 2, *m* = 0). Therefore, this redox couple is pH independent [44].

In addition to the electric and optical properties, doping and deprotonation also have an impact on the morphology of the PANI [27]. Figure 1.25 represents the mechanism of electrochemical-mechanical actuation in a CPs, a volume change (Figure 1.25a, c, e) by two electrochemical pathways with different dopants (Figure 1.25b, d). The same behaviour can be observed in the PANI. The transport of ions for the neutrality of the polymer caused by the pH change and the electrochemistry causes the change in the volume, i.e., the polymer expands. The electrochemistry of the PANI, performed in a pH between 0 and 2, usually follows the path leucoemeraldine base, emeraldine salt to pernigraniline base (Figure 1.23, reaction 1 and 2). For example, during the transformation from leucoemeraldine to pernigraniline, PANI gains mass due to the anion injection (Figure 1.23, reaction 1), but in the second step (Figure 1.23, reaction 2) the mass decreases due to the ion loss. If the electrochemistry is performed in organic solvents, PANI follows the path from leucoemerladine base to pernigraniline salt by reactions 1 and 3 (Figure 1.23) without any proton transfer. Thus, the polymer expands during the whole process [43].

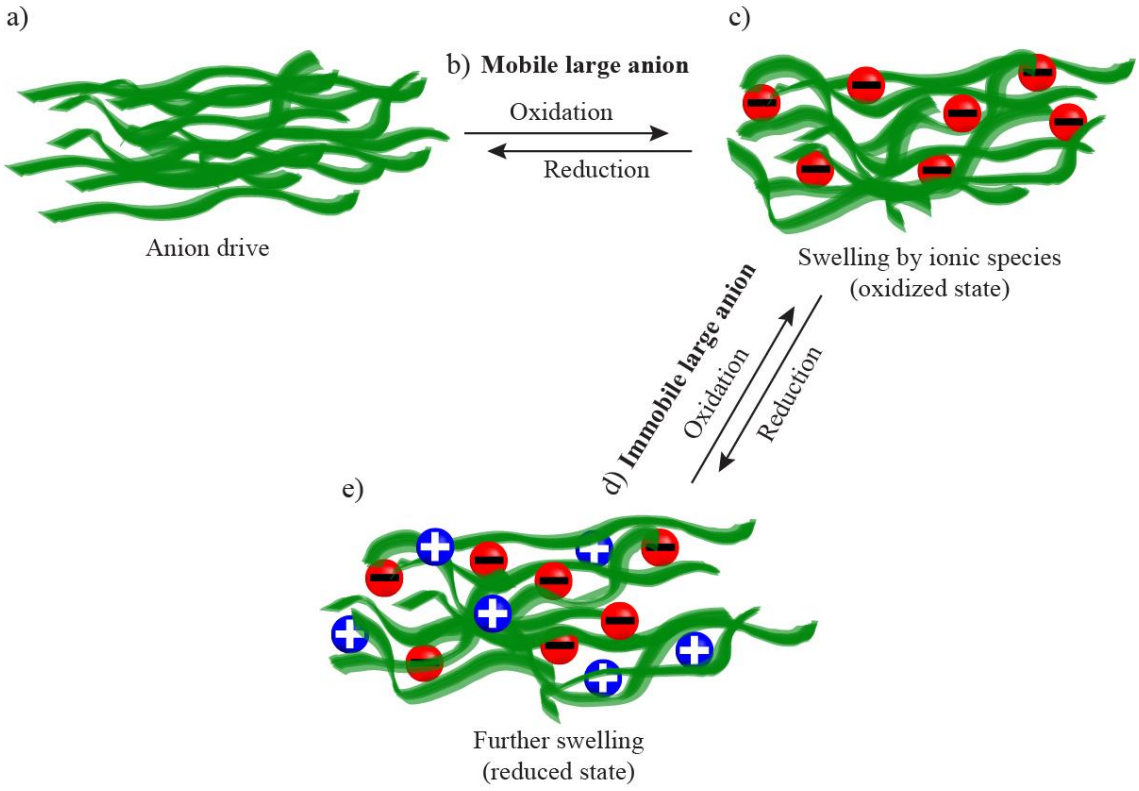

Figure 1.25: Mechanism of actuation, resulting in a volume change (a, c, e) due to two electrochemical pathways (b,d) [19].

1.5.2.1 Polyaniline conductivity

Figure 1.26 presents an electrochemical reaction between reduced and oxidized units of PANI (Figure 1.26a), the basic mechanism for switching between the PANI states, and two types of PANI doping (Figure 1.26b and c), to produce the conductive PANI emeraldine salt. PANI is a combination of completely reduced (Figure 1.26a, red) and oxidised units (Figure 1.26a, blue). The reduced- and oxidised-unit conversion follows an oxidation reaction with the loss of electrons and H^+ (Figure 1.26a). Both units are a base, i.e., without charge, and can be partly or completely protonated into salt units via a protonic acid treatment. From the combination of the base units (Figure 1.19a), the following compositions have been isolated: leucoemeraldine base (only reduced units), protoemeraldine base (3:1 reduced and oxidised units), emeraldine base (1:1 reduced and oxidised units), nigraniline base (1:3 reduced and oxidised units), and pernigraniline base (only oxidised units). The maximum conductivity occurs in a half-oxidised PANI in an acid solution, i.e., emeraldine salt (combination of reduced base units and oxidised salt units) [23], [43].

The PANIs' conductivity mainly depends on the degree of oxidation and the degree of protonation, which makes it unique among other CP group members, and also on the degree of crystallinity and molecular weight or chain length. The conductivity of PANI can be achieved either by non-redox doping, i.e., protonation of the emeraldine base via an acid-base reaction (Figure 1.26b), or redox doping, i.e., oxidation of leucoemeraldine to emeraldine (chemically or electrochemically, Figure 1.26c). The insertion of counter ions is present in both routes, making conductive PANI a salt [16], [17], [23], [26], [28], [34].

PANI exhibits a p-type conduction, meaning that most charge carriers are holes [34]. PANIs' conductivity originates through the hopping mechanism in the PANIs' crystalline region and can occur in the intra-chain or in the inter-chain. After protonation of the emeraldine base (Figure 1.26b), an added proton induces a spin-unpairing mechanism, which leads to a structural change with one unpaired spin per repeated unit. The addition of two protons to the emeraldine base protonates the nitrogen sites on either side of the quinoid rings, resulting in a spinless bipolaron defect, i.e., a double-charged polymeric chain (dication salt, Figure 1.23, the first green emeraldine salt chemical structure) [16], [26]–[28], [46]. The formation of two positive charges

on the neighbouring nitrogen increases the polymers' energy. Therefore, the electron density redistributes, causing one-electron pair of nitrogen atoms, i.e., a formed bipolaron, to convert to an ordered array of stable polarons (polysemiquinone radical-cation salt, Figure 1.26b). At the same time, there is no change in the number of electrons. Such an emeraldine in the metallic state has a half-filled band and a positive charge with the presence of a counter ion in each repeated unit [16], [26], [46]. The polaron structure is responsible for the conductivity, as the cation radical of one nitrogen acts as a hole, i.e., a charge carrier. The electron from a nearby nitrogen jumps into the hole and neutralises it, causing the movement of the hole. In the case of leucoemeraldine and pernigraniline, their structure contains nitrogen atoms with similar electronic environments. Therefore, protons from a dopant can be attracted by any nitrogen atom, creating a few protonated free-nitrogen atoms close by. There is less chance of chain regularity and less chance of forming a polaron as a charge carrier. Hence, leucoemeraldine and pernigraniline are isolated forms of PANI [47], [48].

PANI emeraldine base can be doped with Brönsted acids (HA) to form a conducting PANI/HA emeraldine salt. A wide range of acids can be used, from inorganic acids such as HCl, HNO_3, H_2SO_4, H_3PO_4, and HBF_4, to organic sulfonic and carboxylic acids [28]. The protonation in 1 M HCl results in a complete protonation of the imine nitrogen atom, giving fully protonated emeraldine hydrochloride salt with significant π delocalisation, accompanied by a 9–10 order-of-magnitude increase in the conductivity [23], [46], [49]. Emeraldine hydrochloride salt can also be obtained by oxidation of the leucoemeraldine base, i.e., a p-doping (Figure 1.26c) [17], [46]. The p-doping process involves oxidation of a π system. However, in the case of PANI, oxidation of the σ/π system is preferred [17]. The protonic acid doping, i.e., protonation, and p-doping of PANI results in the formation of a nitrogen base salt (nitrogen radical cation) rather than of a highly reactive carbonium ion, as in the case of the conventional p-doping of other CPs. The latter makes the PANI material very chemically stable in the environment [23], [28].

Similar to Brönsted acid doping, the emeraldine base can also be doped with metal slats and Lewis acids. The metal ions from lithium salts and Lewis acids, such as $AlCl_3$, GaCl, $SnCl_4$ and $FeCl_3$, are bonded to the imine nitrogen sites on the emeraldine base chains [28].

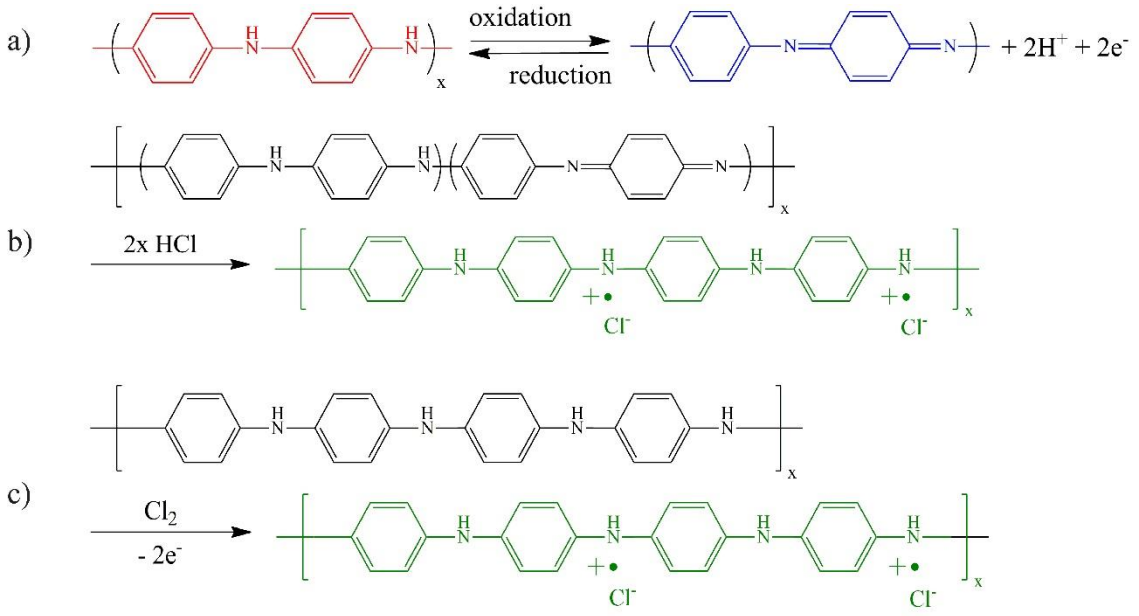

Figure 1.26: a) conversion between reduced (red) and oxidized (blue) PANI unit, and PANI doping: b) non-redox doping, i.e., protonation, and c) redox-doping, i.e. oxidation (Adapted from [17], [29]).

1.5.3 Polyaniline for ammonia detection

Ammonia (NH_3) is a nitrogen-hydrogen compound with a molecular mass of 17.03 g mol^{-1} (NH_3, Figure 1.27a). The NH_3 molecule has some similarities to the water molecule in terms of its electron configuration and bond angles. Both are diamagnetic and behave similarly in many

reactions. In the presence of a proton donor, a proton binds to a free-electron pair of NH_3, forming an ammonium ion (NH_4^+, Figure 1.27b) [50], [51]. The equilibrium of NH_4^+ formation and dissociation depends on the pH of the surroundings. NH_4^+ is considered a weak acid with a pKa of 9.2 at 25 °C. Thus, in a solution at pH < 9.2, NH_4^+ predominates, while at a pH > 9.2, NH_3 is predominant. In the case of pH = 9.2 the proportion of NH_3 and NH_4^+ is 50–50% (Eq. (1.23)) [52].

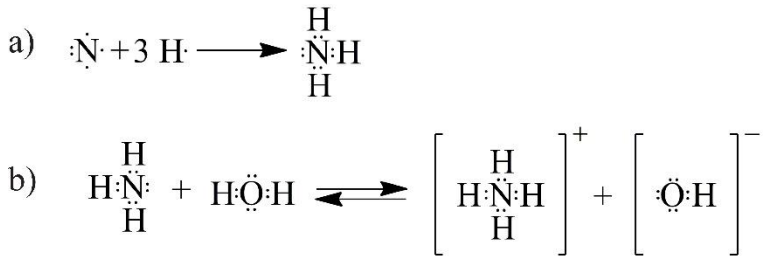

Figure 1.27: Chemical reaction of a) ammonia and b) ammonium-ion formation (Adapted from [51]).

$$\mathrm{pH} = \mathrm{pKa} - \log\left[\frac{\mathrm{NH_3}}{\mathrm{NH_4^+}}\right] \tag{1.23}$$

NH_3 is part of the natural nitrogen cycle as a product of nitrogen-containing organic material's decomposition. In nature, it is mainly in the form of ammonium salts and has significant importance, e.g., ammonium nitrates are an essential supply of nitrogen for growing plants. NH_3 and its salts have an important industrial meaning and have become the world's second-largest synthetic chemical product. It is a highly hydro-soluble gas, present in environmental waters and wastewaters [50], [51]. As a strong local irritant, NH_3 at higher concentrations has a problematic effect on the environment and human health [51]. It can damage an entire aquatic ecosystem by causing extensive growth of algae over the entire surface of the water [53]. According to the Occupation Safety and Health Administration (OSHA), the threshold concentration of ammonia for humans varies between 5 and 50 ppm. NH_3 has a strong and irritating odour, which at higher concentrations triggers skin, eyes, and lung illnesses [51], [54]. Moreover, NH_3 is a toxin and neurotoxin that has harmful effects on cells. The human body naturally contains NH_3 as a by-product of cellular metabolism (e.g., degradation of primary amides and amino acids, hydrolysis of proteins). However, exceeded values cause anomalies such as disruption to the natural pH in cellular organisms and indicates a diseased state. Liver and kidney diseases cause increased urea concentrations in the blood, resulting in elevated ammonia levels in the mouth, nose and skin. Thus, deviations in NH_3 concentrations can act as a potential biomarker for these medical conditions [55], [56] NH_3 is a versatile chemical species with an industrial, environmental, and biological use. Therefore, its monitoring and detection is present over a wide range of applications, from gas to liquid detection systems with different detection ranges, depending on the application [57].

As mentioned above, PANI is one of the most studied members of the CPs. Due to its straightforward synthesis and deposition on the electrode, good thickness control, high surface area, excellent environmental stability, and tuneable properties, it is widely studied and used as a material for sensor applications [38]. Thus, PANI can serve as a sensing layer in conductometric, optical and electrochemical sensors [38], [58]. Its known tuneable electrical conductivity gives it enormous potential, especially for constructing conductometric sensors.

PANI's conductivity depends on its redox state and protonation, e.g., degree of doping. Hence, it is used as a material for pH monitoring and the sensing of gases/vapours, which directly influence its protonation (ammonia (NH_3), H_2O, i.e., humidity) [59]. However, PANI's sensitive electronic properties and conductivity are also a disadvantage in terms of its selectivity. To overcome this restriction, PANI can be functionalised with biomolecules or modified with nanomaterials [60]. The addition of a specific catalytic material, like an organic molecule or a biomolecule to cause the reaction/decomposition of analyte to products, e.g., ions (OH^-, H^+) and molecules (NH_3, HCl) with a known influence on PANI's conductivity, enables an indirect, although selective detection of more complex analytes. Examples of such indirect sensing are the use of Ag nanoparticles for hydrogen peroxide (H_2O_2) [61], $SnCl_2$ for H_2S [62] (both chemi-

resistive gas sensors), the fluoral-P molecule for formaldehyde detection (chemi-resistive gas sensors) [63], and enzyme urease for urea (electrochemical sensor) [64]. PANI can therefore be used as a sensing layer for a variety of toxic and irritating gases such as NH_3, H_2, HCl, NO_2, H_2S, CO, CO_2, volatile organic compounds (chloroform, methanol, formaldehyde) [60], and other hazardous molecules (glucose, hydrogen peroxide, cholesterol, and phenolic compounds) via direct or indirect detection.

PANI is a frequently used material for NH_3 gas detection. As they both contain nitrogen atoms with a similar role in establishing the coordination bonding with protons, resulting in a strong attraction between them. PANI possesses p-type semiconducting properties [65]. After exposing it to a reducing NH_3 gas, it loses its conductivity due to deprotonation (Figure 1.28). The free-electron pair of NH_3 establishes a coordination bonding with the free atomic orbital of the dopant proton. Deprotonation leads to the loss of charge carriers and conductivity (an increase in the electrical resistance). When the PANI is purged with clean air, the process is reversed, and the PANI re-establishes its protonation and recovers its initial resistance [58].

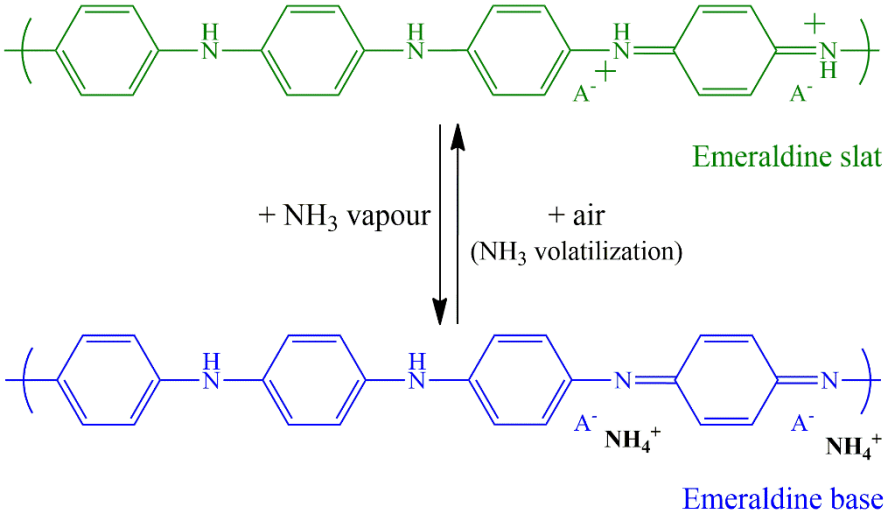

Figure 1.28: PANI-NH_3 gas-sensing mechanism (Adapted from [58]).

Conductometric or chemi-resistive sensors are composed of a sensing material that changes its conductance or resistance upon a reaction with the target analyte (no electrochemical reaction present). Such a sensor is composed of a sensitive material sandwiched between two contacting metal electrodes. The sensing principle is then based on measuring the resistance of the whole device (Figure 1.29) [38], [60]. Conventional materials for chemi-resistive sensors are represented by metal oxide semiconductors. Typical semiconductors (metal oxides such as ZnO) have p- or n-type conduction, depending on whether they conduct via holes (p-type) or electrons (n-type). They are used to detect either reducing or oxidizing gases, which influence their electronic properties upon interacting with them (covalent, hydrogen bonding or molecular recognition). In the case of p-type material, reducing gases (acceptors) will increase the resistance of the material, while oxidizing gases (donors) will decrease the resistance, and vice versa for n-type materials [66]. PANI was shown to be an excellent replacement for metal oxide semiconductors in gas-sensing applications [38]. It has a p-type conductivity [34], so its resistance will increase when it is exposed to a reducing gas (e.g., $NH_{3,(g)}$) and decrease after exposure to an oxidizing gas (e.g., $HCl_{(g)}$). The most significant advantages of PANI over metal oxides are its low cost, facile synthesis, tuneable conductivity, rapid response, and, most importantly, its ability to operate at room temperature. Metal oxide semiconductors operate at elevated temperatures of ~300–400°C [38].

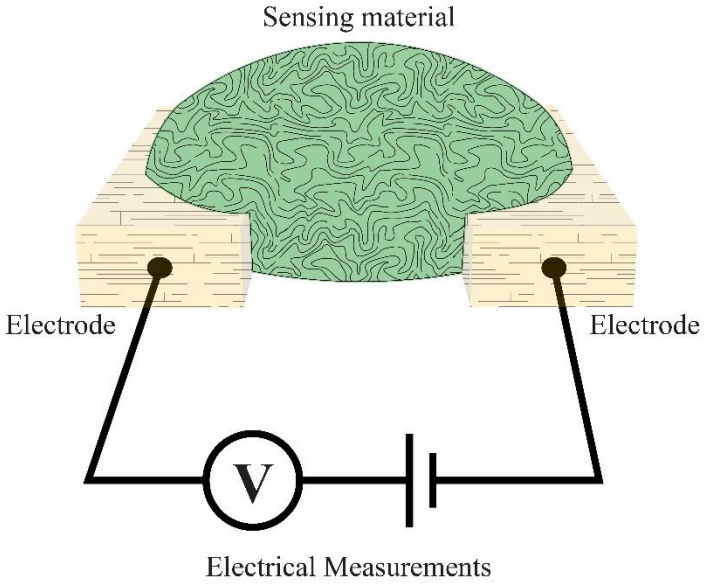

Figure 1.29: Configuration of a conductometric/chemiresistive sensor.

The classic measurement protocol for a chemi-resistive PANI sensor applied to NH_3-gas detection involves three stages (Figure 1.30a): i) exposure to pure air for an estimation of the initial resistance (R_0 [Ω]), ii) exposure to NH_3 gas, and iii) flushing the system with pure air for desorption and recovery. The behaviour of the sensing system is usually described by the sensor's response (Eq. 1.24), defined as the ratio of the change in resistance upon exposure to the target analyte (R_{max} [Ω]) to the sensor's resistance in clean air (R_0).

$$\text{Response} = \frac{(R_{\max} - R_0)}{R_0} \tag{1.24}$$

The curve in Figure 1.30a represents the "ideal" behaviour with an instant change in the electric property of the material, while the real-life time at which the sensor starts to respond is delayed from the switching time (i.e., analyte introduction) [67]–[71].

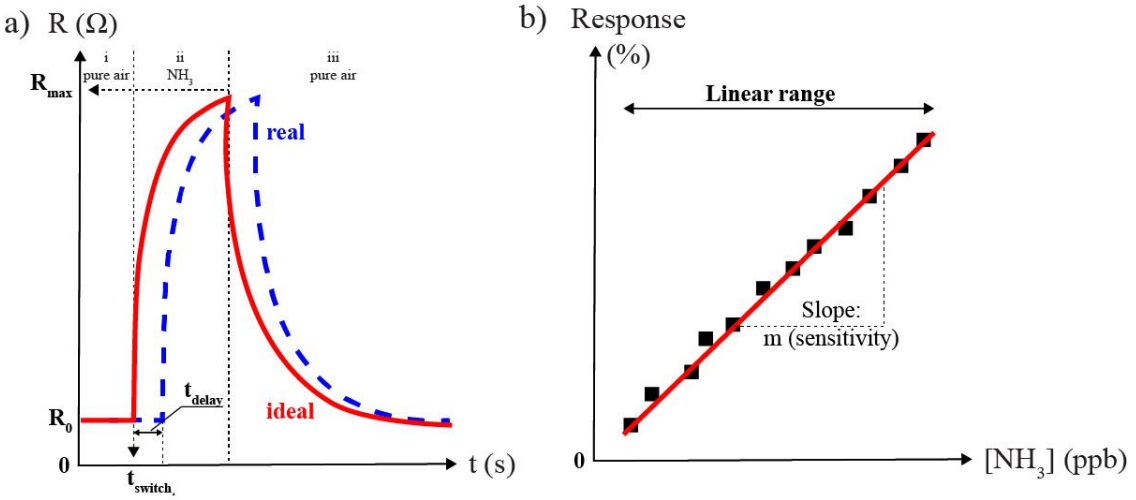

Figure 1.30: a) the dynamics of the chemi-resistive sensor's resistance change, and b) the relationship between the sensor output and the analyte concentration, commonly used for reporting analytical results.

In order to determine the analyte's concentration in a measured sample, the relationship between the maximum deviation of the output of a sensor for a known analyte concertation

needs to be determined, i.e., a "concentration calibration". Figure 1.30b is an example of a plot presenting the measured signal as a function of the concentration of the analyte, i.e., the calibration curve. The more the function fits to a linear relationship between the sensor's output and the concentration, the easier is the calibration. The calibration of the sensor gives us information about the limit of detection (LOD), the quantification limit, and the sensitivity. The LOD, quantification limit, sensitivity, response and recovery time are characteristics of the sensor that are always the targets of improvement by researchers. The LOD is the lowest analyte concentration that can be theoretically detected for a given sensitivity (Eq. 1.25) [72], [73]:

$$\mathrm{LOD} = \frac{3\sigma}{\mathrm{m_{slope}}} \tag{1.25}$$

where three corresponds to the signal/noise ratio, σ is the standard deviation of a blank, and m_{slope} is the calibration sensitivity (the slope of the calibration curve; Figure 1.30b). The sensitivity is the minimum input of analyte that will create a detectable output change. The quantification limit is the lowest analyte concentration that it is possible to be determined/measured using a given analytical procedure [72], [73]. The response time is the time required for the sensor to reach 90% of the maximum response, while the recovery time is the time required for a sensor to return to the baseline value after flushing it with pure air [60], [73].

The selectivity of the sensing material is the ability to detect the presence of the analyte of interest in the presence of other species [73]. PANI is known to be a highly selective material for NH_3 gas. Figure 1.31 presents a comparison between the response of NH_3 gas and other volatile organic vapours (ethanol, acetone, methanol, trichloro ethylene, and isopropanol). It is noted that the PANI response to NH_3 is much higher than for other gases. NH_3 increases PANIs' resistance, while other vapours (except acetone) decrease it. The selectivity of PANI to various gases arises from its qualitatively different response rates [67], [70], [74], [75]).

To boost the sensor's characteristics and overcome the PANI's limitations (e.g., the loss of conductivity with time, humidity effect), PANI as an NH_3-gas sensing material advanced from pure PANI doped with simple molecules ($HClO_4$ [76]) and polymers (polyurethane [75], poly(methyl methacrylate) [77]) to PANI doped with more complex species (dodecylbenzene sulfonic acid – DBSA, camphor sulfonic acid – CSA) [71]) and modified with nanomaterials (carbon nanotubes [78]–[80] and metal or metal oxide NPs (Au, TiO_2, SnO_2, ZnO)) [60].

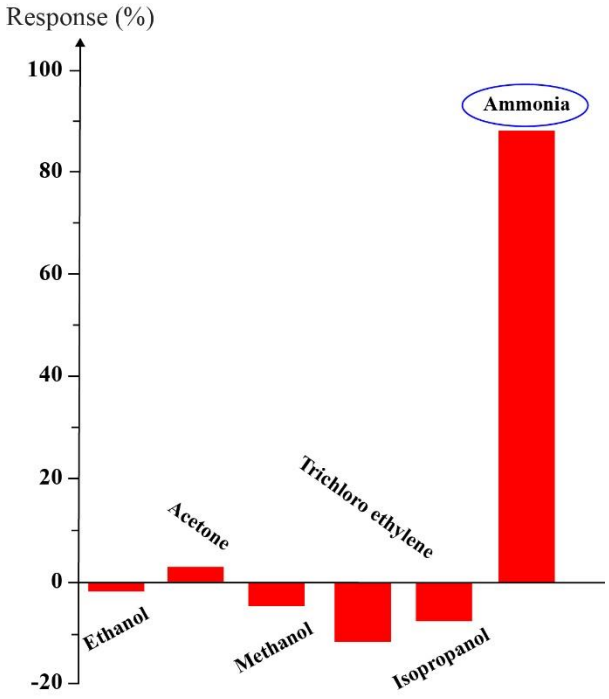

Figure 1.31: Response of PANI to NH_3 gas and other organic volatile-saturated vapours, showing the selectivity for NH_3 (Adapted from [74]).

Aqueous NH_3 detection is mainly based on the detection of the presence of ammonia's nitrogen by analytical techniques such as distillation-titration, chromatography (high-pressure liquid and ion chromatography), and phase molecular absorption spectrometry. However, these analyses require complicated sample preparation and equipment. In modern research, electrochemical methods are replacing complex analytical techniques, surpassing them with their lower cost, straightforward detection and user-friendly apparatus. The most used electrochemical method for the detection of ammonia's nitrogen is the application of ion-selective and nano-modified electrodes [81].

Ion-selective electrodes are an example of an electrochemical sensor composed of a sensitive membrane that is selective for the ions of interest. The most commonly used membrane for NH_4^+ detections is a polyvinyl-chloride-based membrane. When NH_4^+ passes the membrane, a potential is generated between the inside and the outside of the membrane. The correlation between the potential change and NH_4^+ can be determined from the Nernst equation (Eq. (1.9)). Considering the influence of the pH on the concentration ratio between NH_3 and NH_4^+, under more basic conditions (pH > 9.2), the molecular (non-ionic) form predominates. However, its presence can be determined by knowing the coefficient related to the percentage of non-ionic NH_3 (Eq. (1.23)). Thus, the overall concentration of the ammonia's nitrogen can be calculated.

A new direction in the development of ion-selective electrodes is the development of solid-state ion-selective electrodes. These are electrodes composed of an ion-selective film directly coated on the conductive substrate [81]. Due to its high affinity for ammonia, PANI was applied as an in-between solid contact to achieve a high electron transfer between the selective membrane and the conductive substrate. The resulting PANI solid-state ion-selective electrodes were successfully used for NH_4^+ potentiometric detection over a wide range of pH conditions [82]–[84].

Another feasible way of electrochemical detection of ammonia is observing its electro-oxidation. The electro-oxidation mechanism of ammonia (Ed. (1.26)) [85] is well known and widely accepted. It is performed by using electrocatalytic materials, normally noble metals such as Ru, Rh, Pd, Ir and Pt, of which Pt is recognized as the most effective [86]. To perform the electro-oxidation of NH_3, highly basic conditions are required to determine the presence of molecular ammonia [50], [86].

$$2NH_3(aq) \rightarrow N_2(g) + 6H^+ + 6e^- \qquad (1.26)$$

Besides metals, ammonia can be electrochemically detected directly on the PANI surface. Similar to the gas molecule, PANI also attracts a dissolved NH_3 in molecular or ionized form (Figure 1.28), the presence of which can be detected electrochemically. The electrochemical sensing mechanism depends on the form of dissolved NH_3 (molecular or ionized), determined by the pH of the working electrolyte. At high pH, predominant molecular form NH_3 (Figure 1.27b) deprotonates the conductive PANI. Applying an anodic potential, the PANI sensing layer is subjected to an oxidation reaction, the intensity of which is influenced by the presence of NH_3 [87]. Under neutral conditions (pH = 7), ammonia in the form NH_4^+ can be electrochemically detected due to its electro-reduction at the deprotonation sites in PANI. The sensing conditions of a sample should be determined by taking into account the future application of a sensor system, as the actual samples can disturb the operating pH and more importantly, they contain compounds and different ions that can interfere with the sensor's performance. Considering the sensing conditions, the electrochemical response can reflect the direct electrolytic oxidation of NH_3 using, for example, Pt-modified PANI [50], the reduction of NH_4^+ and its influence on the PANI's protonation [57] or the indirect re-oxidation of PANI, previously reduced due to NH_3 oxidation [87].

Chapter 2

Aims and Hypothesis

2.1 Aims

The purpose of this dissertation was to explore electrochemically synthesised polyaniline (PANI) for its further applications in ammonia (NH_3) detection. In order to achieve an effortless and straightforward procedure for electrode preparation, the PANI was electrochemically synthesized and deposited in a one-step procedure on a commercial screen-printed electrode (SPE) with Au working electrode (WE). Since PANI is NH_3 sensitive, the prepared electrode was tested for NH_3 gas and aqueous detection.
Accordingly, the dissertation aims to:

- Provide a straightforward synthesis procedure for the NH_3 receptor element in sensor applications based on electrodeposited PANI and commercial SPE;
- Provide an experimental study for understanding electrochemical aniline polymerisation, since it is important to understand PANI's conductive properties and behaviour and how they can be tailored to the NH_3-sensitive receptor element;
- Construct an NH_3-gas-sensing platform with a novel configuration based on electrochemically prepared PANI as a commercial three-electrode system;
- Electrochemically detect NH_3 in liquids with PANI in a neutral medium for potential biomedical applications.

The main goals of the dissertation are:
1. A construction of conductive and compact PANI deposited directly on commercial SPE;
2. Detailed study of PANI's electrochemical polymerisation process and its electronic properties;
3. Designing a NH_3-gas-sensing platform via the incorporation of electrochemically synthesised PANI deposited on a SPE three-electrode system;
4. Studying the PANI's electrochemical behaviour in a neutral medium to obtain the optimum parameters for aqueous NH_3 detection in biological samples;
5. Improving the electrochemical response of PANI to achieve better sensory performance regarding NH_3 electrochemical detection at neutral pH.

2.2 Hypothesis

2.2.1 Hypothesis 1

PANI can be synthesized via chemical or electrochemical routes. The polymer produced by chemical synthesis is usually deposited on a conductive electrode surface via drop-casting, which results in poor adhesion. If PANI is synthesized via an electrochemical route, it can be directly deposited on the electrode surface. PANI polymerization is most often performed in a highly acidic medium (pH < 1) to avoid the formation of short oligomers and to ensure a sufficient quantity of protons for further protonation. It has three characteristic forms of oxidation state: fully-reduced (leucoemeraldine), half-oxidized (emeraldine) and fully-oxidized (pernigraniline). The most conductive form of PANI is protonated emeraldine, i.e., the emeraldine salt form [28], [31]. For sensory studies, the most studied and desired form is emeraldine, which has semiconducting properties, and its transformation between the base and salt forms (deprotonated and protonated) is accompanied by a change in its electric and electrochemical properties [38], [58]. Electrochemical polymerization can be performed by applying a constant potential, a constant current or performing potential scans. Cyclic voltammetry (CV), a method for potentiodynamic polymerization, is known to give the strongest adhesion of the polymer to the electrode surface. During the CV, the aniline (ANI) monomer is subjected to basic polymerization steps, while the already-produced PANI is in the cyclic potential scans from approximately −0.2 V to 1.0 V vs Ag/AgCl subjected to electrochemical reactions: from leucoemeraldine to emeraldine (~0.2 V vs Ag/AgCl) and further to pernigraniline (~0.8 V vs Ag/AgCl). The rate-determining step of PANI electropolymerization is ANI oxidation with a standard potential of 0.9 V vs SCE. Therefore, a sufficiently high potential must be applied for the polymer to synthesise. However, the potential should not exceed 1 V vs SCE. Otherwise, the polymer can be over-oxidized and degraded [28], [31]. For these reasons, the potential range between −0.3 and 1.0 V vs Ag/AgCl should ensure a high-quality product for later applications.

According to Faraday's first law of electrocatalysis, the deposited polymer's mass on an electrode is directly proportional to the charge ($m \propto q$). The charge involved in the electrochemical experiment can be obtained from the integration of the peak from the CV, i.e., the surface area below the peak, by dividing it by the scan rate (υ; Eq. 2.1) [1], [88], [89]:

$$q = \frac{1}{\upsilon}\int_{E_1}^{E_2} i\mathrm{d}E \tag{2.1}$$

Each completed cycle in the polymerization process results in an increased current, indicating polymer growth. The first oxidation peak, indicating the transformation from leucoemeraldine to emeraldine, is the only peak containing information about the produced polymer. Therefore, with its integration, the charge connected with PANI formation and the mass can be estimated [88], [89]. We assume that by controlling the height of the first oxidation peak, reproducibility of the electrode's preparation will be achieved.

With regards to the **1st aim** and the previously described facts, we hypothesise that by performing CV using a strongly acidic medium (1 M HCl) and a potential range between −0.3 and 1.0 V vs Ag/AgCl for the electrochemical synthesis, the produced PANI will be directly deposited on the surface of the SPE's working electrode. Moreover, electrochemical polymerization should give a more uniform and compact deposit, an important factor when constructing a sensor material. Performing polymerization in strong acid prevents the formation of undesired products and is a source of protons for achieving a highly doped PANI and maximum conductivity.

2.2.2 Hypothesis 2

PANI is known for its tuneable electrochemical, electronic, and optical properties, which are interconnected. Correlated changes in the electrochemical and optical properties place PANI among the electrochromic materials [27]. The origin of the conductivity is the formation of charge carriers: nonlinear excitation in the form of polarons, bipolarons and solitons. Their formation is associated with the energy changes in the band gap, and these are with a specific form of PANI (leucoemeraldine, emeraldine or pernigraniline as a salt or base). Therefore, by

observing PANI's optical changes due to the change in the oxidation state, the formation of charge carriers can be determined and vice versa [16], [22].

Regarding the **2nd aim**, we hypothesise that performing a spectro-electrochemical experiment that combines electrochemistry and spectrophotometry *in situ*, would make a powerful tool for exploring the correlation between the electrochemical and optical behaviours of PANI. PANI's electrochemical synthesis consists of polymer formation, oxidation/reduction, and protonation reactions during polymerisation in acidic media. PANI has a different electronic structure in each oxidation/reduction and protonation state due to the formation of electronic states, accompanied by an optical colour change [38]. Therefore, we postulate that performing a spectro-electrochemical experiment during the PANI's polymerisation will give detailed information regarding the electronic changes connected to the electro-polymerisation process, and the final product deposited on the SPE. The output information will give us an insight into the polymerisation, at which stage of the experiment polymer starts to grow, the form of the final product and which stage of the polymerization process introduces the largest changes in the electronic structure of the PANI. The obtained data will be used to estimate the PANI's electronic-property changes upon electropolymerization, depending on the applied electrochemical parameters, such as the scanning potential range and the quality of the final product in terms of conductivity, an essential feature for further research.

2.2.3 Hypothesis 3

PANI is a widely used conductive polymer for NH_3 sensing based upon their similarities in protonation through nitrogen atoms. As a p-type semiconductor, PANI loses protons in the presence of NH_3 gas, leading to the loss of charge carriers and conductivity. However, the conductivity decrease is reversible since, after cleaning with pure air, PANI reclaims its protonation from NH_4^+. PANI has excellent performance as a gas sensor at room temperature, which makes it more attractive and applicable compared to typical metal/metal oxide semiconductors, as they operate above ~300°C [58], [65].

The most common PANI-NH_3 gas-sensing systems are based on interdigitated electrodes with multiple "fingertips" and drop-casted chemically synthesized PANI [71], [75], [78], [90], [91]. In this case, the PANI is sandwiched between two solid-state electrodes. Electrochemical synthesis has several advantages compared to chemical synthesis, such as easier control over the film thickness and the production of a compact layer of PANI, deposited directly on the electrode surface with good adhesion [31]. However, for successful electro-polymerisation directly onto interdigitated electrodes, the gap between the "fingertips" must not exceed 1–10 µm [61], [91]. Despite the small gap, the direct polymerization of such electrodes presents difficulties in the sense of electrode connection and electrochemical cell set-up.

SPEs are small electrochemical devices composed of printed electrodes (from conductive ink) on a ceramic or plastic substrate. Their development was a step towards the miniaturisation of electrochemical devices and the required sample volumes and lowering production costs [7]. Therefore, they are suitable for application in the field of sensors. As a three-electrode system, SPEs are suitable for the direct electrochemical polymerization of PANI on the working electrode. However, the gap between the electrodes (working, counter, and reference) is too big for conductometric measurements. Suppose that we create/deposit a thin layer of conductive material on the SPE electrodes to create PANI sandwiched between two contacts, the SPE, a three-electrode system, can be used as a conductometric sensor platform.

Regarding the **3rd aim**, we postulate that electrochemically prepared PANI deposited on SPE will be effective as a sensory platform for resistivity measurements upon exposure to NH_3 gas. The facile and straightforward approach to transforming the SPE into an NH_3 gas sensor can compete with more complex systems based on chemically synthesised PANI modified with nanomaterials and PANI-polymer blends.

2.2.4 Hypothesis 4

PANI loses its conductivity when the pH is above 5 as it starts to deprotonate. However, the exact point of the protonation loss depends on the nature of the protons and the counter ions [28], [43]. Regarding the **4th aim,** we hypothesise that electrochemically synthesized PANI will retain sufficient conductivity in a neutral medium by applying optimum electrochemical

parameters, e.g., suitable applied potential (between 0.0 and 0.4 V vs Ag/AgCl) to obtain emeraldine, which would retain the PANI's conductivity due to the redox doping. In that case, the deposited PANI will be suitable for electrochemical sensory experiments at neutral pH values, which will make the sensory system suitable for use in biomedical applications. If we pass the threshold of pernigraniline formation, the conductivity will be lost, and the electrode will be difficult to restore to its initial properties. Therefore, the selection of electrochemical parameters will play a crucial role. Since NH_3 in the gas phase has a deprotonation effect on PANI, it is expected to see a conductivity change also due to the aqueous NH_3.

2.2.5 Hypothesis 5

It is well known that the modification of conductive polymers with nanomaterials can improve their properties and applicability. Nanomaterial modification transfers the physicochemical properties of the modifier to the electrode surface. Different types of nanomaterials (such as metal, metal oxide nanoparticles) can improve the polymer's mechanical, optical, and electrical properties. For example, modification with carbon nanomaterials is known to produce a high-surface electrode with improved thermal and electrical conductivity and mechanical strength [92].

To obtain the best combination of polymer and metal modifier, it is important to know their basic electronic properties as the position of the metal's Fermi level and the lowest unoccupied molecular orbital in a polymer. The electrical properties of the polymer-metal contact are defined by the position of both [93]. PANI with p-type semiconducting properties [34] can be combined with a high-work-function metal such as Au (5.2 eV), forming low-resistance ohmic contacts [93]. Regarding the **5th aim**, hypothesis 5 is the following: Suppose PANI is decorated with Au NPs, the formed composite material has a better ohmic contact between the metal and the polymer, influencing the PANI's electrical character. Indeed, the smaller the particle diameter, the higher the relative surface area, and presumably the higher the output. However, we must distinguish between the morphological surface increase in the overall surface and the increase of the electrochemically active surface area. As active site for NH^{4+} absorption is the PANI, thus it needs to be exposed to the analyte as much as possible. The influence of added Au NPs is hypothesized to have the following effect. According to the fundamental resistance formula (Eq. 2.2).

$$R_r = \frac{\rho L}{A} \tag{2.2}$$

where R_r is the resistance [Ω], L is the length [m], A is the cross-section [m^2], for a round particle $A = \pi r^2$], and ρ is the resistivity [characteristic property, Ωm] [94], the larger the particles the smaller is the resistances. Thus, the largest Au NPs make the largest contribution to the electric conductivity. If this is the case, the Au NPs' presence and size will influence the PANI's sensory performance with respect to NH_3 in the sense of better sensitivity, achieving a lower detection limit.

Chapter 3

Experimental

The central challenge of this doctoral thesis is to study electrochemically synthesised polyaniline (PANI) and its use for ammonia (NH_3) detection. The work is divided into three parts:

- Spectro-electrochemical study of electrochemically prepared PANI;
- Electrochemically prepared PANI for NH_3 gas sensing;
- Electrochemically prepared PANI for NH_3 aqueous detection.

3.1 PANI Synthesis

The electrochemical synthesis of PANI was chosen due to the direct deposition being onto the metal electrode, which should ease its subsequent use for electrochemical sensing. The PANI was electrochemically polymerised by cyclic voltammetry (CV) using a 0.1 M aniline monomer in a highly acidic medium (1.0 M HCl). Depending on further investigations, the polymerisation process was performed directly on a SPE or using a Teflon cell. In the spectro-electrochemical study and NH_3 gas sensing (the first and second parts), the polymerisation was performed directly on the SPE, composed of a Au working electrode (WE), a Pt counter electrode (CE) and a Ag quasi-reference electrode (RE). For the NH_3 aqueous detection, the SPEs' CE and RE were protected using an electrochemical cell, and only the SPEs' Au WE was exposed to the electrolyte. An external Pt mesh and Ag/AgCl were used as the CE and RE. PANI polymerisations were performed in the potential range between – 0.3 and 1.0 V vs RE at 50 mV s^{-1}. The first oxidation peak in the CV PANI polymerisation process contains information regarding the charge of the deposited material. Therefore, the end of the polymerisation process was set by the current of the first oxidation peak. After the polymerisation, the electrode was washed with methanol or ethanol and dried in the air.

3.2 Spectro-electrochemistry

The spectro-electrochemical experiments were performed using an instrument that combines a light source, a bipotentiostat/galvanostat, and a spectrometer with a UV–vis wavelength range. PANI is an electrochromic material, meaning it undergoes a visible colour change due to its redox reactions [19]. Therefore, the device was used to observe the CV polymerisation process and the PANI's electrochemical behaviour in an acidic medium. The polymerisation was performed as described in a previous section by placing an 80 µL drop of monomer suspension on the SPE, in a specifically design cell. After the polymerisation, the electrode was washed with methanol. Spectroscopic measurements from 200 to 900 nm were performed *in situ* by installing an optical probe in the closed cell during the polymerisation. Separately, pure Au-SPE and all the oxidation forms of PANI were observed using UV–vis in the range 200 to 900 nm in air. Different oxidation forms of the deposited PANI were obtained by performing CV in 10 mM HCl, from −0.4 to 0.5 V vs Ag at 50 mV s^{-1} and stopped at a certain potential (−0.2, 0.2 and 0.5 V vs Ag).

3.3 Material Characterization

The morphology at every stage of the electrode preparation was investigated with field-emission scanning electron microscopy (FEG-SEM) Jeol JSM-7600F and Verios G4 HP. In the second and the third parts of the thesis, the secondary-electron images of a top view and a cross-section of a Au WE before and after the PANI polymerisation were compared. In the third section, the backscattered images were included to reveal the position of the added Au nanoparticles (NPs) on the surface of the PANI. The transmission electron microscopy (TEM, EOL JEM-2100) was used to characterize the size of the commercial Au NPs.

The surface relief of the Au WE was examined using a three-dimensional (3D) mapping carried out with a Stylus profilometer DEKTAK (Bruker) having a resolution 0.3 nm in the x, 1 µm in the y, and 0.1 nm in the z directions.

The PANI produced, ready for the detection of NH_3 gas, was characterized with Fourier-transform infrared (FTIR) spectroscopy, using an ATR (attenuated total reflection) crystal with an ATR FTIR Frontier L1280018 spectrometer (Perkin Elmer). A spectrum was obtained by sampling 20 interferograms with a resolution of 4 cm^{-1} in the range 500–4000 cm^{-1}. FTIR analysis provided information on the presence of chemical bonds, based on which the form of PANI was determined.

3.4 Resistivity Measurements

In the second stage, electrochemically prepared PANI via CV on a commercial SPE was used for NH_3 gas sensing. The gas sensing was performed in a dynamic exposure chamber composed of a gas and humidity inlet and outlet controlled by a gas-generation and dilution system. The system contained additional humidity and an NH_3 analyser to control the sensing parameters and conditions better. The sensor resistance was measured continuously with a computerised digital multimeter as a function of the NH_3/humidity concentration and the exposure time.

3.5 Electrochemical Detection

The effect of aqueous NH_3 on PANI in a neutral medium was studied via two electrochemical techniques: CV and chronoamperometry (CA). CV gave information on the PANI behaviour in a neutral medium and the optimal potential for further investigation. Later, a method with a constant applied potential was introduced to avoid the PANI's electrochemical modification due to potential scans. CA enabled fixing of the PANI's electrochemical properties and observing its responses to NH_3 additions.

Chapter 4

A Correlative Study of Polyaniline Electropolymerization and its Electrochromic Behaviour

The aim of this thesis was to study electrochemically synthesized polyaniline (PANI) for ammonia-sensing applications. In this Chapter we focus on understanding PANI, what is the result of the electropolymerization process, how the electronic properties change during the polymerization and which parameters are important for consideration to achieve the product with the desired electronic properties.

PANI can be prepared using chemical or electrochemical synthesis. When aiming for the direct deposition of PANI onto the electrode surface, we chose to perform electrochemical synthesis. i.e., electropolymerization. It was performed in a strong acidic medium (1 M HCl) and via the potentiodynamic technique of cyclic voltammetry (CV) on a commercial screen-printed electrode (SPE). The ANI monomer/HCl electrolyte was cycled (between 21-24 cycles) in the potential range between −0.3 and 1.0 V vs Ag at 50 mV s^{-1}. Despite a successful synthesis and deposition, the current-potential relationship obtained by CV alone does not provide information regarding the optical and electric properties, which are correlated with the electrochemical properties.

PANI is a mixed-oxidation-state polymer with three characteristic states, depending on the oxidation degree (leucoemeraldine, emeraldine and pernigraniline), each with a distinctive colour. Thus, its electrochemical and optical properties are interconnected. Since optical properties reflect not only the change in the oxidation stage, but also changes in the band-gap structure due to the formation of new electronic bands, the electrochemical-optical information also gives an insight into the electronic properties [19], [38].

To investigate PANI's electrochemical polymerization in the sense of a combination of electrochemical and optical data, the electropolymerization process was performed with a spectro-electrochemical technique, performing electrochemical and spectroscopic measurements simultaneously. The PANI was electrochemically synthesized via CV in a specific electrochemical cell, constructed to insert an optical probe, which enabled an *in-situ* experiment of spectro-electrochemistry. The spectro-electrochemical experiments resulted in electrochemical data for CV electropolymerization accompanied by absorption data for 200–900 nm wavelengths. With the data obtained from the CV we determined the electrochemical processes that occur during the polymerization according to the positions of the anodic/cathodic peaks. These are the oxidation of aniline and transformations between leucoemeraldine, emeraldine and pernigraniline. Furthermore, the addition of spectroscopic data gave an insight into the stages of polymerization not visible with the CV. That is the beginning of dimer formation, which part of the cycle undergoes changes, such as protonation, and the conformation of the final product shape.

Our study explains the electrochemical behaviour of PANI during the polymerization process with spectroscopic measurements. By comparing the absorption data obtained at important potentials regarding the CV (−0.3, 1.0 V and all peak potentials), the conclusions are as follows:

- The dimer formation takes part after 6 cycles for given conditions;

- The increasing and decreasing absorbance associated with the quinoid ring is correlated with the emeraldine oxidation to pernigraniline and vice versa;
- The absorbance peaks associated with transitions in the HCl-doped PANI have the highest intensity during the reduction, proving the protonation during the reduction scan and backward deprotonation during the oxidation scan;
- Ending the polymerization at −0.3 V results in an intermediate state of PANI called proto-emeraldine, which is oxidized to emeraldine after exposure to air. Due to the polymerization on a highly acidic medium (1 M HCl), the final product is therefore emeraldine salt.

More on this topic is provided in the article entitled "A Correlative Study of Polyaniline Electropolymerization and its Electrochromic Behaviour", authored by Anja Korent, Kristina Žagar Soderžnik, Sašo Šturm and Kristina Žužek Rožman, published in Journal of the Electrochemical Society, Vol. 167, No. 10, in 2020 [95]. The article is presented on page 51. The presented section achieves the **1st and 2nd aims** of constructing a conducive and compact PANI deposited on a SPE and a detailed study of the process and the product.

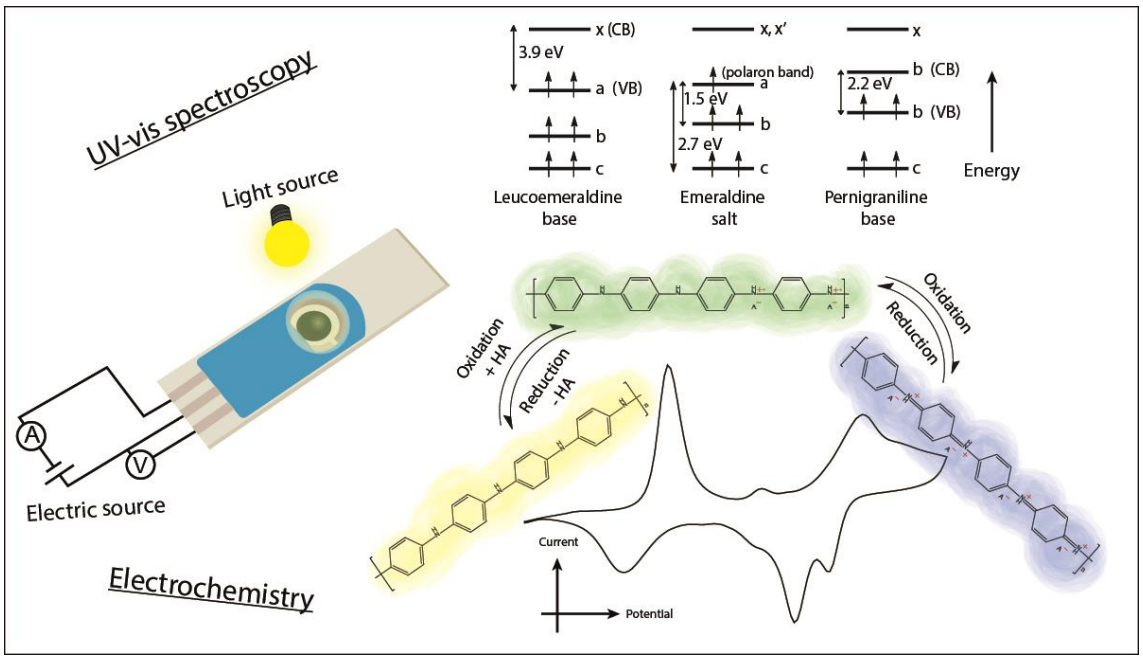

Figure 4.1: Graphical abstract for Chapter: A Correlative Study of Polyaniline Electropolymerization and its Electrochromic Behaviour.

Journal of The Electrochemical Society, 2020 **167** 106504

A Correlative Study of Polyaniline Electropolymerization and its Electrochromic Behavior

Anja Korent,[1,2,z] Kristina Žagar Soderžnik,[1] Sašo Šturm,[1,2] and Kristina Žužek Rožman[1,2]

[1]*Jožef Stefan Institute, Department for Nanostructured Materials, SI-1000 Ljubljana, Slovenia*
[2]*Jožef Stefan International Postgraduate School, SI-1000 Ljubljana, Slovenia*

The electrochemical polymerization of polyaniline (PANI) was studied using correlative measurements of electrochemistry and UV–vis spectroscopy, i.e., spectroelectrochemistry. The electropolymerization of PANI was performed in an acidic medium (1 M HCl) containing 0.1 M aniline with cyclic voltammetry (CV) in a potential window from −0.3 to 1 V and a 50 mV s^{-1} scan rate. At the same time, UV–vis absorbance spectra in the wavelength range from 200 to 900 nm were measured for every 10 mV change in the CV. The CV results show the oxidation of the monomer at a high positive potential (0.9 V vs Ag), the continuous growth of the PANI film and the transformation between the three best-known forms of PANI redox in the potential range between −0.3 V and 1 V. In parallel, the spectroscopic study confirmed the formation of PANI oxidation. The spectroscopic results showed the formation of the final conductive PANI product (emeraldine salt) due to the absorbance of the formed charge carriers (polarons, bipolarons) during the polymerization. The correlative electrochemical/spectroscopy study gave an additional dimension to the PANI polymerization mechanism, where not only was the oxidation the lead type of reaction, but the reduction was also found to play an important role.

 [DOI: 10.1149/1945-7111/ab9929]

Manuscript received March 31, 2020. Published June 11, 2020.

Conductive polymers are synthetic organic materials that can possess metallic conductivity due to their specific π-electronic configuration. One representative is polyaniline (PANI); it has a tunable morphology, environmental stability, controllable electrical conductivity, reversible redox chemistry and can be easily synthesized at low cost.[1,2] This makes PANI suitable for various sensor applications, such as ammonia sensing,[3–6] humidity sensing,[7,8] pH sensing,[9,10] the base material for sensing via molecular imprinting[11] and as a substrate for biosensing.[12] PANI can be synthesized via chemical or electrochemical means,[13] with the latter having several advantages as there is no need to use a toxic oxidizing agent such as ammonium persulfate.[14] In addition, it offers a more straightforward procedure, a direct deposition on the electrode surface, an easier control over the deposition parameters and, consequently, over the thickness and the morphology of the final product. Potentiodynamic deposition via cyclic voltammetry (CV) can be used for the deposition of nanostructured PANI of high purity and in a doped form.[13,14] The term doping refers to the exposure of the polymeric chain to an oxidation or reduction process. As a result, the polymer is transformed from a neutral form to a complex of a positively or negatively charged polymer and its counterion. Such complexes act as charge carriers and are the source of the conductivity.[15] PANI has charge carriers in the form of polaron (radical ion associated with the lattice distortion and the presence of localized electronic states in the gap) and bipolaron (pair of like charges associated with a strong local lattice distortion).[16]

The electrochemical synthesis, i.e., the electropolymerizaiton of PANI, follows a four-step process[13,14] (Fig. 1): 1. formation of a primary cation-radical (oxidation of the monomer at the anode); 2. formation of dimers through deprotonation and re-aromatization; 3. further growth and chain formation with oxidation (oxidation of dimers to a cation-radical and their further reaction with monomer cation-radicals); 4. the last step is a spontaneous doping of the resulting polymeric chain to obtain the polymer in a doped form, which is only the case for the electrochemical approach.[13] The structure of the final PANI polymeric chain is a combination of two repeating units: oxidized (quinoid rings) and reduced (benzene rings). Depending on their ratio and the oxidation state, PANI has three stable characteristic oxidation forms: x = 1 − leucoemeraldine (fully reduced form), x = 0.5 − emeraldine (half-oxidized form); x = 0 − pernigraniline (fully oxidized form)[17,18] (Fig. 1).

The protonation of PANI during the CV sweep is a spontaneous exothermic reaction, which is inevitable in the presence of acid dopants.[19] Due to the presence or absence of a proton, the PANI forms are divided into salts (protonated) and bases (unprotonated), with their conductivity varying, depending on their oxidation state (number of electrons) and degree of protonation (number of protons). The emeraldine salt form (half-oxidized leucoemeraldine in acidic electrolyte, which has a characteristic green color) is the most conductive form of PANI.[1] Emeraldine salt is obtained at an anodic potential of around 0.25 V vs Ag/AgCl in an acidic medium (HCl, pH = 1) during the CV sweep.[1] It has an equal ratio between the amine (–NH–) and imine (=N–) groups. Via acid doping, the imine sites are protonated to bipolarons (a double-charged salt), which further undergoes a rearrangement to form delocalized polarons (radical-cations) that act as charge cariers.[20]

PANI is also an electrochromic material, meaning it undergoes visible color changes, i.e., absorbance changes, due to the reversible redox processes of doping and de-doping mediated by either oxidation or reduction. These changes are closely related to the energies of the band gaps of PANI, obtained from optical measurements via Planck's constant and the speed of light. Thus, the color changes can be interpreted via the formation of sub-bands due to the presence of charge carriers as polarons or bipolarons.[15] By using CV as an electropolymerization technique, a transformation between the reduced, half-oxidized and oxidized PANI forms[14] can be observed, either by following the electrochemical or even the absorption responses.[13] PANI also exhibits chemiresistive properties[21] and is widely studied as a gas-resistivity sensor,[3–5] due to the changes in electrical resistance in response to changes in the chemical environment. In addition, as an electrochromic material, PANI shows potential for optical sensing devices,[6] where the color change is dependent on the transformation between the conductive and isolative forms of PANI.[15] By combining the information from the electrochemical deposition process[12,22–24] with the spectroscopic behavior of PANI, the theory relating to the mechanism of PANI electro-oxidation, deposition and its simultaneous doping and protonation can be revealed in more details using complementary techniques.

In this study a new aspect of the electrochemical deposition of PANI via the potentiodynamic technique CV is presented using correlative experiments of the electrochemistry and UV–vis

[z]E-mail: anja.korent@ijs.si

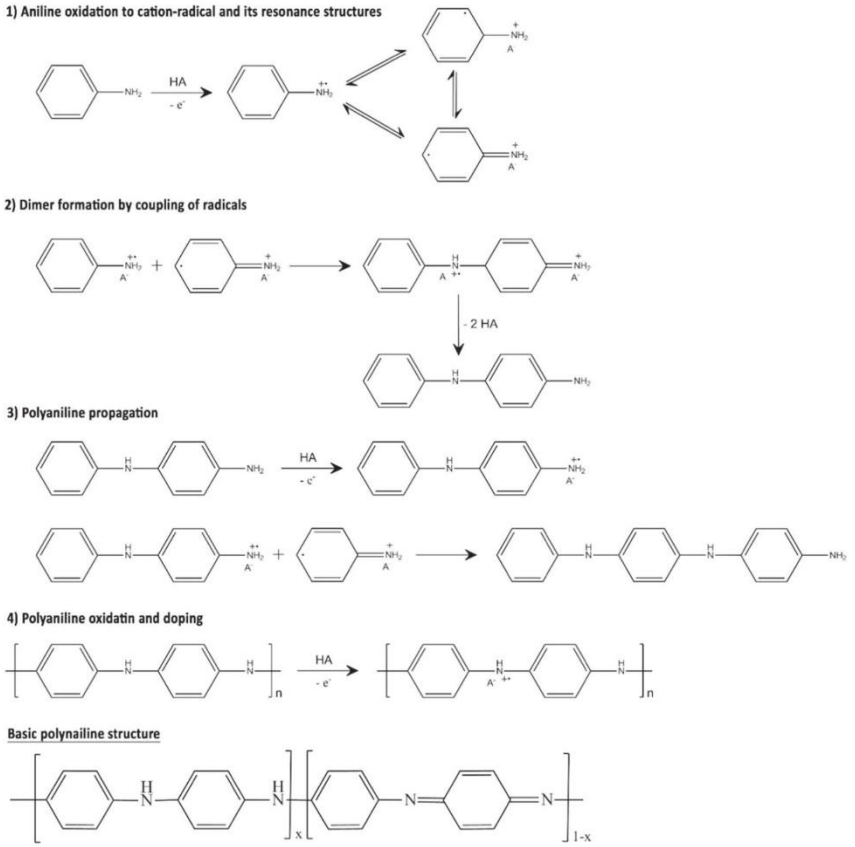

Figure 1. Mechanism of electropolymerization of polyaniline.[13,14]

spectroscopy. From the CV results, three voltammetric redox pairs are observed, which are correlated with gold oxidation/reduction, aniline monomer oxidation, the redox behavior of PANI, and show the current increase after every subsequent cycle, i.e., deposition rate. In contrast to the electrochemical information derived from the CV results, spectroscopy gives an insight into the electronic structure of PANI. The absorbance for π-polaron, polaron-π* and bipolaron transitions confirmed the formation of sub-bands, thus lowering the band gap of PANI and causing a higher conductivity. By combining the CV and the spectroscopy, it was found that the PANI formation mainly proceeds via electro-oxidation. However, during the electroreduction process new and unexpected absorbance peaks appeared, implying that the investigation of reduction processes during the electropolymerization is of equal importance.

Experimental

Commercial DropSens screen-printed electrodes (SPE; Metrohm DropSens, ref. SPE-250AT),[25] with gold as the working electrode, platinum as the counter electrode and silver as the reference electrode, were used for the electrochemical deposition of polyaniline (PANI). Electropolymerization was performed from a monomer suspension, containing 0.1 M aniline (Sigma Aldrich) in a 1 M HCl-containing electrolyte with pH = 0.43 (37% HCl Sigma Aldrich). All the spectroelectrochemical experiments were performed using a SPELEC instrument[26] (Metrohm DropSens), which combines a Lightsource (UV-vis-NIR wavelength range: 215–400 nm deuterium, 360–2500 nm tungsten halogen), a bipotentiostat/galvanostat (±4 V DC potential range, ±40 mA maximum measurable current) combined with a spectrometer with a UV–vis wavelength range: 200–900 nm (ref. SPELEC). The instrument was lent by the representative PRIMAlab, Slovenia for a correlative study of PANI polymerization and its spectroscopic behavior. The polymerization was performed via cyclic voltammetry (CV), by placing an 80 μl drop of monomer suspension into the cell (Fig. 2a) and performing cycles between −0.3 and 1 V vs Ag at a sweep rate of 50 mV s^{-1}. The polymerization was stopped at the end of the cycle in which the first anodic peak achieved a 1.5 mA current.[27,28] After polymerization (Fig. 2b), the electrode was washed with methanol to remove any residual monomer suspension and unattached PANI. Spectroscopic measurements from 200 to 900 nm were performed in situ during the polymerization by installing an optical probe in the closed cell (Fig. 2a). Separately, pure Au-SPE and all the oxidation forms of PANI were observed using UV–vis in the range 200 to

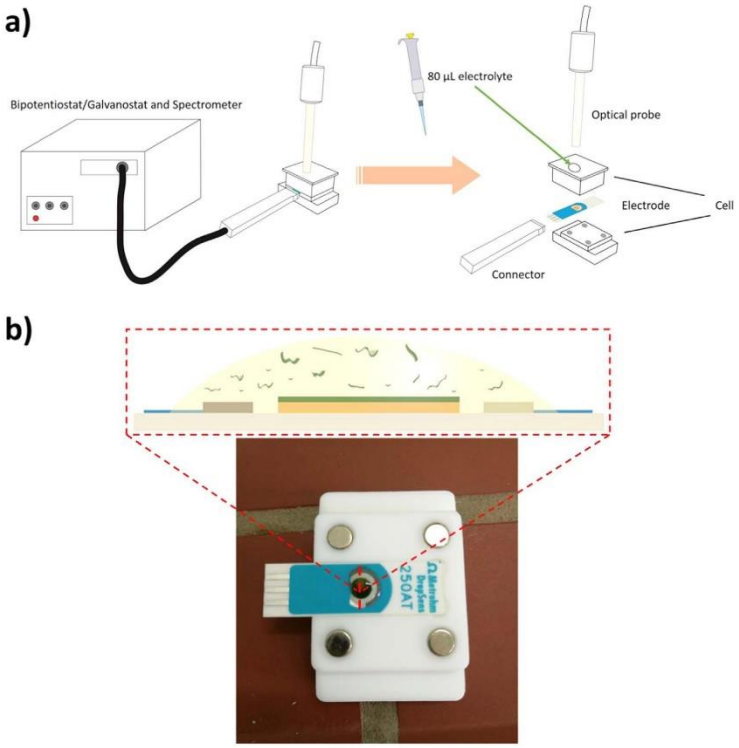

Figure 2. (a) Schematic presentation of in situ spectroelectrochemical measurements with a detailed representation of the measuring cell where an 80 μl drop of aniline was introduced; (b) Au screen-printed electrode (Au-SPE) after the polymerisation of polyaniline (PANI) by cyclic voltammetry (CV). The enlarged scheme shows a cross-section of PANI-Au-SPE covered with a drop containing the residual monomer suspension and unattached PANI.

900 nm in air. Different oxidation forms of deposited PANI were obtained by performing CV in 10 mM HCl (37% HCl Sigma Aldrich), from −0.4 to 0.5 V vs Ag at 50 mV s^{-1} and stopped at a certain potential (−0.2, 0.2 and 0.5 V vs Ag).

Results and Discussion

The electrochemical deposition of the PANI film on the commercial Au-SPE was performed by CV in an aniline monomer suspension at 50 mV s^{-1} and a potential window from −0.3 V to +1 V vs Ag. The electrochemical polymerization was performed in 1 M HCl electrolyte containing 0.1 M aniline, due to the better solubility of the monomer, the formation of the conducting form, and the avoidance of the formation of conjugated oligomers.[14] Figure 3a shows the first two completed polymerization cycles. Both cycles have similar anodic (E (a_2) = 0.9 V, E (a_3) = 1 V) and cathodic peaks (E (c_1) = 0.51 V). The only difference is in the shift of the anodic peak a1 from −0.13 V to −0.06 V. The first stage of polymerization (Fig. 3a) on an inert metal electrode (Au-SPE) in a monomer-acid suspension is the cleaning and activating of the electrode surface, as already observed in the literature,[29–32] and the first polymerization step (see Fig. 1). The anodic peak a_1 is expected to be a result of the Au electrode's nature (Au-SPE), considering that it does not appear in the CV during the polymerization on a polished gold wire[12] using the same conditions and it disappears with subsequent cycling, i.e., polymerization Figs. 3b, 3c. The anodic peak a_2 at 0.9 V (Fig. 3a) is attributed to the irreversible monomer oxidation [14,23] causing the formation of cation-radicals. The anodic peak a_3 most probably represents the formation of gold oxide, as it is not attributed to oxygen evolution. The oxygen evolves at potentials higher than 1.2 V (vs Ag/AgCl[32] and vs Ag[33]). The reduction of the gold oxide is represented by the cathodic peak c_1.

With further polymerization and increasing the number of cycles to 5, 10 (Fig. 3b) and 14, 16, 20 and 23 (Fig. 3c) more pronounced anodic peaks: E (α) = 0.16 V, E (β) = 0.44 V, E (γ) = 0.82 V and cathodic peaks: E (α^*) = 0.02 V, E (β^*) = 0.4 V, E (γ^*) = 0.53 V, E (γ^{**}) = 0.65 V appear. All the represented peak currents increase with each cycle, but retain the same potential, except that the last anodic peak γ is shifted towards a lower potential (Fig. 3b red curve E (γ) = 0.82 V to Fig. 3c blue curve E (γ) = 0.76 V). The anodic peak α is assigned to the oxidation of the dimer (p-aminodiphenylamine) to dimer cation-radicals,[30,34] which is the second polymerization step (see Fig. 1). The anodic peak α is also assigned to the oxidation of leucoemeraldine (a fully reduced form of PANI) to emeraldine (a half-reduced form of PANI).[12] The anodic peak β relates to the formation of the intermediate degradation products (p-benzoquinone) and later to its oxidation. The anodic peak γ is related to the oxidation of emeraldine to pernigraniline (a fully oxidized form of PANI).[12,22,23,34] The cathodic peak γ is split into two peaks, γ^* and γ^{**}, both assigned to the reduction of pernigraniline to emeraldine.[12,22,23,34] The splitting of the cathodic peak γ is related to the acidity of the electrolyte (1 M HCl, pH = 0.43), as at a

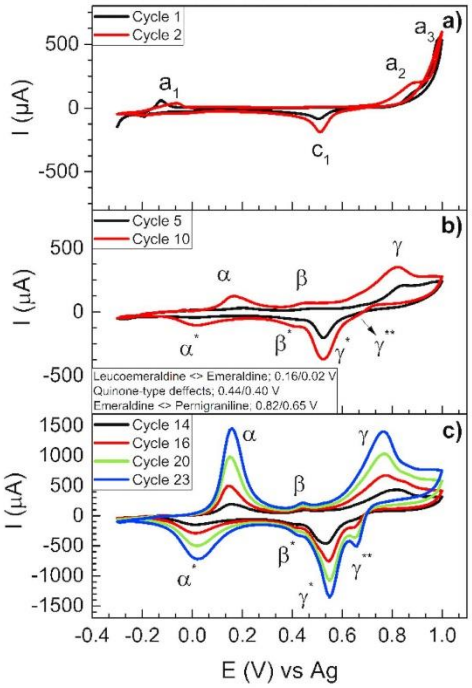

Figure 3. Electrochemical deposition of PANI via CV on Au-SPE. (a) Starting cycles; (b) the first occurrence of PANI formation and (c) further growth of PANI on Au-SPE.

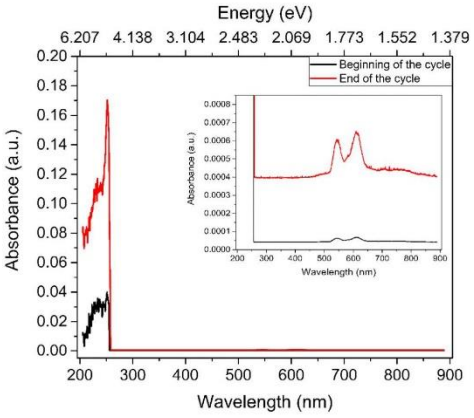

Figure 4. Absorbance spectra at the beginning and the end of the first electropolymerization cycle of PANI. Inset: Close up of absorbance.

lower concentration of HCl (0.5 M, pH = 1.5) the cathodic peak appears as a single wide peak at 0.65 V vs Ag/AgCl.[12] In the more acidic solutions, the redox couple γ/γ^* becomes more irreversible (Fig. 3c 0.76 V/0.55 V in 1 M HCl, and 0.74 V/0.65 V vs Ag/AgCl in 0.5 M HCl[12]), due to the hydrolysis of the imine N–C bond in the –N=(C_6H_4)= groups (quinoid rings) during the polymerization and formation of p-benzoquinone.[35] The cathodic peak β^* relates to the reduction of the intermediate degradation products, p-benzoquinone to hydroquinone. The cathodic peak α^* is related to the reduction of emeraldine to leucoemeraldine.[12,22,23,34]

Furthermore, the special feature of conductive polymers, particularly PANI, is their autocatalytic behaviour;[14,30] meaning, the further formation of the polymer on the already-deposited polymer layer is easier and faster than on the bare electrode. Zotti et al.[36] showed that aniline oxidation is catalyzed by pernigraniline. The above-mentioned can be observed by a rapid increase of the anodic peak α after each cycle, from 3.94 μA to 1500 μA (increased polymerization rate) and in the shift of the anodic peak γ towards lower potentials (from 0.84 V to 0.77 V) with an increased number of cycles.

Figure 4 shows the absorbance spectra measured on Au-SPE at the beginning (black curve) and the end (red curve) of the first polymerization cycle. At the beginning of the polymerization, the absorbance assigned to the presence of benzene rings in the region between 200 and 250 nm is observed. The benzene ring absorbs at 180, 200 and 260 nm due to its π electron system.[37,38] In the case of the substituted benzene (benzene containing a NH_2 group), the peak at 260 becomes more intense.[37] The absorbance peak at 250 nm is observed already at the very beginning of the polymerization (Fig. 4, black curve) due to the presence of a benzene ring in the monomer suspension.[39] There is no other evident absorbance in the first cycle of polymerization, apart from small absorbance peaks at 550 and 612 nm (inset in Fig. 4), which increased during the first cycle. Due to the absence of the aniline cation-radical at low oxidation potentials[13,14] and the intense increase in the absorbance with the number of cycles, it can be assumed that these peaks are related to the formation of the aniline cation-radical and the protonation of nitrogen[37] during the reduction process when the protonation is generated.[18] The black curve in the inset of Fig. 4 represents the absorbance spectra for Au-SPE in the monomer suspension and is the background for all subsequent spectroscopic results.

Figures 5 and 6 show the change in the absorbance behavior in the middle (12th cycle, Fig. 5) and at the end (the last 23rd cycle, Fig. 6) of the PANI polymerization via CV. From the cyclic voltammogram of the 12th cycle (Fig. 5a), potentials for the most important peaks were selected (−0.3, 0.14, 0.43, 0.74, 1 V vs Ag for oxidation and 1, 0.64, 0.53, 0.4, 0, −0.3 V vs Ag for reduction). The absorbance spectra for selected anodic peaks are presented in Fig. 5b, and for the cathodic peaks in Fig. 5d. In the middle of the PANI polymerization, two processes are expected: the ongoing polymerization of PANI due to the presence of the monomer aniline, and the electrochemical reactions of an already-deposited polymer (transformation between the PANI oxidation forms). From the basic PANI structure[17,18] (see Fig. 1), the peaks attributed to the benzenoid and quinoid rings' absorption are expected. At all the selected anodic and cathodic potentials, the absorbance spectra (Figs. 5b, 5d) show an intense peak at 255 nm (4.86 eV), which is assigned to the π-π^* transition (transition of an electron from the valance to the conduction band) of benzenoid segments. The anilinium ion ($C_6H_5NH_3^+$) shows a very similar spectra to benzene, due to the localization of the π electrons in the benzene ring, which causes a shift from 280 (for aniline) to 260 nm (anilinium ion).[37] The second peak observed in all the selected potential steps in the 12th cycle of the polymerization is the peak at 318 nm, which is associated with the π electrons of the benzene rings delocalized on nitrogen atoms[37] and the π-to-π^* transition of the benzenoid rings.[37,40] The wide absorbance peak around 400 nm can be assigned to the oxidized dimer of aniline, diphenyl-*p*-phenylenediimine, which absorbs at 440 nm[37,41] or to the polaron-π^* transition at the same wavelength.[40] Figure 5c shows a close up of the absorbance spectra between 500 and 545 nm. The small absorbance behavior can be assigned to the polaron-π^* electronic transition, related in the

Journal of The Electrochemical Society, 2020 **167** 106504

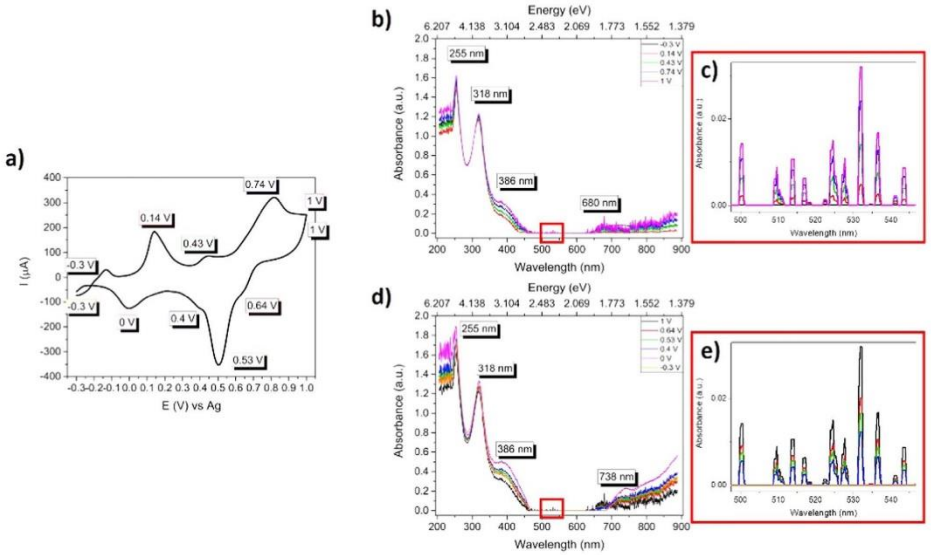

Figure 5. 12th cycle of PANI polymerization via CV: (a) cyclic voltammogram of the 12th cycle; (b) absorbance at certain potentials in the oxidation process; (c) absorbance at certain potentials in the reduction process.

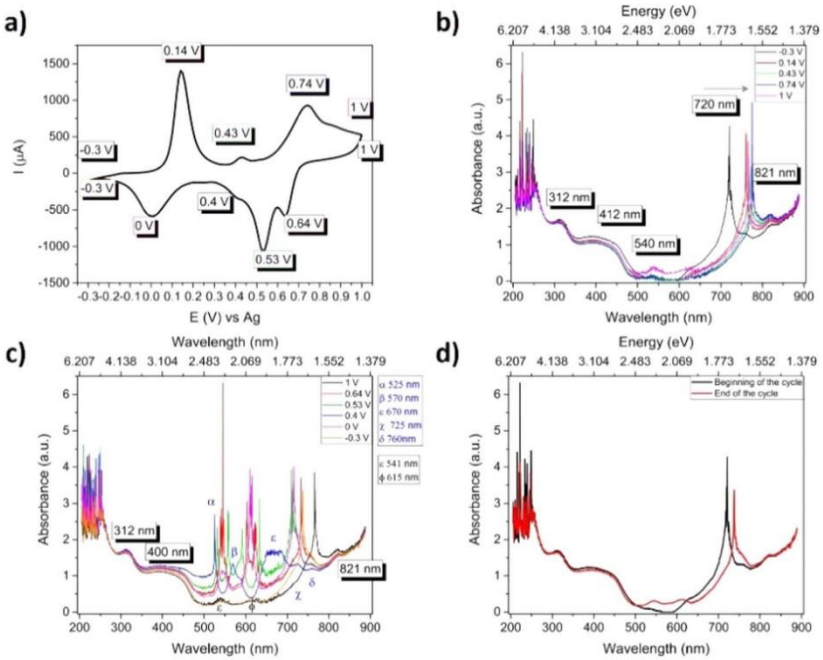

Figure 6. Last cycle of PANI polymerization via CV: (a) cyclic voltammogram of the last cycle; (b) absorbance at certain potentials in the oxidation process; (c) absorbance at certain potentials in the reduction process; (d) absorbance at the beginning and at the end of the last cycle (−0.3 V vs Ag).

quinoid rings in the PANI.[37,42] To summarize, at the starting potential (−0.3 V), of the cycle there are no absorbance peaks, but with further oxidation, the absorbance peaks increase in intensity until the end of the anodic scan at 1 V. The inverse behavior between 500 and 545 nm can be observed following the reduction process (Fig. 5e), where the absorption peaks' intensity is decreasing during the cathodic scan; meaning a lower concentration of quinoid rings is present. Based on this we can conclude that the absorbances around 500 nm start to increase because the transition from the emeraldine to the pernigraniline oxidation form occurs. At the potential 0 V, when emeraldine transforms to leucoemeraldine, the absorbance peaks decrease to zero. The band around 680 nm (1.81 eV) is assigned to the exciton absorption of the quinoid rings, which are attributed to the interchain or intrachain charge transport in PANI.[43] It is known that the nature of PANI doping influences the absorbance shifts of some characteristic absorbance peaks.[38,43] In the case of HCl doping, the band at 680 nm is red-shifted towards longer wavelengths.[42,43] The red-shift of this peak indicates an improvement in the emeraldine structure, correlated with an improvement in the degree of doping.[43] At 700–750 nm the spectra in Figs. 5b, 5d exhibit characteristic absorbances for the polaron-π transition.[40]

The last cycle of the polymerization (23rd cycle) (Fig. 6a) has identical peaks to the 12th cycle (Fig. 5a), only the peak currents are higher due to the larger amount of deposited PANI, as was already shown in Fig. 3. The absorbance spectra for the anodic peaks are presented in Fig. 6b, and for the cathodic peaks in Fig. 6c. In the range between 200 and 280 nm for the oxidation (Fig. 6b) and the same for the reduction (Fig. 6c) process, many intense and noisy absorbance peaks are observed. These absorbance peaks are assigned to the π-electron system in benzene, anilinium ions and possible sifts due to the substitution[37] (NH_2 group on benzene). As already discussed, during the polymerization, not all the produced PANI is attached to the surface of the electrode (see Fig. 2b). Unattached PANI can thus interfere with the light beam, causing the appearance of additional unknown peaks in the range 200 to 280 nm with a high intensity and noise. The absorbance peak at 312 nm is associated with the π electrons of the benzene rings, delocalized on nitrogen atoms[37] and the π-to-π* transition of the benzenoid rings.[37,40] This absorbance peak is unaffected by the doping of the polymer[18,43] and remains unchanged, despite the polymerization from the 12th to the 23rd cycle. The absorbance band at 412 nm could possibly be assigned to the polaron/bipolaron transition that occurs in doped PANI. Bhadra et al.[38] showed that absorbances between 340 and 370 nm and 550 and 650 nm are a consequence of this polaron/bipolaron transition. However, it is important to consider that this behavior was observed for p-toluenesulfonic acid[38] and not for HCl-doped PANI, and thus this explanation can only be used as a general case.

The absorbance around 540 nm in the oxidation part is more intense with the anodic scan's progress and shows the greatest absorbance at the most positive potential (1 V, Fig. 6b). The same behavior of the polaron-π* electronic transition, related to the quinoid rings in PANI, was observed in the 12th cycle (Fig. 5c). The absorbance peaks at 720 and 821 nm can be assigned to the red-shifted peak of the π-polaron transition in HCl-doped PANI.[44] With a higher degree of doping the peak at 720 nm is shifted towards the larger wavelengths (Fig. 6b). To conclude, despite the noise and highly intense absorbances between 200 and 280 nm, the spectra in the oxidation process do not show any new peaks in comparison to the 12th cycle (Fig. 5b). On the other hand, we observed the appearance of new peaks at different positions for each potential during the reduction process (Fig. 6c). This behavior is attributed to the transition from pernigraniline, to emeraldine, to leucoemeraldine. One possible explanation for the appearance of multiple peaks in the reduction process is the already-mentioned interference of unattached PANI in a monomer suspension, and as there is a limited amount of research conducted on PANI oligomers,[18,41] it is difficult to assign these observed peaks to specific processes. However, the polyaniline is, during the CV, subjected not only to electron transfer

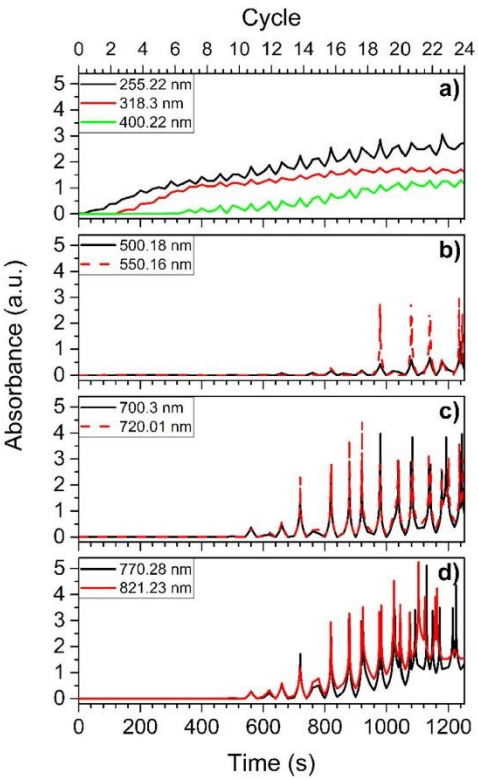

Figure 7. Absorbance of peaks of interest vs PANI electropolymerization time and the number of cycles.

due to the oxidation and reduction, but also to the protonation and deprotonation due to the acidic medium.[18] During the oxidation, the protonation is lost, but it is regenerated by the reduction.[18] The protonation does not only decrease the band gap of the PANI (making it more conductive); it also introduces shallow impurity states (defects in the PANI structure near the band gap),[19] which can contribute to the appearance of these multiple absorbance peaks. However, when leucoemeraldine is formed at the end of the cathodic scan, the system returns to the initial state, as shown in Fig. 6d. The only difference is in the red-shifted peak associated with the degree of protonation (720 to 770 nm).[44]

Figure 7 shows the time/no. of cycles evolvement of the most important absorbance peaks (255.22, 318.3 and 400.22 nm (Fig. 7a); 500.18 and 550.16 nm (Fig. 7b); 700.3 and 720.01 nm (Fig. 7c); 770.28 and 821.23 nm (Fig. 7d)) during the complete polymerization (23 cycles). The absorbance peak at 255 nm associated with benzene is present from the start of the polymerization and is slowly increasing with time during the process (Fig. 7a). The absorbance peaks at 318 and 422 nm start to increase from the 2nd and 6th cycles (Fig. 7a), while the other peaks start to increase from the 10th cycle (Figs. 7b–7d). The peak at 318 nm, associated with the π electrons of the benzene rings delocalized on the nitrogen atoms and the π-to-π* transition of the benzenoid rings,[37] starts to increase in the oxidation process of the 3rd cycle (polymerization at 104 s) and with time becomes constant due to the constant number of aromatic

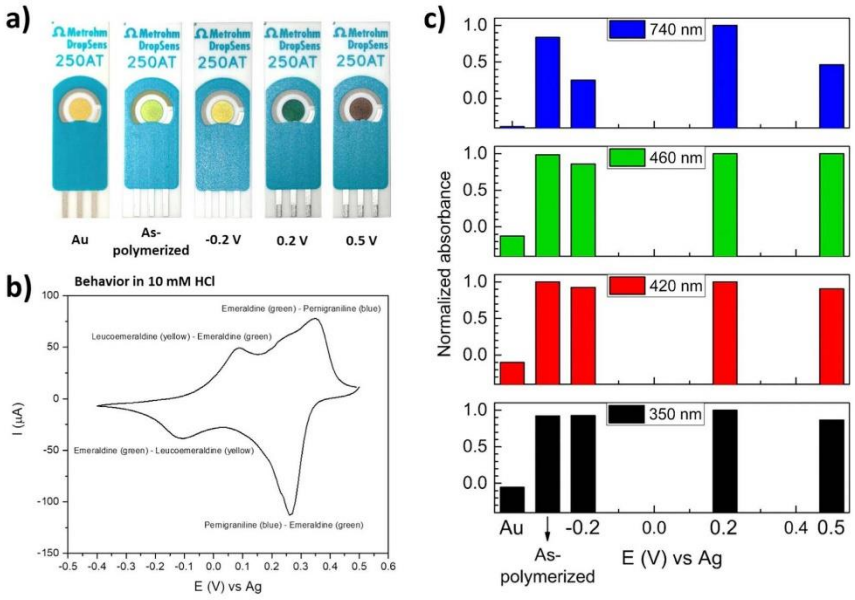

Figure 8. (a) Images of starting Au-SPE, as-polymerized PANI and PANI obtained at certain potentials where different oxidation forms are present (−0.2, 0.2 and 0.5 V vs Ag); (b) cyclic voltammogram of PANI-Au-SPE in 10 mM HCl; (c) UV–vis analysis of the final Au-SPE and PANI-Au-SPE oxidation forms obtained at a certain potential measured at 305, 420, 460 and 740 nm in air.

rings. The absorbance peak at 400 nm (oxidized dimer of aniline, diphenyl-*p*-phenylenediimine),[37,41] increases in the oxidation part in the 6th cycle (polymerization at 261 s). This indicates that until the 6th cycle there is no dimer formation. Peaks at 500 and 550 nm (Fig. 7b) associated with the polaron-π^* electronic transition, related to quinoid rings[42] and an electron transition from the benzenoid ring to the quinoid rings,[37] start to appear in the 12th cycle (polymerization at 675 s). The highest absorbances are achieved from the 19th cycle (polymerization at 966 s) during the reduction process. The peaks from 700 nm (Figs. 7c and 7d) are associated with the π-polaron transition in HCl-doped PANI[44] and they appear from the 11th cycle (polymerization at 548 s) with all the highly intense absorbance peaks in the subsequent reduction parts of the cycles. This indicates the influence of a process present in the cathodic scan such as protonation, on the electron transition from the benzenoid ring to the quinoid rings and the π-polaron transition in the doped PANI.

Figure 8a shows images of the starting Au-SPE, the final (after the 23rd cycle) as-polymerized PANI Au-SPE and the separate oxidation forms of PANI obtained for a certain potential at Au-SPE. These oxidation forms were obtained at the potentials −0.2, 0.2 and 0.5 V vs Ag during CV in the 10 mM HCl electrolyte (Fig. 8b). At −0.2 V the yellow leucoemeraldine is formed, and at 0.2 V the conductive dark-green emeraldine salt is obtained, which is further oxidized to brown pernigraniline (0.5 V). Figure 8c shows the most characteristic wavelengths for the emeraldine-salt oxidation form of PANI (350, 420, 460 and 740 nm). Note, that in all cases, the absorbance spectra of the working electrode were measured in air.

The absorbance values of the Au-SPE are presented as the background for the PANI-Au-SPE absorbance values. It is clear that the PANI oxidation forms show a significantly higher absorbance vs the Au-SPE. As-polymerized PANI is obtained at −0.3 V vs Ag. This is the potential where a completely reduced form of leucoemeraldine is obtained (Fig. 3c). This is known to be an unstable form of PANI and immediately oxidizes in air to the light-green form called protoemeraldine, which is intermediate between leucoemeraldine and emeraldine.[37] The transformation from leucoemeraldine to emeraldine follows a two-step reaction,[18,31,35,37] where protoemeraldine is an intermediate. The as-polymerized PANI obtained shows a higher absorbance at 420 nm than the leucomeraldine (−0.2 V) (Fig. 8c). It can be concluded that exposing the electrode to air after the polymerization caused its partial oxidation. The absorbance increases for the emeraldine salt and decreases for the pernigraniline, as was also observed by Kobayashi et al.[31] The emeraldine salt has characteristic absorbance peaks located between 320 and 360 nm for the π-π^* transition, around 400 nm for the polaron-π^* transition and between 700 and 750 nm for the polaron-π transition.[40] It can be seen that for all the mentioned wavelengths, the green emeraldine salt at 0.2 V shows the highest absorbance (Fig. 8c). According to the theory, the polarons represent charge carriers in conductive polymers.[15,16] Therefore, the emeraldine salt is known to be the most conductive form of PANI. Shacklette et al.,[18] and Huang et al.[37] observed that the absorbance at 350 nm (the π-π^* transition) decreases and the peak at 460 nm (assigned to the reduced form of PANI, due to the presence of bipolaronic structures) increases when prolonging the oxidation. Even though the PANI film was electrochemically deposited on a glass substrate with different dopants,[18,37] we observed the same behavior in HCl-doped PANI that was electrochemically deposited on the Au-SPE (Fig. 8c). The absorbance at 740 nm increases with the oxidation to the green emeraldine salt,[31,37] which confirms its formation at 0.2 V. The observed greater absorbance of the as-polymerized PANI at 740 nm in comparison to the leucoemeraldine form obtained at −0.2 V confirms the presence of protoemeraldine, as already discussed.

Conclusions

The electrochemical synthesis via cyclic voltammetry (CV) of the conductive polymer polyaniline (PANI) was studied by correlative electrochemistry and UV–vis spectroscopy measurements. PANI synthesized via CV in 1 M HCl containing 0.1 M monomer results in a doped and protonated polymer. Despite finishing the polymerization at negative potentials (the fully reduced, nonconductive form of PANI), the polymer quickly oxidizes in air, leading to the formation of the conductive emeraldine form. The electrochemical behavior of PANI interpreted via the absorbances of three forms of PANI with respect to their oxidation states is consistent with the optical studies of chemically synthesized PANI in the relevant literature.[18,37] However, in the case of the electrochemical polymerization of PANI via CV, the second stage of polymerization (dimer formation) happens only after several cycles of cleaning the electrode and monomer oxidation. We showed that by combining the electrochemical processing and spectroscopic methods during the polymerization of PANI, it is possible to correlate the PANIs' oxidation and reduction processes (during CV cycling) with the corresponding PANIs' electronic structures (correlation between the wavelengths and the energies of the electron transfers). A deeper understanding of the polymerization process of PANI in terms of its redox and electronic properties paves the way towards the processing of improved materials for sensing applications, especially for the case of chemiresistors. This work can be considered as a good starting point for further studies of PANI electropolymerization by other in situ/correlative techniques (electrochemistry/Raman, electrochemistry/FTIR, electrochemistry/TEM).

Acknowledgments

The authors are grateful to the DropSens company (representative PRIMAlab, Slovenia) for lending the bipotentiostat/galvanostat and a spectrometer device. We acknowledge the funding of our research activities by the ARRS through the projects and programme PR-08337, J2-1739, Z2-6757, J2-8182 and P2-0084, of which this investigation forms a part.

ORCID

Anja Korent https://orcid.org/0000-0003-4202-1005

References

1. E. Song and J.-W. Choi, *Nanomaterials*, **3**, 498 (2013).
2. M. A. Rahman, P. Kumar, D.-S. Park, and Y.-B. Shim, *Sensors*, **8**, 118 (2008).
3. D. Nicolas-Debarnot and F. Poncin-Epaillard, *Anal. Chim. Acta*, **475**, 1 (2003).
4. T. Mérian, N. Redon, Z. Zujovic, D. Stanisavljev, J. L. Wojkiewicz, and M. Gizdavic-Nikolaidis, *Sensors Actuators B Chem.*, **203**, 626 (2014).
5. J. L. Wojkiewicz, V. N. Bliznyuk, S. Carquigny, N. Elkamchi, N. Redon, T. Lasri, A. A. Pud, and S. Reynaud, *Sensors Actuators B Chem.*, **160**, 1394 (2011).
6. Z. Jin, Y. Su, and Y. Duan, *Sensors Actuators, B Chem.*, **72**, 75 (2001).
7. R. Kumar and B. C. Yadav, *Mater. Lett.*, **167**, 300 (2016).
8. F.-W. Zeng, X.-X. Liu, D. Diamond, and K. T. Lau, *Sensors Actuators B Chem.*, **143**, 530 (2010).
9. Z. Jin, Y. Su, and Y. Duan, *Sensors Actuators B Chem.*, **71**, 118 (2000).
10. H. Mello and M. Mulato, *Sensors Actuators B Chem.*, **213**, 195 (2015).
11. A. K. Roy, C. Dhand, and B. D. Malhotra, *J. Mol. Recognit.*, **24**, 700 (2011).
12. F. Fitriyana and F. Kurniawan, *Indones. J. Chem.*, **15**, 226 (2015).
13. G. Wallace, P. Teasdale, and G. Spinks, *Conductive Electroactive Polymers: Intelligent Polymer Systems* (CRC Press, L.A.) (2008).
14. M. Gvozdenovic, B. Jugovic, J. Stevanovic, and B. Grgur, *Hem. Ind.*, **68**, 673 (2014).
15. T.-H. Le, Y. Kim, and H. Yoon, *Polymers (Basel).*, **9**, 150 (2017).
16. J. L. Bredas and G. B. Street, *Acc. Chem. Res.*, **18**, 309 (1985).
17. G. G. Wallace, *Conductive Electroactive Polymers: Intelligent Polymer Systems* (CRC Press, London) p. 263 (2009).
18. L. W. Shacklette, J. F. Wolf, S. Gould, and R. H. Baughman, *J. Chem. Phys.*, **88**, 3955 (1988).
19. R. X. Wang, L. F. Huang, and X. Y. Tian, *J. Phys. Chem. C*, **116**, 13120 (2012).
20. K. Molapo, P. Ndangili, and R. Ajayi, *Int. J. Electrochem. Sci.*, **7**, 11859 (2012).
21. Y. C. Wong, B. C. Ang, A. S. M. A. Haseeb, A. A. Baharuddin, and Y. H. Wong, *J. Electrochem. Soc.*, **167**, 037503 (2020).
22. W. C. Chen, T. C. Wen, and A. Gopalan, *Synth. Met.*, **128**, 179 (2002).
23. N. Plesu, A. Kellenberger, M. Mihali, and N. Vaszilcsin, *J. Non. Cryst. Solids*, **356**, 1081 (2010).
24. A. Kellenberger, D. Ambros, and N. Plesu, *Int. J. Electrochem. Sci.*, **9**, 6821 (2014).
25. DropScns, http://dropscns.com/en/pdfs_productos/new_brochures/250at-250bt.pdf, http://www.dropsens.com/en/screen_printed_electrodes_pag.html.
26. DropSens, http://dropsens.com/en/pdfs_productos/new_brochures/spelec_spelec1050.pdf, http://www.dropsens.com/en/products.html.
27. Z. Mandić and L. Duić, *J. Electroanal. Chem.*, **403**, 133 (1996).
28. L. Duić and S. Grigi, *Electrochim. Acta*, **46**, 2795 (2001).
29. Pine research Instrumentation, 1–10 (2016) https://pineresearch.com/shop/wp-content/uploads/sites/2/2016/10/DRP10036-Screen-Printed-Electrodes-Overview-REV001.pdf.
30. J. Yano, K. Yoshikawa, and A. Kitani, *Anal. Sci.*, **13**, 741 (1997).
31. T. Kobayashi, H. Yoneyama, and H. Tamura, *J. Electroanal. Chem.*, **177**, 281 (1984).
32. L. Steel, A. C. Ward, C. Jeffrey, D. Alcorn, and D. K. Corrigan, *SCIOL Biotechnol*, **1**, 1 (2017).
33. C. Chen, J. Zhang, Y. Du, X. Yang, and E. Wang, *Analyst*, **135**, 1010 (2010).
34. J. S. Shayeh, P. Norouzi, and M. R. Ganjali, *Russ. J. Electrochem.*, **52**, 933 (2016).
35. W. S. Huang, B. D. Humphrey, and A. G. MacDiarmid, *J. Chem. Soc. Faraday Trans. 1 Phys. Chem. Condens. Phases*, **82**, 2385 (1986).
36. G. Zotti, S. Cattarin, and N. Comisso, *J. Electroanal. Chem.*, **239.1–2**, 387 (1988).
37. W. S. Huang and A. G. MacDiarmid, *Polymer*, **34**, 1833 (1993).
38. S. Bhadra, N. K. Singha, and D. Khastgir, *J. Appl. Polym. Sci.*, **104**, 1900 (2007).
39. NIST Chemistry WeBBook, https://webbook.nist.gov/cgi/cbook.cgi?ID=C62533&Mask=400, https://www.nist.gov/.
40. J. M. Kinyanjui, J. Hanks, D. W. Hatchett, A. Smith, and M. Josowicz, *J. Electrochem. Soc.*, **151.12**, D113 (2004).
41. P. M. McManus, S. C. Yang, and R. J. Cushman, *J. Chem. Soc., Chem. Commun.*, **22**, 1556 (1985).
42. A. G. Baker, *ARO-THE Sci. J. KOYA Univ.*, **7**, 47 (2019).
43. V. Babu, S. Vempati, and S. Ramakrishna, *Mater. Sci. Appl.*, **4.01**, 1 (2013).
44. R. Castagna, R. Momentè, G. Pariani, G. Zerbi, A. Bianco, and C. Bertarelli, *Polym. Chem.*, **5**, 6779 (2014).

Chapter 5

Facile Fabrication of an Ammonia-Gas Sensor Using Electrochemically Synthesised Polyaniline on Commercial Screen-Printed Three-Electrode Systems

Ammonia (NH_3) is an indispensable chemical, used in fertilizer, pharmaceuticals, food and the chemical industries. It is a strong local irritant and a problematic compound, concerning the environment and human health. As a by-product of the degradation of nitrogen-containing compounds, it is formed inside the human body. Organ failures such as kidney and liver diseases cause an increase in NH_3 concentrations, which can be noticed in the exhaled breath [51], [52], [96], [97].

Polyaniline (PANI) is known to have a high affinity for NH_3. In the emeraldine form it behaves as a semiconductor in the presence of NH_3. It changes its conductivity by losing protons to the NH_3, resulting in a transition from emeraldine salt to emeraldine base form. Due to its ability to operate at room temperature, PANI represents an alternative to metal/metal-oxide semiconductors for NH_3 gas-sensing systems. The most common gas-sensing systems are based on conductometric measurements, where the electrical properties of a sensitive material are measured. In this case, PANI is usually synthesized chemically and drop-cast on small, interdigitated electrodes [54].

The second part of the thesis is focused on the **3rd aim,** which is to design a NH_3 gas-sensing platform based on electrochemically synthesised PANI that is deposited on a commercial screen-printed electrode (SPE), a three-electrode system. SPEs are small electrochemical devices that enable electrochemical experiments using just a drop of electrolyte (~50 µL) without the construction of an electrochemical cell [7]. However, the gap between the solid electrodes is too large to connect them with electrodeposited material. Therefore, we sputtered new Au contacts between the reference or the counter electrode and the working electrode.

In the previous study [95] (Chapter 4) we showed that the electrooplymerization of 0.1 M ANI in 1.0 M HCl by cyclic voltammetry (CV) results in the most conductive PANI form, i.e., emeraldine salt. And since the detection of NH_3 gas is observed by PANI deprotonation, the same PANI preparation method was used in this case. Basic surface characterization methods (SEM, profilometer, FTIR) were used to determine the PANI's morphology, roughness and form. To transform SPEs into a suitable platform for conductometric measurements, Au was sputtered through the mask of two different geometries. Both geometries were tested against humidity and the presence of ammonia. The main conclusions of this study are:

- PANI, electropolymerized on a SPE, resulted in a nanofibrous morphology as a uniform layer on the SPE in the emeraldine salt form;
- Au sputtering enabled the transformation of the SPE in a suitable system for conductometric measurements, in this case measurements of the variations in resistance;
- PANI demonstrated a reversible sensibility towards humidity, showing the importance of the measurement conditions;

- The resistance of PANI-Au-SPE was changing linearly with time;
- Both connection geometries showed the same response to ammonia exposure;
- After exposing PANI to NH_3 gas, the PANI's resistance increased; however, it returned to its initial value after introducing clean air. The same behaviour was observed for at least three consecutive cycles;
- All the sensor responses were correlated with the real-time NH_3 concentrations measured by the analyser, allowing more precise and faster characterization of the sensor's performance;
- By measuring the PANI-Au-SPE's response to consecutive changes of NH_3 concentrations, without the purification step, the system demonstrated an ability for real-time measurements;

More on this topic is provided in the article entitled "Facile Fabrication of an Ammonia-Gas Sensor Using Electrochemically Synthesised Polyaniline on Commercial Screen-Printed Three-Electrode System", authored by Anja Korent, Kristina Žagar Soderžnik, Sašo Šturm, Kristina Žužek Rožman, Nathalie Redon, Jean-Luc Wojkiewicz and Caroline Duc, published in Sensors, Vol. 21, No. 169. in 2021 [68]. The article is presented on page 61.

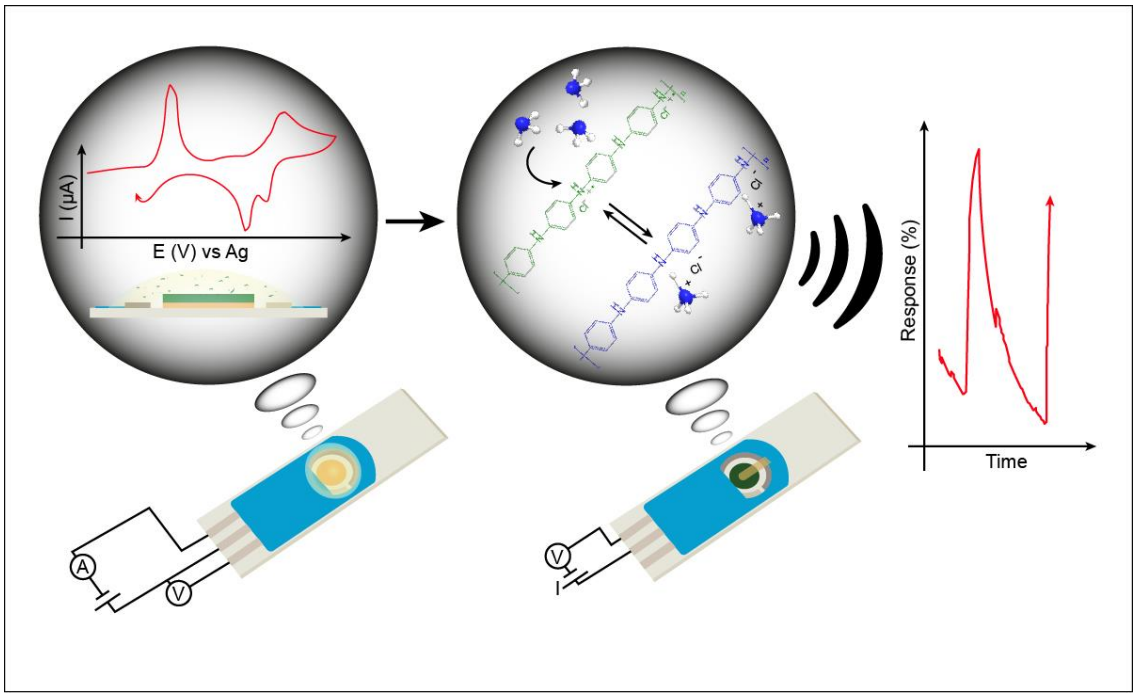

Figure 5.1: Graphical abstract for Chapter: Facile Fabrication of an Ammonia-Gas Sensor Using Electrochemically Synthesised Polyaniline on Commercial Screen-Printed Three-Electrode Systems.

sensors

MDPI

Article

Facile Fabrication of an Ammonia-Gas Sensor Using Electrochemically Synthesised Polyaniline on Commercial Screen-Printed Three-Electrode Systems

Anja Korent [1,2,*], Kristina Žagar Soderžnik [1], Sašo Šturm [1,2], Kristina Žužek Rožman [1,2], Nathalie Redon [3], Jean-Luc Wojkiewicz [3] and Caroline Duc [3]

[1] Department for Nanostructured Materials, Jožef Stefan Institute, Jamova cesta 39, SI-1000 Ljubljana, Slovenia; kristina.zagar@ijs.si (K.Ž.S.); saso.sturm@ijs.si (S.Š.); tina.zuzek@ijs.si (K.Ž.R.)
[2] Jožef Stefan International Postgraduate School, Jožef Stefan Institute, Jamova cesta 39, SI-1000 Ljubljana, Slovenia
[3] IMT Lille Douai, Institut Mines-Télécom, Univ. Lille, Centre for Environment and Energy, F-59000 Lille, France; nathalie.redon@imt-lille-douai.fr (N.R.); jean-luc.wojkiewicz@imt-lille-douai.fr (J.-L.W.); caroline.duc@imt-lille-douai.fr (C.D.)
* Correspondence: anja.korent@ijs.si

Abstract: Polyaniline (PANI) is a conducting polymer, widely used in gas-sensing applications. Due to its classification as a semiconductor, PANI is also used to detect reducing ammonia gas (NH_3), which is a well-known and studied topic. However, easier, cheaper and more straightforward procedures for sensor fabrication are still the subject of much research. In the presented work, we describe a novel, more controllable, synthesis approach to creating NH_3 PANI-based receptor elements. The PANI was electrochemically deposited via cyclic voltammetry (CV) on screen-printed electrodes (SPEs). The morphology, composition and surface of the deposited PANI layer on the Au electrode were characterised with electron microscopy, Fourier-transform infrared spectroscopy and profilometry. Prior to the gas-chamber measurement, the SPE was suitably modified by Au sputtering the individual connections between the three-electrode system, thus showing a feasible way of converting a conventional three-electrode electrochemical SPE system into a two-electrode NH_3-gas detecting system. The feasibility of the gas measurements' characterisation was improved using the gas analyser. The gas-sensing ability of the PANI-Au-SPE was studied in the range 32–1100 ppb of NH_3, and the sensor performed well in terms of repeatability, reproducibility and sensitivity.

Keywords: cyclic voltammetry (CV); electropolymerisation; NH_3 detection; polyaniline (PANI); screen-printed electrode (SPE)

Citation: Korent, A.; Žagar Soderžnik, K.; Šturm, S.; Žužek Rožman, K.; Redon, N.; Wojkiewicz, J.-L.; Duc, C. Facile Fabrication of an Ammonia-Gas Sensor Using Electrochemically Synthesised Polyaniline on Commercial Screen-Printed Three-Electrode Systems. *Sensors* **2021**, *21*, 169. https://doi.org/10.3390/s21010169

Received: 26 November 2020
Accepted: 25 December 2020
Published: 29 December 2020

1. Introduction

Conductive polymers have great potential as gas-sensing materials because of their light weight, low cost, and straightforward production, which are associated with the electronic, magnetic and optical properties of metals [1]. The π-conjugation along the chains of those materials allows the formation of a delocalised electron at the origin of the electrical conduction, which can be modulated by a redox reaction or protonation from a near-insulator to a metallic conductor [2,3]. Integrated into chemiresistive sensors for the detection of oxidising or reducing gases [4–6] (NH_3 [6–10], hydrogen [11], carbon monoxide [10], nitrogen oxides (NO_x) [7,12], and hydrogen sulphide [12]), they enable room-temperature (RT) measurements, i.e., much lower than the operating temperatures of metal oxides that are conventionally used in gas sensing and operate at temperatures ~300–400 °C [5]. Moreover, in comparison with metal oxides, they show good metrological characteristics, such as a high sensitivity and a short response time, combined with the ability to be easily tuned, both chemically and physically [13].

Detecting ammonia (NH_3) at low concentrations is crucial in many environmental and biomedical situations. Firstly, NH_3 is essential to various industries, e.g., chemical, medical, food, and automotive. Still, it can also be problematic concerning the environment and human health, i.e., it is highly reactive and can trigger skin, eye, and lung illnesses [6,14]. According to the Occupational Safety and Health Administration (OSHA) [15], the exposure limit for humans is 50 ppm for 8 h and 35 ppm for 15 min. Humans are incapable of sensing the presence of NH_3 at concentrations below 5 ppm [16,17], and NH_3 is highly reactive. It can form harmful, nanosized aerosols (particulate atmospheric matter such as ammonium nitrate and ammonium sulphate) [14]. Thus, it is essential to develop detection techniques that are quick to react, convenient and reliable for detecting NH_3 in low concentrations. Secondly, NH_3 has been reported to be a relevant marker for liver and kidney diseases [18]. In the case of these organs' failure, the NH_3 concentration from exhaled breath increases from a few hundred ppb to several ppm [19]. The detection of NH_3 over such a broad concentration range in human breath shows promise as a non-invasive and low-cost technique for diagnosing and/or monitoring such diseases [20,21]. The ability to sense NH_3 in a low-ppb range can be transferred to the indirect detection of other toxic gases, where NH_3 is a by-product of a certain chemical reaction triggered by an applied organic compound or catalyst. For example, formaldehyde gas was detected by using polyaniline (PANI) as a sensing material for NH_3 produced as a by-product of an organic reaction between formaldehyde and Fluoral-P [22,23].

Different working principles can be used to detect ammonia, such as electronics, electrochemistry, optical, surface acoustic wave and field-effect transistor. Optical methods such as tuneable-diode-laser adsorption spectroscopy have the highest sensitivity (150 ppt) and selectivity. However, their operating conditions do not match all the application requirements. For this reason, chemiresistive sensors are the most popular. Presenting sensitivities in the range 20 to 100 ppb, they have more cost-effective and simpler fabrication and integration [14,24].

Among the sensitive materials in chemiresistive sensors, PANI is one of the most studied conductive polymers for NH_3 sensing [4]. It is based on the ability of the gas to change the resistance of the material via the well-known deprotonation/protonation mechanism [25,26]. It is, in addition, light weight, inexpensive, and environmentally stable with a straightforward polymerisation reaction that has high yields and reversible redox and pH-switching properties. Its conductivity can be adjusted by changing its oxidation and protonation state, which makes PANI unique in the family of conductive polymers. PANI can be found in various oxidative states, with three being the most known: the fully reduced state (leucoemeraldine), the half-oxidised state (emeraldine) and the fully oxidised state (pernigraniline). Emeraldine is the most conductive form of PANI [27]. Emeraldine has high stability at room temperature and is classified as a semiconductor, which makes it suitable for gas sensing [28]. However, like the other conductive polymers, PANI's main limitations are a sensitivity to humidity and problems with long-term stability [14].

In order to enhance PANI;s conductivity, its switching abilities, and its morphological and structural properties that consequently influence the response to NH_3 [5,6], many different formulations have been developed. They range from using pure PANI with simple dopants such as $HClO_4$ [29] or polymers (polyurethane [30], poly(methyl methacrylate) [31]), in addition to more complex dopants (dodecylbenzenesulfonic acid (DBSA), camphorsulfonic acid (CSA)) [8] or nanomaterials such as carbon nanotubes [21,32,33] and metal particles [5,33] or metal oxides [9,34,35]).

Moreover, various configurations have been used to monitor the changes in the PANI's resistance [8,9,21,30,36–38] or impedance [39] in the presence of NH_3 gas. They consist of (i) two-point resistivity measurements that are usually made using either PANI deposited on interdigitated electrodes with multiple "fingertips" [8,9,21,30,36] (Figure 1a), (ii) a PANI film on glass substrates [40] (Figure 1b), (iii) a PANI pellet connected by wires [38] (Figure 1c), (iv) a PANI film deposited on two electrodes made of different metals [39] (Figure 1d) or (v) PANI in a screen-printed two-electrode system [37] (Figure 1e).

The deposition of PANI on such electrodes is usually completed with drop-casting [9,21,30,37,39], spin-coating [8,41] and layer-by-layer assembly [41]. In all these cases, PANI is synthesised via a chemical polymerisation method.

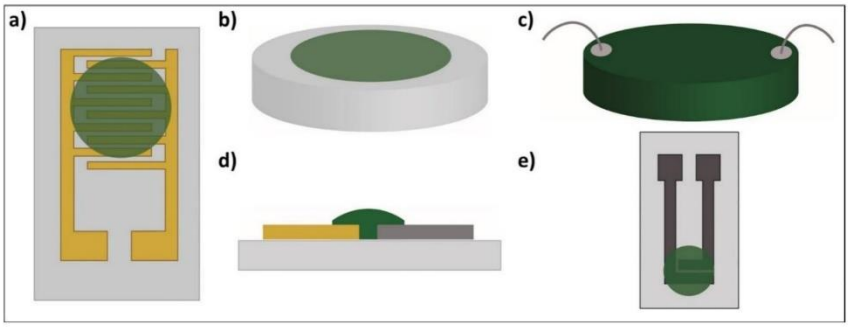

Figure 1. Polyaniline (PANI)-based ammonia/humidity gas sensors: (**a**) interdigitated electrodes [8,9,21,30,36]; (**b**) film [40]; (**c**) pellet [38]; (**d**) two different metal electrodes [39]; (**e**) screen-printed two-electrode system [37].

Knowing the impact of the PANI's morphology and the PANI's film thickness on gas-sensing performance [41,42], the processes of its synthesis and its deposition are thus crucial. In this respect, PANI's electrochemical polymerisation allows easier control over the PANI's film thickness and the morphology of the final product by controlling the parameters of the electrochemical deposition, such as deposition time, applied current or applied voltage. Indeed, the result of such a synthesis is a nanostructured polymer in conductive, doped form due to the polymerisation in an acid electrolyte [27,43]. Such a synthesised polymer is well integrated and compacted with the surface of the working electrode [44] that can be used for gas sensing.

As per the electrochemical synthesis principle, the required three-electrode system (the working, counter and reference electrodes) [27,43] allows the deposition of material only on the surface of the working electrode, which represents a significant drawback and challenge for resistance-based gas measurements. Paul et al. [45] electrodeposited PANI on an eight-electrode array with a 1.7 µm gap between the Au electrodes. Indeed, in the case of a sufficiently small gap (1–10 µm) and long polymerisation times, PANI can assemble over the gap [36,45–47], making it possible to construct two solid-state electrodes, in between which a conducting material is sandwiched. However, such an approach is difficult and expensive in terms of the demand of a particular small electrochemical cell, which needs to enable the contact of the electrolyte with a two-electrode system and a removable reference electrode. In the case of a three-electrode SPE, only a drop of electrolyte is needed, and when a conductive material is electrochemically deposited on the working electrode, for further functionalisation, only suitable contacts on the top of the deposited material still need to be made. These contacts must not be in contact with the working electrode, but must connect the deposited material with the secondary electrode [48]. The deposited material and the type of synthesis represent a bottleneck for these approaches.

By combining a knowledge of resistivity-based gas sensing and electrochemistry, we focused our work on developing a NH_3-detection system based on electrochemically synthesised "pure" PANI without the use of any complex dopants [29–31] and nanomaterials [5,21,32,33,49,50]. PANI was chosen because of its superior sensing performance with regard to ammonia [6,51]. We report on a direct electrodeposition procedure for PANI on a commercial, screen-printed electrode (SPE) that results in the PANI's excellent uniformity, and high reproducibility, with the potential for mass production and in-situ analyses [52]. Moreover, this procedure is suitable for automation processes, and has an increased reliabil-

ity and repeatability. The proposed procedure enables the feasible production of low-cost sensor devices without the extensive use of chemicals/materials. A sensor prepared in this way was characterised in different humidity conditions and NH_3 concentrations. In addition, by including a real-time analyser for NH_3 gas, two different approaches for sensor-sensitivity characterisation were used. As a result, by using this inexpensive and practical fabrication procedure we were able to construct a robust, ppb-range NH_3 sensor. Indeed, at room temperature and under 70% of humidity, the sensor in this study shows a limit of detection of 23 ppb and sensitivities of 12.30 and 4.27%.ppm^{-1} in the ranges 32–200 ppb and 200–1000 ppb, respectively.

2. Materials and Methods

2.1. Polyaniline Synthesis

PANI can be electrodeposited on a metal electrode using three different electrochemical techniques (potentiodynamic, potentiostatic, and galvanostatic). The potentiodynamic method (cyclic voltammetry, CV), exposes the growing polymer to additional processes, i.e., oxidation/reduction reactions, which adds another dimension to the electropolymer's growth [27]. By changing the CV conditions (scan rate, number of cycles) the polymer's properties can be tailored. By applying a slower scan rate (25, 50 mV/s) the peak potential of the first redox couple shifts towards lower potentials and the resulting polymer has a higher growth rate in comparison to the polymer grown with high scan rates (100 mV/s). It was shown that by using 50 mV/s the lowest average diameter of PANI nanofibers is achieved [53]. Controlling the charge consumed for electropolymerisation enables an estimation of the amount of deposited PANI. Only the first oxidation peak of the PANIs' CV behaviour contains information of just the PANI reaction. In all the other peaks, pure bare-electrode material oxidation or reduction is included [53–55]. Therefore, by controlling the equality of the anodic current of the first oxidation, the reproducibility between polymerisations can be achieved. Based on this, the experimental conditions for the PANI's polymerisation were chosen.

The PANI was electrodeposited on a commercial DropSens screen-printed electrode (SPE; MetrohmDropSens, ref. SPE-250AT) [56], with gold as the working electrode, platinum as the counter electrode and silver as the reference electrode. The electropolymerisation was carried out in an acidic medium (1 M HCl prepared from 37% HCl Sigma Aldrich, pH = 0.43) containing a 0.1 M aniline monomer (Sigma Aldrich). The electrochemical experiments were performed on a USB- and battery-powered potentiostat/galvanostat/EIS analyzer PalmSens4. CV, as the deposition method, was performed at a potential of −0.3 V to 1 V using a scan rate of 50 mV/s. The CV was stopped after completing the cycle in which the first oxidation peak reached an anodic current of 1.5 mA to achieve reproducibility for the deposited material. Due to the deviations in weighing the aniline monomer for the polymerisation solution, the anodic current of 1.5 mA of the first anodic peak was achieved in a different number of cycles (from 23 to 25 cycles). Therefore, the experiment was manually stopped at –0.3 V vs. Ag with a 0.1 V uncertainty. After the deposition, the electrode was cleaned with methanol (Sigma Aldrich) to remove the residual monomer/electrolyte suspension and the unattached polymeric parts.

2.2. Material Characterisation

2.2.1. Scanning Electron Microscopy (SEM)

Field-emission scanning electron microscopy (FE-SEM) was used to characterise the morphology of the pure-gold SPE (Au-SPE) and the electrodeposited PANI (PANI-Au-SPE). The specimens for the FE-SEM observations (Jeol JSM-7600F) were prepared by placing the samples on a conductive tape. Cross-section samples were cut perpendicular to the electrode. The Au-SPE surface was observed at an acceleration voltage of 20 kV and the PANI-Au-SPE samples at 5 kV.

2.2.2. Fourier-Transform Infrared (FTIR) Spectroscopy

Fourier-transform infrared (FTIR) spectra of the prepared PANI-Au-SPE were measured using an ATR (attenuated total reflection) crystal with an ATR FTIR Frontier L1280018 spectrometer (Perkin Elmer, Waltham, MA, USA). A spectrum was obtained by sampling 20 interferograms with a resolution of 4 cm^{-1} in the range 500–4000 cm^{-1}.

2.2.3. Profilometer

Three-dimensional (3D) mapping of the surface roughness of the Au-SPE and PANI-Au-SPE was carried out with a Stylus profilometer DEKTAK (Bruker) having a resolution 0.3 nm in the x, 1 µm in the y, and 0.1 nm in the z directions.

2.3. Sensing Characterisation

The prepared PANI-Au-SPE samples were sputtered with gold (Agar Auto Sputter Coater from Agar Scientific) using a 3D-printed template to create an appropriate connection between the separated working, counter and reference electrodes. Two different geometries were used. Connection 1 is composed of one 2-mm-wide electrode deposited on the surface to connect the polymer surface to the counter electrode (Figure 2a). The electric field is oriented longitudinally. For connection 2, two parallel electrodes are deposited on the surface of the polymer with a 1-mm gap in between (Figure 2b), connecting the polymer to the platinum and silver parts of the SPE. A transversal electric field was applied between the counter and the reference electrodes. By using a custom-made connector for the SPE, the PANI-Au-SPE sensors were put in a dynamic exposure chamber, in which the temperature and relative humidity (RH) were controlled for all the experiments: T = 25 °C (RT) and RH for ammonia (NH_3) sensing fixed at 70% and for humidity characterisation varying between 10 and 90%. When the sensor was exposed to the NH_3 and humidity, a variation in the resistance of the active PANI material was measured. The behaviour of the sensor in the presence of NH_3 is presented as a percentage of the relative response Equation (1):

$$Response\ (\%) = \left[\frac{(R_t - R_0)}{R_0}\right] \cdot 100 \quad (1)$$

where R_t is the resistance at a certain time, and R_0 is the initial resistance under zero air. The resistance of the sensor was measured continuously with a computerised digital multimeter (Agilent 34970A) as a function of the NH_3/humidity concentration and the exposure time. The NH_3 concentration was measured at the gas outlet of the gas chamber with the NH_3 analyser (Picarro G2103) and the humidity was measured directly in the chamber with the temperature/RH sensor (Sensirion SHT25). The desired analyte concentration in the chamber was controlled by the flow rate of the two gases (NH_3 gas and humid air) using a gas generation and dilution system (Omicron technologies OMI-SR042A-A). The complete measuring setup is presented in Figure 2c.

For the characterisation of the effect of humidity, the sensor was exposed to a certain percentage of relative humidity for 30 min in both directions (from 0% to 70% RH and back). The sensor's stability in purified air at 70% RH was monitored over 40 h.

The protocol to analyse the behaviour of the sensor in contact with NH_3 involved three phases: 1. Estimation of the initial resistance of the sensor after exposing it to purified air (zero air + humid air); 2. Measuring of the sensor's resistance during exposure to the analyte. In this phase, the sensor's resistance changes due to the interaction of the analyte with the active PANI layer; 3. Blowing the sensor flushed with purified air (zero air + humid air), causing desorption of the analyte and recovery of the sensor's resistance. The NH_3 was sensed by exposing the sensor for 10 min to a particular concentration of NH_3 gas and 50 min to purified gas for the desorption. Then, for simulating real-time measurements without an intermediate process of desorption, the NH_3 gas concentration changed every 10 min. The response time is defined as the time it takes for the sensor to reach 90% of the response change.

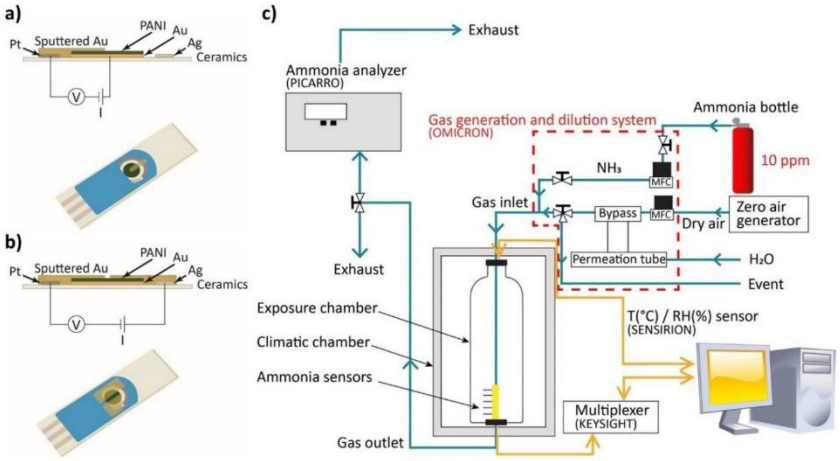

Figure 2. (**a**) Scheme of connection 1; (**b**) scheme of connection 2; (**c**) schematic view of measurement system for sensing.

3. Results and Discussion

3.1. Electrodeposition of Polyaniline (PANI)

The PANI was electrodeposited with CV using a 0.1 M aniline monomer suspension in a 1 M HCl electrolyte. Figure 3 shows all 23 cycles of the electropolymerisation process. There are three peaks observed in the anodic scan (E (a_1) = 0.16 V, E (a_2) = 0.45 V, and E (a_3) 0.77 V vs. Ag) and four in the cathodic scan (E (c_1) = 0.66 V, E (c_2) = 0.55 V, E (c_3) = 0.42 V, E (c_4) = 0.02 V vs. Ag). At the beginning of the electropolymerisation, the CV is performed on the pure Au-SPE, causing Au oxidation (E = 1 V) and reduction (E = 0.51 V) [57,58]. The monomer aniline oxidation, which is the first step in the aniline electropolymerisation occurs at E = 0.9 V [43] in the anodic scan. These later peaks, however, are not visible due to the gradually increasing currents of the peaks, characteristic for the PANI's formation and its redox behaviour. The anodic peak a_1 is the oxidation peak of the leucoemeraldine (the fully reduced state of PANI), which oxidises to emeraldine (half-oxidised state). The anodic peak a_2 is related to the formation of the intermediate degradation products (p-benzoquinone) and their oxidation. The anodic peak a_3 is the oxidation of emeraldine to pernigraniline (fully oxidised state) [55,59,60]. All these processes are reversible during the cathodic scan. The cathodic peaks c_1 and c_2 are the reduction of pernigraniline. The splitting of the peak is associated with the acidity of the electrolyte [59]. The cathodic peak c_3 is the reduction of the intermediate degradation products, p-benzoquinone to hydroquinone, and the cathodic peak c_4 is the reduction of emeraldine to leucoemeraldine [55,59,60]. Leucoemeraldine is known to be an unstable state of PANI [61]; therefore, after exposing the electrode to air at the end of the electropolymerisation, it is oxidised in the direction of emeraldine. The same conclusion was made after a correlative study of the electrodeposition and electrochromic behaviour of PANI [54]. Due to the fact that we are performing the electropolymerisation in an HCl electrolyte [43], the final product is HCl-doped PANI.

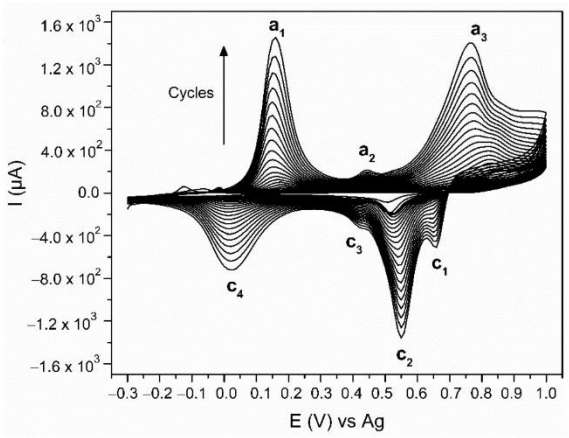

Figure 3. Voltammogram of aniline electropolymerisation via cyclic voltammetry (CV) on the surface of gold screen-printed electrode (Au-SPE) in HCl electrolyte.

3.2. Characterisation and Analysis of the Electrodeposited PANI

The morphology of the Au-SPE and the PANI-Au-SPE in the form of FE-SEM images is presented in Figure 4. The Au-SPE top-view surface (Figure 4a) appears to be a layer with an uneven surface relief and larger, randomly distributed pores. From the cross-section view (Figure 4b) the Au layer takes on the surface relief of the ceramic grains of the SPE substrate. The Au layer's thickness is approximately 250 nm. Figure 4c,d shows the top-view surface and the cross-section of the PANI-Au-SPE. The PANI electrodeposited with CV appears to be a compact film composed of interconnected nanofibers attached to the Au surface. The PANI layer's thickness was estimated to be around 5 μm.

Figure 5a,b presents the 3D surface mapping of the Au-SPE and PANI-Au SPE. A 0.2×0.2 mm^2 surface area was examined in the direction perpendicular to the electrode. The Au-SPE surface has an uneven relief with some randomly distributed, low areas, which is consistent with the Au-SPE SEM surface images (Figure 4a). The roughness factor (Ra) for the Au-SPE surface is approximately 0.58 μm. In the case of the PANI-Au-SPE, the Ra increases to 0.91 μm. The surface relief has fewer higher areas, but more lower areas with an open PANI structure, as seen from the PANI-Au-SPE SEM surface image (Figure 4c). Materials with a higher roughness have abundant surface-adsorption sites, causing an increased response to gas analytes [62]. Therefore, by electrodepositing the PANI with CV, we have successfully completed the first step towards obtaining suitable material for gas sensing, due to the open nanostructure of the PANI and the increased roughness.

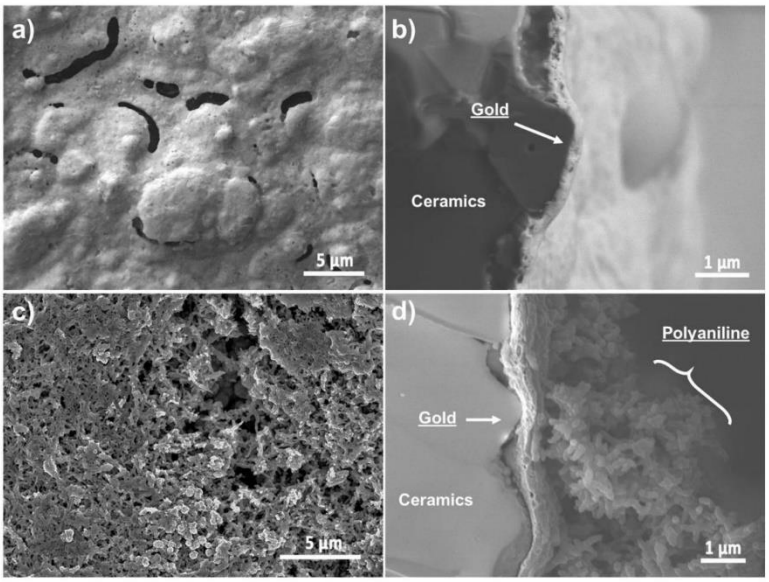

Figure 4. Au-SPE field-emission scanning electron microscopy (FE-SEM-LEI) images: (**a**) top view and (**b**) cross-section view; PANI-Au-SPE FE-SEM-SEI images: (**c**) top view and (**d**) cross-section.

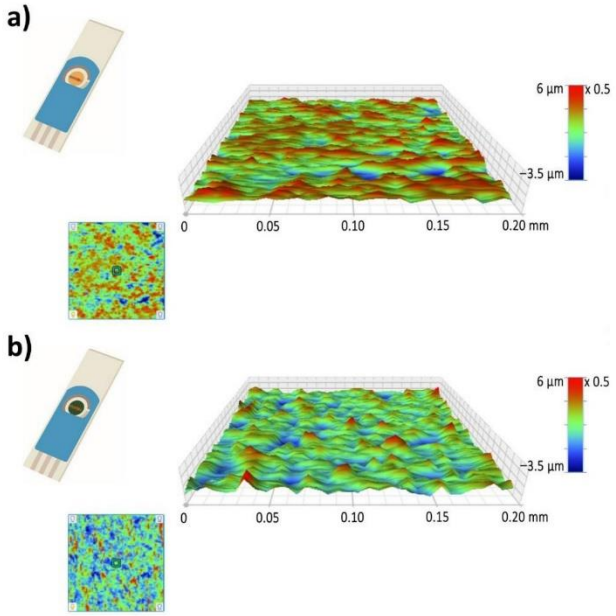

Figure 5. Three-dimensional (3D) mapping of surface area: (**a**) Au-SPE and (**b**) PANI-Au-SPE.

Fourier-transform infrared (FTIR) spectra were used to characterise the state of the PANI-Au-SPE (Figure 6). The band at 1565 cm^{-1} corresponds to the quinoid-ring stretching vibrations, while the band at 1489 cm^{-1} corresponds to the benzenoid-ring stretching vibrations. The bands at 1374 and 1296 cm^{-1} correspond to the C–N stretching in the neighbourhood of the quinoid ring and to the C–N stretching of a secondary aromatic amine. The band at 1240 cm^{-1} corresponds to the C–$N^{+\bullet}$ stretching vibrations in the conductive protonated form of PANI. The broad band at approximately 1136 cm^{-1} corresponds to the C–H aromatic in-plane deformation vibrations [9,63–65]. The bands at approximately 800 cm^{-1} originate from the C–H out-of-plane bending in the 1,4-disubstituted ring structures. These indicate the head-to-tail coupling of the aniline during the polymerisation [30,66]. This type of coupling is known for polymerisation in acidic conditions [59]. The band at 505 cm^{-1} corresponds to the bending vibrations of the PANI backbone due to the presence of a chloride ion [66], which confirms the spontaneous doping of the PANI during electropolymerisation. From the ratio of the area of the peaks corresponding to the quinoid (1565 cm^{-1}) and benzenoid rings (1489 cm^{-1}) (Q/B), the oxidation level can be estimated [65,67]. The oxidation level of the PANI-Au-SPE is 0.8, which is consistent with the electrochemically synthesised PANI via chronoamperometry (polymerisation at constant potential) [65]. The structural form of the emeraldine state has one quinoid ring vs. three benzenoid rings, giving a ratio of 0.75. The FTIR results confirm the formation of a conductive PANI layer on the SPE in the form of an emeraldine salt, which was expected based on the observed green colour of the polymerised electrode.

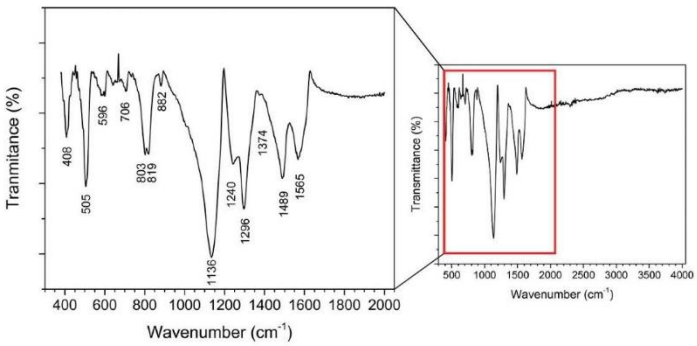

Figure 6. Fourier-transform infrared (FTIR) spectrum of PANI-Au-SPE with magnified fingerprint (500–1500 cm^{-1}) and double bond (1500–2000 cm^{-1}) region.

3.3. Impact of Humidity on the Resistance of the PANI-Au-SPE

The PANI-Au-SPE samples were firstly prepared for a two-point measuring system. The electrochemical SPE-based system has three separate electrodes, a large gap between them (approximately 1 mm) and the electrodeposition of PANI only on the surface of the gold working electrode. Therefore, a suitable connection between the working and counter electrodes (connection 1, Figure 2a) and the counter, working and reference electrode (connection 2, Figure 2b), was created with Au sputtering. The as-prepared PANI-Au-SPE sensors were characterised for the effect of humidity and NH_3 sensing.

Figure 7 shows the typical response of the PANI to humidity for both types of connection (olive circle—connection 1, and navy square—connection 2): the water molecules cause a higher degree of doping, i.e., a lower resistivity by facilitating the proton exchange inside the PANI. The enhancement of the charge transport comes from the transfer from the reduced units (NH_2^+) to the oxidised units (NH^+=) [40,68] and/or the increase of the ionic conduction due to the release of a proton from the water molecules that are adsorbed [69].

Both PANI-Au-SPE sensors have a similar initial resistance (the same exponential range) and show a linear trend ($R^2 > 0.96$ for both connections) in the decreasing resistance with increased RH from 30% to 90% (adsorption of humidity). The difference in the sensitivity to RH (slope of the linear curve; –0.01 $\Omega\%^{-1}$ for connection 1, and –0.02 $\Omega\%^{-1}$ for connection 2) is two-times higher in the case of the sensor with connection 2.

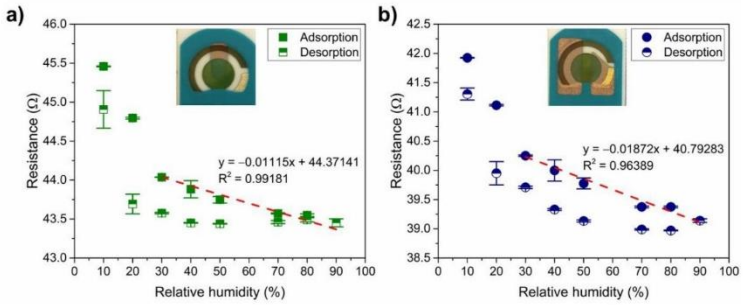

Figure 7. Reversibility of the PANI-Au-SPE sensor after exposing to increasing relative humidity (RH): (**a**) connection 1 and (**b**) connection 2. Both figures, (**a**,**b**), contain linear fitting for the adsorption of water between 30% and 90% RH.

Next, the reversibility of the PANI-Au-SPE sensors' resistance after exposing them to 90% RH was investigated. Figure 7 shows the adsorption and desorption of water vapour in humid air for the PANI-Au-SPE sensor with connection 1 (Figure 7a) and connection 2 (Figure 7b). After continuous exposure to a higher RH, the PANI-Au-SPE did not return to its initial resistance at a certain RH. The desorption resistances are different from the adsorption resistances by 0.14–2.46% for connection 1 and 0.98–2.83% for connection 2. In addition to the "protonation effect", water molecules at high RH can cause swelling of the PANI fibres, which increases the packing disorder [37] and can contribute to the irreversibility. As the PANI acts as water-sensitive material, all further measurements were performed at a constant 70% RH to eliminate the influence of the environment.

The stability of the PANI-Au-SPE was investigated by exposing the PANI-Au-SPE sensors to environmental conditions (room temperature-RT, 70% RH), which were later used for the NH_3 detection (Figure 8). The PANI-Au-SPE sensor with both connection geometries has a linear increase in the resistance with time ($R^2 = 0.99$ for both connections). Connection 1 has a two-times-higher aging effect than connection 2 (slope of the linear curve; 0.1 Ωh^{-1} for connection 1, and 0.05 Ωh^{-1} for connection 2). Thus, the PANI-Au-SPE sensor with connection 1 is more stable with time. As seen in Figure 7, connection 2 has a two-times-higher sensitivity towards RH and a two-times-lower stability with time (Figure 8). Both connections have approximately the same PANI surface area sputtered with Au, i.e., 4 mm^2. The main difference is in the distribution of the current flows across the device, which are difficult to determine precisely given its structure.

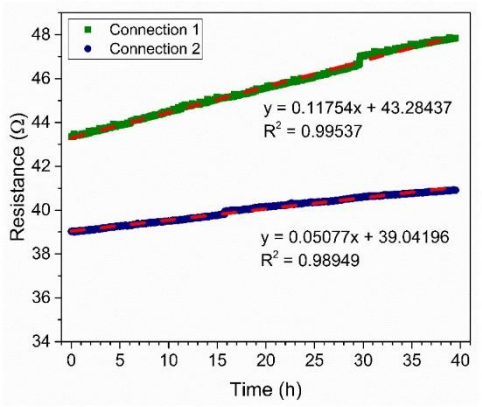

Figure 8. PANI-Au-SPE sensor stability at 70% of RH and room temperature (RT) for connection 1 (olive) and connection 2 (navy).

3.4. NH_3-Sensing Performance of the PANI-Au-SPE

For a comparison of the influence of the connection geometry on the sensor's response to NH_3, PANI-Au-SPE sensors with both connections were exposed to 500-ppb NH_3 at RT and 70% RH (Figure 9a). Both connections exhibit an equivalent relative response to the NH_3 under the same conditions. Even though connections 1 and 2 have differences in terms of humidity characterisation (Figure 7) and sensor stability (Figure 8), they both show linear behaviour. As the PANI-Au-SPE sensor's behaviour towards the NH_3 is presented as a relative response, it is not influenced by this difference. Therefore, we can conclude that the current flow through the PANI film due to the geometry of the connections does not influence the PANI's response to NH_3 gas, which suggests the uniformity of the electrodeposited PANI.

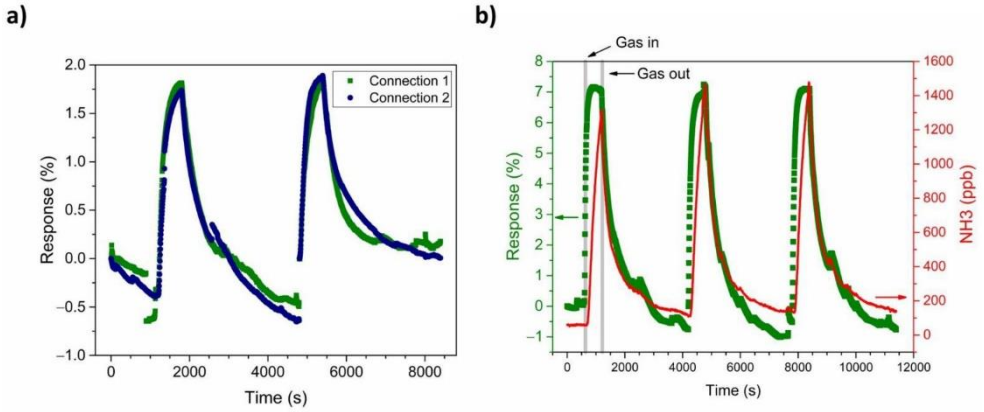

Figure 9. (**a**) Comparison between connection 1 (olive) and connection 2 (navy) of PANI-Au-SPE sensor response to 500 ppb NH3 and (**b**) the dynamics of PANI-Au-SPE-Au resistance change (olive) and NH3 concentration variation monitored by the PICARO analyser (red curve).

As both connections show the same response, either could be used for the subsequent experiments. Our next results, in terms of sensor dynamics, calibration and the simulation of real-time measurements, are presented for connection 1.

Figure 9b shows the repeatability of the PANI-Au-SPE sensor upon exposure to 1400 ppb of NH_3 operating at RT and 70% RH. The olive squares represent the relative PANI-Au-SPE sensor's response and the red curve, the variation in the NH_3 concentration at the same time, monitored by the analyser. The PANI-Au-SPE shows the character of a typical p-type semiconductor [70,71], as its resistance increases upon exposure to NH_3. The NH_3 sensing by the PANI follows the well-known deprotonation/protonation mechanism [25,26]. Polyaniline becomes conductive with the addition of dopants to the polymeric chain, which generates protonation on the nitrogen atom and consequently facilitates the movements of valence electrons, causing hopping conduction. In the presence of NH_3 gas, a proton is removed from the polymeric chain to form an energetically favourable ammonium cation (NH_4^+), compensated in the structure by the dopant (A^-). Removing a proton from the PANI reduces the amount and the mobility of the charge carrier, resulting in an increased resistance of the PANI [6]. In the absence of NH_3, NH_4^+ decomposes to NH_3 and H^+, causing the reversible protonation of the PANI (Equation (2) and Figure 10) [25,26].

$$PANIH^+ + NH_3 = PANI + NH_4^+ \quad (2)$$

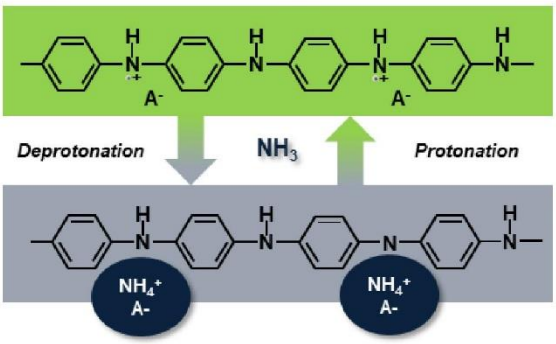

Figure 10. Mechanism of deprotonation/protonation at the origin of the PANI's sensitivity to ammonia gas. A^-, NH_3 and NH_4^+ refer to the dopant, ammonia and ammonium cation, respectively.

Compared with the NH_3 analyser data (Figure 9b), the PANI-Au-SPE sensor follows the behaviour of real-time NH_3 concentration, without reaching the saturation point at the maximum NH_3 concentration, i.e., 1400 ppb. The PANI-Au-SPE sensor shows repeatability during three cycles of exposure to NH_3, having enough time to complete the NH_3 desorption (50 min), and then to respond equally to the NH_3 exposure (10 min).

To obtain the calibration curve of the PANI-Au-SPE sensor for NH_3, a series of NH_3 gases with concentrations ranging from 32 ppb to 1090 ppb were used. Figure 11a shows the PANI-Au-SPE sensor's response to different real-time NH_3 concentrations, monitored by the analyser. A higher concentration of NH_3 has a higher PANI-Au-SPE sensor response. By plotting the maximum sensor response vs. the NH_3 concentration, the calibration plot for the PANI-Au-SPE sensor is obtained (Figure 11b). The PANI-Au-SPE sensor shows two linear ranges, from 32 ppb to 250 ppb ($R^2 = 0.98$) and from 250 ppb to 1100 ppb ($R^2 = 0.99$). The sensitivity of the PANI-Au-SPE sensor to NH_3 detection at 70% RH and RT is 12.3% ppm^{-1} for the first linear range, and 4.27% ppm^{-1} for the second. Due to the synchronic NH_3 concentration monitoring by the analyser, the calibration plot for the PANI-Au-SPE sensor was also made by plotting the responses of the PANI-Au-SPE sensor for the last cycle of 1090 ppb NH_3 (Figure 11a) vs. NH_3 analyser data at the same time (Figure 11c).

The analyser gives more extensive and detailed NH_3 data for all the measurement times. Therefore, the calibration plot of one cycle has more points in comparison to the calibration plot made from the maximum responses of sequential measurements (Figure 11b). The calibration plot of one cycle (Figure 11c) has the same two linear ranges, from 32 ppb to 250 ppb (R^2 = 0.94) and from 250 ppb to 1100 ppb (R^2 = 0.96) with a similar sensitivity (9% ppm^{-1} for the first linear range, and 3.02% ppm^{-1} for the second). As both ways of obtaining the calibration plot provide the same result, the calibration obtained by applying data from the analyser simplifies the sensor's characterisation, i.e., a larger number of points made with only one measurement. The theoretical detection limit is calculated according to the formula from IUPAC recommendations Equation (3):

$$LOD\ (ppb) = \frac{3\sigma}{m}, \tag{3}$$

where σ is the standard deviation of the sensing 15-min baseline before the NH_3 exposure and m is the slope of the first calibration curve (0.0123% pbb^{-1}). The detection limit is calculated to be 23 ppb, which is a realistic number regarding to the lowest detected concentration (quantification limit 32 pbb).

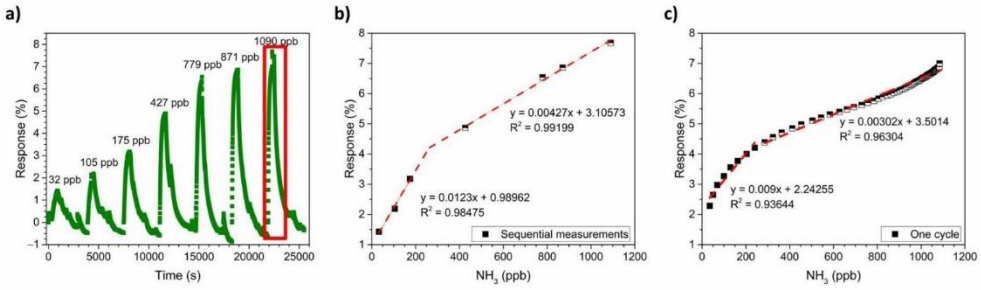

Figure 11. NH_3 calibration: (**a**) PANI-Au-SPE sensor's response after exposing to different concentrations of gas; (**b**) calibration curve obtained from the PANI-Au-SPE sensor's response at maximum achieved gas concentration in sequential measurements and (**c**) calibration curve obtained from one cycle of measurements.

In a real-time environment the sensors are not exposed to absorption and desorption cycles, but the gas concentration varies continuously without a recovery time. Figure 12a shows the PANI-Au-SPE sensor response (olive squares) to a continuously changing NH_3 concentration (red curve). The PANI-Au-SPE sensor follows the same trend as the NH_3 concentration, proving that the system can have the same response trend without any additional recovery time. The out-of-range jump in the sensor's response and the NH_3 analyser at 27 min is a consequence of the RH instability (grey curve) at the same time. It was already proven [30] that different humidity conditions influence the PANI's sensitivity to NH_3, due to the reaction between water and NH_3. Thus, it is important to maintain constant humidity conditions in the case of NH_3 sensing or to monitor simultaneously the humidity to correct the signal. For a comparison of the real-time sensor responses with measurements from a typical laboratory cycle, four points (blue dots in Figure 12a) were inserted into the calibration plot, acquired from sequential measurements (Figure 11b), and are presented in Figure 12b. All the real-time points represent a linear trend in the higher NH_3 concentration range (250 ppb to 1100 ppb) with the same sensitivity.

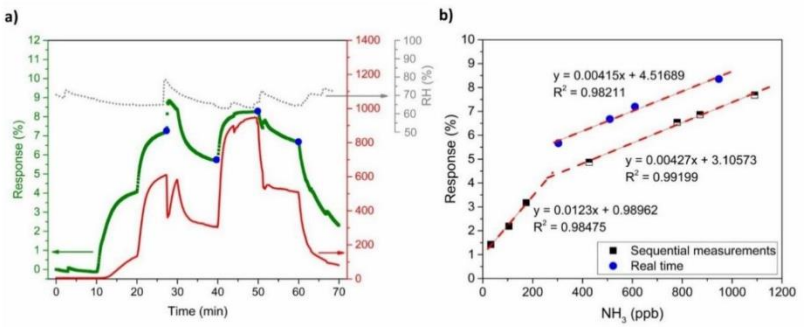

Figure 12. (**a**) PANI-Au-SPE sensor's response, NH_3 concentration, and RH vs. time—simulation of real-time measurement and (**b**) comparison of PANI-Au-SPE sensor's responses obtained from real-time measurement with the calibration curve.

Table 1 summarises the characteristics of the PANI-Au-SPE sensor constructed and studied here with state-of-the-art PANI NH_3 sensors at RT [8,30,70–73]. All the presented PANI systems from the literature were based on a chemically synthesised PANI and without the presence of any nanomaterials. Indeed, the PANI/HCl from a chemical synthesis shows a quantification limit at 1000 ppb [73] when the electropolymerised PANI/HCl from this investigation has a quantification limit 31 times lower. Regarding the response time, we also need to consider preliminary experiments with the reference NH_3 analyser, showing a slow response to the real-time NH_3 concentration increase inside the gas chamber. Because the concentration is not that high, it is impossible to distinguish the response time from the actual filling time. Thus, the calculated response time for the presented system is over-estimated and is probably much shorter.

Table 1. Metrological parameters for the NH_3 gas sensors based on PANI at RT.

Material	PANI Synthesis	Detection Limit [1] [ppb]	Quantification Limit [2] [ppb]	Sensitivity [% ppm^{-1}]	Response Time [min]
PU-PANI (CSA) [8]	Chemical	/	20	0.8	5 at 1 ppm
PBuA-PANI (HCl) [8]	Chemical	/	250	10	2.5 at 1 ppm
PVDF-PANI (DBSA) [8]	Chemical	/	100	17	2.5 at 1 ppm
WO3@PANI [71]	Chemical	3	500	/	4.2 for >0.25 ppm
PANI (H_2SO_4) [30]	Chemical	7	/	15	3 at 50 ppm
PANI-MWCNT (HCl) [70]	Chemical	/	200	/	1.3 at 12 ppm
PANI (DBSA) [3] [72]	Chemical	/	40	7900	/
PANI (HCl) [73]	Chemical	/	1000	/	/
PANI (HCl) [this work]	Electrochemical	23	32	12.3 [32–200 ppb] & 4.27 [200–1000 ppb]	5.2 at 1 ppm

[1] Theoretical detection limit. [2] Lowest measured concentration. [3] Results were only reported as an evolution of relative impedance and not the relative resistance.

Regarding the PANI's' conductivity and sensing performance, the addition of an appropriate nanomaterial, i.e., electron donors or acceptors, in the form of metal, metal oxide nanoparticles or carbon nanotubes, enhances the conductivity due to the p-n heterojunction at the interface between the p-type PANI and n-type nanoparticles [33,34,50]. If the PANI's sensing characteristic is changed to n-type, p-n heterojunctions are formed by the addition of material, which acts as p-type (electron acceptor), e.g., carbon nanotubes [35]. As a result, ultra-low detection limits (0.25 ppb at 60% RH and RT [50], 0.25 ppb [33] and <16 ppb [34] at RT with humidity compensation) can be achieved. In contrast, this work is based on pure PANI with the simplest dopant (HCl) and no additional nanomaterial. Nevertheless, due to the film's morphology and low thickness, a sufficiently low quantification limit

(32 ppb) and good performance (sensitivity: 12.3% ppm^{-1} [32–200 ppb] and 4.27% ppm^{-1} [200–1000 ppb]) were achieved. Comparing the presented sensing system based on PANI with the literature on PANI for NH_3 sensing as presented in Table 1, better sensing properties in terms of sensitivity were found, mainly due to the addition of complex dopants and nanomaterials. Our proposed sensing system is comparable to the best of the state-of-the-art literature for PANI/NH_3 sensors; however, it offers the advantages of ease of fabrication and simplicity where PANI is doped only with an univalent ion (Cl^-). At this stage, any further work on adding nanomaterials to the system has the potential to improve sensitivity. With the good baseline of the current sensor, the addition of nanomaterials could, in the first stage, be focused on adding a certain material that could catalyse the target analyte to produce NH_3 and enable the indirect detection of other toxic compounds.

In the field of sensors, four main characteristics make a material/system suitable: sensitivity, repeatability, reproducibility, and selectivity. As shown in the calibration plots (Figure 11a,b) and by comparing with the literature (Table 1), the PANI-Au-SPE has a high sensitivity in the low-ppb range. Moreover, the reproducibility and the repeatability of our PANI-Au-SPE was proven by comparing electrodes with different connection geometries (Figure 9a) and by performing several continuous cycles (Figure 9b). Finally, as the selectivity of PANI for NH_3 detection was already proven [21,26,30,71], our PANI-Au-SPE sensor is an excellent example of an NH_3 sensor system. Generally, after comparing our work with previously reported studies [6,8,30,70–73] we can conclude that electrochemically deposited PANI is an under-examined but up-and-coming area of NH_3 gas sensing. Due to its practical and controllable preparation via electropolymerisation and SPE's direct use, the proposed procedure reveals novel aspects for NH_3 sensing.

4. Conclusions

We have shown that electrochemically synthesised PANI doped with HCl can be successfully deposited on a gold, screen-printed electrode (Au-SPE) and used as an efficient room-temperature NH_3-gas sensor. With our approach, we have successfully bridged the gap from 3-electrode electrochemical systems suitable for PANI electrodeposition to 2-electrode resistivity systems suitable for NH_3 gas sensing, which was further achieved via additional Au sputtering. Such prepared PANI-Au-SPE sensors show exceptionally good repeatability, reproducibility and sensitivity in the low-ppb NH_3 range. The incorporation of the gas analyser as an additional component for checking and controlling the target gas inlet contributes to the system characterisation, i.e., fewer measurements for a calibration curve with multiple points, enable real-time sensor responses and genuine results, i.e., monitoring the sensor's responses during gas interflow and not only at the maximum concentration. Electrochemical synthesis is considered to be unconventional as it is rarely used in gas sensing, but this fully controllable way of preparing PANI, and its combination with a three-electrode SPE system, leads to novel aspects in PANI gas-sensing systems.

Author Contributions: Conceptualisation, A.K., C.D., J.-L.W. and K.Ž.R.; methodology, A.K., K.Ž.S. and C.D.; software, N.R.; validation, C.D., J.-L.W. and K.Ž.R.; formal analysis, A.K., and K.Ž.S.; investigation, A.K., K.Ž.S. and C.D.; resources, C.D., J.-L.W.; data curation, A.K., K.Ž.S. and C.D.; writing—original draft preparation, A.K.; writing—review and editing, A.K., C.D., N.R., J.-L.W., K.Ž.R., K.Ž.S. and S.Š.; visualisation, A.K., K.Ž.R., C.D. and J.-L.W.; supervision, K.Ž.R., C.D., J.-L.W.; project administration, S.Š., K.Ž.R.; funding acquisition, S.Š. All authors have read and agreed to the published version of the manuscript.

Funding: This research was funded by the ARRS young-researcher project, grant number PR-08337; the ARRS project High performance nanostructured acrylamide sensors, grant number J2-1739; program Nanostructured Materials, grant number P2-0084; and the Erasmus+ program of the European Union, Jožef Stefan International Postgraduate School project, grant number 2019-1-SI01-KA103-060202.

Institutional Review Board Statement.: Not applicable.

Informed Consent Statement: Not applicable.

Data Availability Statement: Data sharing not applicable.

Acknowledgments: The work was performed in the framework of collaboration between Jožef Stefan Institute, Slovenia and Institut Mines-Télécom, Lille Douai France. The authors are grateful to Beno Klopčič for construction and production of the connector, to the ULTRACOOL laboratory for the access to equipment (Director's Fund 2017 project), and to Živa Marinko for performing the profilometry.

Conflicts of Interest: The authors declare no conflict of interest.

References

1. Hangarter, C.M.; Chartuprayoon, N.; Hernández, S.C.; Choa, Y.; Myung, N.V. Hybridized conducting polymer chemiresistive nano-sensors. *Nano Today* **2013**, *8*, 39–55. [CrossRef]
2. Le, T.-H.; Kim, Y.; Yoon, H. Electrical and electrochemical properties of conducting polymers. *Polymers* **2017**, *9*, 150. [CrossRef] [PubMed]
3. Park, S.J.; Park, C.S.; Yoon, H. Chemo-electrical gas sensors based on conducting polymer hybrids. *Polymers* **2017**, *9*, 155. [CrossRef] [PubMed]
4. Wong, Y.C.; Ang, B.C.; Haseeb, A.S.M.A.; Baharuddin, A.A.; Wong, Y.H. Review—Conducting polymers as chemiresistive gas sensing materials: A review. *J. Electrochem. Soc.* **2020**, *167*, 037503. [CrossRef]
5. Pandey, S. Highly sensitive and selective chemiresistor gas/vapor sensors based on polyaniline nanocomposite: A comprehensive review. *J. Sci. Adv. Mater. Devices* **2016**, *1*, 431–453. [CrossRef]
6. Tanguy, N.R.; Thompson, M.; Yan, N. A review on advances in application of polyaniline for ammonia detection. *Sens. Actuators B Chem.* **2018**, *257*, 1044–1064. [CrossRef]
7. Alfano, B.; Massera, E.; de Maria, A.; de Girolamo, A.; di Francia, G.; Delli Veneri, P.; Napolitano, T.; Borriello, A. Polyaniline Proton Doping for Sensor Application. In Proceedings of the 2015 18th AISEM Annual Conference, AISEM 2015, Trento, Italy, 26 March 2015.
8. Wojkiewicz, J.L.; Bliznyuk, V.N.; Carquigny, S.; Elkamchi, N.; Redon, N.; Lasri, T.; Pud, A.A.; Reynaud, S. Nanostructured polyaniline-based composites for ppb range ammonia sensing. *Sens. Actuators B Chem.* **2011**, *160*, 1394–1403. [CrossRef]
9. Mikhaylov, S.; Ogurtsov, N.; Noskov, Y.; Redon, N.; Coddeville, P.; Wojkiewicz, J.L.; Pud, A. Ammonia/amine electronic gas sensors based on hybrid polyaniline-TiO2 nanocomposites. The effects of titania and the surface active doping acid. *RSC Adv.* **2015**, *5*, 20218–20226. [CrossRef]
10. Patni, N.; Jain, N.; Pillai, S.G. Polyaniline-based sensors for monitoring and detection of ammonia and carbon monoxide gases. In *Trends and Applications in Advanced Polymeric Materials*; John Wiley & Sons Inc.: Hoboken, NJ, USA, 2017; pp. 145–162. ISBN 9781119364795.
11. Virji, S.; Kaner, R.B.; Weiller, B.H. Hydrogen sensors based on conductivity changes in polyaniline nanofibers. *J. Phys. Chem. B* **2006**, *110*, 22266–22270. [CrossRef]
12. Nicolas-Debarnot, D.; Poncin-Epaillard, F. Polyaniline as a new sensitive layer for gas sensors. *Anal. Chim. Acta* **2003**, *475*, 1–15. [CrossRef]
13. Bai, H.; Shi, G. Gas sensors based on conducting polymers. *Sensors* **2007**, *7*, 267–307. [CrossRef]
14. Kwak, D.; Lei, Y.; Maric, R. Ammonia gas sensors: A comprehensive review. *Talanta* **2019**, *204*, 713–730. [CrossRef] [PubMed]
15. Occupational Safety and Health Administration Sampling and Analytical Methods; Ammonia in Workplace Atmospheres—Solid Sorbent. Available online: https://www.osha.gov/dts/sltc/methods/inorganic/id188/id188.html (accessed on 16 March 2020).
16. The Fertilizer Institute. *Health Effects of Ammonia*; The Fertilizer Institute: Arlington, VA, USA, 2010.
17. National Research Council (US); Committee on Acute Exposure Guideline Levels Ammonia. Acute exposure guideline levels. In *Acute Exposure Guideline Levels for Selected Airborne Chemicals*; National Academies Press: Washington, DC, USA, 2008; Volume 6, pp. 58–114. ISBN 978-0-309-11213-0.
18. Grabowska-Polanowska, B.; Faber, J.; Skowron, M.; Miarka, P.; Pietrzycka, A.; Śliwka, I.; Amann, A. Detection of potential chronic kidney disease markers in breath using gas chromatography with mass-spectral detection coupled with thermal desorption method. *J. Chromatogr. A* **2013**, *1301*, 179–189. [CrossRef] [PubMed]
19. Davies, S.; Spanel, P.; Smith, D. Quantitative analysis of ammonia on the breath of patients in end-stage renal failure. *Kidney Int.* **1997**, *52*, 223–228. [CrossRef] [PubMed]
20. Di Natale, C.; Paolesse, R.; Martinelli, E.; Capuano, R. Solid-state gas sensors for breath analysis: A review. *Anal. Chim. Acta* **2014**, *824*, 1–17. [CrossRef]
21. Le Maout, P.; Wojkiewicz, J.L.; Redon, N.; Lahuec, C.; Seguin, F.; Dupont, L.; Mikhaylov, S.; Noskov, Y.; Ogurtsov, N.; Pud, A. Polyaniline nanocomposites based sensor array for breath ammonia analysis. Portable e-nose approach to non-invasive diagnosis of chronic kidney disease. *Sens. Actuators B Chem.* **2018**, *274*, 616–626. [CrossRef]
22. Carquigny, S.; Redon, N.; Plaisance, H.; Reynaud, S. Development of a polyaniline/fluoral-P chemical sensor for gaseous formaldehyde detection. *IEEE Sens. J.* **2012**, *12*, 1300–1306. [CrossRef]
23. Antwi-Boampong, S.; Peng, J.S.; Carlan, J.; Belbruno, J.J. A molecularly imprinted fluoral-p/polyaniline double layer sensor system for selective sensing of formaldehyde. *IEEE Sens. J.* **2014**, *14*, 1490–1498. [CrossRef]

24. Feng, S.; Farha, F.; Li, Q.; Wan, Y.; Xu, Y.; Zhang, T.; Ning, H. Review on smart gas sensing technology. *Sensors* **2019**, *19*, 3760. [CrossRef]
25. Kukla, A.L.; Shirshov, Y.M.; Piletsky, S.A. Ammonia sensors based on sensitive polyaniline films. *Sens. Actuators B Chem.* **1996**, *37*, 135–140. [CrossRef]
26. Kumar, L.; Rawal, I.; Kaur, A.; Annapoorni, S. Flexible room temperature ammonia sensor based on polyaniline. *Sens. Actuators B Chem.* **2017**, *240*, 408–416. [CrossRef]
27. Wallace, G.G.; Teasdale, P.R.; Spinks, G.M. *Conductive Electroactive Polymers: Intelligent Polymer Systems*; CRC Press: Boca Raton, FL, USA, 2009; ISBN 9781420067095.
28. Ramohlola, K.E.; Monana, G.R.; Hato, M.J.; Modibane, K.D.; Molapo, K.M.; Masikini, M.; Mduli, S.B.; Iwuoha, E.I. Polyaniline-metal organic framework nanocomposite as an efficient electrocatalyst for hydrogen evolution reaction. *Compos. Part B Eng.* **2018**, *137*, 129–139. [CrossRef]
29. Hirata, M.; Sun, L. Characteristics of an organic semiconductor polyaniline film as a sensor for NH3 gas. *Sens. Actuators A. Phys.* **1994**, *40*, 159–163. [CrossRef]
30. Mérian, T.; Redon, N.; Zujovic, Z.; Stanisavljev, D.; Wojkiewicz, J.L.; Gizdavic-Nikolaidis, M. Ultra sensitive ammonia sensors based on microwave synthesized nanofibrillar polyanilines. *Sens. Actuators B Chem.* **2014**, *203*, 626–634. [CrossRef]
31. Di Zhang, H.; Tang, C.C.; Long, Y.Z.; Zhang, J.C.; Huang, R.; Li, J.J.; Gu, C.Z. High-sensitivity gas sensors based on arranged polyaniline/PMMA composite fibers. *Sens. Actuators A Phys.* **2014**, *219*, 123–127. [CrossRef]
32. Abdulla, S.; Mathew, T.L.; Pullithadathil, B. Highly sensitive, room temperature gas sensor based on polyaniline-multiwalled carbon nanotubes (PANI/MWCNTs) nanocomposite for trace-level ammonia detection. *Sens. Actuators B Chem.* **2015**, *221*, 1523–1534. [CrossRef]
33. Zhang, D.; Wu, Z.; Li, P.; Zong, X.; Dong, G.; Zhang, Y. Facile fabrication of polyaniline/multi-walled carbon nanotubes/molybdenum disulfide ternary nanocomposite and its high-performance ammonia-sensing at room temperature. *Sens. Actuators B Chem.* **2018**, *258*, 895–905. [CrossRef]
34. Liu, C.; Tai, H.; Zhang, P.; Yuan, Z.; Du, X.; Xie, G.; Jiang, Y. A high-performance flexible gas sensor based on self-assembled PANI-CeO_2 nanocomposite thin film for trace-level NH3 detection at room temperature. *Sens Actuators B Chem.* **2018**, *261*, 587–597. [CrossRef]
35. Zhang, W.; Cao, S.; Wu, Z.; Zhang, M.; Cao, Y.; Guo, J.; Zhong, F.; Duan, H.; Jia, D. High-performance gas sensor of polyaniline/carbon nanotube composites promoted by interface engineering. *Sensors* **2020**, *20*, 149. [CrossRef]
36. Krutovertsev, S.A.; Sorokin, S.I.; Zorin, A.V.; Letuchy, Y.A.; Antonova, O.Y. Polymer film-based sensors for ammonia detection. *Sens. Actuators B. Chem.* **1992**, *7*, 492–494. [CrossRef]
37. Zeng, F.-W.; Liu, X.-X.; Diamond, D.; Lau, K.T. Humidity sensors based on polyaniline nanofibres. *Sens. Actuators B Chem.* **2010**, *143*, 530–534. [CrossRef]
38. Manjunatha, S.; Machappa, T.; Ravikiran, Y.T.; Chethan, B.; Sunilkumar, A. Polyaniline based stable humidity sensor operable at room temperature. *Phys. B Condens. Matter* **2019**, *561*, 170–178. [CrossRef]
39. Chani, M.T.S.; Karimov, K.S.; Khalid, F.A.; Moiz, S.A. Polyaniline based impedance humidity sensors. *Solid State Sci.* **2013**, *18*, 78–82. [CrossRef]
40. Jain, S.; Chakane, S.; Samui, A.B.; Krishnamurthy, V.N.; Bhoraskar, S.V. Humidity sensing with weak acid-doped polyaniline and its composites. *Sens. Actuators B Chem.* **2003**, *96*, 124–129. [CrossRef]
41. Nohria, R.; Khillan, R.K.; Su, Y.; Dikshit, R.; Lvov, Y.; Varahramyan, K. Humidity sensor based on ultrathin polyaniline film deposited using layer-by-layer nano-assembly. *Sens. Actuators B Chem.* **2006**, *114*, 218–222. [CrossRef]
42. Zhang, J.; Liu, X.; Neri, G.; Pinna, N. Nanostructured materials for room-temperature gas sensors. *Adv. Mater.* **2016**, *28*, 795–831. [CrossRef]
43. Gvozdenovic, M.; Jugovic, B.; Stevanovic, J.; Grgur, B. Electrochemical synthesis of electroconducting polymers. *Hem. Ind.* **2014**, *68*, 673–684. [CrossRef]
44. Rana, U.; Paul, N.D.; Mondal, S.; Chakraborty, C.; Malik, S. Water soluble polyaniline coated electrode: A simple and nimble electrochemical approach for ascorbic acid detection. *Synth. Met.* **2014**, *192*, 43–49. [CrossRef]
45. Paul, E.W.; Ricco, A.J.; Wrighton, M.S. Resistance of polyaniline films as a function of electrochemical potential and the fabrication of polyaniline-based microelectronic devices. *J. Phys. Chem.* **1985**, *89*, 1441–1447. [CrossRef]
46. Song, E.; Choi, J.W. A selective hydrogen peroxide sensor based on chemiresistive polyaniline nanowires modified with silver catalytic nanoparticles. *J. Micromech. Microeng.* **2014**, *24*, 065004. [CrossRef]
47. Wang, J.; Chan, S.; Carlson, R.R.; Luo, Y.; Ge, G.; Ries, R.S.; Heath, J.R.; Tseng, H.R. Electrochemically fabricated polyaniline nanoframework electrode junctions that function as resistive sensors. *Nano Lett.* **2004**, *4*, 1693–1697. [CrossRef]
48. Mehto, A.; Mehto, V.R.; Chauhan, J.; IB, S.; RK, P. Preparation and characterization of polyaniline/ZnO composite sensor. *J. Nanomed. Res.* **2017**, *5*. [CrossRef]
49. Chen, C.; Zhang, J.; Du, Y.; Yang, X.; Wang, E. Microfabricated on-chip integrated Au-Ag-Au three-electrode system for in situ mercury ion determination. *Analyst* **2010**, *135*, 1010–1014. [CrossRef] [PubMed]
50. Zhang, Y.; Zhang, J.; Jiang, Y.; Duan, Z.; Liu, B.; Zhao, Q.; Wang, S.; Yuan, Z.; Tai, H. Ultrasensitive flexible NH3 gas sensor based on polyaniline/SrGe4O9 nanocomposite with ppt-level detection ability at room temperature. *Sens. Actuators B Chem.* **2020**, *319*. [CrossRef]

51. Fratoddi, I.; Venditti, I.; Cametti, C.; Russo, M.V. Chemiresistive polyaniline-based gas sensors: A mini review. *Sens. Actuators B Chem.* **2015**, *220*, 534–548. [CrossRef]
52. Couto, R.A.S.; Lima, J.; Quinaz, M.B. Recent developments, characteristics and potential applications of screen-printed electrodes in pharmaceutical and biological analysis. *Talanta* **2016**, *146*, 801–814. [CrossRef]
53. Kellenberger, A.; Ambros, D.; Plesu, N. Scan rate dependent morphology of polyaniline films electrochemically deposited on nickel. *Int. J. Electrochem. Sci.* **2014**, *9*, 6821–6833.
54. Korent, A.; Žagar Soderžnik, K.; Šturm, S.; Žužek Rožman, K. A correlative study of polyaniline electropolymerization and its electrochromic behavior. *J. Electrochem. Soc.* **2020**, *167*, 106504. [CrossRef]
55. Plesu, N.; Kellenberger, A.; Mihali, M.; Vaszilcsin, N. Effect of temperature on the electrochemical synthesis and properties of polyaniline films. *J. Non Cryst. Solids* **2010**, *356*, 1081–1088. [CrossRef]
56. DropSens. DropSens Screen-Printed Electrodes. Available online: http://www.dropsens.com/en/pdfs_productos/new_brochures/250at-250bt.pdf (accessed on 8 October 2019).
57. Yano, J.; Yoshikawa, K.; Kitani, A. Kinetic study of the electropolymerization of aniline using chronoamperometric techniques. *Anal. Sci.* **1997**, *13*, 741–746. [CrossRef]
58. Molano Franco, D.; Arevalo-Rodriguez, I.; Roqué i Figuls, M.; Zamora, J. Interleukin-6 for diagnosis of sepsis in critically ill adult patients. *Cochrane Database Syst. Rev.* **2015**, *1*, 1–8. [CrossRef]
59. Fitriyana, F.; Kurniawan, F. Polyaniline-invertase-gold nanoparticles modified gold electrode for sucrose detection. *Indones. J. Chem.* **2015**, *15*, 226–233. [CrossRef]
60. Chen, W.C.; Wen, T.C.; Gopalan, A. Negative capacitance for polyaniline: An analysis via electrochemical impedance spectroscopy. *Synth. Met.* **2002**, *128*, 179–189. [CrossRef]
61. Huang, W.S.; MacDiarmid, A.G. Optical properties of polyaniline. *Polymer* **1993**, *34*, 1833–1845. [CrossRef]
62. Yin, M.; Liu, S. Preparation of ZnO hollow spheres with different surface roughness and their enhanced gas sensing property. *Sens. Actuators B Chem.* **2014**, *197*, 58–65. [CrossRef]
63. Brožová, L.; Holler, P.; Kovářová, J.; Stejskal, J.; Trchová, M. The stability of polyaniline in strongly alkaline or acidic aqueous media. *Polym. Degrad. Stab.* **2008**, *93*, 592–600. [CrossRef]
64. Rangel-Vazquez, N.-A.; Sánchez-López, C.; Felix, F.R. Spectroscopy analyses of polyurethane/polyaniline IPN using computational simulation (Amber, MM+ and PM3 method). *Polímeros* **2014**, *24*, 453–463. [CrossRef]
65. Bhadra, S.; Singha, N.K.; Khastgir, D. Electrochemical synthesis of polyaniline and its comparison with chemically synthesized polyaniline. *J. Appl. Polym. Sci.* **2007**, *104*, 1900–1904. [CrossRef]
66. Dhivya, C.; Vandarkuzhali, S.A.A.; Radha, N. Antimicrobial activities of nanostructured polyanilines doped with aromatic nitro compounds. *Arab. J. Chem.* **2019**, *12*, 3785–3798. [CrossRef]
67. Kinyanjui, J.M.; Hanks, J.; Hatchett, D.W.; Smith, A.; Josowicz, M. Chemical and electrochemical synthesis of polyaniline/gold composites. *J. Electrochem. Soc.* **2004**, *151*, D113–D120. [CrossRef]
68. Travers, J.P.; Nechtschein, M. Water effects in polyaniline: A new conduction process. *Synth. Met.* **1987**, *21*, 135–141. [CrossRef]
69. Cavallo, P.; Acevedo, D.F.; Fuertes, M.C.; Soler-Illia, G.J.A.A.; Barbero, C.A. Understanding the sensing mechanism of polyaniline resistive sensors. Effect of humidity on sensing of organic volatiles. *Sens. Actuators B Chem.* **2015**, *210*, 574–580. [CrossRef]
70. He, L.; Jia, Y.; Meng, F.; Li, M.; Liu, J. Gas sensors for ammonia detection based on polyaniline-coated multi-wall carbon nanotubes. *Mater. Sci. Eng. B Solid State Mater. Adv. Technol.* **2009**, *163*, 76–81. [CrossRef]
71. Fan, G.; Chen, D.; Li, T.; Yi, S.; Ji, H.; Wang, Y.; Zhang, Z.; Shao, G.; Fan, B.; Wang, H.; et al. Enhanced room-temperature ammonia-sensing properties of polyaniline-modified WO3 nanoplates derived via ultrasonic spray process. *Sens. Actuators B Chem.* **2020**, 127892. [CrossRef]
72. Hibbard, T.; Crowley, K.; Killard, A.J. Direct measurement of ammonia in simulated human breath using an inkjet-printed polyaniline nanoparticle sensor. *Anal. Chim. Acta* **2013**, *779*, 56–63. [CrossRef] [PubMed]
73. Chen, J.; Yang, J.; Yan, X.; Xue, Q. NH3 and HCl sensing characteristics of polyaniline nanofibers deposited on commercial ceramic substrates using interfacial polymerization. *Synth. Met.* **2010**, *160*, 2452–2458. [CrossRef]

Chapter 6

Au-Decorated Electrochemically Synthesised Polyaniline-Based Sensory Platform for Amperometric Detection of Aqueous Ammonia in Biological Fluids

Ammonia (NH_3) is a highly water-soluble compound. Therefore, it is also present in the environment and the human body in an aqueous form. In the human body, it is present as a degradation product of primary amides, amino acids and hydrolysis of proteins, and it can be present in biological fluids such as blood, saliva, sweat and urine. Increased concentrations of NH_3 interrupt the pH balance in the body and promote processes like dental caries, for example [98]. NH_3 formation in biological fluids can also originate from the disease state of the body. Thus, if an increasing trend in NH_3 concentrations is observed, the early stages of diseases, such as liver and kidney diseases, can be detected [55], [56].

In the previous study (Chapter 6) [68], electrochemically synthesized polyaniline ($PANI_{el}$) deposited on a screen-printed electrode (SPE) was used for NH_3 gas detection. The material showed an immediate response upon exposure to NH_3 gas, indicating excellent affinity and a reaction between PANI and NH_3. For these reasons, the same material was also tested for aqueous NH_3 detection.

The $PANI_{el}$ was directly deposited on commercial SPE via the electropolymerization of 0.1 M ANI in 1.0 M HCl by cyclic voltammetry (CV). In contrast to the first [68] and second studies (Chapters 4 and 5), the polymerization was performed in an electrochemical cell where only the SPE's working electrode (WE) was exposed, and external counter and reference electrodes (CE and RE) were used. In this way, the CE and RE were protected from electrochemical reactions with PANI and kept clean for further detection measurements.

It is known that PANI, when decorated with metal nanoparticles (NPs), exhibits improved electronic properties, which enhance its electrochemical response. With the same goal, $PANI_{el}$ was in our case decorated with Au NPs of three different sizes (5, 10 and 20 nm). The $PANI_{el}$ and $PANI_{el}$-Au NPs were characterized with a field-emission-gun scanning electron microscope (FEG-SEM) to observe the morphology and the NPs' distribution. The electrochemical characterization by CV in acidic (0.1 M H_2SO_4) and neutral media (phosphate buffered saline, PBS) was used to study its electrochemical behaviour and estimate suitable conditions for NH_3 detection. Chronoamperometry (CA) was used for detecting aqueous NH_3 in pH = 7 buffered media to control the PANI's electrochemical behaviour. NH_3 detection was performed using CA at a constant applied potential of 0.2 V vs Ag by injecting a 1 µL sample aliquot into a 50 µL drop of PBS, placed directly on the SPE. The current response due to the injection of NH_3 into buffered electrolyte during the chrono-amperometric measurement results from protonation and the electrochemical reaction of PANI and the high affinity of NH_4^+ to the PANI's surface and its oxidation. The main conclusions of this study are:

- Electrochemical polymerization, performed in an electrochemical cell, resulted in PANI deposition on the WE and at the same time we obtained a clean CE and RE, which enabled further measurements directly on SPE;

- The $PANI_{el}$ electrochemical characterization by CV in acid and neutral media gave an insight into the PANI's behaviour in the sense of the formation of either emeraldine salt or base, which was important information for selecting the CA conditions for NH_3 detection and the background for developing and proving of a sensing mechanism;
- The $PANI_{el}$ showed a repeatable response for sequential injections of NH_3, demonstrating the potential application as an amperometric platform in an automated analytical system as batch-injection analysis (BIA);
- The 20-nm Au NPs were shown to have the largest contribution to the electrical conductivity of the $PANI_{el}$, since they gave the largest response compared to 5 and 10 nm NPs;
- Both the $PANI_{el}$ and the $PANI_{el}$-Au20 have a linear relationship between the current response and the injected ammonia concentration, allowing a determination of the sensory parameters such as a low detection limit, where the $PANI_{el}$-Au20 had a 17-times-lower value;
- The detection of NH_3 in artificial saliva demonstrated the capability of $PANI_{el}$-Au20 material to perform sensory measurements for more complex samples containing a variety of ions and thus proved the high affinity of PANI for NH_3. Furthermore, it demonstrated the suitability of $PANI_{el}$-Au20 for biomedical applications.

More on this topic is provided in the article entitled "Au-decorated electrochemically synthesized polyaniline-based sensory platform for amperometric detection of aqueous ammonia in biological fluids", authored by Anja Korent, Špela Trafela, Kristina Žagar Soderžnik, Zoran Samardžija, Sašo Šturm and Kristina Žužek Rožman, published in Electrochimica Acta, Vol. 430, in 2022 [99]. The article is presented on page 81, and its Supplementary Material is under Appendix A on page 95. The last section of the thesis covers the **4th and 5th aims** of studying PANI's electrochemical behaviour in a neutral medium for the purpose of the electrochemical detection of aqueous NH_3 and further improving the electrochemical response with nanoparticles.

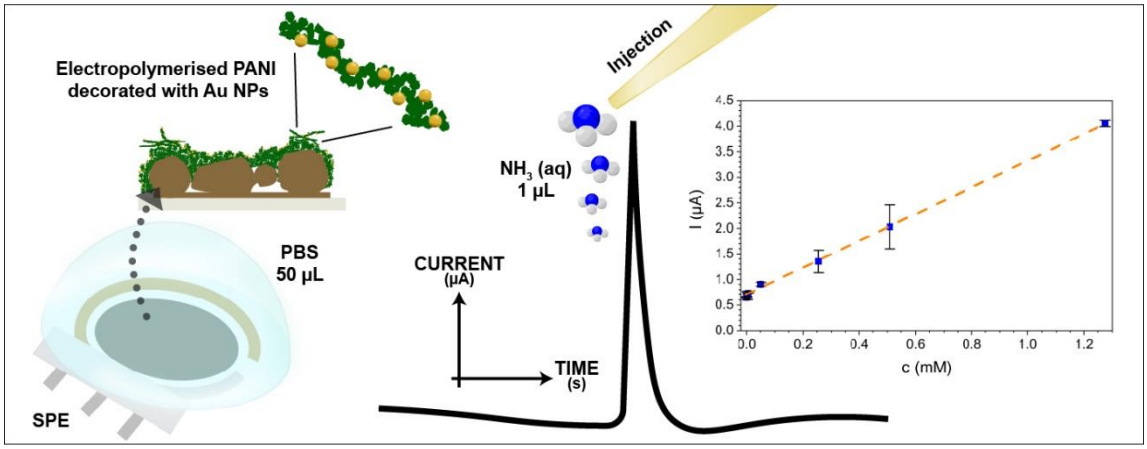

Figure 6.1: Graphical abstract for Chapter: Au-decorated electrochemically synthesised polyaniline-based sensory platform for amperometric detection of aqueous ammonia in biological fluids (Taken from [99].

Electrochimica Acta 430 (2022) 141034

Contents lists available at ScienceDirect

Electrochimica Acta

journal homepage: www.journals.elsevier.com/electrochimica-acta

Au-decorated electrochemically synthesised polyaniline-based sensory platform for amperometric detection of aqueous ammonia in biological fluids

Anja Korent [a,b,*], Špela Trafela [a], Kristina Žagar Soderžnik [a], Zoran Samardžija [a], Sašo Šturm [a,b], Kristina Žužek Rožman [a,b]

[a] Department for Nanostructured Materials, Jožef Stefan Institute, Jamova cesta 39, Ljubljana SI-1000, Slovenia
[b] Jožef Stefan International Postgraduate School, Jamova cesta 39, Ljubljana SI-1000, Slovenia

ARTICLE INFO

Keywords:
Ammonia
Amperometric detection
Electropolymerization
Polyaniline
Screen-printed electrode

ABSTRACT

Ammonia (NH_3) present in biological fluids is biomarker for several disease states. In this work the well-known interaction between polyaniline (PANI) and NH_3 was used for the fabrication of an amperometric sensory platform to detect aqueous NH_3 at neutral i.e. biological pH. Understanding PANI's electrochemical synthesis and redox behaviour in acidic and neutral media was used to determine the NH_3 detection mechanism. The latter is based on the PANI deprotonation reaction, NH_4^+ oxidation and follow-up PANI reduction and oxidation. Chronoamperometry was applied as an NH_3-detection method in a 50 μL background electrolyte in which a 1 μL sample was injected, triggering instantaneous changes to the current. The sensory platform's detection limit, based on pure electrochemically synthesised PANI ($PANI_{el}$) (24.64 μM), was reduced 17 times (1.44 μM) with the addition of 20 nm Au nanoparticles. This Au-decorated $PANI_{el}$ sensory platform showed excellent reversibility, reusability and the possibility for continuously cycled NH_3 measurements, with a recovery rate of 90–99.5% for artificial saliva samples of different pHs. This demonstrates its suitability for more complex samples. The developed sensory platform presents potential from the industry point of view, as a base for an NH_3 batch injection analysis and for preventive home medical self-care.

1. Introduction

Ammonia is an essential compound in every chemistry laboratory and a huge number of industries [1,2]. It is a part of the natural nitrogen cycle, as a product of nitrogen compounds' biological decomposition. In the human body, it is present as a product of several reactions: oxidative degradation of primary amines, degradation of hexoamines, hydrolysis of proteins, deamination of nucleotides and degradation of amino acids [3]. Some of these reactions are a consequence of the diseased state. Chronic kidney disease increases the urea content of the stomach [4] and affects the functioning of the liver, resulting in ammonia being produced.

An increased ammonia concentration can be found in several biological fluids, like blood, urine, saliva and sweat [4,5]. Blood ammonia is an indicator of liver disease and the metabolic condition hyperammonemia. A high ammonia concentration in the urine is an indicator of a disturbed pH balance in the body's extracellular fluid. The ammonia concentration in saliva and sweat increases due to the bacterial hydrolysis of urea in the mouth and skin [5], promoting processes like dental caries.

Depending on the ambient conditions, ammonia can be present as NH_3 and/or the ammonium ion NH_4^+, formed via an equilibrium reaction (Eq. (1)) [3,5]:

$$NH_3\ (g) + H^+ \leftrightarrow NH_4^+ \quad (1)$$

At 25°C, the pKa of NH_4^+ is 9.2 [6], which categorises it as a weak acid, and has a pH at which the proportion of ammonia nitrogen is 50% NH_3 and 50% NH_4^+. In physiological fluids with pH 7–7.4, 99% of the ammonia is NH_4^+ and 1% is in the form of NH_3, called "free ammonia". At pH > 9.2, NH_4^+ reacts with a proton acceptor to form NH_3 [3,5,6]. The presence of both forms has a toxic effect, as they can upset the pH balance of the body's fluids [3].

The sensing of ammonia – as a chemical species, industrial raw material, side-product and biologically and environmentally produced

* Corresponding author at: Department for Nanostructured Materials, Jožef Stefan Institute, Jamova cesta 39, Ljubljana SI-1000, Slovenia.
E-mail address: anja.korent@ijs.si (A. Korent).

https://doi.org/10.1016/j.electacta.2022.141034
Received 19 May 2022; Received in revised form 19 July 2022; Accepted 13 August 2022
Available online 17 August 2022

compound – spans a wide range of applications. Thus, versatile systems need to be studied, from low detection ranges (2.78–111.11 μM) in biomedical applications to higher concentrations (from 5.56 to more than 11.11 mM) in environmental monitoring [7]. Ammonia can be detected either as NH_3 or NH_4^+, which means each detection system needs to be evaluated for its specificity. NH_3 is mainly detected via electro-oxidation in high-pH medium/electrolytes (pH ≥ 10 [8,9], 1 M KOH [10–13]) where ammonium salts ($(NH_4)_2SO_4$ [9,13], NH_4Cl [8, 10]) are the source of the NH_3. Meanwhile, pH < 9 is needed for NH_4^+ detection, for example, from NH_4Cl salt [7,14]. NH_4^+ can be electrochemically detected using all-solid-state ion-selective electrodes composed of metal-wire electrodes (Ag [15–17], Cu [16]) covered with polyaniline (PANI) as a conductive connection between the electrode and ion-selective sensing film [15–17]. Open-circuit-potential measurements are used for the ion-concentration-gradient relationships. However, despite the high selectivity and a wide range of pH conditions, the electrochemical quantification limit lies between 10 and 100 μM of NH_4^+. The NH_4^+ electrochemical detection mechanism can also be based on NH_4^+ reduction, causing a parallel oxidation of the PANI receptor material [7]. An important aspect in analytical practice is the number of samples analysed in a certain time. For these reasons, automated analytical systems were introduced to provide speed, high analytical frequency, and accuracy. Batch injection analysis (BIA), developed in 1991, is an automated analytical system in which a small volume of sample is injected with a micropipette, directly against a nearby detector that is immersed in a large-volume blank solution [18]. BIA can be based on different detection techniques such as amperometry, potentiometry, voltammetry, calorimetry, fluorescence, and spectrophotometry, of which amperometry is the most frequently used. The advantages of BIA are rapid measurements, small sample volume, sensitivity and reproducibility [18,19], which are also interesting for ammonia sensing.

PANI is a member of the conductive polymer family. It can be chemically or electrochemically synthesised at low cost and with little effort. Sensory-potential-wise, it stands out due to its high conductivity, which varies with redox and acid/base (i.e., protonation) reactions that can be directly linked to the analytes' concentration [20]. Chemical species, causing a straightforward conductivity change in PANI, can be monitored by their direct input (H^+ from humidity [21–23], NH_3 [24–29]). As these basic species are often a side product of specific chemical reactions at the PANI's modified surface, their detection can indirectly reflect the concentrations of more complex chemicals. For example, (i) via a conductivity change due to a redox reaction: by modifying PANI with Pd nanoparticles, methanol can be detected via its oxidation, leading to a noticeable parallel reduction of PANI [30]; (ii) or a conductivity change due to an acid/base reaction: H_2S in the presence of metal chloride nanoparticles produces HCl, species causing the protonation of PANI. PANI modified with $SnCl_2$ thus enables H_2S detection via a conductivity change due to HCl formation [31]. The PANI-ammonia system is well studied because it is commonly used for sensing ammonia gas [24–29]. PANI possesses chemiresistive properties and acts as a *p*-type semiconductor, which loses its conductivity due to deprotonation after it is exposed to reducing NH_3 gas. It is also an excellent material for NH_4^+ storage [32], meaning it has the ability to attract and store NH_4^+. As ammonia is a common side-product of several chemical and biochemical reactions, we can use modified PANI-based receptor elements, either modified via organic molecules (fluoral-P [33,34]) or enzymes (urease [9,35,36]), for their indirect sensing.

As mentioned, versatile electrochemical sensing systems have been already developed for aqueous NH_3 sensing using PANI as a sensing material. The majority is focused on NH_3 electrooxidation, which requires a basic electrolyte. The role of NH_3 as a biomarker presents an interest in detecting it in biological fluids, where the concentrations are relatively low. The ammonia concentration in most species, including mammals, varies between approximately 50 and 250 μM, but can increase to over 1 mM [3]. In this study we propose a new sensing mechanism for detecting ammonia as NH_4^+ on electropolymerized PANI ($PANI_{el}$) with commercial screen-printed electrodes (SPEs) at neutral pH. The sensing mechanism is based on the $PANI_{el}$ deprotonation reaction, NH_4^+ oxidation and follow-up $PANI_{el}$ reduction and oxidation. So far, detection systems for aqueous NH_3/NH_4^+ were mainly based on using ammonium salts as analytes in highly basic media for NH_3 [8–11, 13] and in neutral media for NH_4^+ [7,14,37]. However, we have used injections of NH_3 as an analyte source, which represents the most significant difference compared to already-developed systems. The sensory performance of the $PANI_{el}$-based SPE platform was enhanced by introducing Au nanoparticles, resulting in better sensitivity and lower detection and quantification limits. $PANI_{el}$ with 20 nm Au NPs ($PANI_{el}$-Au20) exhibits a three-times-lower detection limit and a 20-times-lower quantification limit than pure $PANI_{el}$, and with a wide detection range. The overall sensing-system performances follow the principle of BIA, as a sample can be injected into the larger volume background solution on the $PANI_{el}$-based SPE. The developed NH_3 sensory platform was implemented for ammonia detection in a medium simulating real-life fluid, i.e., artificial saliva. The system showed a reliable response, with no detectable interference from the species commonly found in biological systems, proving its suitability for biomedical applications. The ability to detect NH_3 presence in artificial saliva shows the potential of further evolution to preventive medical self-care.

2. Experimental

2.1. Reagents and material

Chemicals, including aniline (ANI), hydrochloric acid (HCl, 37%), sulfuric acid (H_2SO_4, 96%), ammonia solution (NH_3, 25%), potassium chloride (KCl), sodium chloride (NaCl), calcium dichloride dihydrate ($CaCl_2 \bullet 2H_2O$), sodium phosphate monobasic (NaH_2PO_4), urea, gold nanoparticle (Au NPs) stabilised suspensions in 0.1 mM PBS of three different sizes (5, 10, and 20 nm), and artificial saliva for pharmaceutical research (pH = 6.8) were purchased from Sigma-Aldrich and used without further purification. BioWhittaker Phosphate Buffered Saline (PBS) – 10x, without Ca and Mg with pH = 6.95 was used for all the chronoamperometry (CA) experiments.

SPEs purchased from the PalmSens company (ItalSens Gold SPE IS-W1-3.C1.RS.35) were used as a base material in the presented research. The chosen SPE is a three-electrode system with a Au working electrode (WE), a Au counter electrode (CE) and a silver pseudo-reference electrode (RE), screen-printed on a polymeric substrate. All the electrochemical experiments, except the electrochemical polymerisation, were performed directly on the SPEs. The electrochemical polymerisation was performed in a Teflon electrochemical cell (volume of 20 mL) with a screen-printed Au WE, and an external Pt mesh as the CE, and Ag/AgCl/3.4 M KCl aqueous solution as the RE (Fig. 1a). The electrochemical cell was assembled in the way to protect CE and RE of SPE, as, during the CV polymerization, as CE is exposed to high positive potentials, that can causthe oxidation of PANI monomer, resulting in the deposition of PANI [1], that is unwanted.

2.2. Electrode preparation

In accordance with the instructions of the producers of the SPEs [38], the electrodes were electrochemically polished before further usage. The electropolishing was performed via cyclic voltammetry (CV). A 100 μL drop of 0.5 M H_2SO_4 was placed on the SPE, covering all three electrodes. The system was cycled between 0 and 1.4 V vs Ag at 100 mV s^{-1} until the cyclic voltammogram for a clean gold electrode was obtained. The electrodes were washed after three cycles with distilled water and dried for further usage.

The PANI was deposited on the Au WE of the SPE via electrochemical polymerisation ($PANI_{el}$). The process was performed via CV using an aniline (ANI) monomer suspended in 20 mL of 1 M HCl to achieve a final

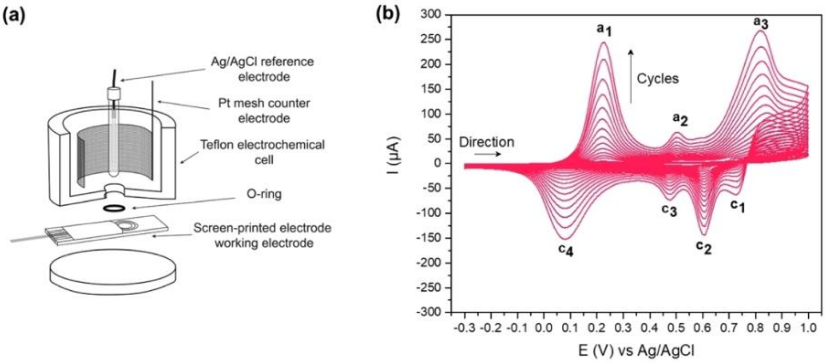

Fig. 1. Schematic representation of electrochemical cell composed of Pt mesh as a counter electrode, Ag/AgCl as a reference electrode and the SPE working electrode (a). Cyclic voltammogram of PANI electropolymerisation in HCl between −0.3 and 1.0 V vs Ag/AgCl at 50 mV s−1 (b).

ANI concentration of 0.1 M. The CV was performed in the potential range between −0.3 and 1.0 V vs Ag/AgCl at 50 mV s^{-1}. The experiment was manually stopped after finishing the cycle in which the first oxidation peak ($E = 0.23$ V vs Ag/AgCl) reached a current of 250 μA. The electrode prepared in this way was washed with ethanol and left to dry in the air at room temperature before further usage.

The $PANI_{el}$ decorated with Au NPs ($PANI_{el}$-Au) was prepared by drop-casting 10 μL of suspended Au NPs of a certain size (diameters of 5, 10 and 20 nm) on $PANI_{el}$ and left to dry overnight in the air at room temperature ($PANI_{el}$-Au5, $PANI_{el}$-Au10, and $PANI_{el}$-Au20). As the $PANI_{el}$-Au20 had the best electrochemical response to NH_3 detection (compared to PANIel-Au5 and PANIel-Au10), all the electrochemical and sensory experiments were focused on the $PANI_{el}$ and $PANI_{el}$-Au20.

2.3. Material characterisation

2.3.1. Morphology characterisation

The Au WE of the SPE, $PANI_{el}$ and $PANI_{el}$-Au (5, 10 and 20 nm Au NPs) samples for scanning electron microscopy were attached to metallic sample holders using conductive carbon adhesive tape and observed at various magnifications in a field-emission-gun scanning electron microscope (FEG-SEM Verios G4 HP, Thermo Fisher Scientific, USA). A preliminary examination of the samples showed that they were sufficiently electrically conductive for the SEM analysis. However, they were also sensitive to damage caused by prolonged exposure to the electron beam. Consequently, the experimental conditions for imaging were set to an accelerating voltage of 2 kV, a beam current between 20 and 50 pA, and a working distance of 4 mm. To avoid sample damage under the electron beam, SEM images were acquired at suitable frame-scanning rates over the analysed area, followed by frame integration to produce high-quality images. The electron micrographs were recorded with two detectors: (i) a through-the-lens detector (TLD) for secondary electrons (SE) and (ii) a mirror detector (MD) for backscattered electrons (BSEs) positioned within the objective lens.

To observe the Au NPs' structure and size, transmission electron microscopy (TEM) with energy-dispersive X-ray spectroscopy (EDS) was used (JEOL JEM-2100, Jeol Ltd., Tokyo, Japan). The samples for the TEM observations were prepared by dispersing the nanoparticles after ultrasonic de-agglomeration in water onto lacey, carbon-coated Cu grids.

2.3.2. Electrochemical characterisation

All electrochemical experiments were performed with a USB and a battery-powered potentiostat/galvanostat/EIS analyser from PalmSens4 supported by PSTrace software. The data were plotted and characterised using the Origin program.

The electrochemical behaviours of the pure Au WE and $PANI_{el}$ were observed in acidic and neutral media using a CV. A 50 μL drop of 0.1 M H_2SO_4 (pH = 1.9) placed directly on the SPE was used in the acid medium. Electrodes were cycled between −0.4 and 0.6 V vs Ag at 50 mV s^{-1} and between −0.4 and 0.2 V vs Ag with varying scan rates (10–100 mV s^{-1}). The reversibility of the $PANI_{el}$s' first redox pair was estimated by plotting the anodic and cathodic peak currents vs the square root of the scan rate, according to the Randles-Sevčik equation (Eq. (2)) [39]:

$$I_p = 2.69 \cdot 10^5 n^{3/2} A D^{1/2} c \nu^{1/2} \quad (2)$$

where n is the number of reacting electrons, A is the surface area [m^2], D is the diffusion coefficient [$m^2\ s^{-1}$], c is the concentration of reacting species [$mol\ L^{-1}$], and ν is the scan rate [$mV\ s^{-1}$]. A 50 μL drop of PBS (pH = 6.95) was used for the CV study in a neutral medium. Electrodes were scanned in potential ranges from −0.40 to 0.85 V vs Ag at 50 mV s^{-1} (1 cycle) and from −0.2 to 0.3 V vs Ag at 50 mV s^{-1} (10 cycles).

2.4. Aqueous ammonia detection

A pristine Au electrode, $PANI_{el}$, and $PANI_{el}$ decorated with Au NPs of three sizes (5, 10 and 20 nm) were used for the amperometric measurements. CA was performed by placing a 50 μL drop of PBS as a background electrolyte directly on the SPE. Potentials −0.1, 0.1 and 0.2 V vs Ag were used to study the potentials' influence on NH_3 detection. All further chrono-amperometric measurements were made with an applied potential of 0.2 V vs Ag. A schematic of the dynamics of the chrono-amperometric measurement of NH_3 detection is presented in Fig. S1. After the current stabilisation of the electrode in the PBS, a 1 μL NH_3 aliquot was injected. NH_3 solutions of different concentrations were prepared in a PBS by diluting 25% NH_3. The resulted output currents of 1 μL NH_3 aliquot injection are presented as a deducted current by subtracting the value of the stabilised current. The final response currents were calculated as reported in Eq. (3):

$$I = I_t - I_0 \quad (3)$$

where I_t is the resulting output current of the 1 μL NH_3 aliquot at a certain time, and I_0 is the value of the stabilised current of the electrode in the background electrolyte, taken 2 s before the aliquot's injection. The maximum response currents were taken to study the relationship between the current's response and the NH_3 concentrations.

2.5. Stability and interference study

$PANI_{el}$-Au20 samples were stored in a desiccator for the stability study. After a certain number of storage days (3, 7, 14, 31, and 61 days), samples were used for NH_3 detection. The studies were made by performing a CA with 0.2 V vs Ag constant applied potential in 50 μL of PBS. After the current stabilisation of the electrode in the 50 μL of PBS background electrolyte at 0.2 V vs Ag, 1 μL of 12.75 mM NH_3 aliquot was injected.

The interference study was performed using NH_3 aliquots prepared in commercial and the Fusayama-Mayer artificial saliva solution and measured as described above. The Fusayama-Mayer artificial saliva solution (pH = 5) was prepared with the following composition [40]: 0.4 g L^{-1} KCl, 0.4 g L^{-1} NaCl, 0.906 g L^{-1} $CaCl_2 \bullet 2H_2O$, 0.531 g L^{-1} NaH_2PO_4 and 1 g L^{-1} urea.

3. Results and discussion

3.1. Polyaniline electropolymerization

The PANI was electrochemically synthesized ($PANI_{el}$) and deposited on a cleaned, gold working electrode (Au WE) of the commercial screen-printed electrode (SPE). The cleaning procedure is described in the Supporting data (Fig. S2). The electropolymerisation process was performed in a Teflon electrochemical cell (Fig. 1a) using external CE and RE. In this way, only the WE of the SPE was exposed to the electrolyte and the CE and RE of the SPE were protected from all possible side reactions on the CE. Fig. 1b shows cyclic voltammograms of a complete polymerization process in 1 M HCl cycled between −0.3 and 1.0 V vs Ag/AgCl at 50 mV s^{-1}. The voltammograms show the typical PANI oxidation ($\mathbf{a_1}$ = 0.23 V, $\mathbf{a_2}$ = 0.50 V, and $\mathbf{a_3}$ = 0.82 V vs Ag/AgCl) and reduction ($\mathbf{c_1}$ = 0.73 V, $\mathbf{c_2}$ = 0.61 V, $\mathbf{c_3}$ = 0.47 V, and $\mathbf{c_4}$ = 0.08 V vs Ag/AgCl) peaks [41–43]. The ANI oxidation peak at a potential of 0.93 V vs Ag/AgCl (0.90 V vs SCE [43]) is visible in the first few cycles of the electropolymerisation and represents the initial and most significant step. However, it is not visible in the final image of the CV experiment (Fig. 1b), since with further polymerisation it becomes masked by the emeraldine oxidation peak ($\mathbf{a_3}$ = 0.82 V vs Ag/AgCl) [42]. During the CV polymerisation process, the $PANI_{el}$ is the subject of basic polymerization reactions (monomer oxidation, dimonomer formation, etc. [44]). At the same time, the already-deposited $PANI_{el}$ goes through typical electrochemical transitions, reflected in the characteristic oxidation ($\mathbf{a_1}$, $\mathbf{a_2}$, and $\mathbf{a_3}$) and reduction ($\mathbf{c_1}$, $\mathbf{c_2}$, $\mathbf{c_3}$, and $\mathbf{c_4}$) peaks (Fig. 1b). The peak $\mathbf{a_1}$ represents the oxidation of leucoemeraldine to emeraldine, $\mathbf{a_2}$ the formation of the intermediate degradation products, and $\mathbf{a_3}$ the oxidation of emeraldine to pernigraniline. Peaks $\mathbf{c_{1\text{-}4}}$ represent the opposite reductive reactions. The separated peaks $\mathbf{c_1}$ and $\mathbf{c_2}$ are for the reduction of pernigraniline to emeraldine. The separation is associated with the electrolyte's acidity [41]. The peak $\mathbf{c_3}$ is the reduction of the intermediate degradation products, and $\mathbf{c_4}$ is the reduction of emeraldine to leucoemeraldine [41–43]. By increasing the number of cycles, the peak currents increase, indicating a larger amount of deposited material, as each higher current reflects the redox transition of a larger amount of material. The polymerization process was manually stopped after finishing the cycle for which the first oxidation peak $\mathbf{a_1}$ (0.23 V vs Ag) reached 250 μA. The oxidation peak $\mathbf{a_1}$ was chosen due solely to the PANI redox transition [45,46]. Controlling the height of peak $\mathbf{a_1}$ in each polymerization process leads to a constant and reproducible amount of deposited $PANI_{el}$. The final product of the electrochemical polymerisation via the CV in the HCl electrolyte is HCl-doped PANI in the form of green emeraldine salt [24,42].

3.2. Material characterization

To gain an insight into the surface changes in the electrode-preparation stages the morphology and composition of a pristine Au SPE after electropolishing, $PANI_{el}$ deposited on Au-SPE via CV, and $PANI_{el}$-Au-SPE decorated with Au NPs of three sizes ($PANI_{el}$-Au5, $PANI_{el}$-Au10, $PANI_{el}$-Au20) were investigated by SEM (Figs. 2., S3, and S4). SE images of the topography/morphology are presented in Figs. 2a, b, S3 and S4a,b and BSE compositional contrast images in Figs. 2c,d and S4c,d. The pristine SPE's Au WE has a granular morphology composed of particles of different sizes and surface textures (Fig. S3). After electropolymerisation (preparation of $PANI_{el}$ via CV), the Au particles of the pristine SPE are completely covered with nanogranular $PANI_{el}$. Further, nanogranular $PANI_{el}$ starts to grow into nanofibers. However, these fibres do not cover the whole surface, but are located as separate islands (Fig. 2a). The latter could be a consequence of an uneven Au electrode surface, as it is known that a uniform surface composed of thin layers [24] results in a more even nanofibrous structure of $PANI_{el}$, covering the entire surface of the Au electrode.

Au NPs were chosen as the material to boost the conductivity and corresponding later sensory properties of $PANI_{el}$. It is known that nanomaterials (carbon nanotubes [47], nanoparticles [11,37], nanosheets [10]) can be used to enhance the surface area of the electrode as well as the conductivity [48]. Song et al. [48] demonstrated Au NPs' excellent electron transfer ability to contribute to material's conductivity, i.e., reducing material impedance. Their SEM analysis shows the Au NPs attachment to the carbon nanofibers increase the surface area. Additionally, Au can cause the oxidative doping of PANI, thus enhancing its conductivity [49]. Figs. 2b and S4a,b present the topography/morphology of $PANI_{el}$ decorated with 20, 5 and 10 nm Au NPs. From the morphological point of view, Au NPs do not affect the initial $PANI_{el}$s' nanogranular and nanofibrous structure, as they are attached just to the $PANI_{el}$s'surface. Their attachment to the $PANI_{el}$s' surface (Fig. 2b) results in an increased overall surface area. NPs' location is clearly seen from the BSE-SEM images of the the $PANI_{el}$-Au (Figs. 2d and FS4c,d). The majority of the Au-NP population is randomly distributed across the $PANI_{el}$, with some concentrated areas.

Before the sensory experiments, the $PANI_{el}$ was characterized in an acidic medium to confirm the deposition of the characteristic PANI material [50,51]. The electrochemical characterisation of the $PANI_{el}$ was performed in 0.1 M H_2SO_4 via CV, and unlike the polymerisation, involved exposing all three SPEs to the electrolyte (Fig. S5a). A typical voltammogram for the $PANI_{el}$ electrochemical reactions in an acidic medium [50,51] is presented in Fig. S5b and described in the supplementary data.

Regarding the detection of NH_3 in biological fluids, $PANI_{el}$ was electrochemically characterized in PBS. A cyclic voltammogram of the $PANI_{el}$'s behaviour in PBS (Fig. 3a) presents two oxidation peaks, ($\mathbf{a_1}$ = 0.16 V and $\mathbf{a_2}$ = 0.46 V vs Ag), which correspond to the main oxidation reactions of PANI (leucoemeraldine/emeraldine and emeraldine/pernigraniline). Emeraldine salt and emeraldine blue share the same electronic environment (just a difference in protonation). Therefore, it is not clear from the CV which emeraldine is the result of the oxidation reaction. Their presence can, however, be determined by observing their pH dependence [52]. The transition from leucomeraldine to emeraldine salt is pH-independent. Meanwhile, leucoemeraldine to emeraldine blue depends on the pH value (−59 mV/decade of pH) [52]. From Figs. S5b and 3 the shift of the $\mathbf{a_1}$ peak's potential (from -0.09 to 0.16 V) due to the pH change indicates the emeraldine blue formation. Performing a CV of PANI at pH ≥ 5 results in the overlapping of two oxidation peaks (leucoemeraldine/pernigraniline) [52,53], as the first oxidation peak shifts towards the second oxidation peak, due to the pH increase. Obtaining two oxidation peaks of HCl-doped $PANI_{el}$ shows the advantage with regards to the ability to focus only on the region of emeraldine formation. After crossing the potential of pernigraniline formation, the current drops rapidly with no reduction peaks in the reverse scan. This exposes the polymer to a higher potential (>0.5 V vs Ag, Fig. 3a) at pH = 7, causing irreversible overoxidation, i.e., rapid structural degradation and a loss of electroactivity [54]. Thus, the electrochemical study of $PANI_{el}$ was focused on the potential region of the first oxidation peak $\mathbf{a_1}$ (i.e.,

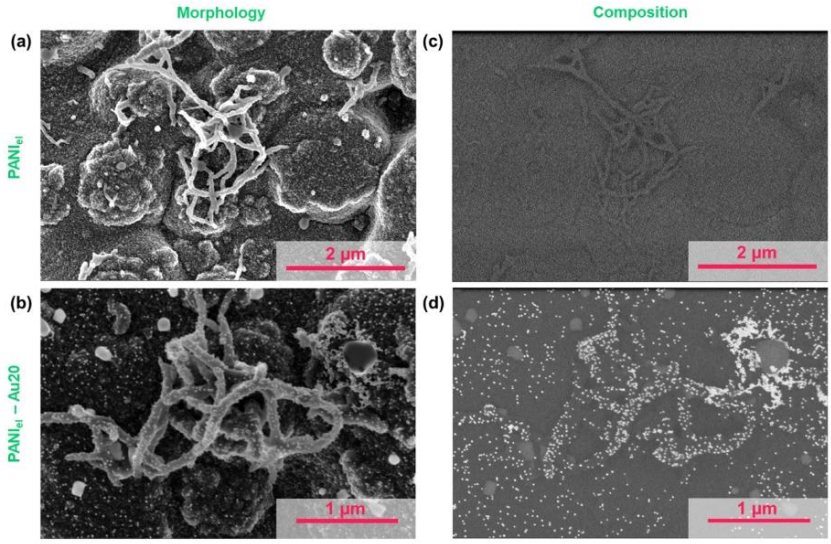

Fig. 2. Secondary-electron (a, b) and backscattered-electron SEM images (c, d) of PANIel (a, c) and PANIel-Au20 (b, d).

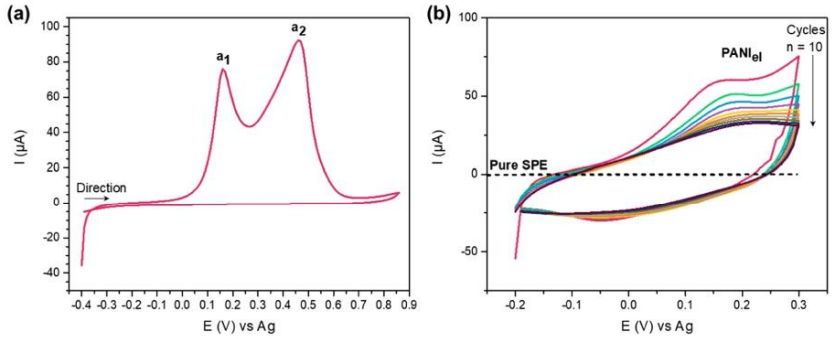

Fig. 3. Electrochemical characterisation of PANIel in PBS electrolyte via CV in the range between −0.40 and 0.85 V vs Ag at 50 mV s−1 (a), and its stability after continuous cycling between −0.2 and 0.3 V vs Ag at 50 mV s−1 (b).

the oxidation of leucoemeraldine to emeraldine). In the potential range between −0.2 and 0.3 V vs Ag (Fig. 3b), both oxidation (0.16 V) and reduction (−0.05 V) peaks are observed. Because PANI's conductivity depends on the degree of oxidation and protonation [20], and the pKa of emeraldine is around 3, some deprotonation and conductivity losses are expected after continuous cycling in the PBS. Thus, the oxidation and reduction peaks become lower and less sharp. However, sufficient constant conductivity remained after 10 cycles, since the $PANI_{el}$ still showed electrochemical behaviour in the sense of oxidation and reduction current.

3.3. NH_3 detection

As $PANI_{el}$ undergoes redox and protonation reactions during a potential scan, CA was used as a detection method. Therefore, three constant potential values (−0.1, 0.1 and 0.2 V vs Ag) according to the CV in PBS (Fig. 3a,b) were chosen to study the $PANI_{el}$'s response to NH_3. −0.1 V represents the redox potential at which $PANI_{el}$ overcomes its redox transition; 0.1 V is the starting potential of the oxidation transition; and 0.2 V is the potential at which $PANI_{el}$ overcomes oxidation to emeraldine. Higher potentials (>0.5 V vs Ag, Fig. 3a) were not chosen as they lead to a loss of conductivity. Fig. 4a presents the amperometric response of $PANI_{el}$ in the PBS electrolyte and its response to the injection of NH_3 at different potentials (−0.1, 0.1 and 0.2 V vs Ag). At potentials of 0.1 and 0.2 V, $PANI_{el}$ starts ($t = 0$ s) with a high oxidation current, which instantly drops and stabilises with time. The stabilised current is above zero, as a consequence of the oxidation reactions at these potentials. At an applied potential of −0.1 V, the resulting initial current is

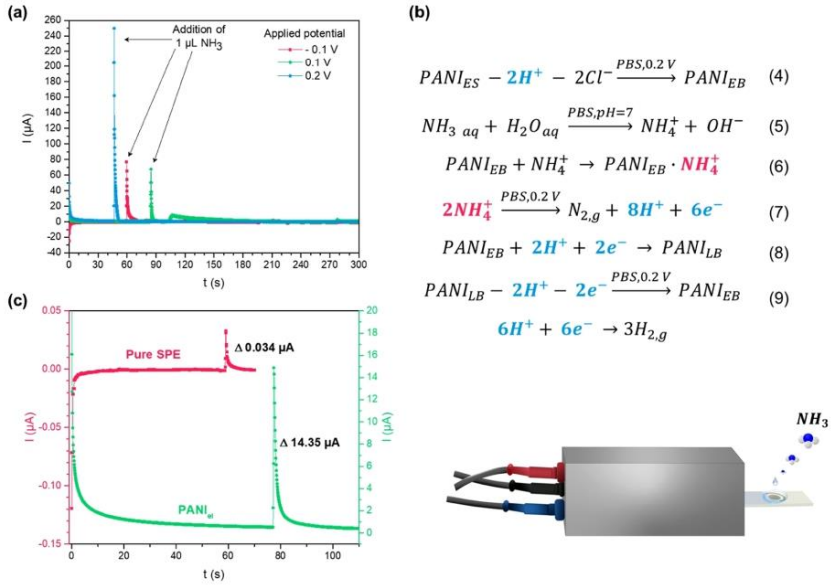

Fig. 4. Amperometric response of PANIel to 263 mM NH3 aliquot injection to PBS at different potentials (−0.1, 0.1 and 0.2 V vs Ag) performed directly on a SPE (a). Comparison between the amperometric response of pristine SPE and deposited PANIel to 25.5 mM NH3 aliquot injection to PBS at applied potential of 0.2 V vs Ag (b). The sensing mechanism of PANIel, due to the injection of NH3 aliquot to PBS at constant potential 0.2 V vs Ag (c).

negative (t = 0 s) and stabilizes below zero, as −0.1 V is the reductive potential for $PANI_{el}$. The injection of NH_3 resulted in an anodic current increase for all three selected applied potentials. At the potential 0.2 V, the injection of NH_3 triggers the highest $PANI_{el}$ response. The potential of −0.1 V was excluded from further investigation since the fully reduced form leucoemeraldine present at this potential is unstable and immediately oxidises in the presence of oxygen [51]. Thus, the background electrolyte PBS would need to be continuously purged with an inert gas [9] to exclude the contribution of the oxidation current due to the presence of oxygen. As 0.2 V resulted in a higher current increase compared to 0.1 V, the oxidative potential of 0.2 V was chosen for all subsequent chrono-amperometric measurements.

On the basis of the voltammetric (Fig. 3) and chrono-amperometric (Fig. 4) observations, the mechanism of chronoamperometric NH_3 detection (at 0.2 V) in a neutral medium is proposed. The starting material for NH_3 detection is the emeraldine salt (protonated half-oxidised form), obtained after the CV polymerisation process in HCl. Once $PANI_{el}$, as an emeraldine salt, is exposed to a neutral medium (PBS, pH = 7) and an oxidative potential of 0.2 V, it loses its protonation and transforms into the emeraldine blue form (Fig. 4b Eq. (4)). As was already explained, the CV study of $PANI_{el}$ in PBS (Fig. 3) showed the loss of protonation and inability to restore the emeraldine salt form in the oxidation scan, where it transforms into emeraldine blue. The transition from emeraldine salt to emeraldine blue was also observed in the chrono-amperometric study at a constant applied potential of 0.2 V (green line in Fig. 4c), where the instant initial oxidation current drops and stabilizes above zero. $PANI_{el}$ in the form of emeraldine blue is the starting point before the injection of the NH_3 aliquot. The injection of NH_3 aliquots into the neutral medium on the electrode surface moves the reaction Eq. (1) towards NH_4^+ (Fig. 4b, Eq. (5)) due to the pH=7. NH_4^+ in the PBS electrolyte instantly triggers the complex formation with $PANI_{el}$ (Fig. 4b, Eq. (6)). NH_4^+ tends to form strong hydrogen bonds with hosts [32] and occupy empty protonation sites in the PANI [7]. The formation of the $PANI_{el}{\cdot}NH_4^+$ complex results in an instant increase in the oxidation current, which is a result of reactions Eqs. (7)–(9). Eq. (7) (Fig. 4b) represents NH_4^+ oxidation due to an applied potential of 0.2 V and is the source of electrons and protons for a simultaneous $PANI_{el}$ emeraldine base reduction, resulting in a protonated reduced $PANI_{el}$ (Fig. 4b Eq. (8)). At the same time, protonated $PANI_{el}$ is subjected to an oxidation reaction since the system is under an applied oxidative potential 0.2 V (Fig. 4b Eq. (9)). After the consumption of reductant and $PANI_{el}$ deprotonation, the current returns to its initial value and stabilizes (Fig. 4b Eq. (9)). This mechanism allows the generation of the transient current response to the presence of NH_3 in amperometric mode. The electro-activity of the $PANI_{el}$ electrode, (Fig. 4b Eq. (7)) was additionally proved with a comparative amperometric measurement of the NH_3 aliquot's injection into the PBS on the pristine Au SPE (pink line in Fig. 4c). The current increase after NH_3 injection indicates the oxidation of the NH_4^+. However, the oxidation current's increase on the pristine Au SPE (Δ 0.034 µA) is negligible compared to the $PANI_{el}$ electrode (Δ 14.350 µA, Fig. 4c) for the same NH_3 concentration (25.5 mM).

The presented mechanism indicates the recovery of $PANI_{el}$ to its initial PBS-stabilised state (Fig. 4b Eq. (9)), which enables sequential measurements in a single experiment. Fig. 5a shows the amperometric response of sequential injections of 12.75 mM NH_3. The sequential injection of the NH_3 aliquot after each current stabilisation gave similar maximum oxidation currents (5.04 ± 0.72 µA) and recovery. For a better interpretation of the results, the currents (I) are represented by subtracting the stabilised current value I_0 (Eq. (3), Fig. 5b), which is specifically determined for each measurement. Fig. 5b presents the deduced current responses from Fig. 5a, with a green standard deviation area presenting the relative standard deviation (RSD) of 9.13% for the $PANI_{el}$'s response to 12.75 mM NH_3. These results show the ability of the reversible sensing mechanism and a great potential for integration into

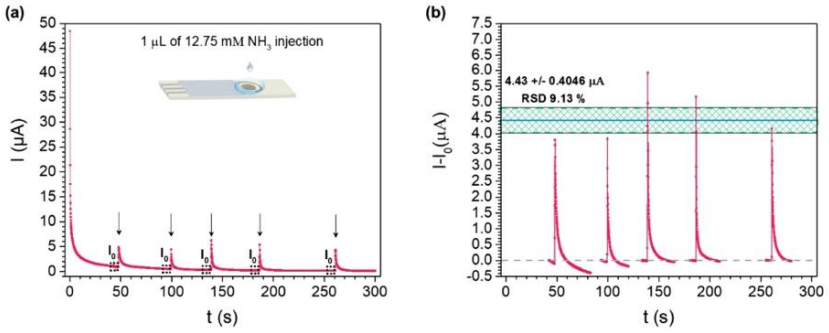

Fig. 5. Amperometric response of PANIel for sequential injections of 12.75 mM NH3 to the PBS at a constant potential of 0.2 V vs Ag, presented with real-time currents (a) and deduced currents (b).

an automated analytical system called batch injection analysis (BIA). Furthermore, the reusability of the $PANI_{el}$ was also proven by separate sequential measurements on the same electrode (Fig. S6). The electrode was washed with distilled water and wiped with a paper towel between each measurement. The deduced currents showed comparable responses (6.62 ± 0.71 μA) in at least six measurements, confirming the complete recovery of the $PANI_{el}$ after each measurement and a compact, consistent and robust electrode after cleaning and wiping.

To gain an insight into the sensory performance of the $PANI_{el}$ for NH_3 detection, the effect of different concentrations was amperometrically studied. Fig. 6a shows the amperometric results of the $PANI_{el}$ for different NH_3 concentrations (51 μM to 2550 mM). Higher NH_3 concentrations give a higher oxidative current increase, according to the proposed sensing mechanism (Fig. 4b). The relationship between the current's response and the concentration was studied in the range from 51 μM to 510 mM NH_3. The calibration plot is linear in two ranges, 0 μM to 5.10 mM with a sensitivity of 0.83 μA μM^{-1} (Fig. 6b) and 5.10 mM to 510 mM with a sensitivity of 0.68 μA μM^{-1} (Fig. 6c). Response reproducibility is presented as error bars obtained from the standard deviations of the response of three ($n = 3$) electrodes at a given concentration. At higher NH_3 concentrations (above 510 mM), the current response does not follow a linear relationship anymore, they are not accurate and have higher error. With a higher concentration, the response starts to decrease. This could be a consequence of the complete occupation of the empty protonation sites by NH_4^+, i.e., saturation region. The split calibration curves for PANI-NH_3 sensing system has been already observed [10,11,13].

To further enhance the $PANI_{el}$'s sensory performances, $PANI_{el}$ was decorated with commercial Au NPs. Fig. 7 shows the improvement in the $PANI_{el}$'s amperometric response to NH_3 in the case of the integration of Au NPs of different sizes (5-, 10- and 20 nm). It is known that metallic NPs on the PANI improve the PANIs' electrochemical properties [35]. The presence of Au NPs improved the stabilisation of the background currents, i.e., less scattering in the measured current in the PBS baseline,

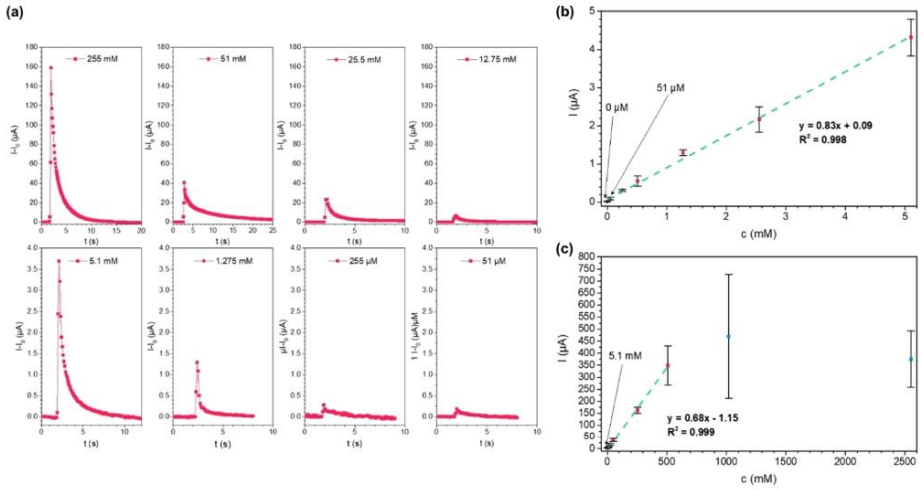

Fig. 6. Relationship between the amperometric response of PANIel and the NH3 concentration in PBS at a constant potential of 0.2 V vs Ag (a) presented in two linear ranges ($n = 3$): 0 μM to 5.10 mM (b) and 5.10 to 510 mM (c).

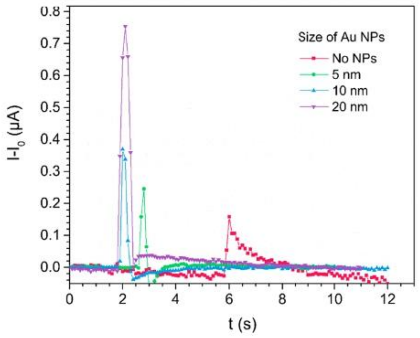

Fig. 7. Effect of Au nanoparticle size, drop casted on PANIel, on its amperometric response to 51 μM NH3 injection to PBS at a constant potential 0.2 V vs Ag.

and resulted in a sharper and increased current response to NH_3 in all three cases. The injection of 51 μM NH_3 triggered a current response of 0.15 μA for pure $PANI_{el}$, 0.25 μA for $PANI_{el}$-Au5, 0.37 μA for $PANI_{el}$-Au10, and 0.76 μA for $PANI_{el}$-Au20. It is evident that the $PANI_{el}$ decorated with 20 nm has an approximately 5-times-better response to the same NH_3 concentration in comparison to the other Au NPs sizes. The electrical character of the polymer-metal contact (in this case PANI-Au NPs) is defined by the position of the metal's Fermi level and the position of the lowest unoccupied molecular orbital in a polymer [49]. PANI has a p-type conduction characteristic [55], and in combination with a high work-function metal such as Au (5.2 eV), it can form low-resistance ohmic contacts [49]. It is observed that 20 nm Au NPs have the largest influence on the amperometric response. According to the fundamental resistance formula Eq. (10) [56]:

$$R = \frac{\rho L}{A} \tag{10}$$

where R is the resistance (a measure of the opposition to the flow of electric current, Ω), L is the length [m], A is the cross-section [m^2, for round particle $A = \pi r^2$], and ρ is the resistivity [characteristic property, Ωm], the 20 nm Au NPs have a lower resistance than the 5 and 10 nm Au NPs. Thus, they make the largest contribution to the electric conductivity in altering the $PANI_{el}$'s electronic properties. The size of the commercial 5, 10 and 20 nm Au NPs was confirmed with the TEM analysis presented in the supplementary data (Fig. S7)

In view of the $PANI_{el}$-Au20's highest amperometric response to NH_3, the $PANI_{el}$-Au20 was characterized using a series of NH_3 concentrations. Fig. 8 shows the current response's dependence on the NH_3 concentration in the range 2.55 μM to 2550 mM. The calibration plot is linear in four ranges: 0 to 5.10 μM with a sensitivity of 16.21 μA μM^{-1} (Fig. 8a inserted), 5.10 μM to 1.275 mM with a sensitivity of 2.60 μA μM^{-1} (Fig. 8a), 125 μM to 51 mM with a sensitivity of 0.91 μA μM^{-1}, and 51 to 510 mM with a sensitivity of 0.03 μA μM^{-1} (Fig. 8b). Compared with $PANI_{el}$, $PANI_{el}$-Au20 has higher current responses and better sensitivity in the low concentration range (0.83 μA μM^{-1} for $PANI_{el}$ vs 16.21 μA mM^{-1} for $PANI_{el}$-Au20). Although at higher concentrations (≥ 25.50 mM) $PANI_{el}$ has higher current responses. This response for the higher NH_3 concentrations could be explained by the assumption that Au NPs are blocking the sites on the active sites on the $PANI_{el}$ surface for NH_4^+ binding. The sensory performances of the $PANI_{el}$ and $PANI_{el}$-Au20 were compared with the detection limit (LOD), as calculated by Eq. (12):

$$LOD = \frac{3\sigma}{m} \tag{12}$$

where 3 stands for sensitivity/noise ratio, σ is the standard deviation of the current's response for the blank ($n = 3$), and m refers to the slope of the calibration graph. The LOD for $PANI_{el}$ is 24.64 μM, and with the addition of a drop of Au NPs, the detection limit was reduced 17 times (1.44 μM for $PANI_{el}$-Au20) (Table S1). The quantification limit (QL) was determined to be 51 μM for $PANI_{el}$ and 2.55 μM for $PANI_{el}$-Au20, which is 20-times lower.

3.4. Stability and interference study

One of the important parameters for PANI as a sensor material is its stability, as it is known to be sensitive to humidity [21–23]. To assess the stability and lifetime of $PANI_{el}$-Au20, the electrodes were stored in a desiccator for 1 to 61 days. The ageing process was estimated with respect to the changes in the current responses to NH_3 (Fig. 9). From Fig. 9 it is clear that the current response decreases with ageing time, since the use of a desiccator does not eliminate the ageing effect [14]. The decrease of the current response can also be a consequence of conductivity loss due to the use of small-molecule volatile acid (HCl) as a dopant [52]. Nevertheless, $PANI_{el}$-Au20 seems to reach its limit after two months of storage as the current response became constant. The results indicate that in the case of the application of $PANI_{el}$-Au20 according to the presented calibration plot (Fig. 8) the time gradient of the current needs to be considered.

Real-life samples have a complex composition, containing different species, which could interfere with the sensing process, having unwanted redox processes, or affect the receptor material's properties. Therefore, the $PANI_{el}$-Au20 electrode was tested for NH_3 dissolved in

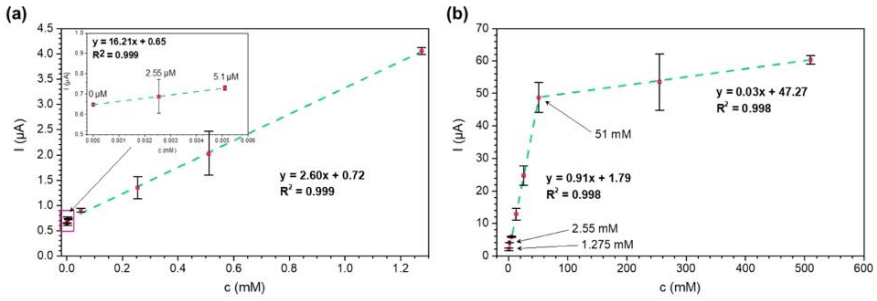

Fig. 8. Relationship between the amperometric response of PANIel-Au20 and NH3 concentration in PBS at a constant potential presented in four linear ranges ($n = 3$): 0 to 5.10 μM ((a) inserted), 5.10 μM to 1.275 mM (a), 1.275 to 51 mM and 51 to 510 mM (b).

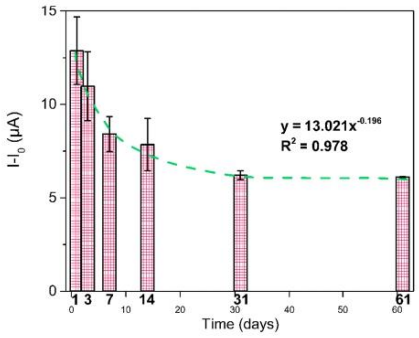

Fig. 9. Lifetime study of PANIel-Au20 stored in a desiccator shown as the PANIel-Au20's response to a 12.75 mM NH3 injection into PBS at a constant potential of 0.2 V vs Ag ($n = 3$).

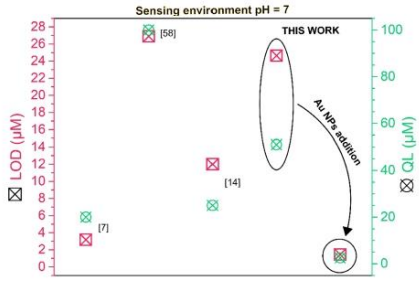

Fig. 10. Illustrative presentation of state of the art values on LOD and QL for conductive polymer PANI-based aqueous NH3 detection systems, obtained for pure analyte samples in neutral medium (pH = 7).

commercial artificial saliva (pH = 7) and prepared Fusayama-Mayer artificial saliva (pH = 5). The actual concentrations of the NH_3 aliquots prepared in both artificial saliva were 1.275 mM, 5.100 mM and 25.50 mM, while those values were 1.258 mM, 4.69 mM and 24.73 mM in commercial artificial saliva and 1.269 mM, 4.573 mM and 24.74 mM in Fusayama-Mayer artificial saliva, determined by the $PANI_{el}$-Au20 electrode (Table 1). The recovery rate is 89–99.8%, which excludes the effect of additional ions on the $PANI_{el}$ and indicates the selectivity of the $PANI_{el}$-Au20 towards NH_4^+. Artificial saliva was used to simulate a biological fluid and a source of different ions (K^+, Cl^-, Na^+, Ca^{2+}, PO_4^{3+}), which could affect the PANI. As PANI is a pH-sensitive material [57] two artificial salivas with different pHs were tested. The recovery rates for both solutions were comparable. Thus, the PBS as a background electrolyte is sufficiently buffered to exclude major impacts due to the injection of a sample with a more acidic pH. Additionally, the predominant ingredient in Fusayama-Mayer artificial saliva is urea, an important component as it is an NH_3 source in the human body. Ingredients of the Fusayama-Mayer artificial saliva (KCl, NaCl, $CaCl_2 \bullet 2H_2O$, NaH_2PO_4, and urea) made no obvious interference, suggesting that $PANI_{el}$-Au20 has an excellent anti-interference performance.

The performance comparison for the developed system with the reported electrochemical NH_3 sensory systems in the literature based on conductive polymers (PANI, polypyrrole) is illustratively presented in Fig. 10 and summarized in the supplementary data (Table S1). The most significant parameter determining the NH_3 detection mechanism is the choice of medium pH. As already mentioned in the introduction, this determines whether NH_3 is in molecular or ionic form. Thus, we classified NH_3-detection based on conductive polymer-based systems into three groups considering the medium pH being 7, 10.5 and 14 (Table S1). It needs to be considered, that the initial construction of sensory material depends on the further application aim. For example, in the case of future modification of initial material into biomolecule-modified material for biosensing, the background electrolyte needs to be suitable for the biomolecule to retain activity. Comparing the sensor characteristics of similar systems' behaviour against ammonium ion presence (Fig. 10) [7,14,58], i.e., operating at a neutral buffered medium, developed PANIel-Au20 surpasses sensory performance including detection limit, quantification limit, and range. However, it needs to be considered that these characteristics are obtained under laboratory conditions, clean and pure electrolyte with a presence of manually added target analyte. Uzunçar et al. [58] demonstrated the PANI-NH_4^+ sensing abilities based on the doping/de-doping process of PANI in the presence of NH_4^+ cation. It was pointed out the importance of the presence of additional anionic group as a charge compensator during doping/de-doping process. PANI, modified with Nafion or polystyrene-sulphonate (source of sulphonate group) enable better intake of NH_4^+ and enable voltammetric detection (CV, DPV), observing loss of protonation or the protonation during the reduction or oxidation scans respectively. $PANI_{el}$-Au20 successfully detected low concentrations of NH_4^+ with the simple HCl-doping, combining electrochemistry of NH_4^+ and PANI. So-prepared catalyst-free material presents a potential starting point for further biomolecule modification (addition of enzymes), a construction of biosensors according to the literature [9,35,36,58]. Regarding the interference study, demonstrating the potential application (Table S1), each system presents an anti-interference performance in the presence of different ions and molecules. $PANI_{el}$-Au20 NH_3 sensing performance was tested in the presence of artificial saliva components, where it showed 89–99.8% recovery. $PANI_{el}$-Au20 is up to now novel in ability to detect NH_3 in artificial saliva. By detecting hazardous NH_3 in saliva, which is the easiest-to-obtain biological sample, the developed PANIel-Au20 sensing platform can be further developed towards preventive medical self-care applications.

4. Conclusion

The electrochemically polymerised polyaniline ($PANI_{el}$) deposited on a Au SPE was demonstrated to be an excellent material for aqueous NH_3 detection at neutral pH. PANI electroplymerization via cyclic voltammetry in 1 M HCl media was selected to obtain the most conductive form of PANI, i.e., emeraldine green. The chronoamperometry (CA) with an applied potential of 0.2 V vs Ag was selected for the detection of NH_3. The latter ensured the emeraldine blue form of $PANI_{el}$ with enough protonation to be conductive and at the same time enough empty protonation spaces for NH_4^+ absorption at a neutral pH. Based on the

Table 1
Detection of aqueous NH_3 in artificial saliva with different pH ($n = 3$).

	Commercial artificial saliva (pH=7)			Fusayama-Mayer artificial saliva (pH = 5)		
Actual [NH_3] (mM)	Response (I-I_0 [μA])	Measured [NH_3] (mM)	Recovery (%)	Response (I-I_0 [μA])	Measured [NH_3] (mM)	Recovery (%)
1.275	3.99 ± 0.35	1.258	98.7	4.03 ± 0.45	1.273	99.8
5.100	6.06 ± 0.84	4.69	92.0	5.92 ± 0.75	4.538	88.9
25.50	24.29 ± 4.32	24.73	97.0	24.16 ± 1.76	24.74	97.0

experimental results and theoretical knowledge, the sensing mechanism for NH_3 at neutral pH was proposed, and is based on the $PANI_{el}$ deprotonation reaction, NH_4^+ oxidation and follow-up $PANI_{el}$ reduction and oxidation. It was found that simple Cl^- doping of $PANI_{el}$ ensures its high sensory performance, without using any additional additives/dopants for charge compensation for NH_4^+ intake. Functionalizing $PANI_{el}$ with Au NPs promoted the system's conductivity, which resulted in a better stabilisation of the current and sensory performances (a 17-times-lower detection limit) in the low NH_3 concentration range. Compared to the reported electrochemical NH_3 sensory systems based on conductive polymers, $PANI_{el}$-Au20 has the widest detection range and better sensory performance (detection and quantification limit, sensitivity) with the detection limit in a range applicable for biomedical applications. A lifetime and interference study further showed that $PANI_{el}$-Au20 is sensitive to long-term ageing; however, its response becomes constant with time. With a very high recovery rate of 90–99.5% for NH_3 measurements in artificial saliva of two different pHs, the $PANI_{el}$-Au20 proved its ability to reliably sense NH_3 with a negligible interference from surrounding ions and even the presence of urea. The developed amperometric sensory platform uses the principle of sample injection into a PBS background electrolyte and has excellent sensory properties together with a significant repeatability, reusability and recovery of $PANI_{el}$ after each injection of NH_3. As such, it represents a base platform for the automated batch injection analysis of NH_3 in biological systems. Additionally, due to the user-friendly electrochemical approach and the ability to detect NH_3 presence in saliva, the presented work is well suited to preventive medical self-care applications.

CRediT authorship contribution statement

Anja Korent: Conceptualization, Data curation, Formal analysis, Investigation, Visualization, Writing – original draft, Writing – review & editing. **Špela Trafela:** Data curation, Visualization, Writing – review & editing. **Kristina Žagar Soderžnik:** Investigation, Project administration, Writing – review & editing. **Zoran Samardzija:** Investigation, Writing – review & editing. **Saša Sturm:** Project administration, Resources, Writing – review & editing. **Kristina Žužek Rožman:** Project administration, Supervision, Visualization, Writing – review & editing.

Declaration of Competing Interest

The authors declare that they have no known competing financial interests or personal relationships that could have appeared to influence the work reported in this paper.

Data Availability

No data was used for the research described in the article.

Acknowledgements

The authors thank to The Arrs Young-Researcher Project, Grant number PR-08337, The Arrs Project High Performance Nanostructured Acrylamide Sensors, Grant number J2-1739, The Arrs Project Development Of High Performance Sensors For Detection Of Persistent And Mobile Chemicals In The Environment (SENSE-PMC), grant number J2-3051, and Program Nanostructured Materials, Grant number P2-0084 for funding.

Supplementary materials

Supplementary material associated with this article can be found, in the online version, at doi:10.1016/j.electacta.2022.141034.

References

[1] D. Li, X. Xu, Z. Li, T. Wang, C. Wang, Detection methods of ammonia nitrogen in water: a review, TrAC Trends Anal. Chem. 127 (2020), https://doi.org/10.1016/J.TRAC.2020.115890.
[2] B. Timmer, W. Olthuis, A. Van Den Berg, Ammonia sensors and their applications—a review, Sens. Actuators B Chem. 107 (2005) 666–677, https://doi.org/10.1016/J.SNB.2004.11.054.
[3] A. Adlimoghaddam, M.G. Sabbir, B.C. Albensi, Ammonia as a potential neurotoxic factor in alzheimer's disease, Front. Mol. Neurosci. 9 (2016) 57, https://doi.org/10.3389/FNMOL.2016.00057/BIBTEX.
[4] P.P. Ricci, O.J. Gregory, Sensors for the detection of ammonia as a potential biomarker for health screening, Sci. Rep. 11 (2021) 1–7, https://doi.org/10.1038/s41598-021-86686-1, 2021 11:1.
[5] J.R. Huizenga, A. Tangerman, C.H. Gips, Determination of ammonia in biological fluids, Ann. Clin. Biochem. 31 (Pt 6) (1994) 529–543, https://doi.org/10.1177/000456329403100602.
[6] D.E. Kissel, M.L. Cabrera, AMMONIA. Encyclopedia of Soils in the Environment, Elsevier, 2005, pp. 56–64, https://doi.org/10.1016/B0-12-348530-4/00177-6.
[7] K. Crowley, E. O'Malley, A. Morrin, M.R. Smyth, A.J. Killard, An aqueous ammonia sensor based on an inkjet-printed polyaniline nanoparticle -modified electrode, Analyst 133 (2008) 391–399, https://doi.org/10.1039/B716154A.
[8] F. Valentini, V. Biagiotti, C. Lete, G. Palleschi, J. Wang, The electrochemical detection of ammonia in drinking water based on multi-walled carbon nanotube/copper nanoparticle composite paste electrodes, Undefined. 128 (2007) 326–333. 10.1016/J.SNB.2007.06.010.
[9] B. Strehlitz, B. Gründig, H. Kopinke, Sensor for amperometric determination of ammonia and ammonia-forming enzyme reactions, Anal. Chim. Acta 403 (2000) 11–23, https://doi.org/10.1016/S0003-2670(99)00594-2.
[10] L. Zhang, T. Liu, R. Ren, J. Zhang, D. He, C. Zhao, H. Suo, *In situ* synthesis of hierarchical platinum nanosheets-polyaniline array on carbon cloth for electrochemical detection of ammonia, J. Hazard. Mater. 392 (2020), https://doi.org/10.1016/J.JHAZMAT.2020.122342.
[11] L. Zhang, J. Liu, X. Peng, Q. Cui, D. He, C. Zhao, H. Suo, Fabrication of a Ni foam-supported platinum nanoparticles-silver/polypyrrole electrode for aqueous ammonia sensing, Synth. Met. 259 (2020), 116257, https://doi.org/10.1016/J.SYNTHMET.2019.116257.
[12] W.L. Liu, Y.Y. Liu, J.S. Do, Room temperature amperometric ammonia sensor based on Pt and Pt-Ir porous ceramic electrodes, IEEE Sens. J. 16 (2016) 1872–1879, https://doi.org/10.1109/JSEN.2015.2510370.
[13] L. Zhang, J. Wan, J. Li, Q. Cui, D. He, C. Zhao, H. Suo, Fabricating a self-supported electrode for detecting ammonia in water based on electrodepositing platinum-polypyrrole on Ni foam, J. Electrochem. Soc. 167 (2020), 027537, https://doi.org/10.1149/1945-7111/AB6C55.
[14] N.T. Brannelly, A.J. Killard, An electrochemical sensor device for measuring blood ammonia at the point of care, Talanta 167 (2017) 296–301, https://doi.org/10.1016/J.TALANTA.2017.02.025.
[15] Y. Huang, J. Li, T. Yin, J. Jia, Q. Ding, H. Zheng, C.T.A. Chen, Y. Ye, A novel all-solid-state ammonium electrode with polyaniline and copolymer of aniline/2,5-dimethoxyaniline as transducers, J. Electroanal. Chem. C (2015) 87–92, https://doi.org/10.1016/J.JELECHEM.2014.12.041.
[16] K. Wu, L. Fu, X. Guo, S. Zhu, The fabrication of all solid-state ammonium ion selective electrodes used in aquaculture, in: Proceedings of IEEE Sensors. 2017-December, 2017, pp. 1–3, https://doi.org/10.1109/ICSENS.2017.8234306.
[17] Y. Kan, C. Han, Y. Ye, X. Zhang, Y. Huang, L. Xing, Y. Zhou, H. Qin, An all-solid-state ammonium ion-selective electrode based on polyaniline as transducer and poly (o-phenylenediamine) as sensitive membrane, Int. J. Electrochem. Sci. 11 (2016) 9928–9940, https://doi.org/10.20964/2016.12.03.
[18] M. Hasšo, Ľ. Švorc, Batch injection analysis in tandem with electrochemical detection: the recent trends and an overview of the latest applications (2015–2020), Monatshefte Chem. Chem. Mon. 1 (2022) 1–16, https://doi.org/10.1007/S00706-022-02898-9/FIGURES/7.
[19] M.S.M. Quintino, L. Angnes, Batch injection analysis: an almost unexplored powerful tool, Electroanalysis 16 (2004) 513–523, https://doi.org/10.1002/ELAN.200302878.
[20] G.G. Wallace, P.R. Teasdale, G.M. Spinks, Conductive Electroactive Polymers: Intelligent Polymer Systems, CRC Press, 2009.
[21] F.W. Zeng, X.X. Liu, D. Diamond, K.T. Lau, Humidity sensors based on polyaniline nanofibres, Sens. Actuators B Chem. 143 (2010) 530–534, https://doi.org/10.1016/J.SNB.2009.09.050.
[22] M.T.S. Chani, K.S. Karimov, F.A. Khalid, S.A. Moiz, Polyaniline based impedance humidity sensors, Solid State Sci. 18 (2013) 78–82, https://doi.org/10.1016/j.solidstatesciences.2013.01.005.
[23] J.P. Travers, M. Nechtschein, Water effects in polyaniline: a new conduction process, Synth. Met. 21 (1987) 135–141, https://doi.org/10.1016/0379-6779(87)90077-4.
[24] A. Korent, K. Žagar Soderžnik, S. Šturm, K. Žužek Rožman, N. Redon, J. L. Wojkiewicz, C. Duc, Facile fabrication of an ammonia-gas sensor using electrochemically synthesised polyaniline on commercial screen-printed three-electrode systems, Sensors 21 (2021) 169, https://doi.org/10.3390/s21010169.
[25] L. Kumar, I. Rawal, A. Kaur, S. Annapoorni, Flexible room temperature ammonia sensor based on polyaniline, Sens. Actuators B Chem. 240 (2017) 408–416, https://doi.org/10.1016/j.snb.2016.08.173.
[26] N.R. Tanguy, M. Thompson, N. Yan, A review on advances in application of polyaniline for ammonia detection, Sens. Actuators B Chem. 257 (2018) 1044–1064, https://doi.org/10.1016/j.snb.2017.11.008.

[27] P. le Maout, J.L. Wojkiewicz, N. Redon, C. Lahuec, F. Seguin, L. Dupont, S. Mikhaylov, Y. Noskov, N. Ogurtsov, A. Pud, Polyaniline nanocomposites based sensor array for breath ammonia analysis. Portable e-nose approach to non-invasive diagnosis of chronic kidney disease, Sens. Actuators B Chem. 274 (2018) 616–626, https://doi.org/10.1016/j.snb.2018.07.178.

[28] Z. Jin, Y. Su, Y. Duan, Development of a polyaniline-based optical ammonia sensor, Sens. Actuators B Chem. 72 (2001) 75–79, https://doi.org/10.1016/S0925-4005(00)00636-5.

[29] A. Javadian-Saraf, E. Hosseini, B.D. Wiltshire, M.H. Zarifi, M. Arjmand, Graphene oxide/polyaniline-based microwave split-ring resonator: a versatile platform towards ammonia sensing, J. Hazard. Mater. 418 (2021), 126283, https://doi.org/10.1016/J.JHAZMAT.2021.126283.

[30] A.A. Athawale, S.V. Bhagwat, P.P. Katre, Nanocomposite of Pd-polyaniline as a selective methanol sensor, Sens. Actuators B Chem. 114 (2006) 263–267, https://doi.org/10.1016/J.SNB.2005.05.009.

[31] C. Duc, M.L. Boukhenane, T. Fagniez, L. Khouchaf, N. Redon, J.L. Wojkiewicz, Conductive polymer composites for hydrogen sulphide sensors working at sub-PPM level and room temperature, Sensors 21 (2021) 6529, https://doi.org/10.3390/S21196529/S1.

[32] S.F. Kuchena, Y. Wang, Superior polyaniline cathode material with enhanced capacity for ammonium ion storage, ACS Appl. Energy Mater. 3 (2020) 11690–11698, https://doi.org/10.1021/ACSAEM.0C01791.

[33] S. Antwi-Boampong, J.S. Peng, J. Carlan, J.J. Belbruno, A molecularly imprinted fluoral-p/polyaniline double layer sensor system for selective sensing of formaldehyde, IEEE Sens. J. 14 (2014) 1490–1498, https://doi.org/10.1109/JSEN.2014.2298872.

[34] S. Carquigny, N. Redon, H. Plaisance, S. Reynaud, Development of a polyaniline/fluoral-P chemical sensor for gaseous formaldehyde detection, IEEE Sens. J. 12 (2012) 1300–1306, https://doi.org/10.1109/JSEN.2011.2169783.

[35] F.N. Crespilho, R.M. Iost, S.A. Travain, O.N. Oliveira, V. Zucolotto, Enzyme immobilization on Ag nanoparticles/polyaniline nanocomposites, Biosens. Bioelectron. 24 (2009) 3073–3077, https://doi.org/10.1016/j.bios.2009.03.026.

[36] W.J. Cho, H.J. Huang, An amperometric urea biosensor based on a polyaniline–perfluorosulfonated ionomer composite electrode, Anal. Chem. 70 (1998) 3946–3951, https://doi.org/10.1021/AC980004A.

[37] H. Zhang, Y. Wang, B. Zhang, Y. Yan, J. Xia, X. Liu, X. Qiu, Y. Tang, Construction of ultrasensitive ammonia sensor using ultrafine Ir decorated hollow graphene nanospheres, Electrochim. Acta 304 (2019) 109–117, https://doi.org/10.1016/J.ELECTACTA.2018.11.215.

[38] ItalSens Gold SPE IS-W1-3.C1.RS.35, (n.d.). https://cdn.palmsens.com/wp-content/uploads/2021/07/ItalSens-IS-W1-3.C1.RS_.35-description.pdf (accessed January 6, 2022).

[39] C.M.A. Brett, A.M.Oliveira. Brett, Electrochemistry: Principles, Methods, and Applications, Oxford University Press, 1993.

[40] K.J. Knutson, D.W. Berzins, Corrosion of orthodontic temporary anchorage devices, Eur. J. Orthod. 35 (2013) 500–506, https://doi.org/10.1093/EJO/CJS027.

[41] F.Kurniawan Fitriyana, Polyaniline-invertase-gold nanoparticles modified gold electrode for sucrose detection, Indones. J. Chem. 15 (2015) 226–233, https://doi.org/10.22146/ijc.21189.

[42] A. Korent, K. Žagar Soderžnik, S. Šturm, K. Žužek Rožman, A correlative study of polyaniline electropolymerization and its electrochromic behavior, J. Electrochem. Soc. 167 (2020), 106504, https://doi.org/10.1149/1945-7111/ab9929.

[43] M. Gvozdenovic, B. Jugovic, J. Stevanovic, B. Grgur, Electrochemical synthesis of electroconducting polymers, Hem. Ind. 68 (2014) 673–684, https://doi.org/10.2298/HEMIND131122008G.

[44] K.E. Ramohlola, G.R. Monana, M.J. Hato, K.D. Modibane, K.M. Molapo, M. Masikini, S.B. Mduli, E.I. Iwuoha, Polyaniline-metal organic framework nanocomposite as an efficient electrocatalyst for hydrogen evolution reaction, Compos. Part B Eng. 137 (2018) 129–139, https://doi.org/10.1016/j.compositesb.2017.11.016.

[45] A. Kellenberger, D. Ambros, N. Plesu, Scan rate dependent morphology of polyaniline films electrochemically deposited on nickel, 2014. www.electrochemsci.org (accessed December 14, 2020).

[46] N. Plesu, A. Kellenberger, M. Mihali, N. Vaszilcsin, Effect of temperature on the electrochemical synthesis and properties of polyaniline films, J. Non Cryst. Solids 356 (2010) 1081–1088, https://doi.org/10.1016/j.jnoncrysol.2010.01.011.

[47] D. Maity, M. Manoharan, R.T. Rajendra Kumar, Development of the PANI/MWCNT nanocomposite-based fluorescent sensor for selective detection of aqueous ammonia, ACS Omega 5 (2020) 8414–8422, https://doi.org/10.1021/ACSOMEGA.9B02885.

[48] J. Song, M. Huang, X. Lin, S.F.Y. Li, N. Jiang, Y. Liu, H. Guo, Y. Li, Novel Fe-based metal–organic framework (MOF) modified carbon nanofiber as a highly selective and sensitive electrochemical sensor for tetracycline detection, Chem. Eng. J. 427 (2021), https://doi.org/10.1016/J.CEJ.2021.130913.

[49] C. Heng Teo, N.S. Karode, K. Abid, F. Rahman, Interfacial behaviour of polyaniline as an organic electronic material, J. Phys. Chem. Solids 72 (2011) 886–890, https://doi.org/10.1016/J.JPCS.2011.04.010.

[50] W.S. Huang, B.D. Humphrey, A.G. MacDiarmid, Polyaniline, a novel conducting polymer. Morphology and chemistry of its oxidation and reduction in aqueous electrolytes, J. Chem. Soc. Faraday Trans. 1 Phys. Chem. Condens. Ph. 82 (1986) 2385–2400, https://doi.org/10.1039/F19868202385.

[51] E. Song, J.W. Choi, Conducting polyaniline nanowire and its applications in chemiresistive sensing, Nanomaterials 3 (2013) 498–523.

[52] J. Tarver, J.E. Yoo, T.J. Dennes, J. Schwartz, Y.L. Loo, Polymer acid doped polyaniline is electrochemically stable beyond pH 9, Chem. Mater. 21 (2009) 280–286, https://doi.org/10.1021/cm802314h.

[53] L. Zhang, The electrocatalytic oxidation of ascorbic acid on polyaniline film synthesized in the presence of β-naphthalenesulfonic acid, Electrochim. Acta 52 (2007) 6969–6975, https://doi.org/10.1016/J.ELECTACTA.2007.05.012.

[54] T.H. Le, Y. Kim, H. Yoon, Electrical and electrochemical properties of conducting polymers, Polymers 9 (2017) 150, https://doi.org/10.3390/polym9040150 (Basel).

[55] S. Bhadra, S. Chattopadhyay, N.K. Singha, D. Khastgir, Improvement of conductivity of electrochemically synthesized polyaniline, J. Appl. Polym. Sci. 108 (2008) 57–64, https://doi.org/10.1002/APP.26926.

[56] N. Kipnis, A law of physics in the classroom: the case of Ohm's law, Sci. Educ. 18 (2009) 349–382, https://doi.org/10.1007/S11191-008-9142-X.

[57] E. Song, J.W. Choi, Self-calibration of a polyaniline nanowire-based chemiresistive pH sensor, Microelectron. Eng. 116 (2014) 26–32, https://doi.org/10.1016/j.mee.2013.10.014.

[58] S. Uzunçar, L. Meng, A.P.F. Turner, W.C. Mak, Processable and nanofibrous polyaniline:polystyrene-sulphonate (nano-PANI:PSS) for the fabrication of catalyst-free ammonium sensors and enzyme-coupled urea biosensors, Biosens. Bioelectron. 171 (2021), 112725, https://doi.org/10.1016/J.BIOS.2020.112725.

Chapter 7

Conclusions

This chapter summarizes the main achievements and conclusions of this research. The thesis provides a review of electrochemically synthesized polyaniline ($PANI_{el}$) and its application in NH_3 gas and liquid sensing. Thus, it is divided into three parts.

The first part of the thesis was dedicated to studying and understanding PANI, synthesized via an electrochemical route. The electropolymerization via cyclic voltammetry (CV) of 0.1 M ANI in 1.0 M HCl was studied by the *in-situ* spectro-electrochemical technique. The chosen CV conditions, a potential range from – 0.3 to 1.0 V at 50 mV s^{-1}, were sufficient to ensure ANI oxidation at 0.9 V vs Ag and the formation of PANI. The appearance of oxidation/reduction peaks, characteristic for PANI formation and transformations between leucoemeraldine, emeraldine and pernigraniline proved the successful formation and deposition of PANI. According to the spectroscopic data the second stage of PANI formation, i.e., dimer formation, delays for approximately 6 cycles, while the anilinium ion was already formed in the first cycle. The polymerization process is an electro-oxidation process. However, the reduction process was shown to have great importance, since the absorbance peaks associated with transitions in HCl-doped PANI have the highest intensity during the reduction. Even though the CV experiment ended at the reduction potential of – 0.3 V vs Ag, the spectroscopic result showed immediate oxidation to protoemeraldine, i.e., the intermediate state, due to the exposure to ambient oxygen, and hence spontaneous oxidation. The final product was the most conductive form of PANI doped with HCl, due to the polymerization in 1.0 M HCl, i.e., the emelardine salt, a compact green deposition on the working electrode of a screen-printed electrode (SPE). Considering the obtained data, the as-prepared PANI results in the most conductive protonated emeraldine form, presenting a conductive base layer for further electric and electrochemical sensory studies.

In the second part of the thesis, the studies were focused on the application of the electrochemically synthesized PANI on SPE, for the purpose of designing a sensory platform suitable for room-temperature NH_3 gas sensing. A straightforward electropolymerization of PANI was applied for the deposition of a compact polymer layer directly on the electrode surface. However, for the resistivity measurements, the sensing material needs to be sandwiched between two contacts. The latter was achieved by Au sputtering to connect the deposited PANI with either the counter or the reference electrode of the SPE. Such prepared Au-modified PANI-Au-SPE was exposed to humidity and NH_3 gas in a chamber. The designed platform showed a reversible sensibility towards humidity and the expected behaviour in the presence of NH_3 gas, i.e., increased resistance after exposure and recovery towards the initial value after introducing clean air. The same behaviour was observed for at least three consecutive cycles. Simultaneous measurements with a commercial NH_3 gas analyser confirmed the instant response of the PANI due to the presence of NH_3 and confirmed the capability for real-time measurements. The presented system achieved a low detection limit (23 ppb) for NH_3 gas that is comparable to more complex PANI-based systems. Electrochemical synthesis used in this study is considered to be unconventional as it is rarely used in gas sensing, but this fully controllable way of preparing PANI, and its combination with a three-electrode SPE system, led to novel aspects in PANI gas-sensing systems.

NH_3 is a highly hydro-soluble gas and a product of degradation reactions of nitrogen-containing compounds. Considering its toxicity and function as a potential biomarker for organ diseases, the thesis's third part aimed at the electrochemical detection of aqueous NH_3 with

already-studied and known electropolymerized PANI on SPE electrodes. The electropolymerization by CV in a highly acidic medium (1.0 M HCl), which results in the conductive emeraldine salt form, was demonstrated to be a suitable material for the electrochemical detection of aqueous NH_3 in a neutral medium. The presence of NH_3 was detected with the chronoamperometric method at an applied potential of 0.2 V vs Ag, the potential of emeraldine formation. Considering the spontaneous deprotonation due to the neutral electrolyte PBS (pH = 7), and the influence of the applied potential on NH_4^+ and PANI, the sensing mechanism was proposed. The latter is based on the PANI deprotonation reaction, $NH4^+$ oxidation and follow-up PANI reduction and oxidation. The detection set-up was based on injecting a small volume of NH_3 aliquot (1 μL) into a larger volume of PBS background electrolyte (50 μL) during the electrochemical measurement. According to the description, the presented system's parameters meet the definition of a batch-injection analysis, which gives it potential as an amperometric component for further industrialization. The suitability for batch-injection analysis was also shown by the repeatability in electrode preparation, separate measurements, and, most importantly, sequential measurements during one experiment. Decorating the PANI surface with 20-nm Au nanoparticles improved the sensory performance by lowering the detection and quantification limit, by 17- and 20-times from 24.64 μm to 1.44 μm and from 51 μm to 2.55 μm, respectively. Along with these measurements, the $PANI_{el}$-Au20 material was tested for the detection of NH_3 in artificial saliva where negligible interferences were observed. This indicates that $PANI_{el}$-Au20 as a material is suitable for detecting NH_3 in more complex samples and demonstrates its suitability for biomedical applications.

In conclusion, this dissertation provides a detailed insight into the electrochemical preparation of PANI and the application of the as-prepared material in two different sensing modes: conductometric and electrochemical. The study opens a number of possibilities, as NH_3 is a common by-product of various catalytic reactions of toxic organic compounds. In that case, an understanding of the basic detection of pure NH_3 opens the way to the indirect detection of more complex toxic organic compounds via formed NH_3. Since PANI shows an excellent affinity for nanoparticles and biomolecules it can be modified with organic molecules, opening further research towards the indirect detection of by-product NH_3, which would be interesting and have a significant scientific contribution.

Appendix A

Au-Decorated Electrochemically Synthesised Polyaniline-Based Sensory Platform for Amperometric Detection of Aqueous Ammonia in Biological Fluids

A.1 Article's Supplementary Material

Supplementary material

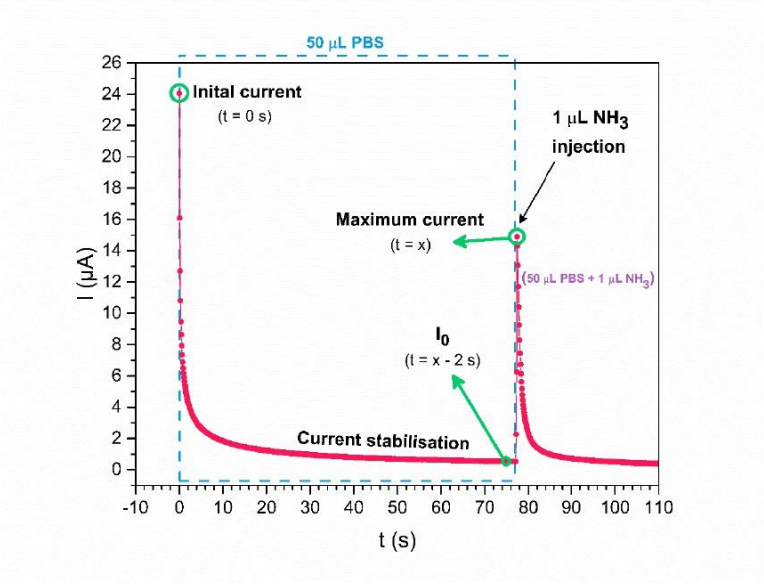

Figure S1. Dynamics of the chronoamperometric measurement of NH_3 detection at an applied potential of 0.2 V vs Ag.

Electrochemical polishing

Electrochemical polishing is a non-mechanical process of removing a thin (micron-level) material layer by converting them into ions, leaving a clean and smooth surface [1]. Due to the further modification of Au WE, the electrochemical polishing process in 0.5 M H_2SO_4 is the initial step in the electrode-preparation process. The electrode was cycled three times (Figure S2), which was enough as all further cycles were identical. A typical CV for the Au electrode was obtained [2,3], with multiple overlapping oxidation peaks in the range 0.8–1.12 V vs Ag and a single sharp gold oxide reduction peak at 0.59 vs Ag.

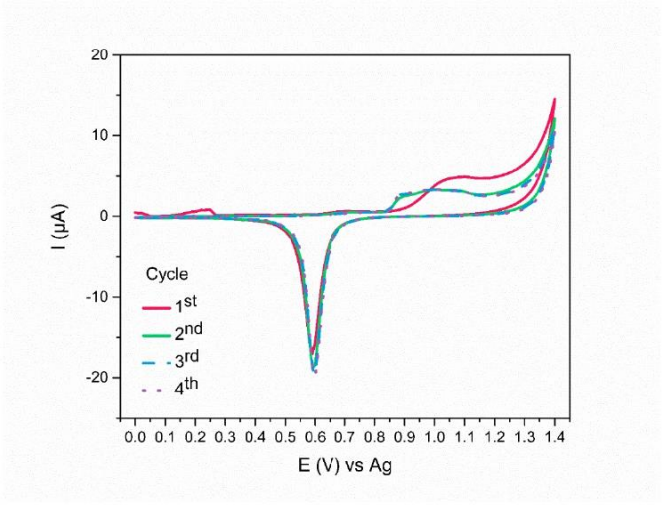

Figure S2. Cyclic voltammogram of electrochemical polishing process for pure gold working electrode on a commercial SPE in 0.5 M H_2SO_4 performed between 0 and 1.4 V vs Ag at 100 mV s^{-1}.

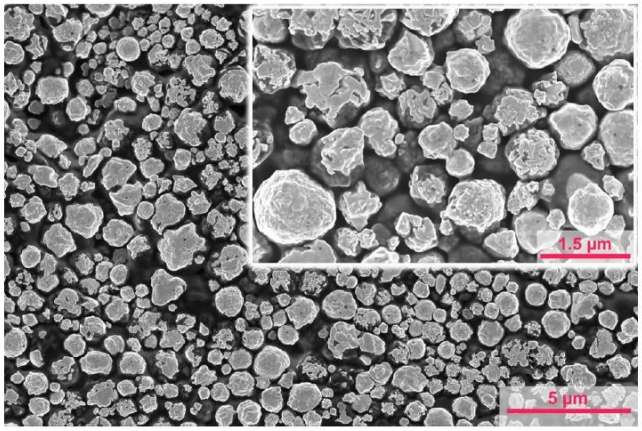

Figure S3. Secondary-electron images of Au SPE's working electrode at two magnifications.

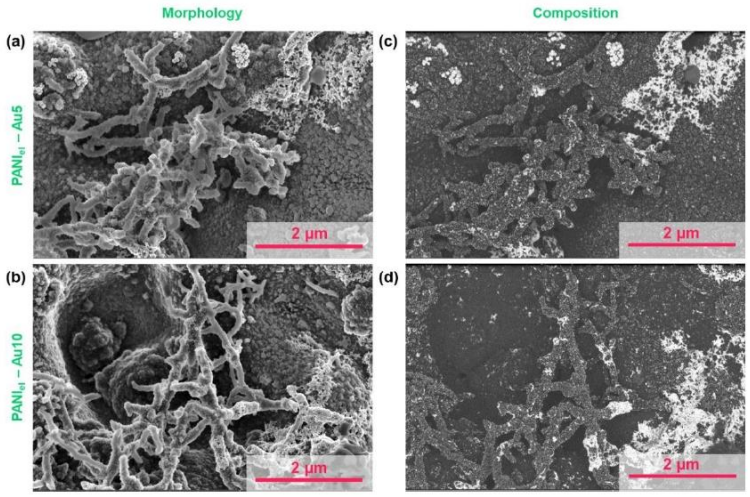

Figure S4. Secondary-electron (a,c) and backscattered-electron SEM image (b, d) of $PANI_{el}$-Au5 (a, b) and $PANI_{el}$-Au10 (c, d).

<u>$PANI_{el}$ electrochemical characterization in acidic medium</u>

In an acidic medium, PANI exists in a fully reduced form (leucoemeraldine) and undergoes two distinct redox transitions to the half-oxidised form (emeraldine) and the fully oxidised form (pernigraniline). Two oxidation ($\mathbf{a_1}$ = −0.09, $\mathbf{a_2}$ = 0.46) and two reduction peaks ($\mathbf{c_1}$ = 0.42, $\mathbf{c_2}$ = −0.23), together form two redox couples ($\mathbf{a_1/c_2}$ and $\mathbf{a_2/c_1}$). The first redox couple ($\mathbf{a_1/c_2}$) is the transition between leucoemeraldine and emeraldine, and the second one ($\mathbf{a_2/c_1}$) is the transition between emeraldine and pernigraniline. Compared to the electrochemical behaviour of pristine Au electrode, the results present an additional confirmation of successful $PANI_{el}$ deposition.
Oxidation $\mathbf{a_2}$ and reduction $\mathbf{c_1}$ peaks are separated by only 40 mV, indicating a high degree of reversibility. Meanwhile, a larger distance between peaks $\mathbf{a_1}$ and $\mathbf{c_2}$ (140 mV) was already observed in HCl-doped PANI [4]. As pernigraniline is unstable due to the quinoid-imine structure [5], the first redox couple ($\mathbf{a_1/c_2}$, leucoemeraldine/emeraldine) is the point of interest. The switching between leucoemeraldine and emeraldine ($\mathbf{a_1/c_2}$) is a diffusion-controlled reaction. The process is scan-rate dependent (Figure S5c) with a peak current increase and a peak potential shift towards more positive and negative values. The linear relationship of peak current vs square root of the scan rate (Figure S5d) from the Randles-Sevćik equation (Eq. 2) confirms the Nernstian behaviour (i.e., reversible system) controlled by diffusion at the electrode surface. The most studied and applicable form of PANI is emeraldine due to its semiconducting properties and easy switching between emeraldine salt and base (emeraldine blue) [5]. And even though the separation potential between $\mathbf{a_1}$ and $\mathbf{c_2}$ (leucoemeraldine and emeraldine) suggests hindering reversibility, continuous cycling showed no current loss or peak potential shift [4].

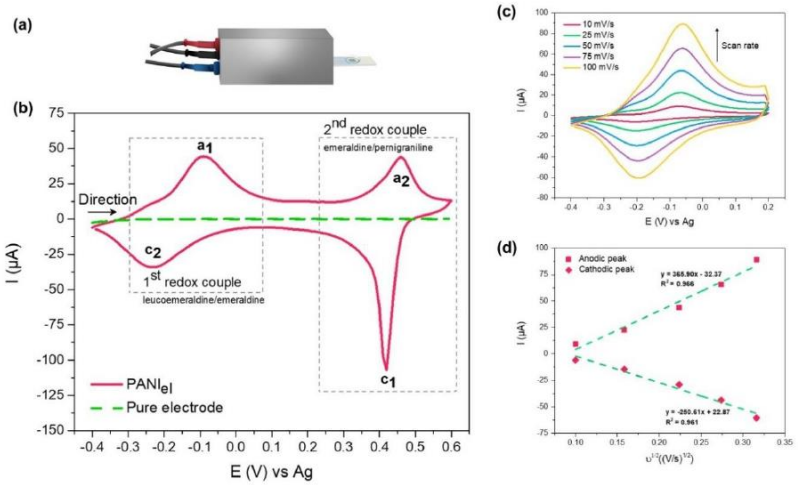

Figure S5. Measuring principle of electrochemical characterization of $PANI_{el}$ by exposing all three SPEs to the drop of electrolyte (a), CV characterization in 0.1 M H_2SO_4 in potential range between −0.4 and 0.6 V vs Ag at 50 mV s^{-1} (b), −0.4 and 0.2 V vs Ag by varying scan range from 10 to 100 mV s^{-1} (c) and relationship anodic/cathodic peak currents and scan-rate square root (d).

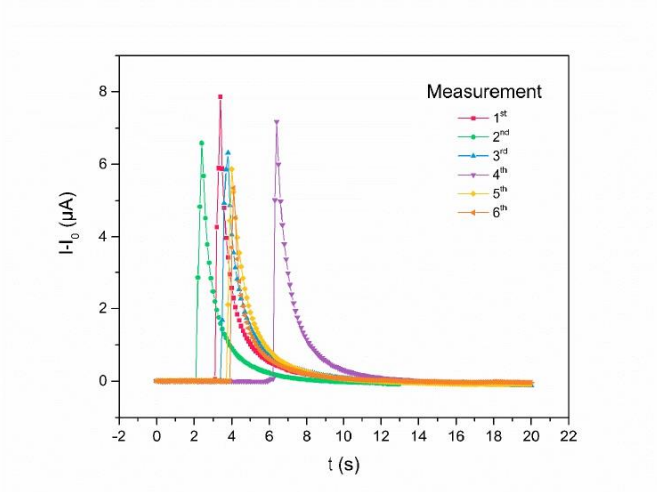

Figure S6. PANI$_{el}$'s amperometric behaviour for one electrode after several separate measurements of 1.275 mM NH_3 injection to PBS at a constant potential of 0.2 V vs Ag.

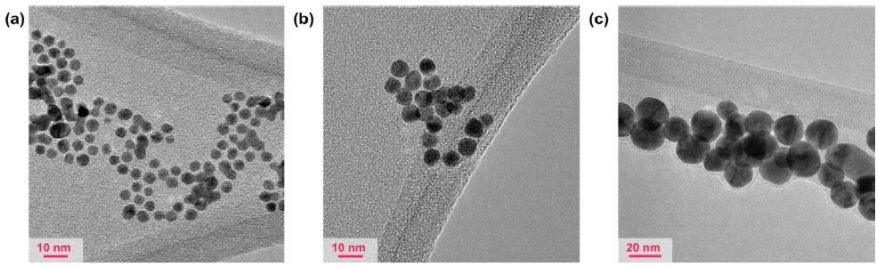

Figure S7. TEM images of commercial Au NPs, drop-cased on TEM Cu grid: 5 nm (a), 10 nm (b), and 20 nm (c).

Table S1.
Analytical performance characteristics for similar conductive polymer-based electrochemical ammonia sensors.

Sensing environment / pH	Composition	Sensing method	Characteristics				Application	Reference
			Detection limit (μM)	Quantification limit (μM)	Sensitivity	Range		
1 M KOH	Pt-PANI-CC	DPV	0.0772	0.5	6.6 μA μM^{-1}	0.5-550 μM	Wastewater	[6]
	Pt-Ag/PPy-Ni foam	LSV	0.037	0.05	89 μA μM^{-1}	0.05-50 μM	Water	[7]
	Pt-PPy/Ni foam	DPV	0.01236	0.5	4.19 μA μM^{-1}	0.5-400 μM	Water	[8]
Buffer, pH = 10	PANI-Nafion	CA [0.3 V vs Ag/AgCl]	5	5	40 ± 20 μA mM^{-1} cm^{-2}	5 μM-1 mM	Enzymatic urea sensing platform	[9]
Buffer, pH = 7.5	PANI (DBSA)	CA [−0.3 V vs Ag/AgCl	3.17	20	0.02 μA μM^{-1}	0-80 μM	Refrigerant wastewater	[10]
PBS, pH = 7	Nano-PANI:PSS	DPV	26.9	100	106 ± 1.8 mA M^{-1} cm^{-2}	100 μM-11.7 mM	Enzymatic urea sensing platform	[11]
	PANI (DVSA)	EIS	12	25	/	20-200 μM	Blood ammonia	[12]
	PANI (HCl)	CA [E = 0.2 V vs Ag]	24.64	51	0.83 μA mM^{-1}	0-510 mM	/	This work
	PANI (HCl)-Au NPs	CA [E = 0.2 V vs Ag]	1.44	2.55	16.21, 2.60, 0.91, 0.03 μA μM^{-1}	0-510 mM	Artificial saliva	This work

[1] T. Jones, Electropolishing of precious metals, Metal Finishing. 102 (2004) 45–57. https://doi.org/10.1016/S0026-0576(04)84698-1.

[2] W. Ma, Y.L. Ying, L.X. Qin, Z. Gu, H. Zhou, D.W. Li, T.C. Sutherland, H.Y. Chen, Y.T. Long, Investigating electron-transfer processes using a biomimetic hybrid bilayer membrane system, Nature Protocols 2012 8:3. 8 (2013) 439–450. https://doi.org/10.1038/nprot.2013.007.

[3] A. Wahl, K. Dawson, N. Sassiat, A.J. Quinn, A. O'Riordan, Nanomolar Trace Metal Analysis of Copper at Gold Microband Arrays, Journal of Physics: Conference Series. 307 (2011) 012061. https://doi.org/10.1088/1742-6596/307/1/012061.

[4] J. Tarver, J.E. Yoo, T.J. Dennes, J. Schwartz, Y.L. Loo, Polymer acid doped polyaniline is electrochemically stable beyond pH 9, Chemistry of Materials. 21 (2009) 280–286. https://doi.org/10.1021/cm802314h.

[5] Z.A. Boeva, V.G. Sergeyev, Polyaniline: Synthesis, properties, and application, Polymer Science - Series C. 56 (2014) 144–153. https://doi.org/10.1134/S1811238214010032.

[6] L. Zhang, T. Liu, R. Ren, J. Zhang, D. He, C. Zhao, H. Suo, In situ synthesis of hierarchical platinum nanosheets-polyaniline array on carbon cloth for electrochemical detection of ammonia, J Hazard Mater. 392 (2020). https://doi.org/10.1016/J.JHAZMAT.2020.122342.

[7] L. Zhang, J. Liu, X. Peng, Q. Cui, D. He, C. Zhao, H. Suo, Fabrication of a Ni foam-supported platinum nanoparticles-silver/polypyrrole electrode for aqueous ammonia sensing, Synthetic Metals. 259 (2020) 116257. https://doi.org/10.1016/J.SYNTHMET.2019.116257.

[8] L. Zhang, J. Wan, J. Li, Q. Cui, D. He, C. Zhao, H. Suo, Fabricating a Self-Supported Electrode for Detecting Ammonia in Water Based on Electrodepositing Platinum-Polypyrrole on Ni Foam, Journal of The Electrochemical Society. 167 (2020) 027537. https://doi.org/10.1149/1945-7111/AB6C55.

[9] B. Strehlitz, B. Gründig, H. Kopinke, Sensor for amperometric determination of ammonia and ammonia-forming enzyme reactions, Analytica Chimica Acta. 403 (2000) 11–23. https://doi.org/10.1016/S0003-2670(99)00594-2.

[10] K. Crowley, E. O'Malley, A. Morrin, M.R. Smyth, A.J. Killard, An aqueous ammonia sensor based on an inkjet-printed polyaniline nanoparticle -modified electrode, Analyst. 133 (2008) 391–399. https://doi.org/10.1039/B716154A.

[11] S. Uzunçar, L. Meng, A.P.F. Turner, W.C. Mak, Processable and nanofibrous polyaniline:polystyrene-sulphonate (nano-PANI:PSS) for the fabrication of catalyst-free ammonium sensors and enzyme-coupled urea biosensors, Biosensors and Bioelectronics. 171 (2021) 112725. https://doi.org/10.1016/J.BIOS.2020.112725.

[12] N.T. Brannelly, A.J. Killard, An electrochemical sensor device for measuring blood ammonia at the point of care, Talanta. 167 (2017) 296–301. https://doi.org/10.1016/J.TALANTA.2017.02.025.

References

[1] C. M. A. Brett and A. M. Oliveira. Brett, *Electrochemistry: principles, methods, and applications*. Oxford University Press, 1993.

[2] D. Pletcher, R. Greff, R. Peat, L. Peter, and J. Robinson, *Instrumental methods in electrochemistry*. Elsevier, 2001.

[3] C. G. Zoski, *Handbook of electrochemistry*. Elsevier, 2006.

[4] B. Pihlar, *Osnove analizne kemije*. Ljubljana: Fakulteta za kemijo in kemijsko tehnologijo, 2007.

[5] R. K. Franklin, S. M. Martin, T. D. Strong, and R. B. Brown, "Chemical and Biological Systems: Chemical Sensing Systems for Liquids," in *Reference Module in Materials Science and Materials Engineering*, Elsevier, 2016. doi: 10.1016/B978-0-12-803581-8.00549-X.

[6] N. Elgrishi, K. J. Rountree, B. D. McCarthy, E. S. Rountree, T. T. Eisenhart, and J. L. Dempsey, "A Practical Beginner's Guide to Cyclic Voltammetry," *J Chem Educ*, vol. 95, no. 2, pp. 197–206, 2017, doi: 10.1021/acs.jchemed.7b00361.

[7] A. García-Miranda Ferrari, S. J. Rowley-Neale, and C. E. Banks, "Screen-printed electrodes: Transitioning the laboratory in-to-the field," *Talanta Open*, vol. 3, p. 100032, 2021, doi: 10.1016/j.talo.2021.100032.

[8] J. X. J. Zhang and K. Hoshino, *Molecular sensors and nanodevices: principles, designs and applications in biomedical engineering*. Academic Press, 2018.

[9] L. M. Moretto and K. Klacher, *Environmental Analysis by Electrochemical Sensors and Biosensors*, vol. 1. New York, NY: Springer New York, 2014. doi: 10.1007/978-1-4939-1301-5.

[10] H. M. Mohamed, "Screen-printed disposable electrodes: Pharmaceutical applications and recent developments," *TrAC Trends in Analytical Chemistry*, vol. 82, pp. 1–11, Sep. 2016, doi: 10.1016/j.trac.2016.02.010.

[11] R. A. S. Couto, J. Lima, and M. B. Quinaz, "Recent developments, characteristics and potential applications of screen-printed electrodes in pharmaceutical and biological analysis," *Talanta*, vol. 146, pp. 801–814, 2016, doi: 10.1016/j.talanta.2015.06.011.

[12] "Metrohm DropSens Screen-Printed electrodes." http://www.dropsens.com/en/screen_printed_electrodes_pag.html (accessed Jul. 28, 2021).

[13] S. A. Ozkan, J.-M. Kauffmann, and P. Zuman, "Screen-Printed Electrodes (SPE) for Drug Compounds Determination," in *Electroanalysis in Biomedical and Pharmaceutical Sciences*, Springer, Berlin, Heidelberg, 2015, pp. 119–140. doi: 10.1007/978-3-662-47138-8_5.

[14] C. K. Chiang *et al.*, "Electrical conductivity in doped polyacetylene," *Phys Rev Lett*, vol. 39, no. 17, pp. 1098–1101, 1977, doi: 10.1103/PhysRevLett.39.1098.

[15] H. Shirakawa, E. J. Louis, A. G. MacDiarmid, C. K. Chiang, and A. J. Heeger, "Synthesis of electrically conducting organic polymers: Halogen derivatives of polyacetylene, (CH)x," *J Chem Soc Chem Commun*, vol. 0, no. 16, pp. 578–580, 1977, doi: 10.1039/C39770000578.

[16] A. J. Heeger, “Semiconducting and metallic polymers: The fourth generation of polymeric materials,” *Journal of Physical Chemistry B*, vol. 105, no. 36, pp. 8475–8491, 2001, doi: 10.1021/jp011611w.

[17] A. G. MacDiarmid, “‘Synthetic metals’: A novel role for organic polymers,” *Current Applied Physics*, vol. 1, no. 4–5, pp. 269–279, 2001, doi: 10.1016/S1567-1739(01)00051-7.

[18] A. J. Heeger, A. G. MacDiarmid, and H. Shirakawa, “The Nobel Prize in Chemistry 2000,” *Nobel Media AB 2020*, vol. 12, no. 1974, pp. 11–20, 2000.

[19] T.-H. Le, Y. Kim, and H. Yoon, “Electrical and Electrochemical Properties of Conducting Polymers,” *Polymers (Basel)*, vol. 9, no. 12, p. 150, Apr. 2017, doi: 10.3390/polym9040150.

[20] J. L. Bredas and G. B. Street, “Polarons, bipolarons, and solitons in conducting polymers,” *Acc Chem Res*, vol. 18, no. 10, pp. 309–315, 1985, doi: 10.1021/ar00118a005.

[21] J. Yue and A. J. Epstein, “XPS Study of Self-Doped Conducting Polyaniline and Parent Systems,” *Macromolecules*, vol. 24, no. 15, pp. 4441–4445, Jul. 1991, doi: 10.1021/ma00015a030.

[22] A. J. Heeger, S. Kivelson, J. R. Schrieffer, and W. P. Su, “Solitons in conducting polymers,” *Rev Mod Phys*, vol. 60, no. 3, pp. 781–850, 1988, doi: 10.1103/RevModPhys.60.781.

[23] J. C. Chiang and A. G. MacDiarmid, “‘Polyaniline’: Protonic acid doping of the emeraldine form to the metallic regime,” *Synth Met*, vol. 13, no. 1–3, pp. 193–205, Jan. 1986, doi: 10.1016/0379-6779(86)90070-6.

[24] A. F. Diaz, J. I. Castillo, J. A. Logan, and W. Y. Lee, “Electrochemistry of conducting polypyrrole films,” *Journal of Electroanalytical Chemistry*, vol. 129, no. 1–2, pp. 115–132, 1981, doi: 10.1016/S0022-0728(81)80008-3.

[25] W. S. Huang, B. D. Humphrey, and A. G. MacDiarmid, “Polyaniline, a novel conducting polymer. Morphology and chemistry of its oxidation and reduction in aqueous electrolytes,” *Journal of the Chemical Society, Faraday Transactions 1: Physical Chemistry in Condensed Phases*, vol. 82, no. 8, pp. 2385–2400, 1986, doi: 10.1039/F19868202385.

[26] W. R. Salaneck *et al.*, “Electronic structure of some polyanilines,” *Synth Met*, vol. 18, no. 1–3, pp. 291–296, 1987, doi: 10.1016/0379-6779(87)90894-0.

[27] K. E. Ramohlola *et al.*, “Polyaniline-metal organic framework nanocomposite as an efficient electrocatalyst for hydrogen evolution reaction,” *Compos B Eng*, vol. 137, no. 12, pp. 129–139, 2018, doi: 10.1016/j.compositesb.2017.11.016.

[28] G. G. Wallace, P. R. Teasdale, and G. M. Spinks, *Conductive electroactive polymers: intelligent polymer systems*. CRC Press, 2009.

[29] A. G. MacDiarmid and A. J. Epstein, “Polyanilines: a novel class of conducting polymers,” *Faraday Discuss Chem Soc*, vol. 88, pp. 317–332, 1989, doi: 10.1039/DC9898800317.

[30] Z. A. Boeva and V. G. Sergeyev, “Polyaniline: Synthesis, properties, and application,” *Polymer Science - Series C*, vol. 56, no. 1, pp. 144–153, 2014, doi: 10.1134/S1811238214010032.

[31] M. Gvozdenovic, B. Jugovic, J. Stevanovic, and B. Grgur, “Electrochemical synthesis of electroconducting polymers,” *Hem Ind*, vol. 68, no. 6, pp. 673–684, 2014, doi: 10.2298/HEMIND131122008G.

[32] C. Li, H. Bai, and G. Shi, “Conducting polymer nanomaterials: Electrosynthesis and applications,” *Chem Soc Rev*, vol. 38, no. 8, pp. 2397–2409, 2009, doi: 10.1039/b816681c.

[33] J. Huang and R. B. Kaner, “The intrinsic nanofibrillar morphology of polyaniline,” *Chemical Communications*, no. 4. Royal Society of Chemistry, pp. 367–376, 2006. doi: 10.1039/b510956f.

[34] S. Bhadra, S. Chattopadhyay, N. K. Singha, and D. Khastgir, “Improvement of conductivity of electrochemically synthesized polyaniline,” *J Appl Polym Sci*, vol. 108, no. 1, pp. 57–64, 2008, doi: 10.1002/app.26926.

[35] J. Kankare, “Electronically Conducting Polymers: Basic Methods of Synthesis and Characterization,” *Electrical and Optical Polymer Systems: Fundamentals, Methods and Applications*. CRC Press, New York, pp. 167–199, 1998.

[36] T. v. Freitas, E. A. Sousa, G. C. Fuzari, and E. P. S. Arlindo, “Different morphologies of polyaniline nanostructures synthesized by interfacial polymerization,” *Mater Lett*, vol. 224, pp. 42–45, 2018, doi: 10.1016/j.matlet.2018.04.062.

[37] L. Brožová, P. Holler, J. Kovářová, J. Stejskal, and M. Trchová, “The stability of polyaniline in strongly alkaline or acidic aqueous media,” *Polym Degrad Stab*, vol. 93, no. 3, pp. 592–600, 2008, doi: 10.1016/j.polymdegradstab.2008.01.012.

[38] E. Song and J.-W. Choi, “Conducting polyaniline nanowire and its applications in chemiresistive sensing,” *Nanomaterials*, vol. 3, pp. 498–523, 2013, doi: 10.3390/nano3030498.

[39] U. Rana, N. D. Paul, S. Mondal, C. Chakraborty, and S. Malik, “Water soluble polyaniline coated electrode: A simple and nimble electrochemical approach for ascorbic acid detection,” *Synth Met*, vol. 192, pp. 43–49, Jun. 2014, doi: 10.1016/j.synthmet.2014.03.013.

[40] S. Mu and J. Kan, “Evidence for the autocatalytic polymerization of aniline,” *Electrochim Acta*, vol. 41, no. 10, pp. 1593–1599, 1996, doi: 10.1016/0013-4686(95)00410-6.

[41] R. Bard, Allen J.; Faulkner, Larry, *ELECTROCHEMICAL METHODS Fundmanentals and Applications (Second Edition)*. John Wiley & Sons, Inc., 2001.

[42] D. Bejan and A. Duca, “Voltammetry of aniline with different electrodes and electrolytes,” *Croatica Chemica Acta*, vol. 71, no. 3, pp. 745–756, 1998.

[43] E. Smela, W. Lu, and B. R. Mattes, “Polyaniline actuators: Part 1. PANI(AMPS) in HCl,” *Synth Met*, vol. 151, no. 1, pp. 25–42, 2005, doi: 10.1016/j.synthmet.2005.03.009.

[44] J. Tarver, J. E. Yoo, T. J. Dennes, J. Schwartz, and Y. L. Loo, “Polymer acid doped polyaniline is electrochemically stable beyond pH 9,” *Chemistry of Materials*, vol. 21, no. 2, pp. 280–286, 2009, doi: 10.1021/cm802314h.

[45] J. P. Travers and M. Nechtschein, “Water effects in polyaniline: A new conduction process,” *Synth Met*, vol. 21, no. 1–3, pp. 135–141, 1987, doi: 10.1016/0379-6779(87)90077-4.

[46] A. J. Epstein *et al.*, “Insulator-to-metal transition in polyaniline: Effect of protonation in emeraldine,” *Synth Met*, vol. 21, no. 1–3, pp. 63–70, 1987, doi: 10.1016/0379-6779(87)90067-1.

[47] C. Dhand, M. Das, M. Datta, and B. D. Malhotra, “Recent advances in polyaniline based biosensors,” *Biosens Bioelectron*, vol. 26, no. 6, pp. 2811–2821, 2011, doi: 10.1016/j.bios.2010.10.017.

[48] S. Stafström *et al.*, “Polaron lattice in highly conducting polyaniline: Theoretical and optical studies,” *Phys Rev Lett*, vol. 59, no. 13, pp. 1464–1467, 1987, doi: 10.1103/PhysRevLett.59.1464.

[49] A. G. Macdiarmid, J. C. Chiang, A. F. Richter, and A. J. Epstein, “Polyaniline: a new concept in conducting polymers,” *Synth Met*, vol. 18, no. 1–3, pp. 285–290, 1987, doi: 10.1016/0379-6779(87)90893-9.

[50] L. Zhang *et al.*, “In situ synthesis of hierarchical platinum nanosheets-polyaniline array on carbon cloth for electrochemical detection of ammonia,” *J Hazard Mater*, vol. 392, 2020, doi: 10.1016/J.JHAZMAT.2020.122342.

[51] Max. Appl, “Physical Properties of Ammonia,” in *Ammonia: principles and industrial practice*, Weinheim ; New York: Wiley-VCH, 1999, p. 301.

[52] D. E. Kissel and M. L. Cabrera, “AMMONIA,” in *Encyclopedia of Soils in the Environment*, vol. 4, Elsevier, 2005, pp. 56–64. doi: 10.1016/B0-12-348530-4/00177-6.

[53] D. Li, X. Xu, Z. Li, T. Wang, and C. Wang, “Detection methods of ammonia nitrogen in water: A review,” *TrAC Trends in Analytical Chemistry*, vol. 127, p. 115890, Jun. 2020, doi: 10.1016/J.TRAC.2020.115890.

[54] N. R. Tanguy, M. Thompson, and N. Yan, “A review on advances in application of polyaniline for ammonia detection,” *Sens Actuators B Chem*, vol. 257, pp. 1044–1064, 2018, doi: 10.1016/j.snb.2017.11.008.

[55] A. Adlimoghaddam, M. G. Sabbir, and B. C. Albensi, “Ammonia as a potential neurotoxic factor in alzheimer’s disease,” *Front Mol Neurosci*, vol. 9, p. 57, 2016, doi: 10.3389/fnmol.2016.00057.

[56] P. P. Ricci and O. J. Gregory, “Sensors for the detection of ammonia as a potential biomarker for health screening,” *Sci Rep*, vol. 11, no. 1, pp. 1–7, 2021, doi: 10.1038/s41598-021-86686-1.

[57] K. Crowley, E. O’Malley, A. Morrin, M. R. Smyth, and A. J. Killard, “An aqueous ammonia sensor based on an inkjet-printed polyaniline nanoparticle -modified electrode,” *Analyst*, vol. 133, no. 3, pp. 391–399, 2008, doi: 10.1039/B716154A.

[58] D. Nicolas-Debarnot and F. Poncin-Epaillard, “Polyaniline as a new sensitive layer for gas sensors,” *Anal Chim Acta*, vol. 475, no. 1–2, pp. 1–15, 2003, doi: 10.1016/S0003-2670(02)01229-1.

[59] E. Song and J. W. Choi, “Self-calibration of a polyaniline nanowire-based chemiresistive pH sensor,” *Microelectron Eng*, vol. 116, pp. 26–32, 2014, doi: 10.1016/j.mee.2013.10.014.

[60] S. Pandey, “Highly sensitive and selective chemiresistor gas/vapor sensors based on polyaniline nanocomposite: A comprehensive review,” *Journal of Science: Advanced Materials and Devices*, vol. 1, no. 4, pp. 431–453, 2016, doi: 10.1016/j.jsamd.2016.10.005.

[61] E. Song and J. W. Choi, “A selective hydrogen peroxide sensor based on chemiresistive polyaniline nanowires modified with silver catalytic nanoparticles,” *Journal of Micromechanics and Microengineering*, vol. 24, no. 6, p. 065004, 2014, doi: 10.1088/0960-1317/24/6/065004.

[62] C. Duc, M. L. Boukhenane, T. Fagniez, L. Khouchaf, N. Redon, and J. L. Wojkiewicz, “Conductive polymer composites for hydrogen sulphide sensors working at sub-PPM level and room temperature,” *Sensors*, vol. 21, no. 19, p. 6529, 2021, doi: 10.3390/S21196529/S1.

[63] S. Carquigny, N. Redon, H. Plaisance, and S. Reynaud, “Development of a polyaniline/fluoral-P chemical sensor for gaseous formaldehyde detection,” *IEEE Sens J*, vol. 12, no. 5, pp. 1300–1306, 2012, doi: 10.1109/JSEN.2011.2169783.

[64] F. N. Crespilho, R. M. Iost, S. A. Travain, O. N. Oliveira, and V. Zucolotto, “Enzyme immobilization on Ag nanoparticles/polyaniline nanocomposites,” *Biosens Bioelectron*, vol. 24, no. 10, pp. 3073–3077, 2009, doi: 10.1016/j.bios.2009.03.026.

[65] Y. C. Wong, B. C. Ang, A. S. M. A. Haseeb, A. A. Baharuddin, and Y. H. Wong, “Review—Conducting Polymers as Chemiresistive Gas Sensing Materials: A Review,” *J Electrochem Soc*, vol. 167, no. 3, p. 037503, 2020, doi: 10.1149/2.0032003jes.

[66] P. Shankar and J. B. B. Rayappan, “Gas sensing mechanism of metal oxides: The role of ambient atmosphere, type of semiconductor and gases - A review,” *Science Letters*, vol. 4, no. 126, 2015.

[67] G. Fan *et al.*, “Enhanced room-temperature ammonia-sensing properties of polyaniline-modified WO3 nanoplates derived via ultrasonic spray process,” *Sens Actuators B Chem*, p. 127892, 2020, doi: 10.1016/j.snb.2020.127892.

[68] A. Korent *et al.*, “Facile Fabrication of an Ammonia-Gas Sensor Using Electrochemically Synthesised Polyaniline on Commercial Screen-Printed Three-Electrode Systems,” *Sensors*, vol. 21, no. 1, p. 169, 2021, doi: 10.3390/s21010169.

[69] A. L. Kukla, Y. M. Shirshov, and S. A. Piletsky, “Ammonia sensors based on sensitive polyaniline films,” *Sens Actuators B Chem*, vol. 37, no. 3, pp. 135–140, 1996, doi: 10.1016/S0925-4005(97)80128-1.

[70] L. Kumar, I. Rawal, A. Kaur, and S. Annapoorni, “Flexible room temperature ammonia sensor based on polyaniline,” *Sens Actuators B Chem*, vol. 240, pp. 408–416, 2017, doi: 10.1016/j.snb.2016.08.173.

[71] J. L. Wojkiewicz *et al.*, “Nanostructured polyaniline-based composites for ppb range ammonia sensing,” *Sens Actuators B Chem*, vol. 160, no. 1, pp. 1394–1403, 2011, doi: 10.1016/j.snb.2011.09.084.

[72] D. A. Skoog, D. M. West, F. J. Holler, and S. R. Crouch, *Fundamentals of analytical chemistry*. Cengage learning, 2013.

[73] E. Desimoni and B. Brunetti, “Presenting Analytical Performances of Electrochemical Sensors. Some Suggestions,” *Electroanalysis*, vol. 25, no. 7, pp. 1645–1651, 2013, doi: 10.1002/elan.201300150.

[74] A. Maity, A. K. Raychaudhuri, and B. Ghosh, “High sensitivity NH3 gas sensor with electrical readout made on paper with perovskite halide as sensor material,” *Scientific Reports 2019 9:1*, vol. 9, no. 1, pp. 1–10, 2019, doi: 10.1038/s41598-019-43961-6.

[75] T. Mérian, N. Redon, Z. Zujovic, D. Stanisavljev, J. L. Wojkiewicz, and M. Gizdavic-Nikolaidis, “Ultra sensitive ammonia sensors based on microwave synthesized nanofibrillar polyanilines,” *Sens Actuators B Chem*, vol. 203, pp. 626–634, 2014, doi: 10.1016/j.snb.2014.07.004.

[76] M. Hirata and L. Sun, “Characteristics of an organic semiconductor polyaniline film as a sensor for NH3 gas,” *Sens Actuators A Phys*, vol. 40, no. 2, pp. 159–163, 1994, doi: 10.1016/0924-4247(94)85024-0.

[77] H. di Zhang *et al.*, “High-sensitivity gas sensors based on arranged polyaniline/PMMA composite fibers,” *Sens Actuators A Phys*, vol. 219, pp. 123–127, 2014, doi: 10.1016/j.sna.2014.09.005.

[78] P. le Maout *et al.*, “Polyaniline nanocomposites based sensor array for breath ammonia analysis. Portable e-nose approach to non-invasive diagnosis of chronic kidney disease,” *Sens Actuators B Chem*, vol. 274, pp. 616–626, 2018, doi: 10.1016/j.snb.2018.07.178.

[79] S. Abdulla, T. L. Mathew, and B. Pullithadathil, “Highly sensitive, room temperature gas sensor based on polyaniline-multiwalled carbon nanotubes (PANI/MWCNTs) nanocomposite for trace-level ammonia detection,” *Sens Actuators B Chem*, vol. 221, pp. 1523–1534, 2015, doi: 10.1016/j.snb.2015.08.002.

[80] D. Zhang, Z. Wu, P. Li, X. Zong, G. Dong, and Y. Zhang, “Facile fabrication of polyaniline/multi-walled carbon nanotubes/molybdenum disulfide ternary nanocomposite and its high-performance ammonia-sensing at room temperature,” *Sens Actuators B Chem*, vol. 258, pp. 895–905, Apr. 2018, doi: 10.1016/j.snb.2017.11.168.

[81] D. Li, X. Xu, Z. Li, T. Wang, and C. Wang, “Detection methods of ammonia nitrogen in water: A review,” *TrAC - Trends in Analytical Chemistry*, vol. 127, 2020, doi: 10.1016/j.trac.2020.115890.

[82] K. Wu, L. Fu, X. Guo, and S. Zhu, “The fabrication of all solid-state ammonium ion selective electrodes used in aquaculture,” *Proceedings of IEEE Sensors*, vol. 2017-December, pp. 1–3, 2017, doi: 10.1109/ICSENS.2017.8234306.

[83] Y. Huang *et al.*, “A novel all-solid-state ammonium electrode with polyaniline and copolymer of aniline/2,5-dimethoxyaniline as transducers,” *Journal of Electroanalytical Chemistry*, vol. C, no. 741, pp. 87–92, Mar. 2015, doi: 10.1016/J.JELECHEM.2014.12.041.

[84] Y. Kan *et al.*, “An all-solid-state ammonium ion-selective electrode based on polyaniline as transducer and poly (o-phenylenediamine) as sensitive membrane,” *Int J Electrochem Sci*, vol. 11, no. 12, pp. 9928–9940, 2016, doi: 10.20964/2016.12.03.

[85] H. Gerischer and A. Mauerer, “Untersuchungen Zur anodischen Oxidation von Ammoniak an Platin-Elektroden,” *J Electroanal Chem Interfacial Electrochem*, vol. 25, no. 3, pp. 421–433, 1970, doi: 10.1016/S0022-0728(70)80103-6.

[86] A. C. A. de Vooys, M. T. M. Koper, R. A. van Santen, and J. A. R. van Veen, “The role of adsorbates in the electrochemical oxidation of ammonia on noble and transition metal electrodes,” *Journal of Electroanalytical Chemistry*, vol. 506, no. 2, pp. 127–137, 2001, doi: 10.1016/S0022-0728(01)00491-0.

[87] B. Strehlitz, B. Gründig, and H. Kopinke, “Sensor for amperometric determination of ammonia and ammonia-forming enzyme reactions,” *Anal Chim Acta*, vol. 403, no. 1–2, pp. 11–23, 2000, doi: 10.1016/S0003-2670(99)00594-2.

[88] A. Kellenberger, D. Ambros, and N. Plesu, “Scan Rate Dependent Morphology of Polyaniline Films Electrochemically Deposited on Nickel,” *Int J Electrochem Sci*, vol. 9, pp. 6821–6833, 2014, Accessed: Dec. 14, 2020. [Online]. Available: www.electrochemsci.org

[89] N. Plesu, A. Kellenberger, M. Mihali, and N. Vaszilcsin, “Effect of temperature on the electrochemical synthesis and properties of polyaniline films,” *J Non Cryst Solids*, vol. 356, no. 20–22, pp. 1081–1088, 2010, doi: 10.1016/j.jnoncrysol.2010.01.011.

[90] S. Mikhaylov *et al.*, “Ammonia/amine electronic gas sensors based on hybrid polyaniline-TiO2 nanocomposites. the effects of titania and the surface active doping acid,” *RSC Adv*, vol. 5, no. 26, pp. 20218–20226, 2015, doi: 10.1039/c4ra16121a.

[91] S. A. Krutovertsev, S. I. Sorokin, A. v. Zorin, Y. A. Letuchy, and O. Y. Antonova, “Polymer film-based sensors for ammonia detection,” *Sens Actuators B Chem*, vol. 7, no. 1–3, pp. 492–494, 1992, doi: 10.1016/0925-4005(92)80350-7.

[92] Á. Terán-Alcocer, F. Bravo-Plascencia, C. Cevallos-Morillo, and A. Palma-Cando, “Electrochemical Sensors Based on Conducting Polymers for the Aqueous Detection of Biologically Relevant Molecules,” *Nanomaterials 2021, Vol. 11, Page 252*, vol. 11, no. 1, p. 252, 2021, doi: 10.3390/NANO11010252.

[93] C. Heng Teo, N. S. Karode, K. Abid, and F. Rahman, “Interfacial behaviour of polyaniline as an organic electronic material,” *Journal of Physics and Chemistry of Solids*, vol. 72, no. 7, pp. 886–890, 2011, doi: 10.1016/J.JPCS.2011.04.010.

[94] N. Kipnis, “A Law of Physics in the Classroom: The Case of Ohm’s Law,” *Sci Educ (Dordr)*, vol. 18, no. 3–4, pp. 349–382, 2009, doi: 10.1007/S11191-008-9142-X.

[95] A. Korent, K. Žagar Soderžnik, S. Šturm, and K. Žužek Rožman, “A Correlative Study of Polyaniline Electropolymerization and its Electrochromic Behavior,” *J Electrochem Soc*, vol. 167, no. 10, p. 106504, 2020, doi: 10.1149/1945-7111/ab9929.

[96] National Research Council (US) and Committee on Acute Exposure Guideline Levels, “Ammonia: acute exposure guideline levels,” in *Acute exposure guideline levels for selected airborne chemicals*, vol. 6, no. 2, Washington (DC): National Academies Press (US), 2008, pp. 58–114. Accessed: Apr. 24, 2020. [Online]. Available: https://www.ncbi.nlm.nih.gov/books/NBK207883/

[97] The Fertilizer Institute, “HEALTH EFFECTS AMMONIA of,” 2010. Accessed: Apr. 24, 2020. [Online]. Available: https://www.tfi.org/sites/default/files/documents/HealthAmmoniaFINAL.pdf

[98] J. R. Huizenga, A. Tangerman, and C. H. Gips, “Determination of ammonia in biological fluids,” *Ann Clin Biochem*, vol. 31 (Pt 6), no. 6, pp. 529–543, 1994, doi: 10.1177/000456329403100602.

[99] A. Korent, Š. Trafela, K. Ž. Soderžnik, Z. Samardžija, S. Šturm, and K. Ž. Rožman, “Au-decorated electrochemically synthesised polyaniline-based sensory platform for amperometric detection of aqueous ammonia in biological fluids,” *Electrochim Acta*, p. 141034, 2022, doi: 10.1016/j.electacta.2022.141034.

Bibliography

Publications Related to the Thesis

Journal Articles

A. Korent, Š. Trafela, K. Žagar Soderžnik, Z. Samardžija, S. Šturm and K. Žužek Rožman, " Au-decorated electrochemically synthesised polyaniline-based sensory platform for amperometric detection of aqueous ammonia in biological fluids, " *Electrochimica Acta*, vol. 430, pp. 141043, 2022.

A. Korent, K. Žagar Soderžnik, S. Šturm, K. Žužek Rožman, N. Redon, J-L. Wokjkiewicz and C. Duc, "Facile fabrication of an ammonia-gas sensor using electrochemically synthesised polyaniline on commercial screen-printed three-electrode systems, " *Sensors*, vol. 21, no. 1, pp. 169-1-169-18, 2021.

A. Korent, K. Žagar Soderžnik, S. Šturm and K. Žužek Rožman, " A correlative study of polyaniline electropolymerisation and its electrochromic behavior, " *Journal of the Electrochemical Society*, vol. 167, no. 10, pp. 106504-1-106504-9, 2020.

Conference Paper

A. Korent, K. Žagar Soderžnik and K. Žužek Rožman, "In-situ spectroelectrochemical study of conductive polyaniline forms for sensor applications," in *Proceedings of the 4th International Conference nanoFIS - Functional Integrated nanoSystems*, *MDPI, Proceedings,* vol. 56, no. 1, pp. 32-1-32-3, 2020.

A. Korent, Š. Trafela and K. Žužek Rožman, " Nanostructured molecularly imprinted polyaniline for acrylamide sensing," in *Proceedings of the 7th International Symposium on Sensor Science*, Napoli, Italy: *MDPI, Proceedings,* vol. 15, no. 1, pp. 2504-3900, 2019.

Scientific Conferences Contributions Abstracts

A. Korent, Š. Trafela, K. Žagar Soderžnik and K. Žužek Rožman, "Polyaniline and its sensing abilities rowards ammonia, a potenctial biosensors element," *Slovenski kemijski dnevi 2022 = 28th Annual Meeting of the Slovenian Chemical Society*, September 21 – 23, Portorož, Slovenia. Book of abstracts, pp. 210, 2022.

A. Korent, Š. Trafela, K. Žagar Soderžnik and K. Žužek Rožman, "Indirect detection of acrylamide using PANI-amidase biosensor element," *57th International Conference on Microelectronics, Devices and Materials & The Workshop on Energy Harvesting: Materials and Applications*, September 14 – 16, Maribor, Slovenia. Book of abstracts, pp. 90, 2022.

A. Korent, K. Žagar Soderžnik, S. Šturm, K. Žužek Rožman, N. Redon, J-L. Wokjkiewicz and C. Duc, "Novel architecture of ppb range ammonia gas sensor based on eletrochemically synthesized polyaniline on comercial screen-printed three-electrode system," *56th International Conference on Microelectronics, Devices and Materials & the Workshop on Personal Sensor for Remote Health Care Monitoring*, September 22 – 24, Ljubljana, Slovenia. Book of abstracts, pp. 26, 2021.

Other Publications

Journal Articles

N. M. Santhosh, A. Vasudevan, A. Jurov, A. Korent, P. Slobodian, J. Zavašnik and U. Cvelbar, " Improving sensing properties of entangled carbon nanotube-based gas sensors by atmospheric plasma surface treatment, " *Microelectronic engineerin*, vol. 232, pp. 111403-1-111403-10, 2020.

M. Lorenzetti, A. Korent, S.Šturm and S. Novak, "TiO_2 (nano)particles extracted from sugar-coated confectionery," *Journal of nanomaterials,* vol. 2017, pp. 6298307-1-6298307-14, 2017.

S. Novak, M. Lorenzetti, A. Korent, J. Vidmar, J. Ščančar and M. Filipič, " Diversity of TiO_2 nanopowders' characteristics relevant to toxicity testing, " *Journal of nanoparticle research,* vol. 18, pp. 130-1-130-13, 2016.

Scientific Conferences Contributions Abstracts

K. Žagar Soderžnik, A. Korent, Š. Trafela, P. Trebše and M. Bavcon Kralj, "Electrochemical detection of bisphenols in water samples," *Slovenski kemijski dnevi 2022 = 28th Annual Meeting of the Slovenian Chemical Society*, September 21 – 23, Portorož, Slovenia. Book of abstracts, pp. 158, 2022.

Š. Trafela, A. Korent, A. Krishnamurthy, K. Žagar Soderžnik, K. Žužek Rožman and S. Šturm, "Highly sensitive and selective biosensor platform for SARS-CoV-2 electrochemical detection," *57th International Conference on Microelectronics, Devices and Materials & The Workshop on Energy Harvesting: Materials and Applications*, September 14 – 16, Maribor, Slovenia. Book of abstracts, pp. 88, 2022.

Š. Trafela, A. Korent, A. Krishnamurthy, K. Žagar and K. Žužek Rožman, "Electrochemical detection of Sars-CoV-2 using a polyanaline/polystyrene/Au nanocomposite," *27th Annual Meeting of the Slovenian Chemical Society*, Septrember 22 – 24, Portorož, Slovenia. Book of abstracts, pp. 165, 2021.

K. Žužek Rožman, Š. Trafela, A. Korent, K. Žagar, U. Kavčič, I. Karlovits and S. Šturm, "Electrochemical sensing of toxic organic compounds (formaldehyde and acrylamide) in solutions using nanostructured electrodes," *European Congress on Exhibition on Advanced Materials and Processes*, Septrember 1 – 5, Stockholm, Sweden. Book of abstracts, pp. 509, 2019.

A. Korent, Š. Trafela and K. Žužek Rožman, "Imprinted polyaniline-based screen printed electrodes for sensing of toxic organic compounds," *Electrochem 2019*, August 26 – 28, Glasgow, UK. Book of abstracts, pp. 118, 2019.

K. Žužek Rožman, Š. Trafela, A. Korent, K. Žagar, U. Kavčič, I. Karlovits and S. Šturm, "Nanostructured electrochemical sensors for detecting toxic organic compounds (formaldehyde, acrylamide) in living environments," *IUMRS-ICAM International Conference on Advanced Materials, Spring Meeting*, May 27 – 31, Nice, France. Book of abstracts, 2019.

S. Novak, V. Golja and A. Korent, "Are there titania nanoparticles in my food?," *1st ISO-FOOD International Symposium on Isotopic and Other Techniques in Food Safety and Quality*, April 1 – 3, Portorož, Slovenia. Book of abstracts, 2019.

K. Žužek Rožman, D. Pečko, M. S. Arshad, A. Pintar, Š. Trafela, A. Korent, S. Šturm and N. Kostevšek, "Electrodeposited nanostructures for magnetic, energy and sensing applications," *EMN Meeting 2018, Energy Materials Nanotechnology*, May 14 – 18, Heraklion, Crete, Greece. Book of abstracts, pp. 37, 2018

A. Korent, Š. Trafela, S. Šturm and K. Žužek Rožman, "Novel functionalized nanomaterials for acrylamide sensing," *13th International Workshop on Electrodeposited Nanostructures, EDNANO*, August 30 – September 1, Bristol, UK. Book of abstracts, pp. 27, 2018.

A. Korent, Š. Trafela, S. Šturm and K. Žužek Rožman, "Electrochemical sensor for acrylamide detection," *54th International Conference on Microelectronics, Devices and Materials & the Workshop on Sensors and Transducers*, October 3 – 5, Ljubljana, Slovenia. Book of abstracts, pp. 65-66, 2018.

Š. Trafela, A. Korent, S. Šturm and K. Žužek Rožman, "KOH-modified nickel nanowires as effecient catalysts for electro-oxidation of formaldehyde for sensing applications," *54th International Conference on Microelectronics, Devices and Materials & the Workshop on Sensors and Transducers*, October 3 – 5, Ljubljana, Slovenia. Book of abstracts, pp. 63-64, 2018.

A. Korent, M. Lorenzetti, N. Drnovšek and S. Novak, "A method for detection of TiO_2 nanoparticles presence in food based on colorimetric assay," *25th International Conference on Materials and Technology*, October 16 – 19, Portorož, Slovenia. Book of abstracst, pp. 55, 2017.

A. Korent, M. Lorenzetti, N. Drnovšek and S. Novak, " Colorimetric assay for TiO_2 nanoparticles detection in complex matrices as food samples," *9th Jožef Stefan International Postgraduate School Students' Conference and 11th Young researchers' Day*, April 19 – 20, Ljubljana, Slovenia. Book of abstracts, pp. 88, 2017.

Biography

The author of this thesis, Anja Korent, was born on the 1st of August 1993 in Celje, Slovenia. After graduating from high school in 2012, she enrolled in the program Chemical Engineering at the Faculty of Chemistry and Chemical Technology at the University of Ljubljana. In 2015, she finished her B.Sc. work entitled "*Extraction and characterization of TiO_2 nanoparticles in chewing gums"* under the supervision of her mentor prof. dr. Polona Žnidaršič Plazl from The Faculty of Chemistry and the co-mentor dr. Martina Lorenzetti from the Jožef Stefan Institute. She continued her studies at the Jožef Stefan International Postgraduate school, programme Nanoscience and Nanotechnologies. For her M.Sc study she continued her work with TiO_2 nanoparticles as a food additive. The research work was carried out under the supervision of prof. dr. Saša Novak Krmpotič and co-supervision by dr. Martina Lorenzetti. She defended the M.Sc thesis entitled "Colorimetric assay for TiO_2 nanoparticles in complex matrices as food samples" in 2017. In October 2017 she continued with her PhD studies at the Jožef Stefan Postgraduate School in the field of Sensor Technologies, and she was enrolled as a young researcher under the supervision of Prof. Dr. Kristina Žužek Rožman at the Department for Nanostructured Materials, Jožef Stefan Institute, Ljubljana, Slovenia.